

ELECTRODEPOSITION OF CHROMIUM USING NOVEL DEEP EUTECTIC SOLVENTS

Thesis submitted for the degree of
Doctor of Philosophy
at the University of Leicester

in

Material Science

by

Azeez Abdullah Azeez Al-Barzinjy

(MSc. in Physics)

University of Leicester

Supervisors

Prof Andrew P. Abbott

Prof Karl S. Ryder

September 2014



**University of
Leicester**

Parts of this work have already been published in the following occasions

(a) Papers:

A. P. Abbott, **Azeez A. Al-Barzinjy**, P. D. Abbott, G. Frisch, R. C. Harris, J. Hartley and K. S. Ryder, *Phys. Chem. Chem. Phys.*, 2014, **16**, 9047-9055.

(b) Conferences:

(i) Talks:

- **Azeez A. Al-Barzinjy**, Andrew. P. Abbott & Karl S. Ryder, *Chromium electroplating using a novel deep eutectic solvent*, The Midlands Electrochemistry Group Meeting (MEG 2013) Postgraduate Students' Meeting, 17th April 2013 Nottingham.
- **Azeez A. Al-Barzinjy**, Andrew. P. Abbott & Karl S. Ryder, *Chromium electrodeposition using a novel type IV deep eutectic solvent*, the Molten Salt Discussion group, Christmas Meeting 16th December 2013, London.
- **Azeez A. Al-Barzinjy**, *Chromium plating from environmentally friendly liquids*, East Midlands Universities Postgraduate Research Student Conference, 6th September 2013, University of Derby, Derby.
- **Azeez A. Al-Barzinjy**, A. P. Abbott and K. S. Ryder, *Chromium plating from the novel environmentally friendly liquid*, Iraqi Cultural Attaché Conference, 28th February 2014, University of Nottingham, NG7 2RD, Nottingham.
- **Azeez A. Al-Barzinjy**, *Chromium plating using new ionic liquid systems*, Kurdistan Medical and Scientific Federation (KMSF), 1st Special Seminar Postgraduate Students and HCDP Programme, 19th May 2012, Aston University, Birmingham.

(ii) Posters:

- **Azeez A. Al-Barzinjy**, Andrew. P. Abbott & Karl S. Ryder, *Chromium electrodeposition using type IV deep eutectic solvent*, the Molten Salt Discussion group, Christmas Meeting 21th December 2013, Leicester.
- **Azeez A. Al-Barzinjy**, *Chromium plating from a novel DES, The best 50 research student winner from 1400 member of postgraduate research community, University of Leicester 27th June 2013.*
- **Azeez A. Al-Barzinjy**, A. P. Abbott and K. S. Ryder, *Chromium Electrodeposition using a Novel Type IV Deep Eutectic Solvent*, Electrochem conference September 1-3, 2013 Southampton University, 2013, 171, Southampton.
- **Azeez A. Al-Barzinjy**, *Chromium plating using new ionic liquid systems*, Kurdistan Medical and Scientific Federation (KMSF), 1st Special Seminar Postgraduate Students and HCDP Programme, 19th May 2012, Aston University, Birmingham.
- **Azeez A. Al-Barzinjy**, *Chromium plating from a novel DES*, the first international scientific conference for Kurdistan's postgraduate students, KSC2013, 16th September, 2013, Nottingham University Jubilee Campus, Nottingham.

Statement of originality

The experimental work in this thesis has been carried out by the author in the material centre at the University of Leicester between October 2011 and October 2014. The work has not been submitted, and is not presently submitted, for any other degrees at this or any other university.

Signed.....

Date.....

Azeez Abdullah Al-Barzinjy
Material Centre
University of Leicester,
University Road,
Leicester,
LE1 7RH.

Electrodeposition of chromium using novel deep eutectic solvents

Azeez Abdullah Azeez Al-Barzinjy

Abstract

Chromium electrodeposition is important for the production of anti-wear and anti-corrosion coatings. It has been carried out for over 50 years in a multi-billion dollars industry using essentially the same technology based on chromic acid. The toxicity of the electrolyte makes the search for an alternative process an environmental imperative.

In this study a variety of novel formulations of deep eutectic solvents are produced and tested to determine their efficacy for chromium deposition. The study concentrates on using urea as a complexing agent with a variety of trivalent chromium salts.

In the first results chapter complexes of $\text{CrCl}_3 \cdot 6\text{H}_2\text{O}$ with urea are formed. It is shown that this system displays high conductivities, despite relatively high viscosities compared with the previously reported chromium based deep eutectic solvents. Thick, adherent, non-cracked black chromium could be deposited and produce relatively hard chromium coatings. EXAFS suggests that there are a variety of chromium species but they are probably cationic with a variety of oxygen donors as ligands.

In the next section $[\text{Cr}(\text{en})_3]^{3+}$ species was produced as the cationic species and this had a higher conductivity than any similar system previously described. Bright, adherent, hard chromium was obtained by electroreduction with constant speciation. A novel solvatochromic shift, that we are unaware of in the literature, demonstrates the charge transfer complex results in an unexpected colour change.

In an endeavour to remove Cl^- from the formation chrome-alum ($\text{KCr}(\text{SO}_4)_2 \cdot 12\text{H}_2\text{O}$) was used as the metal salt. This produced unprecedented high conductivity for this type of medium with a low viscosity. It was proposed that unlike most ionic liquids mass transport is not limited by hole transport and instead it is proposed that these liquids function more like very concentrated electrolytes where ion pairing becomes important.

In the final result section a variety of additives are tested. Some are shown to have a significant effect on the morphology and hardness of the deposit. Ultimately bright metallic chromium films could be reproducibly produced with a hardness of 800 ± 10 HV. This is the first process based on Cr(III) to be able to achieve these rigorous requirements and suggests the first real alternative to hexavalent chromium for hard chrome.

Acknowledgements

I would like to express my deepest appreciation and sincere gratitude to my supervisor, Professor Andrew Abbott for his skilful guidance, encouragement, opportunities, patience, support, and great concern, which made this work successful. Thank you for being the best supervisor anyone could have asked for.

I would also like to thank my second supervisor Professor Karl Ryder for his insightful ideas, suggestions, and time for serving in our discussions.

I am thankful to all my colleagues from the Leicester ionic liquid group both past and present for their individual contributions to my experience, academically and socially. I would particularly like to express my gratitude to Prof Robert Hillman, Dr Gero Frisch and Dr Robert Harris, Dr Jennifer Hartley, Dr Andrew Ballantyne, Dr William Wise, Essa Ismaeil and Jamil Abdullah for their invaluable assistance and guidance, not least their friendship, throughout my PhD.

A scholarship and study leave granted by the Ministry of High Education in the Iraqi Kurdistan Region, HCDP program and University of Salahaddin/Hawler is also gratefully acknowledged.

I would like to thank the team of ESRF beamline BM25A (SpLine) for beam time and support in Grenoble-France, and Dr Philippe Verpoort the project Leader at OCAS in Belgium for analysing some of my samples.

Last but not least, I wish to express my immeasurable appreciation and thanks to my father and my mother's pure soul. Thank you for your prayers and support. Most of all, I would like to thank my wife, for her patience and for staying up with me through all those tiredness. To my two precious daughters, Ala'a and Ashna, and my beloved son Abdullah thank you for your unconditional love. All of you have been the source of my strength and motivation for success especially in periods of uncertainties and difficulties.

Dedication

I dedicate this thesis to the memory of my beloved mother, who would have been happy to see me at this stage.

Azeez Abdullah Al-Barzinjy

Leicester, 2014

Table of contents

Abstract	i
Acknowledgements	ii
Dedication	iii
Table of contents	iv
Abbreviations	vii
Chapter 1: Introduction	1
1.1 Electrodeposition	2
1.2 Chromium electrodeposition	4
1.3 Hexavalent chromium electrodeposition alternatives	5
1.4 Non-aqueous electrodeposition	6
1.5 Ionic liquids	7
1.6 History of ionic liquids	10
1.7 Electroplating using ionic liquids	11
1.8 Deep eutectic solvents (DESs)	14
1.9 Type 4 DESs	16
1.10 Chromium plating in deep eutectic solvents	17
1.11 Hardness	18
1.12 Research aims	21
1.13 References	22
Chapter 2: Experimental procedures	27
2.1 Introduction	28
2.2 Materials	28
2.3 Preparation of solution	28
2.4 Physical properties	29
2.4.1 Viscosity measurements	29
2.4.2 Conductivity measurements	29
2.4.3 Surface tension measurements	29
2.4.4 Density measurements	30
2.5 Thermal properties	30
2.6 Electrochemical measurement	31
2.6.1 Cyclic voltammetry	31
2.6.2 Potential step experiment	32
2.7 Electrochemical quartz crystal microbalance (EQCM)	32
2.8 Hull cell testing	33
2.9 Surface analysis	34
2.9.1 SEM and EDX	34
2.9.2 3D-microscope	34
2.9.3 X-ray diffraction	35
2.10 EXAFS	36
2.11 UV-Vis spectroscopy	38
2.12 Fast atom bombardment mass spectroscopy (FAB MS)	40
2.13 Hardness test	41
2.14 References	42
Chapter 3: Chromium chloride based deep eutectic solvents	43
3.1 Introduction	44
3.2 Eutectic mixture based on urea and $\text{CrCl}_3 \cdot 6\text{H}_2\text{O}$	45
3.3 Physical properties	46
3.3.1 Phase behaviour	46
3.3.2 Viscosity	47
3.3.3 Conductivity	50
3.3.4 Molar conductivity	52
3.4 Solution speciation	54

3.4.1	Mass spectrometry	54
3.4.2	UV-visible spectrum	54
3.4.3	Speciation and extended X-ray absorption fine structure (EXAFS)	55
3.4.3.1	Theory of EXAFS	56
3.4.3.2	Generation of X-rays	57
3.4.3.3	Absorption coefficients	58
3.4.3.4	Absorption edges	59
3.4.3.5	Origin of EXAFS signal	61
3.4.3.6	Generation of EXAFS spectra	62
3.4.3.7	Speciation of metal salts in DESs	63
3.4.3.8	Chromium species in the novel DES	63
3.5	Density and surface tension	65
3.6	Hole theory	66
3.7	Cyclic voltammetry	69
3.8	Quartz crystal microbalance (QCM)	69
3.8.1	Electrochemical quartz crystal microbalance (EQCM)	71
3.9	Bulk deposition	73
3.10	Hardness and thickness	75
3.11	Conclusions	76
3.12	References	77
	Chapter 4: [Cr(en)₃]³⁺ based deep eutectic solvents	80
4.1	Introduction	81
4.2	Ligand field theory	82
4.2.1	Crystal field theory	83
4.3	Colour of transition-metal coordination compounds	88
4.4	Eutectic mixtures based on urea and [(Cr(en) ₃)Cl ₃ ·3H ₂ O]	90
4.5	Physical properties	91
4.5.1	Phase behaviour	91
4.5.2	Viscosity	92
4.5.3	Conductivity	94
4.5.4	Molar conductivity	97
4.6	Solution speciation	99
4.6.1	UV-visible spectrum	99
4.6.2	EXAFS	100
4.7	Density	100
4.8	Molar volume	101
4.9	Cyclic voltammetry	103
4.9.1	Under-potential deposition (upd)	103
4.9.2	The effect of the viscosity on the voltammograms	106
4.10	Bulk deposition	109
4.11	Hardness and thickness	110
4.12	Current efficiency	110
4.13	Conclusions	111
4.14	References	112
	Chapter 5: Cr alum based deep eutectic solvents	114
5.1	Introduction	115
5.2	Eutectic mixture based on urea and chrome alum	115
5.3	Physical properties	115
5.3.1	Phase behaviour	115
5.3.2	Viscosity	116
5.3.3	Conductivity	119
5.3.4	Molar conductivity	122
5.4	Solution speciation	124
5.4.1	UV-visible spectrum	124

5.4.2 EXAFS	125
5.5 Density	126
5.6 Molar volume	127
5.7 Cyclic voltammetry	128
5.8 Bulk deposition	128
5.9 Hardness and thickness	130
5.10 Current efficiency	130
5.11 Conclusions	131
5.12 References	132
Chapter 6: The role of additives in the electrodeposition of chromium	134
6.1 Introduction	135
6.2 Levelling and brightening	135
6.3 Effect of brighteners on the morphology	137
6.4 Use of additives for electrodeposition from ionic liquids	139
6.5 Results and discussion	142
6.6 Effect of additives on bulk deposition	142
6.7 Viscosity and conductivity	146
6.8 Solutions speciation	149
6.9 Cyclic voltammetry	151
6.10 Hardness and thickness	153
6.11 X-ray diffraction	154
6.12 Conclusions	155
6.13 References	157
Chapter 7: Summary and future directions	159
7.1 Summary	160
7.1.1 Cr electrodeposition from deep eutectic solvents	160
7.1.2 The effect of ligands exchange	161
7.1.3 The effect of additives on the Cr electrodeposition	162
7.2 Future directions	163
7.3 References	164
Chapter 8: Appendix	165

Abbreviations and symbols

[BMIM][PF ₆]	1-Butyl-3-methylimidazolium
AFAC	Amplitude correction factor
AFM	Atomic force microscopy
BA	Boric Acid
BASIL	Biphasic Acid Scavenging utilising Ionic Liquids
CFT	Crystal field theory
ChCl	Choline chloride
cP	Centi Poise
CT-band	Charge transfer band
CV	Cyclic voltammetry
DES	Deep eutectic solvent
DSC	Differential scanning calorimeter
EDX	Energy dispersive analysis using X-rays
Δ_o	Splitting parameter
EG	Ethylene glycol
en	Ethylene diamine
EPA	Environmental Protection Agency
EQCM	Electrochemical quartz crystal microbalance
E_Λ	Activation energy for conductivity
EXAFS	Extended X-ray absorption fine structure
E_η	Activation energy for viscous flow
FAB-MS	Fast atomic bombardment mass spectrometry
GC	Glassy carbon
HBD	Hydrogen bond donor
hcp	Hexagonal closed packed
HOMO	Highest occupied molecular orbital
HV	Vickers Hardness
IL	Ionic liquid
LUMO	Lowest unoccupied molecular orbital
MO	Molecular orbital
O	Octahedral crystal
OD	Oxygen Donor

Pa	Pascal
PF ₆	Hexa-fluorophosphate
Pt	Platinum
REACH	Registration, Evaluation, Authorisation and Restriction of Chemicals
RTIL	Room Temperature Ionic Liquid
SEM	Scanning electron microscopy
SIMS	Secondary ion mass spectrometry
STM	Scanning tunnelling microscope
TCLP	Toxicity Characteristic Leaching Procedure
T _f	Freezing temperature
T _g	Glass transition temperature
T _m	Melting temperature
UV-vis	Ultra violet visible
Λ	Molar conductivity
XANES	X-ray Absorption Near Edge Structure
XRD	X-Ray diffraction spectrometry
η	Viscosity
σ	Conductivity

Chapter 1: Introduction

1.1	Electrodeposition	2
1.2	Chromium electroplating	4
1.3	Hexavalent chromium electroplating alternatives	5
1.4	Non-aqueous electrodeposition	6
1.5	Ionic liquids	7
1.6	History of ionic liquids	10
1.7	Electroplating using ionic liquids	11
1.8	Deep eutectic solvents (DESs)	14
1.9	Type 4 DESs	16
1.10	Chromium plating in deep eutectic solvents	17
1.11	Hardness	18
1.14	Research aims	21
1.15	References	22

1.1 Electrodeposition

Electroplating is an electrodeposition process for producing a thick, uniform, and adherent coating, commonly of metal or alloys, upon a surface by the act of electric current.¹ The coating formed changes the properties of the underlying substrate and is generally applied to improve wear and corrosion resistance of the interface or improve the aesthetic properties of the object. The piece to be electroplated is made into the negative electrode in an electrochemical cell and a current is passed through an electrolyte containing the ions of the metal to be electrodeposited.

There has been little change in the method of electroplating over 100 years and almost all processes are based on aqueous solutions of metal salts with a variety of additives to control morphology and properties. The industry is dominated by a relatively small number of coating materials. Anti-wear coatings are mostly Cr, Ni and Co and their alloys with other metals.^{2,3} For aesthetic purposes Cr, Ag and Au are used. Zn and Cd and their alloys are applied for anti-corrosive coatings.^{2,3} Copper and silver have been used extensively for electronic and optoelectronic products.^{4,5} A few other metals and alloys are deposited but these are very much niche applications.

The use of aqueous solutions has many issues for electroplating primarily due to the narrow potential window so metals with a large negative reduction potentials, e.g. Cr and Zn, are deposited with poor current efficiencies and suffer from hydrogen embrittlement.⁶ Furthermore, although water is a green solvent the inclusion of high metal concentrations means that the water has to be extensively cleaned before it can be returned to the environment.⁷ The electroplating process is also a complex series of pre- and post-treatment steps to prepare the substrate and remove the electrolyte after coating. An example for chromium plating is shown schematically in **Figure 1.1**.

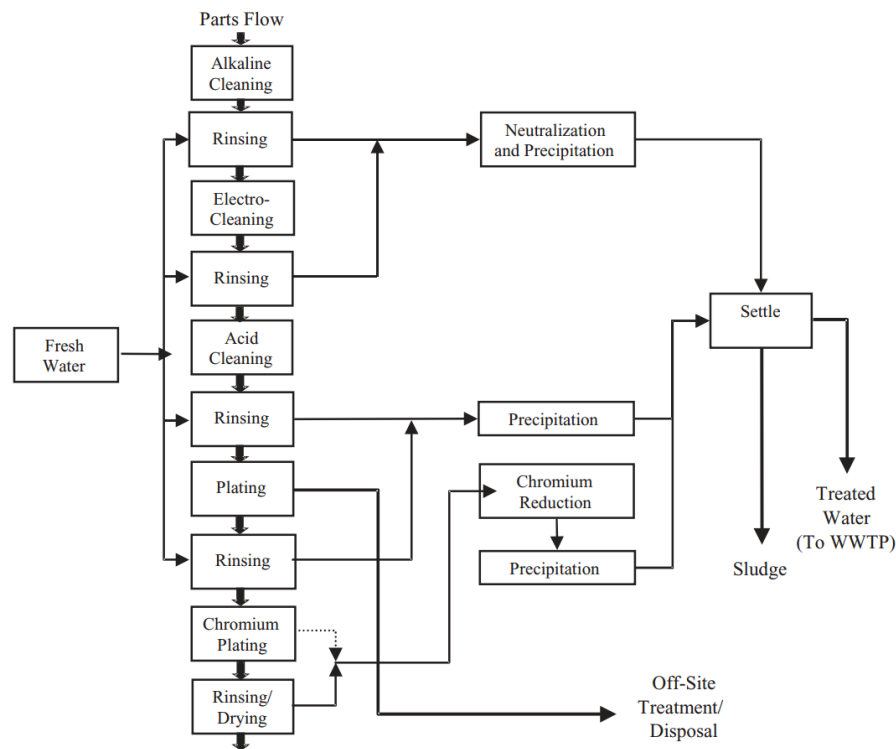


Figure 1.1: Process flow-sheet of a typical electroplating plant.⁸

Obviously the main advantages of using aqueous solutions are:

- Cost
- Non-flammable
- High solubility of electrolytes
- High conductivities resulting in low ohmic losses and good throwing power
- High solubility of metal salts
- High rates of mass transfer.

For these reasons water will remain the backbone of the metal plating industry, nevertheless, there are also limitations of aqueous solutions comprising:

- Limited potential windows
- Gas evolution processes can be technically not easy to handle and result in hydrogen embrittlement
- Passivation of metals can cause issues with both anodic and cathodic materials
- Requirement for complexing agents such as cyanide
- All water must finally be returned to the water course.

These issues stop aqueous solutions being useful to the deposition of several technically

vital materials. The main research areas in electroplating include replacement of environmentally toxic metal coatings, such as chromium, deposition of novel alloys and semiconductors and new coating methods for reactive metals.

1.2 Chromium electroplating

Chromium plays an important role in a number of modern industries, for example as a protective material in automotive and aerospace applications as well as for decorative purposes. It is the 22nd most common element the Earth's crust, and is ahead of technically important metals such as Ni, Zn and Cu. With a density of 7.14 g cm^{-3} , it no longer belongs to the class of light metals. It is however for its almost unparalleled hardness that the metal has become so valuable. Without the wear- and corrosion resistance of chromium most hydraulic systems would have considerably shorter lifetimes.²

Although chromium with a standard redox potential, E^0 , of $(\text{Cr}/\text{Cr}^{3+}) = -0.744 \text{ V}$ is a base metal its ease of surface passivation makes it a good anti corrosion coating. It is weather- and tarnish-resistant, thermally stable up to $500 \text{ }^\circ\text{C}$ and is not corroded by hydrochloric acid, hot sulphuric acid and many other chemicals.

Chromium is traditionally electroplated from chromic acid which is a mixture of CrO_3 and H_2SO_4 . Although this has been the basis of a successful technology for over 50 years it is highly toxic and carcinogenic. There has been cumulative anxiety due to environmental, health and safety concerns related with the emission, treatment, storage which has led to reduced usage of hexavalent chromium compounds.⁹ In general hexavalent chromium electroplating baths produce trivalent chromium ions and hydrogen gas at the cathode, whereas oxygen gas is the major product at the anode. These gases increase to the top of the bath and then into the atmosphere. Workers can breathe in this mist in the electroplating shop.¹⁰ Hexavalent chromium is strongly linked with lung cancer. It also causes burns, ulceration of the skin and the mucous membrane, and loss of respiratory sensation.¹⁰ Indeed, the Environmental Protection Agency (EPA) indicate a limit of $100 \text{ } \mu\text{g/L}$ of total chromium Cr(III) and Cr(VI) in drinking water and $52 \text{ } \mu\text{g/m}^3$ of the same contaminant in the inhaled air for 8-hour work shifts.¹¹ EPA also issued the Toxicity Characteristic Leaching Procedure (TCLP) in soil which gives the extreme tolerated concentration of pollutants which for Cr is 5 ppm.¹² Chromium (III) is

however a vital micronutrient for animals and human being. It is also thought to be significant for the action of insulin.¹²

1.3 Hexavalent chromium electroplating alternatives

In addition to its toxicity there are other issues associated with the deposition of chromium from chromic acid electrolytes. These have been summarized by Smart *et al.*¹³ as follows:

- Chromium electrodeposition utilising Cr(VI) has a low efficiency i.e. 15–22% where the remainder of the applied current is used in hydrogen evolution.
- The average cathodic current densities are high (typically 10-15 Adm^{-2}).
- The procedure has poor covering power across low current density areas.
- Burning is observed as grey deposits in high current density zones.
- Chromium electroplating has low throwing power, which results in thick electrodeposits on the boundaries and protruding parts of cathodes and thin deposits over the rest of the surface.
- Breaks in power during electrodeposition produce milky deposits known as white washing.
- Chromic acid poses instant harmful effects on human tissue, burning the skin and even dilute solutions cause ulcers.
- Chromic acid is a strong oxidizing agent and hence is a fire hazard.
- High cost of chemical treatment.

Numerous studies have attempted to develop trivalent chromium formulations for chromium plating and while several have been commercialised they are all used for decorative coatings.¹⁴ Trivalent chromium is at least 100 times less toxic to humans and the environment than hexavalent. Thermal spray techniques, nickel-based coatings and trivalent chromium electroplating have all been used as alternatives to Cr(VI) but none have comparable hardness.^{15, 16}

Electroplating with trivalent chromium has been used in the metal finishing industry since 1973. Jeffrey and Stanley¹⁷ invented the first commercial trivalent chromium bath based on chromium chloride, boric acid, ammonium chloride and bromide salts. Barclay¹⁸ created a trivalent electrolyte based on chromium sulphate and thiocyanate utilising a divided cell arrangement to avoid anodic oxidation of trivalent chromium. In

1984, Deeman produced another sulphate-based bath.¹⁹ All these trivalent chromium processes were used for depositing less than 0.5 μ m thick chromium films.²⁰⁻²⁴ Ibrahim²⁴ and El-Sharif²¹ similarly detected that deposits from trivalent electrolytes possess comparable features to that of hexavalent chromium electrolytes for thin, bright deposits. The standard hardness of the deposits from trivalent chromium baths is between 600 to 1000 HV.²⁵ The trivalent chromium bath also has the ability to tolerate current interruptions without passivation or making white misting on the coating.

The most common bath is an electrolyte using chloride or sulphate salts with graphite or compound anodes and different additives to hinder the oxidation of Cr(III) at the anode.²⁶ Conductive metal oxide coated anodes have been effectively utilised in trivalent chromium electroplating. The main issue with the deposition from Cr(III) electrolytes is related to the reactions happening at the cathode. Shahin²⁷ suggested that electrodeposition of chromium from trivalent baths contains two successive reduction steps via the Cr²⁺ species. The standard reduction potential for the various chromium species are:²⁸



It is clearly thermodynamically favourable to produce hydrogen instead of chromium metal which leads to low current efficiency and hydrogen embrittlement.

The aim of this thesis is to use alternative electrolytes for the electrodeposition of chromium to circumvent the issues of using Cr(VI), to improve current efficiency and optimise the hardness and aesthetic finish of the deposit.

1.4 Non-aqueous electrodeposition

In the last few years, electrodeposition of metals from non-aqueous solutions has attracted attention of researchers. Traditional aqueous solutions cannot be always utilised as electrolytes due to the hydrogen evolution during electrolysis, narrow electrochemical potential windows, poor thermal stability, and evaporation.

There are obviously a variety of other solvents that could be utilised, ionic and molecular; polar and non-polar. Polar solvents are preferable to dissolve electrolytes

and produce high conductivities. In general the small solvent molecules will usually offer a high fluidity. Undesirably all polar molecules possess electronegative elements such as oxygen which by their nature make them good electron donors. These will powerfully coordinate to metal ions making them less easy to reduce. Some of the more electropositive metals have been plated from polar organic solvents but these do not provide significant technical advantages.

Non-polar organic solvents, mostly aromatic hydrocarbons have been utilised for metal electrodeposition. These possess the advantage of wide-ranging potential windows but the clear disadvantage of poor conductivity. The Alumiplate procedure was technologically advanced in the late 1980s to plate aluminium from toluene.^{29, 30} Triethyl aluminium was utilised as the basis of aluminium but it is pyrophoric and this in grouping with a highly flammable solvent makes the procedure not easy to run. A variety of other metals have also been electrodeposited from aromatic solvents including Sn, Cu, Pd, Pb, Cd, Ti and Cr.³¹⁻³⁵ A review explaining the electrochemistry in non-aqueous solutions is given by Izutsu.³⁶

1.5 Ionic liquids

High temperature molten salts have long been used for extraction of metals such as Al, Ti, Na and Li.^{37,38} The main limitation with high temperature molten salts is obviously the operation temperature which makes difficult in operation and limits the range of substrates that can be used. In an attempt to reduce the melting temperature of salts various studies focused on $\text{Li}^+/\text{K}^+/\text{AlCl}_3$ eutectics which have freezing points close to 100 °C.³⁹

The use of organic salts with melting points below 100 °C, normally referred to as ionic liquids (ILs)⁴⁰⁻⁴⁵ has seen unparalleled growth since 2000. **Figure 1.2** shows some of the main developments in the field of ILs.

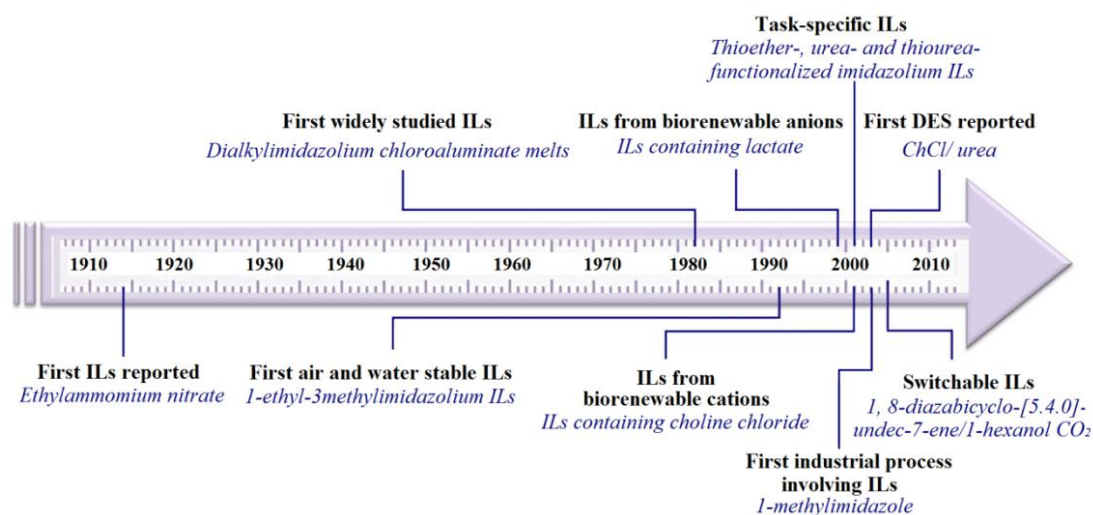


Figure 1.2: Selected milestones in the development of ILs and DESs.

Indeed, the term “ionic liquids” has been used to differentiate between high temperature and low temperature systems. There are many ionic liquids with melting points below ambient-temperature which makes them of fundamental interest to chemists, since both the thermodynamics and kinetics of reactions carried out in ionic liquids are different to those in conventional molecular solvents and the chemistry is different. Imidazolium, pyrrolidinium, pyridinium, tetraalkylphosphonium, and tetraalkylammonium ions are the common cations. Alternatively, the anions of common ionic liquids include halides (X^-), hexafluorophosphate (PF_6^-), tetrafluoroborate (BF_4^-), trifluoromethylsulfonate (TfO^-), nitrate (NO_3^-), acetate (OAc^-) and bis(trifluoromethanesulfonyl)imide (NTf_2^-). The amalgamations of such cations and anions can lead to a huge number of ionic liquids that can provide substantial flexibility in the assignment of the most suitable pair for a particular chemical application. A number of the common cations and anions are shown in **Figure 1.3**.

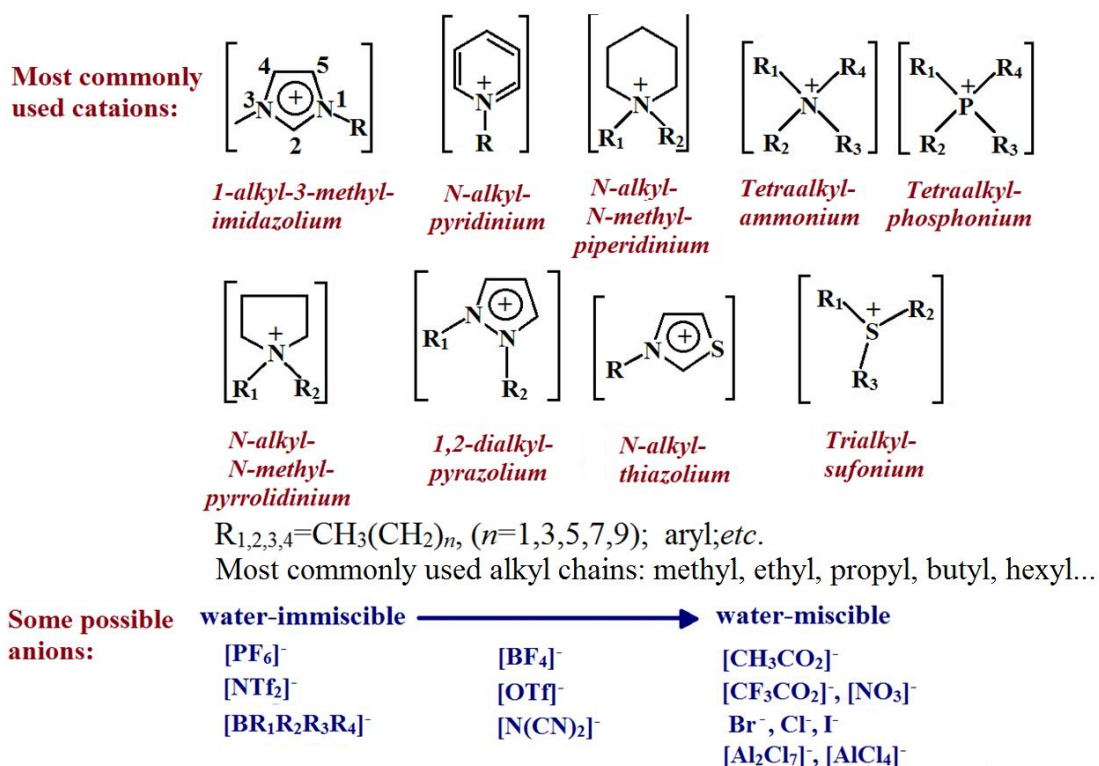


Figure 1.3: Common cations and anions used in the formation of ionic liquids

Each different combination of anion and cation changes both the physical and chemical properties of the liquid leading to their description as designer solvents.⁴⁶

Currently, the term ionic liquid is used almost exclusively to refer to room temperature ionic liquids and the term molten salt indicates salts with melting points above 100 °C.⁴⁷ This fluidity of ionic liquids near room temperature challenges usual expectations for ionic compounds.⁴⁸ Holbrey and Rogers have discussed contributing factors to the low melting point.⁴⁹ The charge, size, distribution of charge on the respective ions and asymmetry of the cation are believed to be key factors influencing the melting point. In general, larger ions result in a decrease in melting point by having more charge delocalization, less charge density and hence reduced Coulombic attractions between the ions.⁴⁹ The inability of the ions to fit into a crystal lattice owing to the sizes of the ions involved, described as “packing inefficiency” has been proposed as an important factor in rationalizing the low melting points of some ionic liquids.⁵⁰ Large anions with many degrees of freedom slow down crystallization until lower melting temperatures are obtained.⁴¹

1.6 History of ionic liquids

Walden is commonly recognized with the first synthesis of an ionic liquid as early as 1914.⁵¹ The field of ionic liquids has been extensively reviewed by many authors, including Welton,⁵² Holbrey,⁵³ and Seddon.⁵⁴ Interest in the electrochemistry of ionic liquids has increased significantly over the past decade. After nearly two decades Graenacher⁵⁵ received the 1st patent in the ionic liquid field. In his patent he stated that certain organic salts have the aptitude to dissolve cellulose. Unfortunately, this publication did not generate any remarkable attention in the scientific community. In 1948, Hurley, used a low melting salt, to demonstrate aluminium deposition.⁵⁶ Osteryoung and Gilbert in 1975 used ionic liquid salts as potential electrolyte replacements in batteries.⁵⁷⁻⁵⁸ Later in 1982 Wilkes and Hussey⁵⁹ attempted to look for a less reducible cation, which led to the use of imidazolium cation in an ionic liquid.⁶⁰ These ILs, (**Figure 1.4**), have subsequently been intensively studied, but the water sensitivity, general custom of 1st generation, of the involved chloroaluminate(III) anion slowed down their potential industrial applications.⁶¹ A second generation of air- and moisture-stable 1-ethyl-3-methylimidazolium-based ILs was presented one decade later using discrete anions such as BF_4^- and PF_6^- , and this led to their use in a wide variety of application.^{62,63}

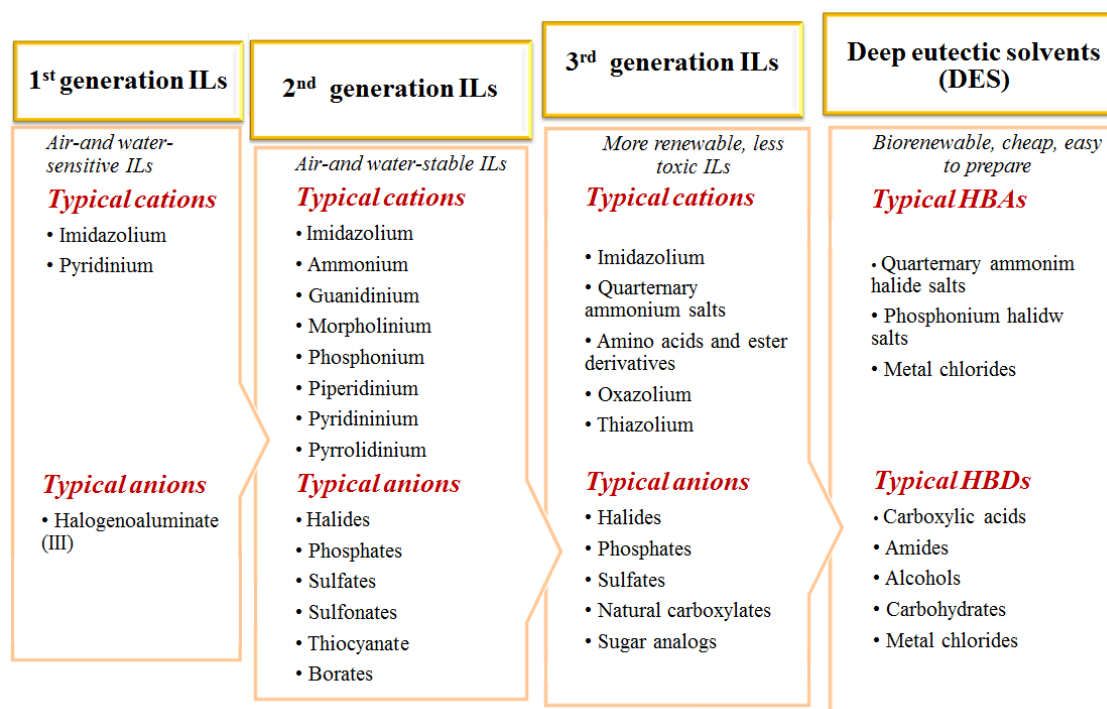


Figure 1.4: Common Classification of ILs and DESs

More recently, the use of readily obtainable, biorenewable anions and/or cations was described for the preparation of sustainable ILs.^{64, 65} Significantly, the first industrial progression including ILs, BASIL (biphasic acid scavenging utilizing ILs), was announced in 2003.⁶⁶

Moreover, these “first generation” ionic liquids had a significantly lower viscosity than the equivalent pyridinium liquids and it is the imidazolium cation that still governs the ionic liquid literature. Discrete anion or “second generation” ionic liquids are composed of simple anions, as opposed to a combination of anions in equilibrium. Their finding is attributed to Wilkes and Zaworotko who formed 1-ethyl-3-methylimidazolium tetrafluoroborate and acetate for the first time⁶⁷. It is this class of ionic liquid which has dominated the literature ever since. Later Seddon and Hussey tried to understand spectroscopic and chemical aspects of these metal compounds by investigating metal complexes in ionic liquids.^{68, 69} The potential toxicity of ionic liquids has also received a great deal of attention with respect to their likely use as greener solvents and new materials for a broad number of prospective purposes.⁷⁰ Chauvin⁷¹ and Wilkes⁷² in 1990 used transition metal catalysts in acidic ionic liquids to catalyse the dimerisation of propane and the polymerisation of ethane. Two year later Wilkes and Zaworotko established a uniform reaction in ionic liquid by applying more steady species.⁷³

ILs have attracted substantial attention in a variety of fields including chemical synthesis, catalysis, electrochemistry, engineering, and biology^{43, 61, 74-76} due to their tuneable physicochemical properties. Likewise, they have been employed in a variety of areas of analytical chemistry, including sample preparation, analytical separation, and detection procedures.⁷⁷⁻⁷⁹ Some of these applications are based upon their characteristic properties including amphiphilic solvation power, wide liquid temperature range, insignificant volatility, non-flammability, wide electrochemical window, etc.^{49,52, 80} There is a vast range of both cations and liquids which, joint together, might give as many as a 10^{12} different ionic liquids. A comprehensive review by Seddon *et al.* has detailed the successful application of ionic liquids to date.⁶¹

1.7 Electroplating using ionic liquids

The main interest in using ionic liquids for metal deposition arises from the very wide potential windows which have been reported which in some cases exceed 5 V. Many

imidazolium and pyridinium salts are stable below -2.5 V suggesting that the majority of electronegative metals can be electro-reduced within the potential window of the liquid. The vast majority of metals have been deposited from ionic liquid electrolytes and this has been extensively reviewed by Abbott and Endres *et al.*^{81, 82, 37}

While numerous metals have been deposited onto a variety of substrates the true potential of using ionic liquid has not been achieved to date. Most studies have approached ionic liquids as a direct substituent for water and have applied similar conditions those used in aqueous solutions. A review by Abbott and McKenzie has highlighted the differences between aqueous solutions and ionic liquids in terms of the conductivity, speciation, mass transport, anodic reaction and double layer structure. Most have also failed to take issues such as diluents, brighteners, pre- and post-treatment protocols and complexing agents into account.⁸²

The avoidance of water chemistry seems easy, even though ionic liquids have different weaknesses and no systems are accurately water free. However, liquids having Lewis basic anions such as chloride are much less sensitive to water content than are weakly coordinating anions. It is a common mistaken belief that a high concentration of ions necessarily leads to high conductivities; in ionic liquids the viscosity controls the conductivity, and values are generally less than 10 mS·cm⁻¹. The commonly high viscosity of ionic liquids can also present important concerns related to throwing power and can cause inhomogeneity of coating thickness.⁸³ A clear limitation of ionic liquids to metal deposition will be cost. Plating tanks are generally in excess of 1 m³ and with liquids currently in the region of £500 kg⁻¹ ionic liquids would be prohibitively expensive for most metals.

It is therefore not sensible to expect ionic liquids to be applicable to all aspects of electroplating but it is helpful to consider the aspects in which ionic liquids are unique.

Electronegative metals: Clearly of most interest is the ability to deposit electronegative metals that be deposited from any other media. While numerous groups have studied the electrodeposition of aluminium from imidazolium chloroaluminate liquids the water sensitivity of the liquid is still too great to make it viable on a long term process. Studies in the group at Leicester have scaled up the technology to 20 litres but found that the bath deteriorated after a couple of months. Of more interest in this area may be the ability to obtain unique alloys and numerous aluminium based systems have been studied to this end.⁸⁴⁻⁸⁶

Novel architectures: Ionic liquids are well known to allow metals to grow with unusual morphologies. Numerous groups have shown that deposits tend to form with nanocrystalline morphologies. It has recently been shown that nanowires can be obtained from ionic liquids both with and without templates on the electrode surface. Of note is the work of Sun *et al.* who showed that zinc nanowires form with Type 1 DESs.⁸⁷ Endres has also shown that the use of polymer beads and etched polymer films can be used to make both photonic crystals and nanowires respectively.⁸⁸ This has been achieved for important metals such as Cu, Ag, Al and Si.

Semiconductor deposition: Numerous groups have used ionic liquids to deposit semiconductors. The unique aspect of this research has been the ability to tailor the band-gap of the deposit to change the semiconductor properties. Endres has studied a variety of materials based on silicon, germanium, gallium and indium.^{37, 89} Golgovici *et al.* used DESs to deposit Te, Bi-Te and Sb-Te alloys.⁹⁰ These areas are discussed in more depth in a recent review by Abbott *et al.*^{37, 82, 83}

In addition some of the most useful applications of ionic liquids and particularly DESs will probably arise from their ability to deposit metals circumventing the use of hazardous precursors. It is the aim of this research to circumvent the use of chromic acid for chromium deposition. This approach has already been shown to be viable for the removal of cyanide from immersion silver coating.⁸²

Perhaps the main issue to be highlighted with the design of ionic plating systems is the coordination chemistry and concentration of the metal complex. It influences not only the thermodynamics, but also kinetics of metal ion reduction and therefore is a key liable factor to deposit morphology and properties. To comprehend the issues it is strongly suggested that to make a comparison with current water-based plating systems.

Table 1.1 shows some components of the most frequently utilised aqueous electroplating solutions. It is obvious that many have strong ligands such as oxides or cyanides or oxidising agents present, which considerably influences the coordination geometry of the metal complexes. Additionally, a mixture of brighteners is added to most commercial electroplating systems which influence adsorption, mass transport and coordination chemistry.^{82, 91}

Table 1.1: Typical concentrations of metal salts used in commercial aqueous electroplating solutions⁹¹

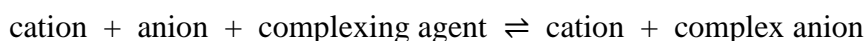
Metal	Electrolyte	Concentration of metal salts/ g· dm ⁻³
Chromium	CrO ₃ , H ₂ SO ₄	250-450
Copper	CuSO ₄ , Potash alum, H ₂ SO ₄	60-200
Nickel	NiSO ₄ , NiCl ₂ , Boric acid	200-350
Silver	Ag salts (various), KCN	80-200

Most of the ionic liquid systems have been made using chlorides, and the metal complexes formed are reliant on the Lewis acidity of the metal and Lewis basicity of the ionic liquid. In aqueous plating solutions chlorides are not often used as they have a tendency to produce black powdery deposits. This is believed to be as a result of the ease of nucleation producing large numbers of small nuclei formed at the electrode surface.

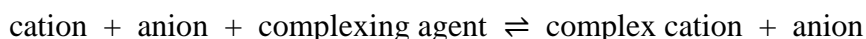
One of the principal differences between ionic liquids and aqueous solutions is the relatively high viscosity of the former. The viscosities are normally in the range 10 - 500 cP (0.01 - 0.50 Pa.s) and this influences the diffusion coefficients of species in solution. Abbott has fitted the viscosity of ionic liquids using hole theory.⁹² The theory was settled for molten salts but has been shown to be very convenient for ionic liquids. It was shown that the value of activation energy is related to the size of the ions and the size of the voids existing in the liquid.³⁸ The viscosity of ionic liquids is several orders of magnitude higher than high temperature molten salts due partly to the dissimilarity in size of the ions, but also because of the increased void volume in the final. It has been shown⁹³ that hole theory can be utilised for both ionic and molecular fluids to explain viscosity and can assistance with the design of new ionic liquids.⁹⁴

1.8 Deep eutectic solvents

Abbott has suggested that ionic liquids can be expressed by the following equilibria;



or potentially:



For example first generation ionic liquids use metal salts as the complexing agent with a halide as the anion and a quaternary ammonium cation. The Leicester group suggested this could be significantly extended using a variety of complexing agents which were

not simple metal salts. These so-called Deep Eutectic Solvents (DESs) are eutectic mixtures of simple salts with either Lewis acidic or Brønsted acidic complexing agents. While they do not have the same chemical inertness of some of the ionic liquids with discrete anions they are simple to prepare, are insensitive to water content, do not need to be registered as their toxicological properties are known and probably most importantly for large scale applications like electroplating they are inexpensive **Figure 1.5** shows the formation of a eutectic schematically.

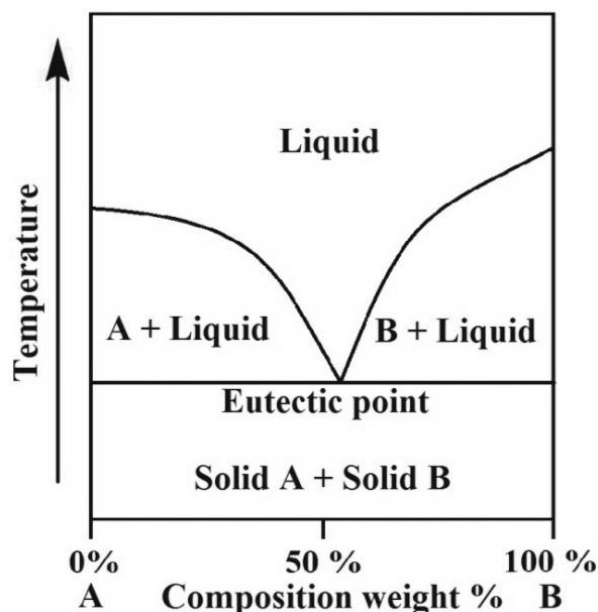


Figure 1.5: Schematic illustration of eutectic mixture formation

DESs These comprise of quaternary ammonium salts (e.g. choline chloride, ChCl), metal salts or metal salt hydrates and hydrogen bond donors (e.g. urea) and are commonly divided into four groups (**Table 1.2**),⁹⁵ and have been particularly successful on a large scale for metal polishing^{96,97} and immersion silver deposition.^{98,99}

Researchers have already reported numerous applications of DESs. For example, the Abbott group dissolved silver salts in the DESs to dip coat copper surfaces with silver without the need for catalysts.¹⁰⁰⁻¹⁰⁴ Choline chloride-based DESs replaced phosphoric and sulphuric acids for electropolishing stainless steel.¹⁰⁵ Choline chloride addition to a biodiesel preparation removed the glycerol side product by forming a choline chloride-glycerol DES as a second phase.¹⁰⁶

Table 1.2: Classification of deep eutectic solvents (DESS)

Type 1	• Quaternary ammonium salt + metal chloride
Type 2	• Quaternary ammonium salt + metal chloride hydrate
Type 3	• Quaternary ammonium salt + hydrogen bond donor
Type 4	• Metal chloride(hydrate)+ hydrogen bond donor

There are now over 300 publications on DESs and some of the applications have recently been reviewed.^{107, 108}

1.9 Type 4 deep eutectic solvents

The majority of ionic liquids are based on quaternary ammonium or phosphonium cations (type 1, 2 and 3),¹⁰⁹ however the Abbott group showed that it is likely to make ionic liquids without the use of quaternary or phosphonium salts. They showed that eutectics can be formed between metal salts and simple organic alcohols or amides, these have both metal-containing anions and cations and the physical properties are reliable with other ionic liquids.¹¹⁰ These form ionic liquids through the disproportionation of ZnCl_2 to form ZnCl^+ and ZnCl_3^- although they possess somewhat low conductivities.

Inorganic cations usually do not form eutectics with low melting point as a result of their high charge density, nevertheless, previous investigations have shown that mixtures of metal halides with urea can form eutectics with melting points of less than 150 °C.^{111, 112} The Abbott group have built upon this effort and presented that a range of transition metals can be combined into ambient temperature eutectics. It would be predicted that these metal salts would not usually ionise in non-aqueous media, but ZnCl_2 has been shown to form eutectics with urea, acetamide, ethylene glycol and 1,6-hexanediol.¹¹⁰

In another attempt, Abbott *et al.* shows that AlCl_3 can also undergo disproportionation by forming a complex with acetamide or urea and the complex is liquid at ambient temperature with a 3 to 4 fold higher conductivity than the corresponding zinc chloride

eutectics.¹¹³ The AlCl_3 based liquids only form with a narrow range of amides and only over a comparatively small compositional choice.

These so called Type 4 eutectics are useful as they produce cationic metal complexes, ensuring that the double layer close to the electrode surface has a high metal ion concentration. An analogous approach was used by Binnemans, who complexed $\text{Cu}((\text{CF}_3\text{SO}_2)_2\text{N})_2$ with acetonitrile, to form the complex cation $[\text{Cu}(\text{CH}_3\text{CN})_4]^{2+}$.¹¹⁴

1.10 Chromium plating in deep eutectic solvents

Due to health, safety and environmental stresses, a search for replacements to hexavalent hard chrome plating has been in progress for many years. The deposition of chromium from aqueous electrolytes suffers from low current efficiency and the use of toxic CrO_3 . An alternative to metal electrodeposition from aqueous solutions is through the use of ionic liquids. The electroreduction of most metals has been studied using a range of ionic liquids and novel deposit architectures have been demonstrated.⁸³ So far, the main focus of the current research has been on metals and semiconductors which cannot be electrodeposited from water, e.g. aluminium,¹¹⁵ silicon,¹¹⁶ and very few studies have been carried out on other important metals, such as chromium.³⁷ However, the difference in the electrochemical behaviour of metals in ionic liquids compared to traditional aqueous electrolytes presents the prospect of using new, and potentially less toxic, precursors for electrodeposition, e.g. replacing hexavalent chromium with $\text{CrCl}_3 \cdot 6\text{H}_2\text{O}$.¹¹⁷⁻¹¹⁹

Chromium deposition has been demonstrated from a Type 2 DES system, composed of ChCl and $\text{CrCl}_3 \cdot 6\text{H}_2\text{O}$ in a 1:2 molar ratio.^{15, 120} Amorphous crack-free chromium deposits were obtained, although they were relatively soft and could easily be removed during wear testing. On the other hand, the black coatings produced from the type 2 system had a similar appearance to 'Black Chrome' coatings produced from sulphate free hexavalent aqueous solutions. Furthermore, the coating thicknesses were greater than those obtained from aqueous baths. These are extremely encouraging because they give confidence that the ILs are promising candidates for commercial application in chromium plating.

Choline chloride forms eutectic mixtures with $\text{CrCl}_3 \cdot 6\text{H}_2\text{O}$, $\text{CoCl}_2 \cdot 6\text{H}_2\text{O}$, and $\text{Zn}(\text{NO}_3)_2 \cdot 4\text{H}_2\text{O}$ and these liquids are relatively highly conducting. Researchers have

shown that chromium can be effectively deposited from these liquids. The high ionic strength prevents the hydrated water molecules acting as bulk water as they are powerfully coordinated to the ions and therefore they are not easily reduced at the electrode surface. As a result the deposition of metals such as chromium can be accomplished with high current efficiencies. The Abbott group showed that the addition of up to 10 wt % LiCl, may possibly produce the deposition of black chromium which is amorphous in morphology hence free from surface cracks.¹²⁰ The progression has been operated at pilot plant scale even though no studies about the development have been given in the open literature.

1.11 Hardness

Hardness is defined as a property of something that is not easily penetrated, spread, or scratched. This behaviour relates to; elastic rigidity, plastic distortion, and cracking. For many materials, the mechanisms of these are widely related because they all include the strength of chemical bonding (cohesion). Therefore discussion of the mechanism for one case may provide some understanding of all three.

Various semi-empirical models that characterize experimentally observed phenomena at standards of indentation strain at or near a circumstance of full plasticity have been assumed significant attention in the literature.¹²¹⁻¹²⁵ These models in different ways depict the response of the specimen material in terms of slip lines, elastic displacements, and radial compressions. For sharp wedge or conical indenters, considerable upward flow is typically detected, and since elastic strains are thus insignificant related to plastic strains, the specimen can be stated as being rigid plastic.

Since hardness of the material is the resistance to penetration of the indenter. The indentation tests fall into three types of indentations:¹²⁶

- (i) Macro-indentations as determined by the Brinell (Meyer) and Rockwell indenters using a hard smooth ball.
- (ii) Micro-indentation as determined by the Knoop and Vickers indenters, for Knoop the indenter used is a rhombic-based pyramidal diamond and for Vickers a diamond indenter, in the form of a square-based pyramid with an angle of 136 between the opposite faces.

- (iii) Nano-indentation as determined by the Berkovich indenter, which is a diamond indenter that has a triangular pyramid with a true point since only three sides have to meet.

The hardness of a metal also relies on the grain size: The smaller the grain size, the higher the hardness values as the dislocations generated by the indenter are blocked by the grain boundaries. Therefore, high-strength metals are achieved by grain sizes in the nano-meter range. Additionally, grain size is the first, but not certainly most important reason. It has been shown that in polycrystalline samples grain size has a vital influence when it is of the same order as the indent diameter.

The important advantage of indentation techniques is that the size of the impression, made by applying a known load for a defined time, is calculated using a microscope fitted with a standardized eye piece. The hardness of electrodeposits is typically determined utilising a traditional micro-hardness method employing a Vickers or Knoop pyramid indenter instead of a macro technique. If the test is carried out on the surface of the deposit, the coating must be enough thick to avoid the ‘anvil’ effect; if not, the substrate effects the hardness value obtained for the coating.

The hardness and wear resistance of chromium deposits are, in general, very good and are relatively insensitive to the plating conditions. This is valid as long as a suitable thickness is applied for the intended use.¹²⁷

Chromium is the hardest of the most commonly deposited metals. Hard chrome is used as a wear resistant coating not only on steel but also on a wide variety of other metals. Hard chromium differs from decorative chromium not only because of its use but also because of the difference in deposit thickness. The thickness of the hard chrome plate is undoubtedly thicker than those used for decorative purposes. The thicknesses of hard chrome coatings are normally between 2.5 and 500 μm thick. The hardness of the crack-free plate is between 800 to 1200 HV (**Figure 1.6**). This absence of lustre and comparative softness of the crack-free chromium deposits can be suitable for certain applications due to the greater protection it gives to a substrate, which is not exposed through any discontinuities. Combination of non-metallic material results in harder deposits; the grain size is smaller and the tensile strength higher than in the absence of organic additives in the bath.¹²⁸

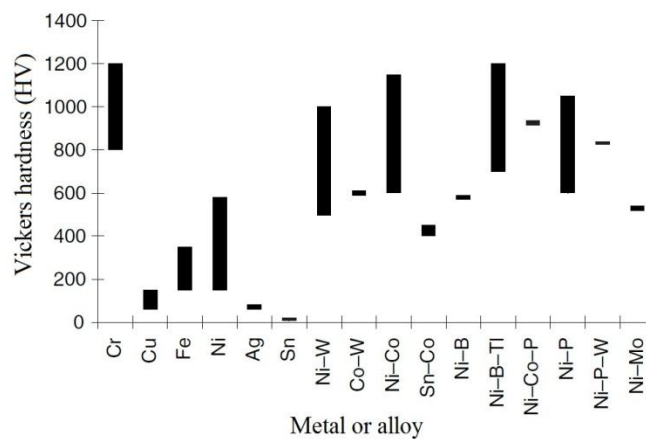


Figure 1.6: Vickers hardness for a selection of pure metals and metal alloy coatings.¹²⁹

Approximately the same values of hardness are obtained for hard chromium plating whether on the Brinell, Knoop, Vickers, or diamond pyramid scale¹³⁰, and it delivers excellent wear and corrosion resistance.¹³¹ The coating from the bath with an optimised additive content had high hardness due to its reduced grain size (11 ± 2 nm) and improved tribological properties due to the high proportion of crystals with a *hcp* structure. The coatings with the grain size in the range of 11-23 nm had varying surface morphologies and different porosities. A cluster-pore mixture model has been proposed by considering no contribution from pores to the hardness.

On the other hand, relatively soft deposits produced from hot solutions have often given especially good service, possibly owing to freedom from cracks or to greater strength and cohesion of this type of plate. Trivalent chromium deposits become harder when heated. Chrome carbides are thought to form by a reaction between the chromium and codeposited carbon.²

Hardness measurements are problematic to make since so many other factors are involved in service life. Unfortunately, hardness is not a straightforward property; it relies on other factors in a poorly understood way.²

In general, the hardness of bright hexavalent chromium deposits is given as about 900–1000 kgmm^{-2} .¹³² Approximately the same values are obtained whether on the Brinell, Knoop, Vickers, or diamond pyramid scale.¹³³ After heat treatment the hardness can reach 1500 Knoop or Vickers. It is recommended that the plate thickness should be at least 10 times the depth of penetration of the indenter.^{134, 135} Low loads often result in a considerable increase in the hardness number. Tests are sometimes made on the cross section of the deposit if it is thick enough and well supported.¹³⁶

1.12 Research aims

Environmental concerns dictate a need for the replacement of hazardous super acids with benign solutions for chromium plating. Legislation such as REACH (Registration, Evaluation, Authorisation and Restriction of Chemicals) is seeking to limit the use of chromic acid and the development of alternative technologies is urgently needed. The project aims to develop new eutectic mixtures based on a type 4 formulation whereby hydrated chromium salts are mixed with hydrogen bond donors to produce liquids with high chromium content but also with optimal conductivity and fluidity.

Three different formulations are studied. In each case urea is used as the HBD (although others are also demonstrated). The three chromium salts which have been used are; $\text{CrCl}_3 \cdot 6\text{H}_2\text{O}$, $[\text{Cr}(\text{en})_3]\text{Cl}_3 \cdot 3\text{H}_2\text{O}$ and $\text{KCr}(\text{SO}_4)_2 \cdot 12\text{H}_2\text{O}$. These three salts were chosen to demonstrate the role of speciation in controlling morphology. Clearly ethylene diamine (en) is a strong ligand, whereas sulphate is a weak ligand. The eutectics have very different physical and chemical properties and the aim of the project is to determine the effect of these on the deposit morphology.

For each eutectic the physical properties are determined such as phase behaviour, conductivity, viscosity and density as a function of composition. The speciation of chromium is demonstrated using both visible spectroscopy, FAB-MS and EXAFS. The electrochemical behaviour of the liquids is studied using a variety of voltammetric techniques and electrochemical quartz crystal microbalance. Chromium electrodeposits are characterised in terms of their hardness and morphology. In all cases the results are contrasted with those obtained using the Type 2 DES of $\text{CrCl}_3 \cdot 6\text{H}_2\text{O}$ and choline chloride. In the final results chapter the role of additives is described and it is shown that these liquids can be scaled up to produce thick, hard chromium on a large scale process.

1.13 References

1. M. Kulkarni, K. Elangovan and K. Reddy, *Bangladesh Journal of Scientific and Industrial Research*, 2013, **48**, 205-212.
2. M. Schlesinger and M. Paunovic, *Modern Electroplating*, John Wiley & Sons, 2010.
3. Z. Zeng and J. Zhang, *Journal of Physics D: Applied Physics*, 2008, **41**, 185303.
4. H. E. Boyer, T. L. Gall and A. S. f. Metals, *Metals Handbook: Desk Edition*, American Society for Metals, 1985.
5. A. Więckowski, *Interfacial electrochemistry : theory, experiment, and applications*, Marcel Dekker, New York, 1999.
6. A. P. Abbott and K. J. McKenzie, *Phys Chem Chem Phys*, 2006, **8**, 4265-4279.
7. R. D. Rogers and K. R. Seddon, *Ionic Liquids As Green Solvents: Progress and Prospects*, American Chemical Society, 2003.
8. F. A. Lowenheim, *Modern electroplating*, Electrochemical Society, Wiley, 1974.
9. K. Legg, M. Graham, P. Chang, F. Rastagar, A. Gonzales and B. Sartwell, *Surface and Coatings Technology*, 1996, **81**, 99-105.
10. D. L. Snyder, *Metal Finishing*, 2000, **98**, 215-222.
11. J. Guertin, J. A. Jacobs and C. P. Avakian, *Chromium(VI) Handbook*, Taylor & Francis, 2004.
12. N. V. Prasad, *Trace Elements as Contaminants and Nutrients: Consequences in Ecosystems and Human Health*, Wiley, 2008.
13. D. Smart, T. Such and S. Wake, *Trans. Inst. Met. Finish.*, 1983, **61**, 105-110.
14. G. Dubpernell, *Plat. Surf. Finish.*, 1984, **71**, 84-91.
15. A. P. Abbott, G. Capper, D. L. Davies and R. K. Rasheed, *Chemistry – A European Journal*, 2004, **10**, 3769-3774.
16. A. Baral and R. D. Engelken, *Environmental Science & Policy*, 2002, **5**, 121-133.
17. J. Gyllenspetz and S. Renton, UK Patent no. 1,455,841, 1976.
18. D. J. Barclay and W. M. Morgan, UK Patent no. 1,431,693, 1976.
19. N. Deeman, European Patent no. 58,044, 1982.
20. S. Nikolova, T. Dobrev and M. Monev, *Metal Finishing*, 1995, **93**, 12-18.
21. M. El-Sharif, S. Ma and C. Chisholm, *T I Met Finish*, 1995, **73**, 19-25.
22. P. Lansdell and J. Farr, *T I Met Finish*, 1997, **75**, 219-223.
23. A. Gardner, *Metal Finishing*, 2006, **104**, 41-45.
24. S. Ibrahim, A. Watson and D. Gawne, *T I Met Finish*, 1997, **75**, 181-188.
25. K. Geels, *Metallographic and Materialographic Specimen Preparation, Light Microscopy, Image Analysis, and Hardness Testing*, ASTM International, 2007.
26. I. Shuker and K. Newby, *Transactions of the IMF*, 2005, **83**, 272-274.
27. G. E. Shahin, US Patent no. 5294326 A, 1994.
28. D. R. Lide, *CRC Handbook of Chemistry and Physics, 84th Edition*, Taylor & Francis, 2003.
29. E. Peled and E. Gileadi, *J Electrochem Soc*, 1976, **123**, 15-19.
30. S. Simanavicius, *Chemija*, 1990, **3**, 178.
31. G. Geblewicz, R. Potter and D. SCHRIFFRIN, *T I Met Finish*, 1986, **64**, 134-136.
32. A. Abbott, A. Bettley, R. Potter and D. Schiffrin, *T I Met Finish*, 1988, **66**, 99-101.
33. A. Abbott, E. Long, A. Bettley and D. Schiffrin, *Journal of Electroanalytical Chemistry and Interfacial Electrochemistry*, 1989, **261**, 449-453.

34. A. Abbott, A. Bettley and D. J. Schiffrin, *Journal of Electroanalytical Chemistry*, 1993, **347**, 153-164.
35. A. Abbott, *Chemical Society Reviews*, 1993, **22**, 435-440.
36. K. Izutsu, *Electrochemistry in Nonaqueous Solutions*, Wiley, 2009.
37. F. Endres, D. MacFarlane and A. Abbott, *Electrodeposition from ionic liquids*, John Wiley & Sons, 2008.
38. A. P. Abbott, D. Boothby, G. Capper, D. L. Davies and R. K. Rasheed, *Journal of the American Chemical Society*, 2004, **126**, 9142-9147.
39. A. P. Abbott, R. C. Harris, K. S. Ryder, C. D'Agostino, L. F. Gladden and M. D. Mantle, *Green Chem*, 2011, **13**, 82-90.
40. J. Ranke, S. Stolte, R. Störmann, J. Arning and B. Jastorff, *Chemical Reviews*, 2007, **107**, 2183-2206.
41. J. S. Wilkes, *Green Chemistry*, 2002, **4**, 73-80.
42. S. Zhu, R. Chen, Y. Wu, Q. Chen, X. Zhang and Z. Yu, *Chemical and Biochemical Engineering Quarterly*, 2009, **23**, 207-211.
43. H. Niedermeyer, J. P. Hallett, I. J. Villar-Garcia, P. A. Hunt and T. Welton, *Chemical Society Reviews*, 2012, **41**, 7780-7802.
44. R. N. Das and K. Roy, *Molecular diversity*, 2013, **17**, 151-196.
45. Z. Du, Z. Li, S. Guo, J. Zhang, L. Zhu and Y. Deng, *The journal of physical chemistry. B*, 2005, **109**, 19542-19546.
46. M. J. Earle and K. R. Seddon, *Pure Appl Chem*, 2000, **72**, 1391-1398.
47. C. Reichardt, *Green Chem*, 2005, **7**, 339.
48. K. Xu, *Chemical Reviews*, 2004, **104**, 4303-4418.
49. P. Wasserscheid and T. Welton, *Ionic Liquids in Synthesis*, Wiley-VCH, 2008.
50. A. Mohammad, *Green Solvents II: Properties and Applications of Ionic Liquids*, Springer, 2012.
51. S. Sugden and H. Wilkins, *Journal of the Chemical Society (Resumed)*, 1929, 1291.
52. T. Welton, *Chemical Reviews*, 1999, **99**, 2071-2084.
53. J. D. Holbrey, W. M. Reichert, R. P. Swatloski, G. A. Broker, W. R. Pitner, K. R. Seddon and R. D. Rogers, *Green Chem*, 2002, **4**, 407-413.
54. K. R. Seddon, *J Chem Technol Biot*, 1997, **68**, 351-356.
55. 1943176, 1934.
56. F. H. Hurley and T. P. Wier, *J Electrochem Soc*, 1951, **98**, 207.
57. H. L. Chum, V. R. Koch, L. L. Miller and R. A. Osteryoung, *Journal of the American Chemical Society*, 1975, **97**, 3264-3265.
58. K. Grennan, A. J. Killard and M. R. Smyth, *Electroanal*, 2005, **17**, 1360-1369.
59. J. S. Wilkes, J. A. Levisky, R. A. Wilson and C. L. Hussey, *Inorg Chem*, 1982, **21**, 1263-1264.
60. S. Sowmiah, V. Srinivasadesikan, M. C. Tseng and Y. H. Chu, *Molecules*, 2009, **14**, 3780-3813.
61. N. V. Plechkova and K. R. Seddon, *Chemical Society Reviews*, 2008, **37**, 123-150.
62. F. Endres and S. Zein El Abedin, *Phys Chem Chem Phys*, 2006, **8**, 2101-2116.
63. J. S. Wilkes and M. J. Zaworotko, *J. Chem. Soc., Chem. Commun.*, 1992, 965-967.
64. M. J. Earle, P. B. McCormac and K. R. Seddon, *Green Chem*, 1999, **1**, 23-25.
65. A. P. Abbott, G. Capper, D. L. Davies, H. L. Munro, R. K. Rasheed and V. Tambyrajah, *Chemical Communications*, 2001, 2010-2011.
66. K. R. Seddon, *Nature materials*, 2003, **2**, 363-365.
67. J. S. Wilkes and M. J. Zaworotko, *J Chem Soc Chem Comm*, 1992, 965-967.

68. B. Clare, A. Sirwardana and D. R. Macfarlane, *Topics in current chemistry*, 2010, **290**, 1-40.
69. A. J. Dent, K. R. Seddon and T. Welton, *Journal of the Chemical Society, Chemical Communications*, 1990, 315.
70. D. Zhao, Y. Liao and Z. Zhang, *CLEAN – Soil, Air, Water*, 2007, **35**, 42-48.
71. Y. Chauvin, B. Gilbert and I. Guibard, *Journal of the Chemical Society, Chemical Communications*, 1990, 1715.
72. C. A. Angell, N. Byrne and J. P. Belieres, *Accounts of chemical research*, 2007, **40**, 1228-1236.
73. J. S. Wilkes and M. J. Zaworotko, *Journal of the Chemical Society, Chemical Communications*, 1992, 965.
74. H. G. Joglekar, I. Rahman and B. D. Kulkarni, *Chemical engineering & technology*, 2007, **30**, 819-828.
75. H. Zhao, *Chemical Engineering Communications*, 2006, **193**, 1660-1677.
76. S. Werner, M. Haumann and P. Wasserscheid, *Annual review of chemical and biomolecular engineering*, 2010, **1**, 203-230.
77. P. Sun and D. W. Armstrong, *Analytica Chimica Acta*, 2010, **661**, 1-16.
78. J. L. Anderson, D. W. Armstrong and G.-T. Wei, *Anal Chem*, 2006, **78**, 2892-2902.
79. M. D. Joshi and J. L. Anderson, *RSC Advances*, 2012, **2**, 5470-5484.
80. J.-f. Liu, G.-b. Jiang and J. Å. Jönsson, *TrAC Trends in Analytical Chemistry*, 2005, **24**, 20-27.
81. S. Zein El Abedin and F. Endres, *Chemphyschem*, 2006, **7**, 58-61.
82. A. P. Abbott and K. J. McKenzie, *Phys Chem Chem Phys*, 2006, **8**, 4265-4279.
83. A. P. Abbott, G. Frisch and K. S. Ryder, *Annu Rev Mater Res*, 2013, **43**, 335-358.
84. S. Zein El Abedin, P. Giridhar, P. Schwab and F. Endres, *Electrochemistry Communications*, 2010, **12**, 1084-1086.
85. Q. Zhang, Q. Wang, S. Zhang and X. Lu, *Journal of Solid State Electrochemistry*, 2014, **18**, 257-267.
86. A. P. Abbott, R. C. Harris, Y.-T. Hsieh, K. S. Ryder and I. W. Sun, *Phys Chem Chem Phys*, 2014, **16**, 14675-14681.
87. J.-M. Yang, S.-P. Gou and I.-W. Sun, *Chemical Communications*, 2010, **46**, 2686-2688.
88. M. Al Zoubi and F. Endres, *Electrochim Acta*, 2011, **56**, 5872-5876.
89. F. Endres, *ChemPhysChem*, 2002, **3**, 144-154.
90. F. Golgovici, A. Cojocar, M. Nedelcu and T. Visan, *Chalcogenide Letters*, 2009, **6**, 323-333.
91. *The Canning handbook: surface finishing technology*, W. Canning plc., 1982.
92. A. P. Abbott, *ChemPhysChem*, 2004, **5**, 1242-1246.
93. A. P. Abbott, *ChemPhysChem*, 2005, **6**, 2502-2505.
94. A. P. Abbott, G. Capper and S. Gray, *ChemPhysChem*, 2006, **7**, 803-806.
95. A. P. Abbott, A. A. Al-Barzinjy, P. D. Abbott, G. Frisch, R. C. Harris, J. Hartley and K. S. Ryder, *Phys Chem Chem Phys*, 2014, **16**, 9047-9055.
96. A. Abbott, G. Capper, B. Swain and D. Wheeler, *Transactions of the IMF*, 2005, **83**, 51-53.
97. A. P. Abbott, G. Capper, K. J. McKenzie, A. Glidle and K. S. Ryder, *Phys Chem Chem Phys*, 2006, **8**, 4214-4221.
98. A. P. Abbott, J. Griffith, S. Nandhra, C. O'Connor, S. Postlethwaite, K. S. Ryder and E. L. Smith, *Surface and Coatings Technology*, 2008, **202**, 2033-2039.

99. A. P. Abbott, S. Nandhra, S. Postlethwaite, E. L. Smith and K. S. Ryder, *Phys Chem Chem Phys*, 2007, **9**, 3735-3743.
100. D. Carriazo, M. C. Serrano, M. C. Gutierrez, M. L. Ferrer and F. Del Monte, *Chem Soc Rev*, 2012, **41**, 4996-5014.
101. A. P. Abbott, G. Capper, D. L. Davies, H. Munro, R. K. Rasheed and V. Tambyrajah, 2003, **856**, 439-452.
102. A. P. Abbott, K. J. McKenzie and K. S. Ryder, 2007, **975**, 186-197.
103. A. P. Abbott, D. Boothby, G. Capper, D. L. Davies and R. K. Rasheed, *J Am Chem Soc*, 2004, **126**, 9142-9147.
104. A. P. Abbott, G. Capper, D. L. Davies, K. J. McKenzie and S. U. Obi, *Journal of Chemical & Engineering Data*, 2006, **51**, 1280-1282.
105. D. F. Perepichka, M. R. Bryce, E. J. L. McInnes and J. P. Zhao, *Organic Letters*, 2001, **3**, 1431-1434.
106. F. van Rantwijk, F. Secundo and R. A. Sheldon, *Green Chem*, 2006, **8**, 282.
107. F. Pena-Pereira and J. Namieśnik, *ChemSusChem*, 2014.
108. A. Ispas and A. Bund, *Electrochemical Society Interface*, 2014, 47.
109. P. Wasserscheid and T. Welton, *Ionic liquids in synthesis*, Wiley Online Library, 2008.
110. A. P. Abbott, J. C. Barron, K. S. Ryder and D. Wilson, *Chemistry – A European Journal*, 2007, **13**, 6495-6501.
111. M. Gambino, P. Gaune, M. Nabavian, M. Gaune-Escard and J. Bros, *Thermochimica Acta*, 1987, **111**, 37-47.
112. M. Gambino and J. P. Bros, *Thermochimica Acta*, 1988, **127**, 223-236.
113. H. M. A. Abood, A. P. Abbott, A. D. Ballantyne and K. S. Ryder, *Chemical Communications*, 2011, **47**, 3523-3525.
114. N. R. Brooks, S. Schaltin, K. Van Hecke, L. Van Meervelt, K. Binnemans and J. Franssaer, *Chemistry-a European Journal*, 2011, **17**, 5054-5059.
115. Q. Liao, W. R. Pitner, G. Stewart, C. L. Hussey and G. R. Stafford, *J Electrochem Soc*, 1997, **144**, 936-943.
116. S. Zein El Abedin, N. Borissenko and F. Endres, *Electrochemistry communications*, 2004, **6**, 510-514.
117. S. Eugenio, C. M. Rangel, R. Vilar and S. Quaresma, *Electrochim Acta*, 2011, **56**, 10347-10352.
118. S. Eugenio, C. M. Rangel, R. Vilar and A. M. B. do Rego, *Thin Solid Films*, 2011, **519**, 1845-1850.
119. A. P. Abbott, G. Capper, D. L. Davies, R. K. Rasheed, J. Archer and C. John, *T I Met Finish*, 2004, **82**, 14-17.
120. A. P. Abbott, K. S. Ryder and U. König, *T I Met Finish*, 2008, **86**, 196-204.
121. M. Swain and J. Hagan, *Journal of Physics D: Applied Physics*, 1976, **9**, 2201.
122. D. Tabor, *The Hardness of Metals*. Oxford, Clarendon Press, 1951, 1970.
123. S. Chiang, D. Marshall and A. Evans, *Journal of Applied Physics*, 1982, **53**, 298-311.
124. T. Mulhearn, *Journal of the Mechanics and Physics of Solids*, 1959, **7**, 85-88.
125. K. Johnson, *Journal of the Mechanics and Physics of Solids*, 1970, **18**, 115-126.
126. M. Yovanovich, Micro and macro hardness measurements, correlations, and contact models, 2006.
127. B. Inwood and A. Garwood, *Tribology International*, 1978, **11**, 113-119.
128. J. K. Dennis and T. E. Such, *Nickel and Chromium Plating*, Woodhead Publishing, 1993.
129. B. G. Mellor, *Surface Coatings for Protection Against Wear*, Woodhead Publishing Limited, 2006.

130. P. Morriset, J. Oswald, C. Draper and R. Pinner, *Robert Draper, Teddington, Middlesex, UK*, 1954.
131. P. Andersson, J. Tamminen and C.-E. Sandström, *A literature survey. VTT Tiedotteita-Research Notes*, 2002, **2178**.
132. A. H. Guenther, *Optical Interferograms - Reduction and Interpretation*, American Society for Testing and Materials, 1978.
133. P. Morriset, J. Oswald, C. Draper, R. Pinner and R. Ehrhardt, *J Electrochem Soc*, 1955, **102**, 143C-144C.
134. W. D. Callister, *Materials Science and Engineering: An Introduction*, John Wiley & Sons, Incorporated, 2006.
135. C. Peters and F. Knoop, *Metals and Alloys*, 1940, **13**, 292.
136. C. A. Snavely and C. L. Faust, *J Electrochem Soc*, 1950, **97**, 99-108.

Chapter 2: Experimental procedures

2.1	Introduction	28
2.2	Materials	28
2.3	Preparation of solutions	28
2.4	Physical properties	29
	2.4.1 Viscosity measurements	29
	2.4.2 Conductivity measurements	29
	2.4.3 Surface tension measurements	29
	2.4.4 Density measurements	30
2.5	Thermal properties	30
2.6	Electrochemical measurements	31
	2.6.1 Cyclic voltammetry	31
	2.6.2 Potential step experiment	32
2.7	Electrochemical quartz crystal microbalance	32
2.8	Hull cell testing	33
2.9	Surface analysis	34
	2.9.1 SEM and EDX	34
	2.9.2 3D-microscope	34
	2.9.3 X-ray diffraction	35
	2.9.4 EXAFS	36
2.10	UV-Vis spectroscopy	38
2.11	Fast atom bombardment mass spectrometry (FAB MS)	40
2.12	Hardness test	41
2.13	References	42

2.1 Introduction

This chapter covers the standard experimental conditions and protocols used throughout this thesis. The theories underlying standard electrochemical techniques are not described in detail.

2.2 Materials

Table 2.1: List of compounds used in the project. All the chemicals were used as obtained.

Compound	Abbreviation	MW g/mol	Purity
Chromium(III)chloride hexahydrate	$\text{CrCl}_3 \cdot 6\text{H}_2\text{O}$	266.45	Aldrich, >98%
Choline chloride (ChCl)	$\text{HOC}_2\text{H}_4\text{N}(\text{CH}_3)^+\text{Cl}^-$	139.63	Aldrich, >98%
Urea	NH_2CONH_2	60.06	Aldrich, >99%
Ethylene glycol (EG)	$\text{C}_2\text{H}_4(\text{OH})_2$	62.07	Aldrich, >99%
Glycerol	$\text{C}_3\text{H}_8\text{O}_3$	92.09	Aldrich, >99%
Chromium(III) potassium sulphate dodecahydrate (Chrome alum)	$\text{KCr}(\text{SO}_4)_2 \cdot 12\text{H}_2\text{O}$	499.40	Aldrich, >98%
Methanol	CH_3OH	32.04	Aldrich, >99%
Ethylenediamine	$\text{C}_2\text{H}_4(\text{NH}_2)_2$	60.10	Aldrich, >99%
Boric acid	H_3BO_3	61.83	Aldrich, >99%
Sodium bromide	NaBr	102.89	Aldrich, >99%
Zinc	Zn	65.39	Aldrich, >99%
p-Benzoquinone	$\text{C}_6\text{H}_4\text{O}_2$	108.09	Aldrich, >98%

2.3 Preparation of solutions

The deep eutectic solvents used in this study were mixtures of hydrogen bond donors with a) $\text{CrCl}_3 \cdot 6\text{H}_2\text{O}$ b) $\text{KCr}(\text{SO}_4)_2 \cdot 12\text{H}_2\text{O}$ and c) $[\text{Cr}(\text{en})_3]\text{Cl}_3 \cdot 3\text{H}_2\text{O}$ system. These systems were compared with previously reported type 2 (ChCl/ $\text{CrCl}_3 \cdot 6\text{H}_2\text{O}$) system. The H-bond donors for the complex anions used in this study were: ethylene glycol (EG), glycerol and urea. The deep eutectic mixtures were formed by continuous stirring of the two components at 333 K until a homogeneous, liquids were formed. Boric acid, sodium bromide and benzoquinone were used as additive to study their effect on the

levelling and grain refined. The concentration of these additives used was between 0.01-0.5 mol·dm⁻³ in the solutions.

2.4 Physical properties

2.4.1 Viscosity measurements

Viscosity measurements of the compositions were obtained in the temperature range 293-343 K. A Brookfield DV-E Viscometer (Brookfield Instruments, USA) fitted with a temperature probe was used. The mixtures were first heated up to 343 K and then measurements of viscosity were taken from that temperature, all the way down to 293 K. It was maintained with an accuracy of temperature ± 274 K. An average of three readings of viscosity was used for the analysis.

2.4.2 Conductivity measurements

The conductivity of various compositions was measured in the temperature range 20-70 °C. Using a Jenway 4510 conductivity meter fitted with an inherent temperature probe (cell constant = 1.01 cm⁻¹). The mixtures were heated up to 343 K and measurements were taken from 293 K then on up to 343 K.

2.4.3 Surface tension measurements

Surface tension measurements of various compositions were obtained using a Krüss K9-tensiometer with a platinum plate, fitted with a thermostatted-water bath jacket to control the heating. A glass sample dish was used to hold the 40 mL sample volume used for each analysis. A rectangular platinum plate was used which was made to just touch the surface of the liquid, at this point the resulting readings were recorded. The measurements for this method were based on the geometry of a fully wetted plate in contact with, but not submerged in, the liquid phase. In this technique, the position of the platinum plate relative to the surface is important. Since the surface is brought into contact with the platinum plate, the equipment will respond to this action by the change in forces it experiences. Each composition was analysed in triplicate and the average value is reported. The temperature ranges used were 293-343 K. The plate was thoroughly washed with deionised water followed by heating to red hot in a Bunsen flame to ensure the removal of any adherent material and then cooled to room temperature.

2.4.4 Density Measurements

Density measurements were also obtained using a Krüss K9-tensiometer fitted with a thermostated jacket which was heated by a water bath. A platinum cylinder was fully submerged in the compositions for 1 minute so the equipment can reach equilibrium and the measurements were taken. Each measurement was repeated 3 times and the average value is reported. The temperature range used was 293-373 K.

2.5 Thermal properties

Differential Scanning Calorimetry (DSC) is a thermoanalytical technique wherein the difference in heat flow between a sample and reference material is measured as a function of time or temperature when they are subjected to the same heating rate in a controlled atmosphere.¹ It is used to investigate thermal transitions comprising energy or heat capacity changes, for instance melting, glass transitions, recrystallization, mesomorphic transition temperature, equivalent entropy and enthalpy changes, and exothermic decompositions of numerous materials with high sensitivity.² The technique was first developed by E.S. Watson and M.J. O'Neill in 1960.³ Numerous thermal transitions of materials can be perceived such as glass transition, melting, crystallization, oxidation and decomposition as shown in **Figure 2.1**.⁴

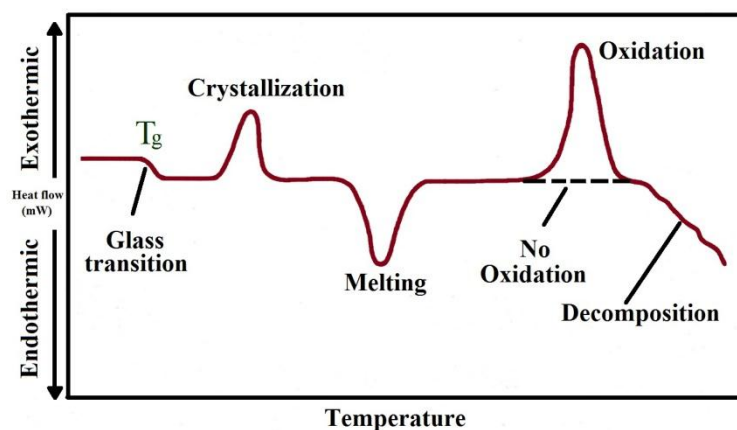


Figure 2.1: Typical DSC thermogram showing normally observed transitions⁴

Figure 2.1 shows a phase diagram typical eutectic character of the DES mixtures, having a eutectic point localized at a eutectic temperature. The glass transition can be found to be the midpoint of a heat capacity variation, while the melting and crystallization temperatures can be determined as the onset of the change. The key sources of uncertainty in the temperature measurements originate from instrument variation for a sample that has not been removed from the instrument and uncertainties resulting from inaccurate location of the sample in the furnace that produces somewhat

different thermal contact with instrument thermocouples. It should be also pointed out that the outcomes may depend slightly on the temperature scan rate. For instance, we have observed samples that solidify in the laboratory at room temperature only after several months. Therefore, we would not expect these transitions to be observed for the period of a DSC run that is achieved over a short period of time (e.g. one hour).

Freezing points were determined using a Mettler Toledo DSC1 differential scanning calorimeter (DSC). The mixtures were cooled to 77 K and heated up to 343 K at 283 K min^{-1} for two cycles. The thermogram exhibited a typical sharp exothermic peak corresponding to the melting point of the compositions. To avoid the variability in the temperature measurements, the freezing point determined by three replicate scans of the same sample.

2.6 Electrochemical measurements

All electrochemical processes e.g. cyclic voltammetry and chronoamperometry were carried out using an Autolab PGSTAT20 potentiostat (Ecochemie, Holland) which is controlled by GPES2 software. A 3-electrode system consisting of a working electrode (platinum/GC disc electrode; 1mm diameter), counter electrode (platinum flag; area 1cm^2) and pseudo-reference electrode (silver wire) was used for all experiments. The working electrode was first cleaned electrochemically and then mechanically polished with $0.3\ \mu\text{m}$ alumina paste followed by rinsing with deionised water and dried before every single measurement.

2.6.1 Cyclic voltammetry

In cyclic voltammetry (CV),⁵ the current response of a small stationary electrode in an unstirred solution is excited by a triangular voltage waveform, such as that shown in **Figure 2.2**. This excitation cycle is often repeated several times. The voltage excesses at which reversal takes place (in this case, E_i and E_λ) are called switching potentials. The current found rely on two procedures: mass transfer of electro-active material to the electrode surface and electron transfer process. The direction of the early scan may be either negative or positive, depending on the composition of the sample (a scan in the direction of more negative potentials is called a forward scan, and one in the opposite direction is termed a reverse scan). As electrolysis proceeds the reactant is exhausted near the electrode surface and diffusion becomes the principal means of moving reactant to the surface. The average distance reactant molecules must transfer to reach the electrode surface increases and therefore the rate of mass transfer decreases.

Ultimately, with the increasing rate of electron transfer, mass transport becomes rate determining and a current maximum is detected. Away from the peak, the current is time dependent and independent of potential. On the reverse scan, the product formed is reoxidised and the anodic peak is observed.

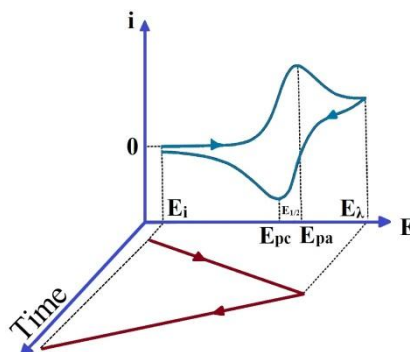


Figure 2.2: Cyclic voltammogram for reversible redox couple

All cyclic voltammograms were made at a scan rate of 20 mV s^{-1} . The peak analysis of the voltammograms was performed by using the GPES ver. 4.9.

2.6.2 Potential step experiment

The chronoamperometric data were obtained by stepping the potential of the platinum working electrode from a potential where no chromium reduction takes place to adequately negative values where the reduction process take place. The working electrode was mechanically polished with Buehler micropolish II (0.05 micron Deagglomerated gamma alumina) after each measurement.

2.7 Electrochemical quartz crystal microbalance (EQCM)

The crystal impedance spectra were recorded using a Hewlett Packard 87512A transmission/ reflectance unit via a 50Ω coaxial cable such that the centre of the recorded spectra was close to the resonant frequency, f_o , of the crystal (ca. 10 MHz). To recover the temporal resolution, network analyser data acquisition was controlled by a computer running HP VEE. This program was adept of recording admittance spectra every 2-3 sec.

In this study, 10MHz AT-cut polished (flat mirror) finish quartz crystal with a gold film thickness of 900 \AA , deposited in a keyhole shape on both sides with central disc active area of 0.211 cm^2 was used (International Crystal Manufacturing Co., Oklahoma City, USA.). The crystal was located into a tube such that one face of the crystal was exposed

to the solution and one face was exposed to air. The three electrode electrochemical cell was completed with a Pt mesh counter electrode.

Through this technique and using Sauerbrey equation (**Equation 2.1**):

$$\Delta f = -\frac{2f_o^2}{A\sqrt{\rho_q\mu_q}} \Delta m \quad \text{Equation 2.1}$$

where f_o is the resonant frequency in Hz, Δf is the frequency change in Hz, Δm is the mass change in grams, A is the surface area of the resonator, ρ_q is the density of quartz, and μ_q is the shear stiffness of quartz for an AT-cut crystal, the deposited mass of Cr^0 at the electrode was studied through the variation in resonant frequency (Δf) of the gold coated quartz crystal working as cathode and the response of the quartz crystal's resonance frequency from its base value (f_o) was observed as a function of time during potentiostatic deposition. A full resonance spectrum of the in situ mass loaded crystal at any point in time was picked up and the resonance curves were conventionally presented as admittance (reciprocal of impedance, Z / Ω), U/ Siemens and frequency plot.

The measured data were fitted to a Lorentzian equivalent circuit model, **Equation 2.2**, combining the in-phase impedance, inductance and centre frequency, with an iterative difference method. Using in-house written software in Microsoft Excel using the Visual Basic the data were fitted.

$$U(f) = a + \left(\frac{R}{R^2 + 16\pi^2 L^2 (f - f_o)^2} \right) \quad \text{Equation 2.2}$$

Where $U(f)/\Omega^{-1}$ is the measured admittance curve as a function of applied frequency f Hz (and $U(f) = 1/Z(f)$), R/Ω is the real component of the impedance (Z), L/Henry is the inductance, f_o/Hz is the centre frequency and a/Ω^{-1} is the baseline offset. The latter was used during fitting to compensate for variations in the static calibration of the network analyser.

2.8 Hull cell test

The Hull cell is a plating test cell that was designed to allow a quick analysis of the plating and to allow the effect of additions to the bath to be simply scaled up to an industrial system.⁶ An example is shown in **Figure 2.3**. The Hull cell is a trapezoidal plating cell that uses a cathode placed diagonal to the anode to cause a variation of current density across the cathode surface. The Hull cell allows a panel to be plated that shows qualitatively the effects of current density variations on the deposit properties

(generally deposit morphology or brightness). Small additions of additives can be made to the solution in the Hull cell, which in our case contains 33 mL volume of plating bath. Hull cell tests were done in a miniature plating cell. This specific cell set up (**Figure 2.3**) was used for studying the impact of additives on the deposit characteristics at various current densities. The cathodic plate (mild steel, copper, brass and nicked 50 mm × 42 mm × 1 mm) were mechanically polished and cleaned with acetone and rinsed with water. An iridium oxide-coated titanium mesh electrode, 40 mm × 50 mm, was used as an anode and degreased with acetone before being placed into the Hull cell. In all of the experiments the solution temperature was 313 K, with a constant cell voltage of 4 V. Experiments were carried out over a period of 2 hours, after which the substrates were removed from the Hull cell and washed with deionised water and acetone.

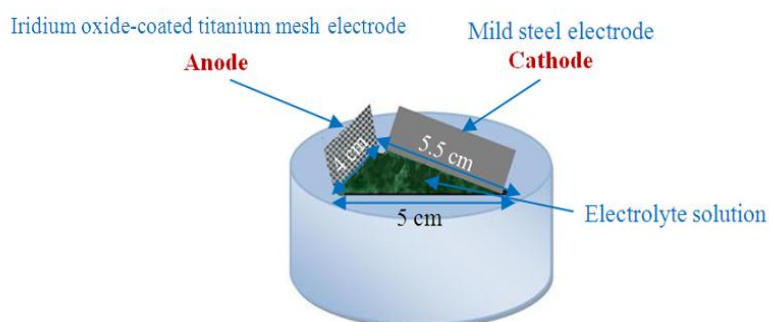


Figure 2.3: Schematic representation of the Hull cell

2.9 Surface analysis

2.9.1 SEM and EDX

The surface morphology and compositions have been characterised using scanning electron microscopy (SEM) and elemental analysis by energy dispersive X-ray Spectroscopy (EDX) using a Phillips XL30 ESEM instrument with an accelerating voltage between 15 and 20 keV, giving an average beam current of *ca.* 120 μ A.

2.9.2 3D-Microscope

3D optical images were captured on a Zeta Instruments Zeta-2000 optical profiler using the inbuilt Zeta3D software version 1.8.5. The Zeta-2000 Optical Microscope is a fully integrated microscope based system that provides 3D imaging and metrology capability in a small, robust and cost effective package. Based on branded technology, the Zeta-2000 enables imaging of surfaces with very low reflectivity and very high roughness.

The Zeta system scans a sample over a user specified vertical (or Z) range. At each Z location, it records the XY location and the accurate Z height of the pixels using the

Zeta Optics Module. This data is used to create a true colour 3D image and a 2D composite image. The resulting image has a protracted depth of focus so the whole surface is seen clearly. The Zeta 3D software can be used to determine dimensional and roughness information. An optional film thickness unit allows calculation of transparent layer thicknesses on the surface. To give a 3D image of the sample we need to regulate the objective lens to focus first on the lowest point of the sample and then on the highest one. The profilometer then scans the sample adjusting the focus from these two extreme points and gives a 3D sketch of the sample. The highest magnification possible with this instrument is 100x and it can measure the profile of a sample with an accuracy of at least 0.5 μm .

2.9.3 X-ray diffraction

William Bragg⁷ presented a simple clarification of the diffracted beams from a crystal. He expected that the X-ray wave incidents on parallel planes of atoms in the crystal are reflected, with each plane reflecting only a very small fraction of the radiation. The diffracted beams are formed when the reflections from parallel planes of atoms interfere constructively, as in the **Figure 2.4**. Bragg derived the **Equation 2.3**, now called the Bragg Law, which allows the determination of the interatomic spacing, d , of the atoms in the specimen or the wavelength, λ , of the X-rays (depending on what is known):

$$2d \sin\theta = n\lambda \qquad \text{Equation 2.3}$$

where θ is the angle of reflection at which constructive interference occurs and n is the order of diffraction ($n = 1, 2, 3, \dots$ corresponding to occasions when the path difference between the two reflected rays in the diagram is an integral number, n , of wavelengths, allowing constructive interference to occur).⁷

X-ray diffraction method provides qualitative and quantitative information about the compounds present in a solid sample. Powder X-ray diffraction was conducted using a Phillips model PW 1730 X-ray generator, with a PW 1716 diffractometer and PW 1050/25 detector. The X-ray tube was a long fine focus Cu anode with Ni $K\alpha$ filtered radiation. Typical operating settings were 40 KV, 30 mA scanned between 15 and 110° 2θ with a step size of 0.02° 2θ . Angle calibration was carried out using a synthetic Si sintered standard.

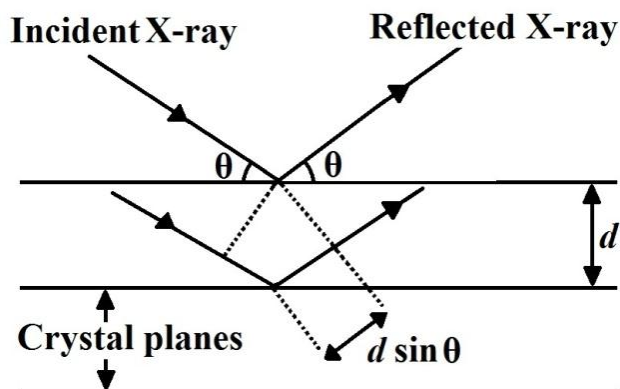


Figure 2.4: A schematic representation for derivation of the Bragg law

2.10 EXAFS

EXAFS (extended X-ray absorption fine structure) is a technique that involves firing monochromatic X-rays at a sample to excite an atom, at which point it will produce a photoelectron wave. From the oscillations in absorptivity after the absorption edge caused by interference between the emitted and backscattered wave, properties for instance atomic number, distance and coordination number of the atoms surrounding the central excited atom can be determined. As a broad tuneable source of X-rays is necessary, a synchrotron should be used to produce them.

The Cr-speciation in the liquid phase of these eutectics was determined by extended X-ray absorption fine structure (EXAFS) at the SpLine beamline (BM25A) of the ESRF synchrotron (Grenoble).

Measurements were carried out at the Cr K-edge, nominally 5989 eV, in transmission mode, using a Si(111) monochromator and ionisation chamber detectors. Liquid samples were sandwiched between two strips of polycarbonate, with plastic gaskets between 20 and 200 μm in thickness, such that an edge step between 0.5 and 1.5 was achieved (**Figure 2.5**). Solid reference samples for amplitude calibration were made of CrCl_3 and $\text{CrCl}_3 \cdot 6\text{H}_2\text{O}$ by grinding these salts with cellulose powder and pressing them into tablets.



Figure 2.5: *Experimental set-up at BM25A, including sample stage, sample holder and both detectors. The fluorescence detector is centre and back, with black ring around end. The transmission detector is at the far left.*

After processing the raw spectra in ATHENA, the EXCURV⁸ program was used to fit the data by calculating interatomic distances and their root mean square variation (σ^2). Electron scattering parameters were calculated and used to determine the type and number of coordinating atoms, using the Hedin-Lundqvist potential.⁹ Uncertainties in the fitted parameters, R(min), are quoted to two standard deviations. Two spectra were recorded for every sample, and then averaged, calibrated and background subtracted with the program Athena.¹⁰

EXCURV98 provides fitted values of interatomic distances (from the Cr atom) R , coordination numbers N , atomic type and the root mean square variation in interatomic distance σ^2 for the scattering atoms included in the fit. There is also an energy offset E_0 corresponding to the energy between the mean potential in the sample and the energy of the lowest unoccupied molecular orbital (E^0 is always negative as defined in the program). EXCURV98 also provides estimates of the uncertainty in these fitted parameters and an overall goodness of fit.

The amplitude correction factor (AFAC) is not the same for each metal and was determined from fitting known numbers of atoms, shells and distances from a crystal structure to an experimentally determined reference spectrum of either a metal foil or a solid metal salt sample.

To achieve the precise speciation for each of the solutions, several fitting parameters needed to be determined: atom type and number, their distance from the excited atom, the number of shells around the excited atom, Debye-Waller factor, and Fermi Energy.

The Debye-Waller factor is a degree of thermal vibration and static disorder in the system which can give an indication of the size and number of any close by atoms. A

larger Debye-Waller factor will shrink and broaden the Fourier transform of the EXAFS spectrum, showing more atomic wobbling. The signal will start large and quickly decay. In contrast, a small Debye-Waller factor will increase and narrow the EXAFS signal, representing less atomic wobbling. Each different type of atom will cause a certain phase shift. The Fermi energy displays where the defined zero energy state for the system is and modifies for this phase shift. There is also an energy offset E^0 (or E_{\min}) associated with the EXAFS spectra, consistent to the energy between the mean potential in the sample and the lowest vacant molecular orbital (LUMO). This is effectively the location of the edge with regard to the nominal value.

To confirm that the data fit was accurate, all sensible species were examined. The improper data fits could simply be recognized by unusually long or short M-X bond lengths associated to the solid crystal structure, unreasonably large coordination numbers, or a Debye-Waller factor that was significantly different for the atom being fitted.

2.11 UV-Vis spectroscopy

UV-Visible spectroscopy is very convenient as an analytical technique in chemical and biochemical research for two reasons: to classify some functional groups in the molecules and to measure concentration of a material in solution.¹¹ Furthermore, UV-Visible spectroscopy can be used as a complementary technique to EXAFS to measure the speciation of a metal salt in solution, along with the concentrations of these salts if two different species are seen to be present. UV-Vis spectroscopy is based on the absorption of light by the sample, such that electronic transitions will be produced. The energy that a molecule owns can be assigned definite energy levels, or states. In UV-Visible spectroscopy, a photon beam is passed through a sample, and absorption causes excitation of electrons in the discrete states of the molecules in the sample. These excitations can cause transitions between the energy levels (**Figure 2.6**).¹²

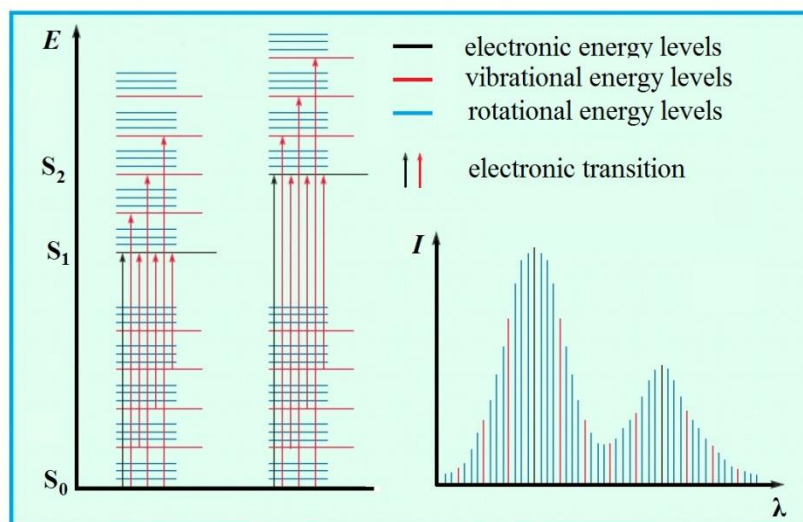


Figure 2.6: *Electronic transitions and the corresponding spectra*¹²

Figure 2.6 shows that the numerous absorption energies are related to different wavelengths that create a unique response for each sample. Each electronic transition has a regular energy requirement and will only absorb specific wavelengths of light. In this region, charge transfer bands (CT bands) and d-d transitions will be observed for metal complexes. The molar absorptivity of these absorptions can be calculated from the Beer-Lambert law:

$$A = \epsilon cl \quad \text{Equation 2.4}$$

where A is absorbance, ϵ is molar absorptivity ($\text{dm}^3 \text{mol}^{-1} \text{cm}^{-1}$), c is concentration ($\text{mol} \cdot \text{dm}^{-3}$) and l is path length (cm). There are two selection rules which must be taken into consideration for how strong these transitions will be. Firstly, there is the Laporte selection rule ($\Delta l = +/-1$), which states that if a molecule has an inversion centre of symmetry (i.e. octahedral compounds); electronic transitions within a given set of p- or d-orbitals are forbidden. The second is the spin selection rule ($\Delta S = 0$), where the electronic transitions are spin forbidden if the overall electron spin changes¹³. CT bands are predicted to be very strong ($\epsilon_{\text{max}} = 10^3 - 10^5$) as they are totally allowed. Any d-d transitions would be likely to be much weaker than the CT bands, as they tend to be forbidden by at least one of the two selection rules ($\epsilon_{\text{max}} = 1 - 10^3$ if partly allowed or $\epsilon_{\text{max}} = 10^{-3} - 1$ if entirely forbidden). The reason that entirely forbidden transitions can still be observed is that these rules can be relaxed in a number of ways, such as spin-orbit coupling (shows weak spin forbidden bands), vibronic coupling (an octahedral complex can have permissible vibrations where the molecule is temporarily asymmetric), or mixing of the d-orbitals with pi-acceptor and donor ligands.

When light either UV or visible is absorbed by molecules, the valence electrons are promoted from their normal state to a higher energy state. The colour of the sample affects the absorption of photons in the visible ranges, where molecules undergo electronic transitions. Only (π to π^*) and (n to π^*) transitions that occur in the UV-Vis region are observed. In UV/Visible Spectroscopy, the term chromophore is used to point out a group of atoms that absorbs radiation in the UV or visible region. They cause electronic transitions inside a molecule, supporting bonding and non-bonding electrons into higher and less stable antibonding orbitals¹⁴. In general, chromophores are conjugated species, such as alkenes, aromatics, conjugated dienes, trienes etc. The absorption of UV-visible light normally leads not to single, sharp lines as sometimes observed in IR absorption, but to broad bands. Due to the contribution of vibrational and rotational energy levels of these electronic transitions, broad spectra are obtained.

A Shimadzu Model UV-1601 Spectrophotometer was carried out to measure the solvatochromic shift of the different solution compositions in the visible absorbance spectrum. The program UV PROBE was used to obtain the values for λ_{\max} of the UV-Vis spectra of all composites. Neat samples of ionic liquids were analysed by smearing a thin film of the liquid in between two quartz plates. The reference cell was filled with air. The spectrums of the solvatochromic probe in the systems were measured at a resolution of 0.05 nm per data point. Therefore, the estimated uncertainty in the wavelength maximum is less than 0.5 nm. The cells were synthetic quartz glass with a path length of 10 mm and the baseline was obtained with the empty cells in place. Measurements were taken between 1100 and 220 nm at 0.1 nm intervals. The metal salt solutions were originally made up to 0.1 mol dm⁻³ but were diluted as necessary, down to a minimum of 0.1 mmol dm⁻³, to confirm a clear signal of the absorption peaks. Spectra were measured from 1100 nm to 220 nm, at ambient temperature.

2.12 Fast atom bombardment mass spectrometry (FAB MS)

The FAB method involves, first and foremost, providing a mass spectrometer with an atom gun. A beam of fast atoms is produced by ionizing the atoms, accelerating them through a potential (typically 2-8 keV), and finally allowing the fast ions to be neutralized through resonant gas phase charge exchange.

FAB involves the bombarding of a sample in a liquid matrix, with a neutral beam of atoms having energies of 2-8 keV to obtain sputtered negative and positive ions. The ionization process and inlet techniques are combined. FAB can be considered an outgrowth of Secondary Ion Mass Spectrometry (SIMS) which uses 2-8 keV ions

without a matrix liquid. In FAB, the sample is usually dissolved in a liquid matrix of low vapour pressure (glycerol is the most common and versatile). When this solution is exposed to the bombarding particles, the sputtered sites on the matrix surface are continually replenished with analyte by the process of diffusion.

FAB MS was carried out in order to understand the behaviour of the eutectics and to determine the metal species present in the system by using a Kratos Concept IIIH Mass spectrometer, using Xe gas at about 7-8 keV.

2.13 Hardness test

In Vickers hardness testing, the indenter is a regular four-sided diamond pyramid with an interfacial angle, α , of 136° . The hardness was evaluated as the resistance to indentation, in the form of force of indentation and depth of indentation, for chromium deposits on the mild steel by using a Mitutoyo model MVK-G100. The specimens were indented using different forces (0.01 to 1 kgF) and a loading rate of 0.1 mm/s for 10 s. The Vickers number is the number obtained by dividing the kg-force load by the square area of indentation. The depth of indentation was noted as the hardness.

The Vickers pyramid is pressed vertically into the specimen with a test force F (kgf) shown schematically in **Figure 2.7**. d_1 and d_2 are the diagonals of the impression (mm). The mean diagonal diameter d of the indentation is used to calculate the Vickers hardness.

$$HV = 1.8544 \frac{F}{d^2} \quad \text{Equation 2.5}$$

Where: HV is Vickers hardness, F is a test force in kgf and d is an arithmetical mean value of the measured indentation diagonals in mm

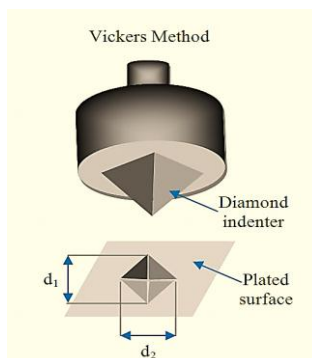


Figure 2.7: Schematic illustration of the Vickers hardness test

2.14 References

1. B. Wunderlich, *Journal of thermal analysis*, 1987, **32**, 1949-1955.
2. C. Schick, *Analytical and bioanalytical chemistry*, 2009, **395**, 1589-1611.
3. E. S. Watson, Google Patents, 1966.
4. D. A. Skoog, F. J. Holler and S. R. Crouch, *Principles of Instrumental Analysis*, Thomson Brooks/Cole, 2007.
5. J. J. Van Benschoten, J. Y. Lewis, W. R. Heineman, D. A. Roston and P. T. Kissinger, *Journal of Chemical Education*, 1983, **60**, 772.
6. T. McColm and J. Evans, *J Appl Electrochem*, 2001, **31**, 411-419.
7. W. L. Bragg, *Proceedings of the Royal Society of London. Series A*, 1913, **89**, 248-277.
8. J. Kotaś and Z. Stasicka, *Environmental pollution*, 2000, **107**, 263-283.
9. C. Hardacre, *Annu. Rev. Mater. Res.*, 2005, **35**, 29-49.
10. A. Ravel and M. Newville, *Journal of synchrotron radiation*, 2005, **12**, 537-541.
11. D. Pavia, G. Lampman, G. Kriz and J. Vyvyan, *Introduction to Spectroscopy*, Cengage Learning, 2008.
12. T. Owen, *Fundamentals of Modern UV-visible Spectroscopy: Primer*, Agilent Technologies, 2000.
13. C. E. Housecroft and A. G. Sharpe, *Inorganic Chemistry*, Pearson Prentice Hall, 2005.
14. H. H. Perkampus, *UV-VIS spectroscopy and its applications*, Springer-Verlag, 1992.

Chapter 3: Chromium chloride based deep eutectic solvents

3.1	Introduction	44
3.2	Eutectic mixtures based on urea and $\text{CrCl}_3 \cdot 6\text{H}_2\text{O}$	45
3.3	Physical properties	46
	3.3.1 Phase behaviour	46
	3.3.2 Viscosity	47
	3.3.3 Conductivity	50
	3.3.4 Molar conductivity	52
3.4	Solution speciation	54
	3.4.1 Mass spectrometry	54
	3.4.2 UV-visible spectrum	54
	3.4.3 Speciation and extended X-ray absorption fine structure (EXAFS)	55
	3.4.3.1 Theory of EXAFS	56
	3.4.3.2 Generation of X-rays	57
	3.4.3.3 Absorption coefficients	58
	3.4.3.4 Absorption edges	59
	3.4.3.5 Origin of the EXAFS signal	61
	3.4.3.6 Generation of EXAFS spectra	62
	3.4.3.7 Speciation of metal salts in DESs	63
	3.4.3.8 Chromium species in the novel DES	63
3.5	Density and surface tension	65
3.6	Hole theory	66
3.7	Cyclic voltammetry	69
3.8	Quartz crystal microbalance (QCM)	69
	3.8.1 Electrochemical quartz crystal microbalance (EQCM)	71
3.9	Bulk deposition	73
3.10	Hardness and thickness	75
3.11	Conclusions	76
3.12	References	77

3.1 Introduction

The electrodeposition of corrosion- and wear- resistant coatings is an extremely important manufacturing process, particularly in the automotive and aerospace sectors. The main metals of interest are chromium, cobalt and nickel and, although these coatings have been studied in detail, toxicological issues remain about the precursor solutions from which the metals are deposited. One of the most important of these is the electrodeposition of chromium, which has classically been achieved using aqueous chromic acid ($\text{H}_2\text{SO}_4 + \text{CrO}_3$).¹ Chromic acid is extremely hazardous because it is carcinogenic.² However, there are also practical issues and these have been summarized by Smart *et al.*³

An alternative to metal electrodeposition from aqueous solutions is through the use of ionic liquids. The electroreduction of most metals has been studied using a range of ionic liquids and novel deposit architectures have been demonstrated.⁴ So far, the main focus of the current research has been on metals and semiconductors which cannot be electrodeposited from water, *e.g.* aluminium⁵, silicon,⁶ and very few studies have been carried out on other important metals, such as chromium.⁷ However, the difference in the electrochemical behaviour of metals in ionic liquids compared to traditional aqueous electrolytes presents the prospect of using new and potentially less toxic precursors for electrodeposition, *e.g.* replacing hexavalent with trivalent chromium.⁸⁻¹⁰

In addition to ionic liquids with discrete anions, the electrodeposition of a range of metals has been previously carried out in Deep Eutectic Solvents (DESs).⁷ These comprise quaternary ammonium salts (*e.g.* choline chloride, ChCl), metal salts or metal salt hydrates and hydrogen bond donors (*e.g.* urea) and are commonly divided into four groups (**Table 1.1**), and have been particularly successful on a large scale for metal polishing^{11, 12} and immersion silver deposition.^{13, 14}

While most ionic liquids and DESs include a quaternary ammonium ion as the cationic component, it has recently been shown that eutectics can also be formed between a metal salt (hydrate) and a simple amide or alcohol to form a metal-containing solution composed of cations and anions *via* disproportionation processes¹⁵ *e.g.*



These so called Type 4 eutectics are useful as they produce cationic metal complexes, ensuring that the double layer close to the electrode surface has a high metal ion concentration. An analogous approach was used by Binnemans, who complexed $\text{Cu}((\text{CF}_3\text{SO}_2)_2\text{N})_2$ with acetonitrile, to form the complex cation $[\text{Cu}(\text{CH}_3\text{CN})_4]^{2+}$.¹⁶ In

previous research, chromium deposition has been demonstrated from a Type 2 DES system, composed of ChCl and $\text{CrCl}_3 \cdot 6\text{H}_2\text{O}$ in a 1:2 molar ratio.^{17, 18} Amorphous crack-free chromium deposits were obtained, although they were relatively soft and could easily be removed during wear testing.

In the current study we have taken mixtures of $\text{CrCl}_3 \cdot 6\text{H}_2\text{O}$, as a metal salt that is weakly ionic and/or that contains a multiply-charged metal ion, with urea, as a neutral organic molecule, (Type 4 DES) and compared them to the analogous mixtures of $\text{CrCl}_3 \cdot 6\text{H}_2\text{O}$ with ChCl (Type 2 DES). Physical properties, such as phase behaviour, viscosity, conductivity, density and surface tension have been determined. It has been identified through the use of extended X-ray absorption fine structure, EXAFS that cationic chromium complexes are formed in solution, whereas the Type 2 DES also forms anionic metal complexes. Finally, these properties will be applied to the electrodeposition behaviour of chromium, along with an examination of the hardness of these deposits.

3.2 Eutectic mixtures based on urea and $\text{CrCl}_3 \cdot 6\text{H}_2\text{O}$

The mixture was prepared by mixing the metal salt, $\text{CrCl}_3 \cdot 6\text{H}_2\text{O}$, with the complexing agent, urea as a hydrogen bond donor. In order to facilitate preparation of the mixture, the components may be heated together at elevated temperature, such as any temperature from 323 to 333 K (**Figure 3.1**). The molar ratio of $\text{CrCl}_3 \cdot 6\text{H}_2\text{O}$ to urea was studied in the range from 4:1 to 1:3. The eutectic mixture, i.e. the mixture with the lowest freezing point was found to occur at $2(\text{CrCl}_3 \cdot 6\text{H}_2\text{O})$ and urea.



Figure 3.1: The DES was formed by mixing the two solids together at 323K.

While urea and thiourea are recognized to interact with numerous metal cations in solution,^{19, 20} no eutectic mixtures of this type have been prepared.

3.3 Physical properties

3.3.1 Phase behaviour

Melting points (T_m) and glass-transition temperatures (T_g) of ILs, are frequently measured using differential scanning calorimetry (DSC). **Figure 3.2** shows the melting points of urea: $\text{CrCl}_3 \cdot 6\text{H}_2\text{O}$ mixtures as a function of composition and it can be seen that the eutectic is formed at a composition of 1:2 urea: $\text{CrCl}_3 \cdot 6\text{H}_2\text{O}$. The melting points of mixtures of urea and $\text{CrCl}_3 \cdot 6\text{H}_2\text{O}$ are always lower than either melting point of the pure components (urea: 407K (134 °C)); $\text{CrCl}_3 \cdot 6\text{H}_2\text{O}$: 356K (83 °C). The melting temperature of the eutectic composition is *ca.* 282 K (9 °C), producing a melting point depression of 364 K (91 °C), with respect to the weighted average of the pure components.

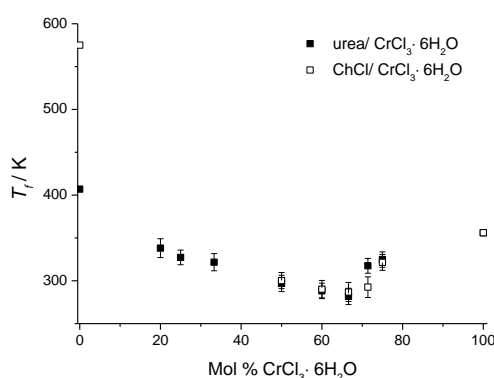


Figure 3.2: Melting points of urea: $\text{CrCl}_3 \cdot 6\text{H}_2\text{O}$ as a function of composition together with those for the ChCl: $\text{CrCl}_3 \cdot 6\text{H}_2\text{O}$ system for comparison.

Figure 3.2 also shows the analogous Type 2 DES, composed of choline chloride and $\text{CrCl}_3 \cdot 6\text{H}_2\text{O}$, and it should be noted that the melting points of the Type 4 DES are generally slightly lower although the trends are very similar.¹⁶ This is as expected, as the freezing point of a deep eutectic solvent is partially determined by the melting points of the pure constituent parts, T_f (*cf.* urea m.p. 407 K and ChCl m.p. 576 K).

Interestingly, the eutectic compositions for both Type 4 and Type 2 DES occurred at the same composition with a 0.67 mole fraction chromium salt. Analogous anhydrous eutectics formed from urea and ZnCl_2 were shown to have a eutectic composition at 0.22 mole fraction ZnCl_2 with a melting point of 282 K (9 °C) and a depression of melting point of 423 K (150 °C) with respect to the urea and ZnCl_2 .²¹ In the ZnCl_2 case the speciation is known to be $[\text{ZnCl}_2 \cdot 2\text{urea}]^+ [\text{ZnCl}_4]^-$ and the markedly different eutectic point suggests that disproportionation is not the mechanism by which these chromium DESs conduct charge.

In all cases, the original reduction in the melting points up to the eutectic compositions is caused not only by the interaction between the components, but also the formation of the complex ions that are the basis of the DES. At the eutectic composition, the species have the smallest degree of interaction between the cation and anion and thus the lowest melting point. DSC shows that all compositions lose water above 353 K (80 °C) and a visual change in colour from dark green to dark purple is observed. According to thermogravimetry studies on the Type 2 liquid, the system released 3 hydrate water molecules at about 358 K (85 °C), and another 3 at about 453 K (180 °C).⁶ This indicates a change in speciation and may be important for future applications. Around 323 K (50 °C) the liquids can be utilized in an open atmosphere without considerable change in the liquid composition because the water concentration in the liquid remains approximately unaltered.

It was believed in the beginning that these type 4 liquids are simply a mixture between type 1 and 3 but these eutectics only form for a limited number of metal salts and an even narrower range of donors. A number of other donors were also examined but it was found that only a limited number of amides were effective at forming room temperature liquids. Amongst these were glycerol and ethylene glycol and these are the examples that will not be described here. It was found that carboxylic acids do not form ambient temperature eutectic liquids with ZnCl_2 as they do with quaternary ammonium salts. This perhaps suggests that the complex is not formed through a hydrogen bond, but more probably through an oxygen bond between the donor and the metal centre.²¹

3.3.2 Viscosity

DESs are relatively viscous compared with molecular liquids.²² **Figure 3.3** shows the viscosity of urea: $\text{CrCl}_3 \cdot 6\text{H}_2\text{O}$ mixtures as a function of temperature and composition. Some samples were investigated in the super-cooled liquid state. A qualitative variation in the character of molecular motion occurs with this reducing of dynamics. Nearby the glass transition, dynamics in one region of a super-cooled liquid can be orders of magnitude faster than dynamics in another area only a few nano-meters away. This heterogeneity in dynamics has significant effects for understanding transport properties and the kinetics of chemical reactions in such materials.²³

For a wide range of DESs, viscosity decreases in an exponential manner with increasing temperature.²² However, this is not the case for the majority of the compositions described here and especially not for the mixtures with high chromium salt content, as shown in **Figure 3.3**.

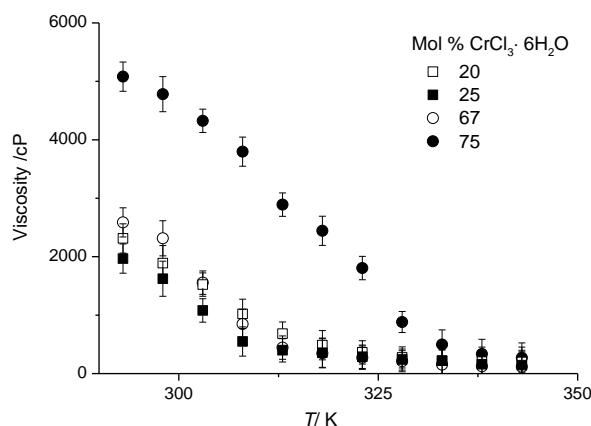


Figure 3.3: Viscosity of urea: $\text{CrCl}_3 \cdot 6\text{H}_2\text{O}$ as a function of temperature and composition.

The viscosity of the medium is reduced as the mole fraction of $\text{CrCl}_3 \cdot 6\text{H}_2\text{O}$ decreases. The minimum viscosity is not observed at the eutectic composition, which is what is observed for all other DESs systems studied to date.^{21, 24} It should however be noted that the viscosity of these Type 4 eutectics is significantly lower compared to Type 2 DESs, *e.g.* $\text{ChCl}:\text{CrCl}_3 \cdot 6\text{H}_2\text{O}$,¹⁸ and anhydrous Type 4 DESs, *e.g.* urea: ZnCl_2 , previously reported.²¹ At 20 °C the viscosity of the **ChCl**: $\text{CrCl}_3 \cdot 6\text{H}_2\text{O}$ system at the eutectic composition (1:2) is 4800 cP while the **urea**: $\text{CrCl}_3 \cdot 6\text{H}_2\text{O}$ is 2602 cP (1:2). This reduction in viscosity means improved mass transport and should cause an increase in electrical conductivity. The change in viscosity, η with temperature can be described by the following equation:

$$\ln \eta = \ln \eta_0 + \frac{E_\eta}{RT} \quad \text{Equation 3.2}$$

where η_0 is a constant and E_η is the energy for activation of viscous flow. Applying **Equation 3.2** to the data in **Figure 3.3** the E_η were calculated and are shown in **Table 3.1**. The obtained data compared with analogues type 4 and type 2 systems. Earlier studies have shown that the E_η values for ionic liquids are noticeably larger than traditional liquids and high temperature molten salts.²² This is caused by the large ion to hole radius ratio in ionic solvents. **Table 3.1** also shows that the donor has an important influence on the viscosity, for instance a conclusive difference can be seen between urea and acetamide, in the zinc systems, even though the two molecules are similar in size. The variation between the two liquids must originate from the ability of urea to form hydrogen bonds through its two NH_2 functionalities whereas acetamide only has one. It

has been shown empirically that E_η values are related to the melting point of liquids (T_m) by **Equation 3.3**.²⁵

$$E_\eta = 3.74 RT_m \quad \text{Equation 3.3}$$

This has been found to be accurate for a range of molecular liquids and high-temperature molten salts.²⁵ This would propose an E_η value of approximately 10 kJmol^{-1} for the urea/ $\text{CrCl}_3 \cdot 6\text{H}_2\text{O}$ mixtures, which is considerably smaller than that shown in **Table 3.1**. The values for the chromium containing liquid are, however, similar to other room-temperature ionic liquids. Branco *et al.*²⁶ described the viscosity of a variety of imidazolium salts and through these data the energy for activation of viscous flow was found to range from $37.2 \text{ (C}_4\text{mimBF}_4)$ to $59.7 \text{ kJmol}^{-1} \text{ ((C}_5\text{O}_2\text{mimCl})$.

Table 3.1: Activation energies for viscous flow (E_η) and conductivity (E_Λ) as a function of liquid composition. Coefficients of correlation (r) for the fits to **Equations 3.2** and **Equation 3.3** are also given.

	DESS	$E_\eta[\text{kJ}\cdot\text{mol}^{-1}]$	r	$E_\Lambda[\text{kJ}\cdot\text{mol}^{-1}]$	$-r$
Type 4	urea : $\text{CrCl}_3 \cdot 6\text{H}_2\text{O}$				
	1:3	53.4	0.973	18.2	0.990
	1:2	57.3	0.986	13.7	0.994
	3:1	45.2	0.991	18.3	0.995
	4:1	46.8	0.964	17.5	0.987
	urea : ZnCl_2 ²¹				
	3.5:1	135	0.991	77	0.992
	acetamide : ZnCl_2				
	4:1	62	0.998	28	0.998
Type 2	urea : AlCl_3 ¹⁵				
	1:1	38.2	0.996	21.2	0.993
	acetamide : AlCl_3 ¹⁵				
	1:1	25.6	0.993	23.4	0.986
	ChCl : $\text{CrCl}_3 \cdot 6\text{H}_2\text{O}$ ¹⁸				
1:1	58.5	0.997	43.7	0.999	
1:2	54.2	0.998	41.2	0.996	
1:2.5	52.4	0.996	40.6	0.992	
Type 2	ChCl : $\text{MgCl}_2 \cdot 6\text{H}_2\text{O}$ ²⁷				
	1:1	41.8	0.998	136.4	0.953
	1:2	44.2	0.973	132.3	0.935
	1:2.5	53.4	0.997	183.7	0.925

Abbott *et al.*¹⁸ showed that the empirical relationship observed in **Equation 3.3** for molecular liquids and high temperature molten salts, is not valid for ambient-temperature ionic liquids and may result from the large size of the solvent ions found in ionic liquids.

The eutectic mixture has a very high refractive index (1.581), which is larger than that of most molecular solvents and comparable to many of the imidazolium-based ionic liquids and high-temperature molten salts.²⁸⁻³⁰

3.3.3 Conductivity

Figure 3.4 shows the conductivity of the urea: $\text{CrCl}_3 \cdot 6\text{H}_2\text{O}$ system as a function of temperature and composition. Conductivity increases with temperature in an approximately linear fashion for all compositions, whilst in most other DESs the conductivity increases exponentially with temperature.²² Similarly to viscosity, conductivity does not change regularly as the mole fraction of $\text{CrCl}_3 \cdot 6\text{H}_2\text{O}$ increases. The highest conductivity is observed for the 4:1 urea: $\text{CrCl}_3 \cdot 6\text{H}_2\text{O}$ composition, which is also the least viscous. This indicates that ionic mobility rather than the concentration of charge carriers controls conductivity. This is common to other eutectic mixtures and ionic liquids and a strong indication for the applicability of hole-theory to describe transport properties.^{31, 32}

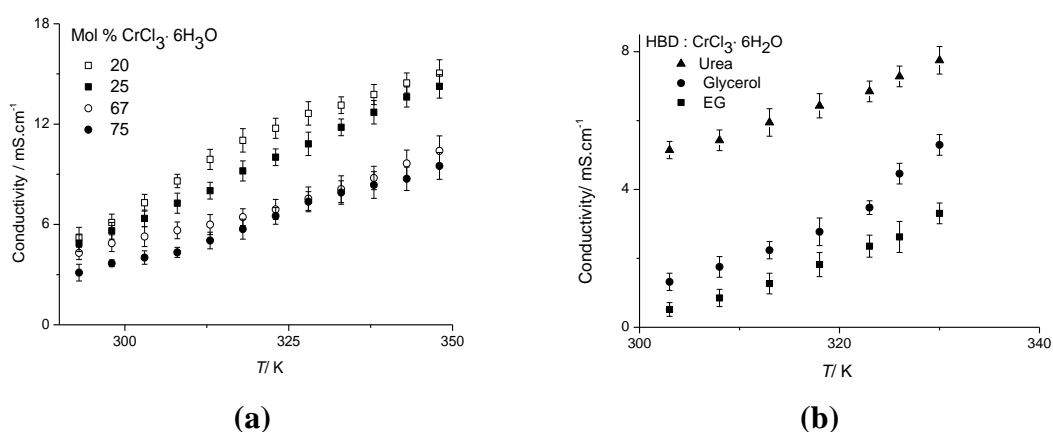


Figure 3.4: (a) Conductivity of urea/ $\text{CrCl}_3 \cdot 6\text{H}_2\text{O}$ as a function of temperature and composition, and (b) Conductivity of HBD/ $\text{CrCl}_3 \cdot 6\text{H}_2\text{O}$ (1:1) as a function of temperature.

Generally, the conductivities observed for the urea systems are much higher than any other DES previously reported. As it is shown in **Figure 3.5** at 313 K (40°C) for

example, conductivities of the urea: $\text{CrCl}_3 \cdot 6\text{H}_2\text{O}$ system are an order of magnitude larger (5 mS cm^{-1}) than those of the analogous $\text{ChCl} : \text{CrCl}_3 \cdot 6\text{H}_2\text{O}$ (0.5 mS cm^{-1}).¹⁸ This can be partly associated to the viscosity of the ionic liquids, but may also be due to the change in the type of charge carrier. These values are also comparable to some of the highest conductivities reported for room temperature ionic liquids with discrete anions.³³

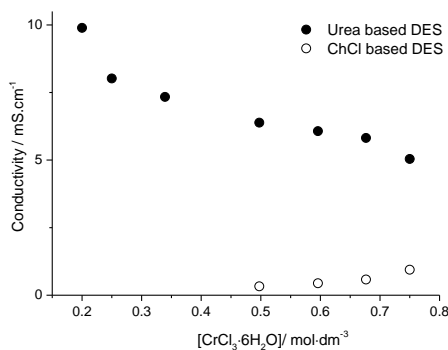


Figure 3.5: The conductivity of urea based DES and ChCl based DES as a function of $\text{CrCl}_3 \cdot 6\text{H}_2\text{O}$ concentration, at 313 K.

The current study focusses on urea as a hydrogen bond donor (HBD) although other HBDs also form eutectic mixtures with hydrated metal salts. **Figure 3.4b** compares the conductivity for different Type 4 DESs. Ethylene glycol and glycerol have been shown to form good hydrogen bond donors (HBDs) forming eutectic mixtures with choline chloride (Type 3 DES).³¹ In the Type 4 DESs with $\text{CrCl}_3 \cdot 6\text{H}_2\text{O}$, the urea system exhibits the highest conductivity. The converse is observed with the Type 3 DESs with choline chloride¹⁷ and it is recommended that this topic should be investigated in greater detail in the future.

An equivalent expression to **Equation 3.2** has been shown to valid for the variation of conductivity, σ , with temperature, namely:²⁵

$$\ln \sigma = \ln \sigma_0 + \frac{E_{\Lambda}}{RT} \quad \text{Equation 3.4}$$

The activation energy for conduction (E_{Λ}) is listed in **Table 3.1** as a function of composition. Similar to the E_{η} values, they are considerably larger than high-temperature molten salts (usually group I halides have values of 5 to 20 $\text{kJ} \cdot \text{mol}^{-1}$).²⁹

Comparing the data in **Table 3.1** for both of the activation energies for viscous flow (E_{η}) and conductivity (E_{Λ}) as a function of liquid composition it can be seen that the activation energies of conductivity for the novel type 4 system is much lower than the

activation energies for viscous flow which perhaps mean this system charge transfer dominant system.

For ionic fluids, the conductivity is normally controlled by the mobility of the charge carriers. Therefore a plot of conductivity versus fluidity must be linear for a certain charge carrier. Although the case of chromium chloride, is to some extent complex, because of the different ligand arrangements, that are conceivable.

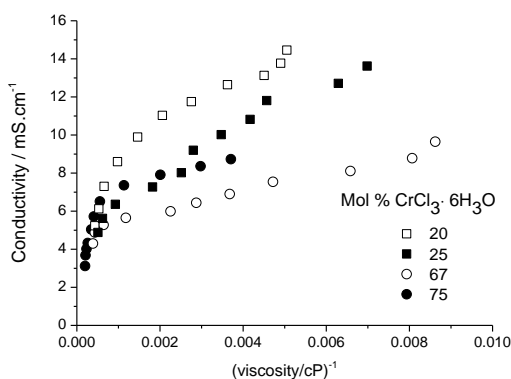


Figure 3.6: Conductivity as a function of $1/\text{viscosity}$ for the data in Figures 3.3 and 3.4a

Figure 3.6 shows a non-linear relationship between conductivity and the reciprocal of viscosity (i.e. fluidity). This trend will be discussed in more detail in the next chapter.

3.3.4 Molar conductivity

Recently, it has been stated that the Walden rule is approximately valid in ILs, and is a suitable extent for analysis of the ion pairing issue in electrolyte solution. If the viscosity and conductivity of the electrolyte follows Walden's rule, the ionic conductivity is linked to viscosity using the qualitative method of Angell.³⁴

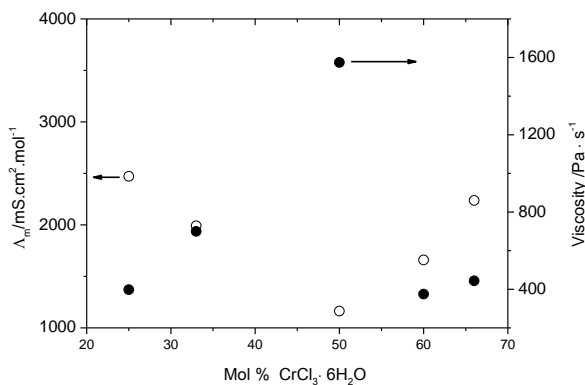


Figure 3.7: Molar conductivity and viscosity as a function of composition for the urea: $\text{CrCl}_3 \cdot 6\text{H}_2\text{O}$ system at 313 K.

In aqueous solutions molar conductivity is usually observed to decrease with increasing electrolyte concentration because of ionic atmosphere and ion pairing effects at low concentrations. As the concentration increases the molar conductivity increases again due to triple ion effects and at high electrolyte concentrations it decreases again due to increases in viscosity.²⁵

Figure 3.7 shows the molar conductivity and viscosity as a function of composition at 313 K. Although there are more charge carrying species as the $\text{CrCl}_3 \cdot 6\text{H}_2\text{O}$ content increases the viscosity of the system slows down the flow of ions through the system.

Numerous studies have found empirically that the molar conductivity of an ionic liquid is inversely proportional to the viscosity of the liquid and have erroneously invoked the Walden rule ($\Lambda_m^0 \eta^0 = \text{constant}$) as a method of describing an ionic liquid.^{35, 36} It has subsequently been shown that this arises from the low density of suitably sized holes in the liquid and since the size of suitable voids is at infinite dilution then the Nernst Einstein **Equation 3.5** is valid.^{32, 37}

$$\Lambda_m^0 = \frac{z^2 F e}{6\pi\eta} (R_+^{-1} + R_-^{-1}) \quad \text{Equation 3.5}$$

where z is the charge on the ion, F is the Faraday constant, e is the electronic charge, η is the viscosity of the liquid and R_+ and R_- are the radii of the cation and anion.

Figure 3.8 shows a plot of logarithmic molar conductivity, $\log(\Lambda_m)$, vs. fluidity, η^{-1} , these systems are non-linear as a function of temperature at each composition unlike most ionic systems. In most ionic liquids the ionic species and hence the charge carrying species remains constant with temperature. In the $\text{CrCl}_3 \cdot 6\text{H}_2\text{O}$: urea system the complex equilibria between the Cr centre and the three possible ligands suggest a variety of charge carrier sizes and charges could exist and this could explain the non-linearity of **Figure 3.8**.

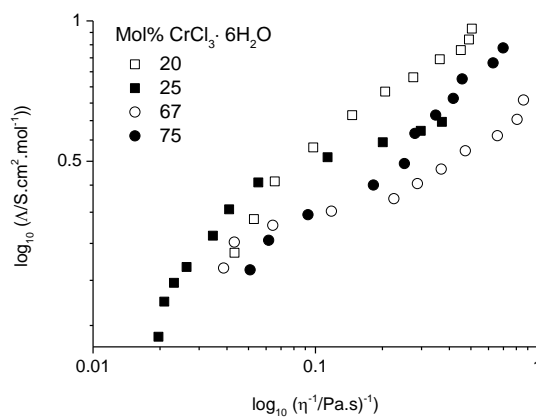


Figure 3.8: Molar conductivity as a function of fluidity for the urea:CrCl₃·6H₂O system.

3.4 Solution speciation

In order to understand the behaviour of the eutectic mixtures it is vital to have an understanding of the metal species present in the system. The liquids are highly conducting and, since chromium and chloride ions are the only charge carriers, the conducting species must originate from dissociation of CrCl₃·6H₂O.

3.4.1 Mass spectrometry

Generally, the physical properties of deep eutectic solvents are reliant upon both the ionic speciation and the inner interactions of the liquid components. Although, the speciation of metals dissolved in ionic liquids is reasonably understudied and this observation has been highlighted in a number of relevant reviews.^{7, 38}

In previous FAB-MS studies¹⁸ Type 2 DESs of ChCl:CrCl₃·6H₂O showed Ch⁺ cations and [Cr(H₂O)₂Cl₄]⁻.¹⁸ In FAB-MS with urea: CrCl₃·6H₂O no chromium-containing anions were detected, indicating that Cl⁻ may be the main anionic species. Analysis also showed several chromium containing cations including CrCl₂⁺. However, it must be acknowledged that mass spectrometry is an inherently destructive ex-situ technique, so that is not a reliable technique for determining *in-situ* speciation of weak transition metal chloro-aquo complexes.^{39, 40} It is therefore essential to use technique which is both *in-situ* and non-destructive.

3.4.2 UV-visible spectrum

To determine the speciation of metals in ionic liquids an extensive range of techniques have been formerly utilised, most of which have largely been focused on EXAFS,

Raman, FAB-MS and UV-visible spectroscopy.^{38, 41} UV-Vis spectroscopy is a frequently used method for qualitatively and quantitatively analysing solute speciation and composition.⁴²

Elving and Zemel showed that the number of chloride and water ligands bound to the metal affected the UV-visible spectrum of the chromium species.⁴³ They indicated two bands varying from 407 to 475 nm ($4T_{1g} \leftarrow 4A_{2g}$) for the first and from 575 to 665 nm ($4T_{2g} \leftarrow 4A_{2g}$) for the second band. For each band the lower end of the wavelength absorbance was assigned to the hexaqua complex and the upper end to the trichloro species. The addition of each chloride ligand moves the wavelength of each band by about 20 to 30 nm. In a neutral aqueous solution, the hexaqua species dominates but the trichloro species dominates in 12 M HCl. Generally, this UV-Vis spectroscopy has provided some useful insight. **Figure 3.9** shows the difference between the 1:2 urea: $\text{CrCl}_3 \cdot 6\text{H}_2\text{O}$ system and the 1:2 ChCl: $\text{CrCl}_3 \cdot 6\text{H}_2\text{O}$ mixture. While these spectra are indicative of more than one complex co-existing in solution, the maxima of the two bands are both shifted by about 25 nm suggesting that, on average, the 1:2 urea: $\text{CrCl}_3 \cdot 6\text{H}_2\text{O}$ system contains 1 less chloride than the 1:2 ChCl: $\text{CrCl}_3 \cdot 6\text{H}_2\text{O}$ mixture.

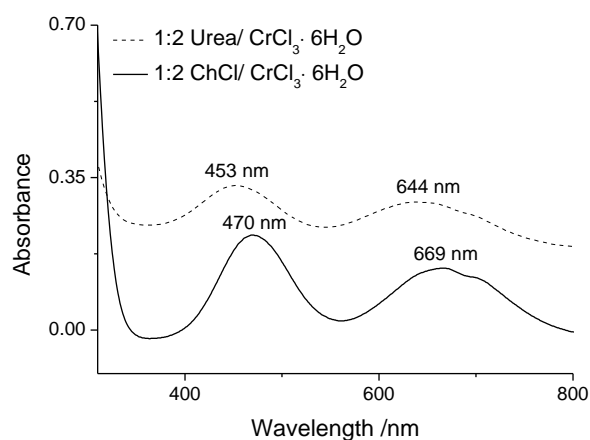


Figure 3.9: UV-Vis spectra of 1:2 urea: $\text{CrCl}_3 \cdot 6\text{H}_2\text{O}$ and 1:2 ChCl: $\text{CrCl}_3 \cdot 6\text{H}_2\text{O}$.

3.4.3 Speciation and extended X-ray absorption fine structure (EXAFS)

EXAFS indicates to the oscillatory structure in the x-ray absorption coefficient just above an x-ray absorption edge. This concludes to be an exclusive signature of a given material; it also relies on the comprehensive atomic structure and electronic and vibrational characteristics of the material. Therefore, EXAFS is a very good probe of materials providing information of local atomic structure, *viz.* types of atoms and their locations.⁴⁴ A limited number of groups have utilised EXAFS as a technique to

determine speciation in ionic liquids and this area of research has recently been studied by Hardacre *et al.*⁴¹

3.4.3.1 Theory of EXAFS

EXAFS spectroscopy measures the X-ray absorption as a function of energy and allows the local arranging of atoms to be explained. The absorption produces from the excitation of a core electron within an atom. Traditional EXAFS is typically linked with hard X rays, greater than 3–4 keV, and needs synchrotron radiation to supply the intensity at the energies used. At these energies, the core electrons expelled correspond to the 1s (K-edge), 2s (L_I-edge), 2p_{1/2} (L_{II}-edge), and 2p_{3/2} (L_{III}-edge) levels. Meanwhile the photon energy is increased past the absorption edge, an oscillatory structure is originated, which is characterized as the X-ray fine structure. The X-ray fine structure starts at around 30 eV past the edge and expands to a range of 1000 eV. The EXAFS is observed as a regulating change in the absorption coefficient affected by the expelled electron wave back scattering from the surrounding atoms. It is defined as:

$$\chi(k) = \frac{\mu(k) - \mu_0(k)}{\Delta\mu_0(k)} \quad \text{Equation 3.6}$$

where $\chi(k)$ is the EXAFS as a function of the wavenumber of the photoelectron, k ; $\mu(k)$ is the measured absorption above the absorption edge; $\mu_0(k)$ is the absorption spectrum without the EXAFS oscillations, *i.e.*, the background; and $\Delta\mu_0$ is a normalization factor. The wavenumber is defined at a photon energy, E , above the absorption edge energy, E_0 , with regard to the mass of the electron, m_e .

$$k = \sqrt{\frac{2m_e}{\hbar^2} (E - E_0)} \quad \text{Equation 3.7}$$

The EXAFS is related to the wavenumber by:

$$\chi(k) \approx \sum_i \frac{N_i f_i(k)}{k r_i^2} e^{-2\sigma_i^2 k^2} e^{-2r_i/\lambda} \sin[2kr_i + \alpha_i(k)] \quad \text{Equation 3.8}$$

where $\chi(k)$ is the summation over N_i back scattering atoms I ; f_i is the scattering amplitude term feature of the atom, $\exp(-2\sigma_i^2 k^2)$ is the Debye-Waller factor related to the vibration of the atoms; r_i is the distance from the absorbing atom, λ is the mean free path of the photoelectron, and α_i is the phase shift of the sphere-shaped wave as it

scatters from the back-scattering atoms. A real space radial distribution function of the back scattering atoms around the absorbing atom can be produced, by taking the Fourier transform of the amplitude of the fine structure, $\chi(k)$. Multiple scattering is vital in many systems, as discussed to in detail below.

On study of the EXAFS data, the local surroundings around a certain absorbing atom, can be found, *i.e.*, the type, number, and distance of the back scattering atoms. It should be recognised that it is not essential for the nearby atoms to be properly bonded to the absorbing atom. Normally, the distance has an uncertainty of $\pm 1\%$ in a radius of approximately 6 Å; nevertheless, the miscalculation in the coordination number is intensely reliant on the system studied and can be high. Calibration with standard materials and the use of EXAFS in combination with other techniques to confirm a realistic clarification of the data are vital.

Since the fine structure is linked with only the specific absorption edge being studied, and the energy of the absorption edge is reliant on the element and its oxidation state, the EXAFS observes the local structure around one particular element, and in some circumstances, an element in a given oxidation state. Hence by monitoring more than one absorbing element in the sample, a whole picture can be gained. EXAFS theory and application continue to development and grow, and a number of resources are accessible that provide thorough background, review, and discussion. Among them the reviews that offer the theory more evidently and reiterate much of the data on general liquid systems.^{45, 46}

Equation 3.8 only refers to the EXAFS for single scattering atoms and not for multiple scattering atoms. Single scattering is satisfactory for most of the samples used in this project although certain linear molecules, for instance SCN, can display strong multiple scattering effects. This is principally important when one atom lies directly behind the emitting atom and any contributions to the EXAFS from it are significantly affected by the forward scattered photoelectron waves.⁴⁷

3.4.3.2 Generation of X-rays

Synchrotrons create electromagnetic radiation by forcing charged particles, usually electrons, which are moving having a speed close to the speed of light to change direction inside a magnetic field. Obviously, the electrons are first produced by an electron gun and are then speeded up by a sequence of accelerators. As soon as the electrons have reached just below the speed of light, they are introduced to the storage

ring, where they will pass through sequences of bending magnets or wigglers, both to direct the electrons around the ring and to make the synchrotron radiation. As the electrons pass through each magnet, they lose energy in the form of light. As this emission spans a wide frequency range, it must then be passed through a monochromator to attain the specific X-ray wavelengths required, which are then concentrated onto the sample.

To be capable of measuring the intensity of the X-rays before and after they have acted together with the sample, a grouping of three ion chamber detectors filled with a specific gas mix is utilised. The first of these ion chamber detectors (I_0) measures the intensity of the X-rays before hitting the sample, the second measures the intensity after transmission or fluorescence (I_T or I_F) and the last chamber measures the intensity after the X-rays have passed within a reference foil for the specific element edge for the absorbing atom (I_R). This collection is shown in **Figure 3.10**.

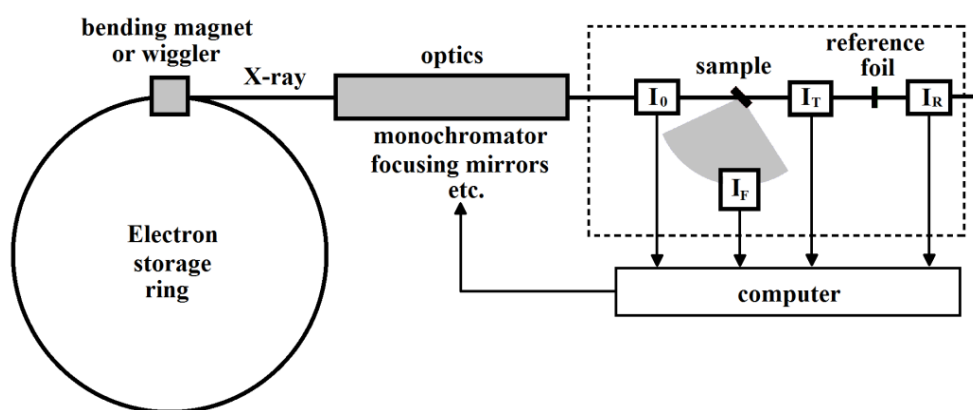


Figure 3.10: Schematic diagram of the synchrotron beam-line.

3.4.3.3 Absorption coefficients

When a collimated beam of monochromatic X-rays travels through matter, it unavoidably loses its intensity through interaction with the material. The loss in intensity (I) is proportional of the original intensity and the thickness x :

$$dI = -\mu I dx \quad \text{Equation 3.9}$$

with the proportionality constant μ being the linear absorption coefficient.

Integrating **Equation 3.9** gives rise to:

$$\frac{I}{I_0} = e^{-\mu x}$$

Equation 3.10

where I_0 and I are the incident and the transmitted X-ray intensities upon passage through a homogeneous sample of thickness x (**Figure 3.11**).

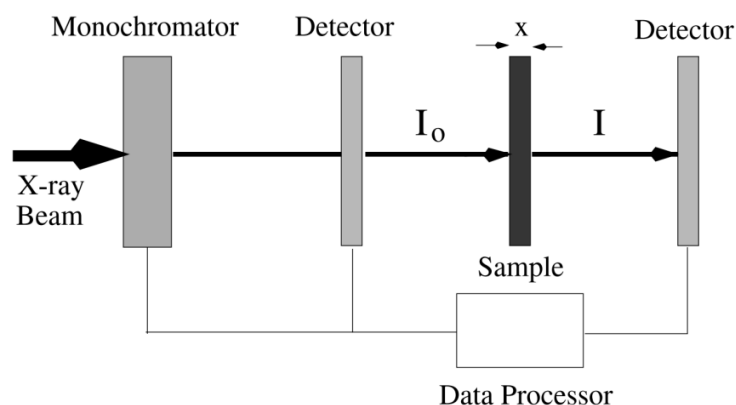


Figure 3.11: Representation view of the experimental arrangement of a typical EXAFS experiment.

Since the attenuation (or absorption) of intensity is determined by the quantity of matter crossed by the X-ray beam, the absorption coefficient is every so often stated as mass absorption coefficient, μ/ρ , calculated by dividing the linear absorption coefficient μ by the density ρ of the material. For μ in cm^{-1} and ρ in g/cm^3 , μ/ρ has a unit of cm^2/g . μ/ρ is approximately independent of the physical state of the material and is roughly additive:

$$\frac{\mu}{\rho} = \sum_i g_i \left(\frac{\mu}{\rho}\right)_i \quad \text{Equation 3.11}$$

where g_i is the mass fraction of the element i with mass absorption coefficient $(\mu/\rho)_i$. An additional frequently used unit is the atomic absorption coefficient μ_a which is defined as:

$$(\mu_a)_i = \left(\frac{\mu}{\rho}\right)_i \left(\frac{A_i}{N}\right) \quad \text{Equation 3.12}$$

where A_i is the atomic weight of the element i and N is Avogadro's number. μ_a has a unit of cm^2 . The absorption cross section of 10^{-24}cm^2 is sometimes referred to as 1 barn.

3.4.3.4 Absorption edges

As the wavelength λ of the X-rays is slowly decreased (or consistently as the energy of the photons is increased), the absorption coefficient μ commonly decreases up to a

definite critical wavelength is reached where the absorption coefficient increases sharply. This cut-off in the absorption coefficient relates to the expulsion of a core electron from an atom and is named the absorption edge. An additional decrease in λ causes an analogous decrease in μ , but at a slightly different rate, until another absorption edge is reached. As is clear from the previous section, there are one, three, five ... absorption edges for the $K, L, M \dots$ shells, respectively.

To produce the EXAFS spectra, hard X-rays of greater than 3-4 keV are applied and photon absorption within this range is determined by core electron excitations. When the energy of an X-ray photon resembles that of the binding energy of a core shell electron in a sample, a sharp rise in absorption coefficient, μ , happens as the electron is excited and ejected into the surroundings. This is recognized as the absorption edge. For single isolated atoms, the absorption falls monotonically as a function of energy after the edge. For molecules or reduced phases, any difference of the absorption coefficient at energies above the edge shows EXAFS. These spectra are typically observable at 40-1000 eV above the absorption edge and possess a tendency to possess amplitudes of a few tenths of the edge step magnitude.^{41, 44}

In X-ray absorption spectroscopy the absorption edges perceived has a typical energy which counterparts to the related atomic core orbitals. For example, excitation of the 1s orbital gives rise to the K-edge, the 2s, 2p_{1/2} and 2p_{3/2} related to the L_{I-III} edges respectively and the 3s, 3p_{1/2} and 3p_{3/2} orbitals to the M edges (**Figure 3.12**).

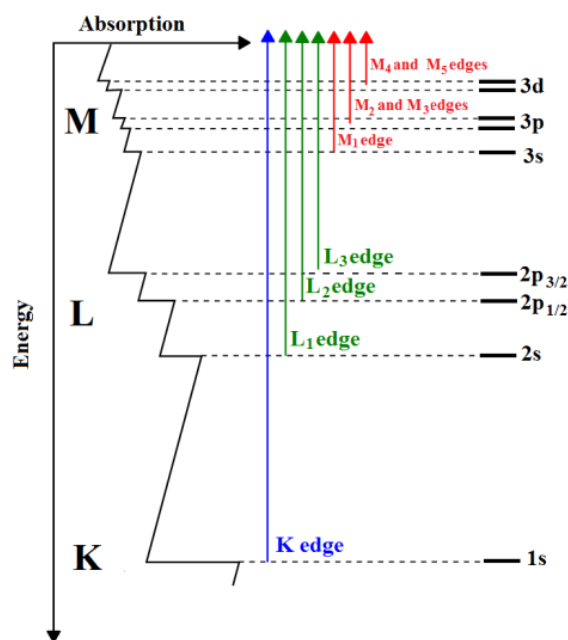


Figure 3.12: Schematic diagram presenting the core orbitals of a 3d-element atom and their corresponding X-ray absorption edges.

3.4.3.5 Origin of the EXAFS signal

An absorption edge on its own is of little value away from elemental identification.⁴⁸ On the other hand, if one observes any of the edges in **Figure 3.12** in more appropriate way, they may found to cover a wealth of information. This is demonstrated by the schematic absorption edge shown in **Figure 3.13**.

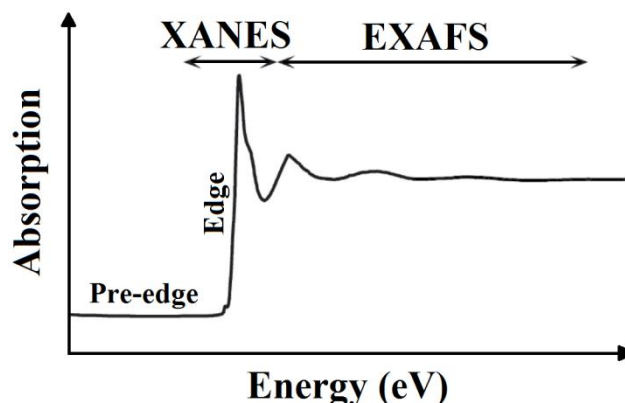


Figure 3.13: Schematic representation of an X-ray absorption spectrum, presenting the structured absorption that is seen both within ca. 50 eV of the edge (the XANES) and for several hundred to >1,000 eV above the edge (the EXAFS).

Different regions of the EXAFS spectrum can be understood for different sets of information and these regions are presented in **Figure 3.13**. From the energy of the edge data on the absorbing atom, for instance structure and oxidation state can be extracted. From the interloping after the edge, information about the local short-range environment around the absorbing atom can be determined, for instance the number of scattering neighbouring atoms, their characteristics and distances away from the absorbing atom.⁴⁹

The absorption edge is not simply a discontinuous increase in absorption, as proposed by **Figure 3.12**, but in fact displays structure both in the instant vicinity of the edge jump and well above the edge. The structure in the vicinity of the edge is every so often point out as X-ray absorption near-edge structure (XANES). XAS spectra are frequently divided into the X-ray absorption near edge structure (XANES) region, for absorption within 50 eV of the edge and the extended X-ray absorption fine structure (EXAFS) region, for absorption well above the edge. Reliant on the nature of the absorbing site, EXAFS structure can cover till 1000 eV or more above the edge. The XANES and EXAFS regions of an iron X-ray absorption spectrum are illustrated in **Figure 3.13**.^{50, 51} As a result, XANES provides a “fingerprint” of the structure such as oxidation state and

symmetry around the absorber atom, while the EXAFS region can uncover the kind and the structure, i.e. distances and coordination numbers, of nearest neighbour atoms by applying suitable fitting routines using the EXAFS theory. Since the EXAFS function is oscillatory, Fourier transforms of the EXAFS data are frequently helpful, resulting in a radial distribution function.

It must be understood that, during using EXAFS, the amplitude of the fine structure of μ vs. E is reliant on the type and bonding of neighbouring atoms, whereas the frequency is reliant on the distance away the neighbouring atom is from the absorbing atom, while these neighbouring atoms do not essentially need to be bonded to the absorbing atom. Errors in coordination number will be determined by the particular system and can be high depending on the structure of the coordinating ligands, for instance a linear molecule can cause multiple scattering in the EXAFS. If the sample contains multiple potential absorbers, accurate determination of the speciation can be obtained by studying all of these absorbing atoms.^{41, 45} To attain the best results, EXAFS should be utilised in combination with other speciation techniques to be certain of a realistic clarification of the structure of the species of interest.

3.4.3.6 Generation of EXAFS spectra

When an outgoing photoelectron wave has been produced by absorption of an X-ray and ejection of a core shell electron from the absorbing species, this photoelectron wave is then backscattered from any nearby atoms in the sample (**Figure 3.14**) and the meddling between these two waves creates a distinctive pattern which is recognized as the fine structure.

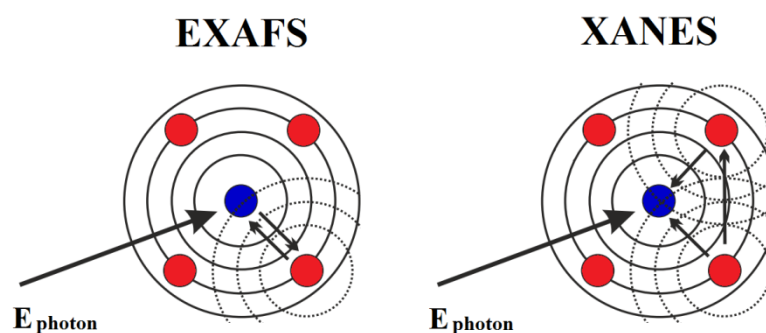


Figure 3.14: Schematic of electron scattering processes giving rise to EXAFS and XANES in x-ray absorption.

EXAFS probes the absorption continuum above the ionization edge. Oscillatory features, in this range, take place as a result of the interference of the outgoing and re-

scattered photoelectron waves. The EXAFS results from single re-scattering proceedings from the nearest neighbours due to the strong damping of the outgoing electron wave by inelastic scattering proceedings. This interference, specifically the EXAFS, can be defined as the fractional oscillation of the absorption coefficient above the edge with respect to the atomic background absorption. On the other hand, the XANES around the absorption edge denotes multiple scattering events of the photoelectron (**Figure 3.14**), in this way investigative both the atomic arrangement and the electronic structure of the environment.⁵² Additionally, Fourier transform of the fine structure produces a real space radial distribution function for the back scattering atoms around the central absorbing atom.

3.4.3.7 Speciation of metal salts in DESs

The speciation of metal salts in DESs has formerly been investigated by the Abbott group utilising fast atom bombardment-mass spectroscopy (FAB-MS)⁵³ and EXAFS.^{39, 54} Comparing the data collected with these methods for Zn^{2+} , it can simply be seen that there is a disparity between the proposed speciation. For example, FAB-MS proposes that complex anions are formed in Ethaline (ChCl: 2EG), such as $[\text{ZnCl}_3]^-$, $[\text{Zn}_2\text{Cl}_5]^-$ and $[\text{Zn}_3\text{Cl}_7]^-$,⁴⁰ whereas EXAFS points toward the existence of a single tetrachloro species, $[\text{ZnCl}_4]^{2-}$.³⁹

FAB-MS probably does not provide a comprehensive representation of the solution phase as a result of potential fragmentation of the metal chloro-complexes in the gas phase. By using EXAFS to study speciation as an alternative, an in situ study of the species of interest can therefore be made, without damaging the sample or breakdown of the solution species.

Generally, for the DESs used, it was found that the M^+ salts have a tendency to form $[\text{MCl}_2]^-$ complexes, whilst the M^{2+} salts tended to form $[\text{MCl}_4]^{2-}$ complexes, with a few unusual exceptions for the strong ligands.⁵⁵

3.4.3.8 Chromium species in the novel DES

EXAFS was recorded to elucidate the nature of the chromium species, in particular with respect to their overall charge. In most cases, the Fourier transforms (**Figure 3.15**) exhibit a double peak at *ca.* 2 Å, resulting from a mixed 1st coordination shell consisting of O and Cl donor ligands.

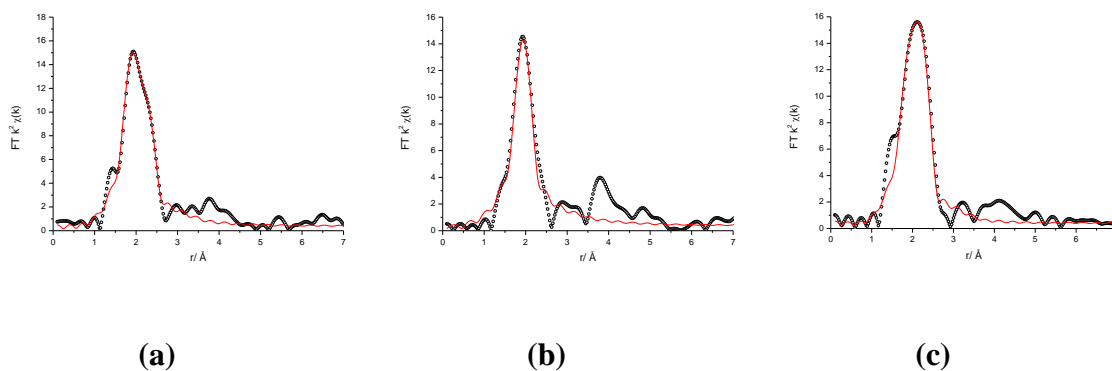


Figure 3.15: Fourier transforms of the EXAFS data (black circles) and fits (red line) for (a) 1:2 and (b) 4:1 urea: $\text{CrCl}_3 \cdot 6\text{H}_2\text{O}$ and (c) 1:2 $\text{ChCl}:\text{CrCl}_3 \cdot 6\text{H}_2\text{O}$

Only the spectrum of 4:1 urea: $\text{CrCl}_3 \cdot 6\text{H}_2\text{O}$ shows a single peak. This is confirmed by the least square fits (**Table 3.2**). In the samples with no more than 67% urea, Cr is coordinated by 4 oxygen donor ligands (urea or water, OD) and 2 chloride ions, hence resulting in the cationic species $[\text{CrCl}_2(\text{OD})_4]^+$. This is even maintained if a significant amount of water is added to the sample.

In all Fourier transforms there is a broad peak at *ca.* 4 Å, which indicates the presence of coordinating urea molecules. The peak is more pronounced in the samples with high urea content. However, it was not possible to include these in the fits and the urea: water ratio in the coordination shells remains unknown.

Table 3.2: EXAFS fit parameters of Cr DESs.

urea: $\text{CrCl}_3 \cdot 6\text{H}_2\text{O}$	coordinating atom	Number of atoms, N	distance from Cr $r / \text{Å}$	Debye-Waller factor $a / \text{Å}^2$	fit index, $R1$
4:1	O	4.5(5)	1.970(9)	0.005(3)	12.1%
2:1	O	4.8(6)	1.984(7)	0.007(3)	7.6%
1:1	Cl	1.5(8)	2.27(3)	0.020(15)	4.1%
	O	3.5(4)	1.96(1)	0.004(2)	
1:2	Cl	2.0(5)	2.26(1)	0.006(4)	4.3%
	O	3.8(4)	1.944(9)	0.004(2)	
1:2 (+ 20 % H_2O)	O	3.6(4)	1.95(1)	0.004(2)	4.8%
	Cl	1.8(6)	2.25(1)	0.007(5)	
$\text{ChCl}:\text{CrCl}_3 \cdot 6\text{H}_2\text{O}$	coordinating atom	Number of atoms, N	distance from Cr $r / \text{Å}$	Debye-Waller factor $a / \text{Å}^2$	fit index, $R1$
1:2	O	3.7(4)	1.97(1)	0.006(3)	5.5%
	Cl	2.4(5)	2.268(8)	0.006(4)	

In the Type 2 DES 1:2 ChCl: CrCl₃·6H₂O liquid, EXAFS shows that chromium ions are coordinated by 2.5 chloride ions on average. This is consistent with the higher chloride content of these mixtures compared to the Type 4 system. The presence of anionic species in FAB-MS suggests that the solution contains a mixture of anionic and cationic complexes, probably in a ratio of 3:1. The charge carriers in these solutions would hence be choline and [CrCl₂(H₂O)₄]⁺ as cations, and chloride and [CrCl₄(H₂O)₂]⁻ as anions.

3.5 Density and surface tension

Knowing the density and surface tension as a function of temperature and composition can provide information of structure. Methods for calculating saturated liquid densities as a function of temperature were reviewed and evaluated by Spencer and Danner.⁵⁶ Due to the close similarity of the physicochemical characteristics of DESs to ILs, prediction methods appropriate for ILs may be acceptable for DESs.

The variation of density and surface tension as a function of temperature and composition are shown in **Figure 3.16**. The densities for all compositions decrease with increasing temperature, as expected. Surprisingly the densities of the liquids are higher than those of the solid state components (density urea = 1.2 g·cm⁻³, CrCl₃·6H₂O = 1.76 g·cm⁻³). Motin studied the molar volume of concentrated salt/water/urea systems and found that urea was strongly structure forming.⁵⁷ Extrapolating Motin's data suggests that a water free system would also have a density higher than the components. The observation that the density of the liquid is higher than the solid components indicates that hydrogen bonding is different in the solid and liquid forms, similar to the case with ice. This is supported by the observation that the liquid freezes from the top of the container, *i.e.* the solid floats on top of the liquid.

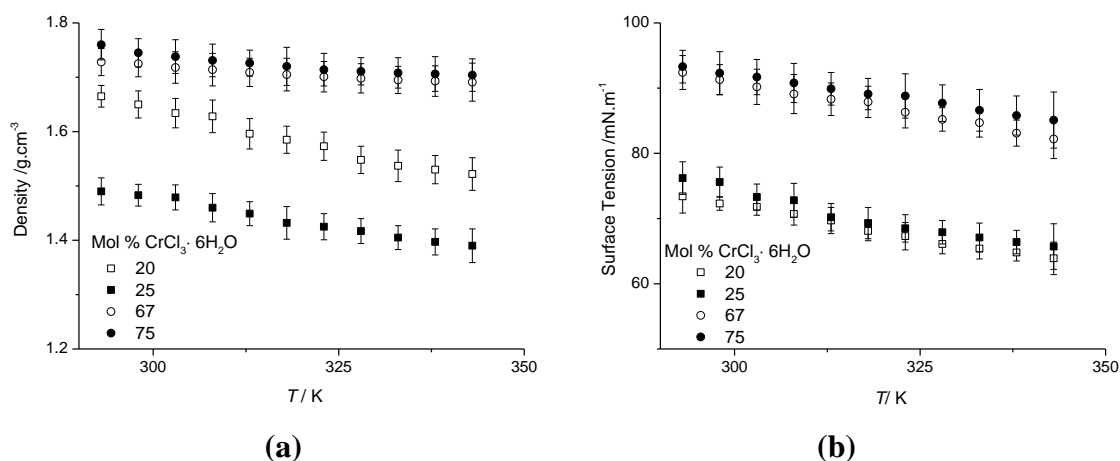


Figure 3.16: (a) Density and (b) surface tension of the urea: $\text{CrCl}_3 \cdot 6\text{H}_2\text{O}$ system as a function of temperature and composition.

Figure 3.16b shows the surface tension as a function of temperature and composition. The values of the surface tension range from 63.9 to 93.34 mN m^{-1} . These are higher than those of typical high temperature molten salts, (*e.g.* $\text{KBr} = 77.3 \text{ mN m}^{-1}$ at 1173 K vs. $\text{ChCl} : 2\text{CrCl}_3 \cdot 6\text{H}_2\text{O} = 77.68 \text{ mN m}^{-1}$ at 313 K)^{18, 29} and are similar to the previously studied Type 3 system but higher than those of molecular liquids (*e.g.* Benzene = 28.9 mN m^{-1} and other room temperature ionic liquids $[\text{BMIM}][\text{PF}_6] = 44.1 \text{ mN m}^{-1}$ and $\text{ChCl} : \text{ZnCl}_2 = 50.9 \text{ mN m}^{-1}$).⁵⁸⁻⁶⁰

3.6 Hole theory

A model has been proposed to predict the viscosities and conductivities of ionic liquids and deep eutectic solvents.^{32, 37, 58} The central hypothesis of hole theory is that as a solid melts, voids of random size and orientation are formed. The capability of an ion to move is therefore considered to be reliant on the presence of a neighbouring void of an equal or greater size than the ion. The possibility of ion motion can hence be considered to be a product of the size of the ions in consideration and the relative population of appropriately sized holes.

It has been shown that Hole theory developed by Fürth and later extended by Bockris for use with molten salts can be used to determine the average radius, r , of the voids in an ionic liquid using **Equation 3.13**:⁶¹

$$4\pi\langle r^2 \rangle = 3.5 k_B / \gamma \quad \text{Equation 3.13}$$

where k is the Boltzmann constant and γ is the surface tension at absolute temperature T . The most commonly practical model to study ion motion in high temperature ionic liquids is the hole theory.²⁵ In this theory ions are expected to migrate through empty holes formed and destroyed by statistical fluctuations. Abbott has confirmed the application of the hole model to RTILs with relative success.³⁷ The prediction of conductivity can delightfully reach the correct orders of magnitude. However, for many widely used RTILs, there still remain marked deviations between the estimated and measured value. For instance, the conductivity of almost all imidazolium-based salts is greatly underestimated. This is because the model was originally designed for the systems of molten salts, where the composition and structure of the components are distinctly different from those of RTILs. Molten salts, such as NaCl, consist of small inorganic ions; accordingly, the ions are considered as tiny spheres in the model. By comparison, RTILs are in general involved of inorganic anions and bulky organic cations with complex structure.

The influence of the salt upon the structure of the liquid can be obviously seen by measuring the liquid density. The amount of free volume can be determined using a hard sphere model. Using the density data shown in **Figure 3.16a** the molar volume V_m can be calculated using:

$$V_m = \frac{M_r}{\rho} \quad \text{Equation 3.14}$$

Where M_r is the relative molar mass of the liquid calculated from:

$$M_r = x_{CrCl_3 \cdot 6H_2O} M_{CrCl_3 \cdot 6H_2O} + x_{urea} M_{urea} \quad \text{Equation 3.15}$$

where x is the mole fraction and M the relative molar mass of the two components. The actual volume occupied by the components can be calculated in a similar manner *i.e.*

$$V_{comp} = (x_{CrCl_3 \cdot 6H_2O} V_{CrCl_3 \cdot 6H_2O} + x_{urea} V_{urea}) N_A \quad \text{Equation 3.16}$$

where V is the molecular volume of the component and N_A the Avogadro constant. Using this approach the fractional molar free volume can be obtained using;

$$V_{free} = (V_m - V_{comp})/V_m \quad \text{Equation 3.17}$$

Using the data in **Figure 3.16b** the average void radius for the urea: $\text{CrCl}_3 \cdot 6\text{H}_2\text{O}$ eutectic at 313 K was found to be 1.16 Å, whilst this was 1.24 Å for $\text{ChCl} : 2\text{CrCl}_3 \cdot 6\text{H}_2\text{O}$.¹⁸ The radius of the choline ion is 3.29 Å. KBr at 1173 K has an average void radius of 2.1 Å,²⁵ which shows a the major difference between the viscosity of ionic liquids and molten salts: the ratio of ionic radius to void radius is noticeably larger for ionic liquids than molten salts, making ionic motion significantly easier in the latter case.¹⁷ The relatively low viscosity shown in **Figure 3.17** is probably due to Cl^- acting as the main mobile species.

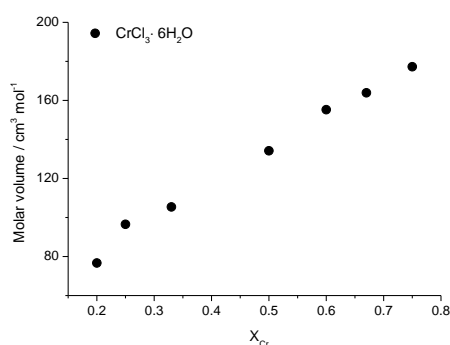


Figure 3.17: *Relative changes in liquid free volume as a function of composition*

Obviously these liquids have relatively high densities which are even higher than the $\text{ChCl} : \text{CrCl}_3 \cdot 6\text{H}_2\text{O}$ system. The free volume of the liquid was calculated using the data in **Figure 3.16a** and the following ionic and molecular volumes; $[\text{CrCl}_2(\text{H}_2\text{O})_4]^+ = 128 \text{ \AA}^3$, $\text{Cl}^- = 24.84 \text{ \AA}^3$, $\text{H}_2\text{O} = 19.51 \text{ \AA}^3$, urea = 52.62 \AA^3 . The urea: $3\text{CrCl}_3 \cdot 6\text{H}_2\text{O}$ is harder to model as the speciation is extremely complex and changes with composition. It is known that the main species is $[\text{CrCl}_2(\text{OD})_4]^+$ where OD is an oxygen donor which could be water or urea. For the purposes of fitting the OD will be assumed to be water and an ionic volume of 128 \AA^3 will be used for $[\text{CrCl}_2(\text{H}_2\text{O})_4]^+$. There is significant error associated with the chromium ions depending on the modelling method used, however the trend is always the same. It is therefore pertinent to plot the relative changes in free volume normalised to the largest value (**Figure 3.17**). It can be seen that the free volume decreases significantly at low $[\text{CrCl}_2(\text{H}_2\text{O})_4]^+$ mole fractions. For this system (urea: $\text{CrCl}_3 \cdot 6\text{H}_2\text{O}$) the maximum density occurs at the eutectic composition. This corresponds with the changes in conductivity and this is may be due to that in ionic liquids the conductivity is related to the mobility of charge carriers rather than the number of them.

3.7 Cyclic voltammetry

Cyclic voltammetry is a useful technique whereby electrolysis mechanisms of redox couples can be determined by sweeping a potential between two values at a fixed rate to monitor a change in current. Peaks in current will be observable wherever species are oxidised or reduced in solution. Redox potentials are usually determined from the average of either the peak positions or from the half wave potential.⁶² **Figure 3.18** shows cyclic voltammograms for the urea: $\text{CrCl}_3 \cdot 6\text{H}_2\text{O}$ system at different compositions, recorded at 313 K on a Pt disc electrode with a sweep rate of 20 mV s^{-1} . The cathodic current increases with increasing $\text{CrCl}_3 \cdot 6\text{H}_2\text{O}$ content, as expected.

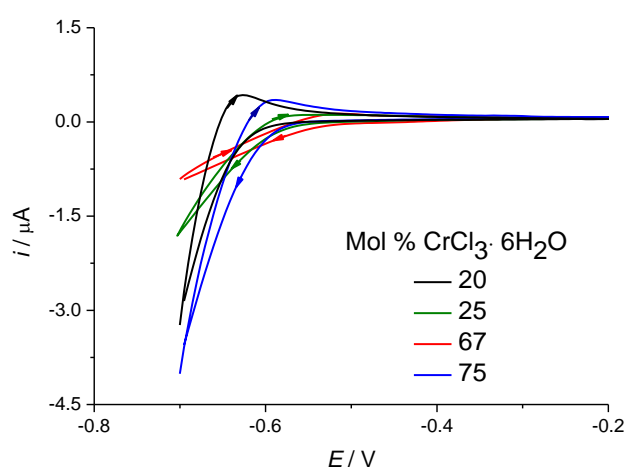


Figure 3.18: Cyclic voltammogram for the urea: $\text{CrCl}_3 \cdot 6\text{H}_2\text{O}$ system at 313 K on a Pt microelectrode, at a sweep rate of 20 mV s^{-1} for different compositions.

The voltammograms are poorly resolved which appears to be a feature of Cr, Ni and Fe complexes in the liquids studied to date. This does appear to be substrate dependent and it is a topic which is currently being investigated.

3.8 Quartz crystal microbalance (QCM)

Piezoelectric devices are very sensitive to mass changes at the surface of the crystal and provide the competence of detecting extremely small amounts (ng) of deposited material.⁶³⁻⁶⁵ The operation of the device depend on the excitation of a normal mode of oscillation by the application of a radio frequency field across a thin disc of the material.⁶⁶ For AT cut crystals (**Figure 3.19**), the resonant condition matches with a shear oscillation wherein the shear wave propagates through the bulk of the material, perpendicular to the faces of the disk.

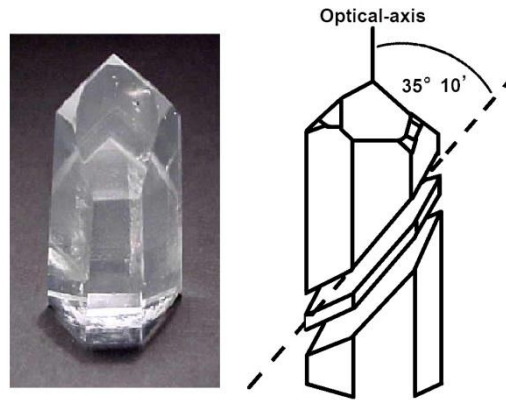


Figure 3.19: Illustration of AT-cut quartz crystal.

The atomic displacements corresponding to this shear motion are therefore parallel to the disk faces. The resonant frequency decreases due to deposition of material on either or both faces of the crystal. The first quantitative study of this effect was that by Sauerbrey⁶⁷, who derived the relationship between the frequency change (Δf) caused by the added mass (ΔM). Sauerbrey discussed that the elastic properties of the deposited film cannot contribute to the resonant frequency since the film is thin and located entirely inside the anti-nodal region of the resonator, where no shear deformation happens either in the film or in the quartz crystal close to the surface. The unloaded resonant frequency f_0 , is found⁶⁸ from the condition that the bulk material thickness d is an integral multiple n of half wave length λ_Q , i.e., $d = n\lambda_Q/2 = nV_Q/2f_0$, where V_Q is the shear wave velocity in quartz. Therefore:

$$f_0 = nV_Q/2d \quad \text{Equation 3.18}$$

and if we assume that at the fundamental frequency ($n = 1$), $N_{AT} = df_Q$ is the frequency constant of the ordinarily used AT-cut crystal and is 0.1666 MHz.cm.⁶⁹ A variation of thickness of the quartz plate will cause a change of frequency as given by:

$$\frac{f}{f_0} = \frac{\Delta d}{d} \quad \text{Equation 3.19}$$

The density, mass, and thickness of the quartz are related by $d = M_Q / A \rho$ where A is the surface area, and this yields:

$$\frac{f}{f_0} = \frac{M_Q}{dA\rho} \quad \text{Equation 3.20}$$

The variation in frequency resulting from the deposition of a thin, uniform film of any foreign substance would be equal to that resulting from a layer of quartz of the same mass.^{67, 68} Utilising the relationship between the thickness and N_{AT} , one obtains:

$$\Delta f = \Delta M f_0^2 / A \rho N_{AT} \quad \text{Equation 3.21}$$

where Δf is the mass of film of any substance added to the quartz plate. Utilising values of the constants mentioned and for the density of quartz ($\rho = 2.648 \text{ g/cm}^3$) it follows:

$$\Delta f = -2.275 \times 10^6 f_0^2 \left(\frac{\Delta M}{A} \right) \quad \text{Equation 3.22}$$

where Δf is the change in frequency due to the added film (Hz), f_0 is the resonant frequency of the quartz plate without deposited film (MHz), ΔM is the mass of deposited film (g), and A is the area (cm^2) for a 5 MHz crystal, one finds:

$$\Delta M = -1.74 \times 10^{-8} A \Delta f \quad \text{Equation 3.23}$$

so that the mass sensitivity is $-1.74 \times 10^{-8} \text{ g/cm}^2 \text{ Hz}$. **Equation 3.23** is the essential equation (Saubery equation) which links the frequency decrease to the increase of mass loading on the quartz crystal, and the mass sensitivity can be calculated from first principles. **Equations 3.22** and **3.23** predict that the QCM is sensitive to sub-monolayer quantities of material deposited on the quartz plate and that the sensitivity increases as the square of the frequency of the plate, f_0 .

3.8.1 Electrochemical quartz crystal microbalance (EQCM)

In the electrochemical application, the quartz crystal is coated with a gold/platinum disc on both sides. One side is exposed to the solution in the electrochemical cell, whereas the other is exposed to air. Voltammetry is carried out using the gold/ platinum disc exposed to solution as the working electrode. This EQCM setup allows instantaneous measurement of mass and current in a voltammetric experiment. The use of the QCM in electrochemistry was first demonstrated by Jones and Meiore^{70, 71} who determined trace metals by deposition of metal onto a QCM electrode in an electrochemical cell followed by the *ex-situ* (in air) analysis of the deposited mass. Successful development in the liquid environment was demonstrated by Konash and Bastiaans⁷² in 1980, and a year

later by Nomura⁶⁵. The first *in-situ* electrochemical application of the QCM cell to investigate the electrochemical reduction was applied to Cu(II) and Ag(I) in electrolyte solutions.^{64, 65}

Once used as an *in-situ* technique for measuring mass changes at electrode surface, one of the EQCM electrodes is exposed to the solution and simultaneously provides the altering electric field which drives the oscillation of the crystal and acts as the working electrode in conventional electrochemical cell. The other electrode leftovers exposed to air and serves only to complete the oscillation circuit. Therefore, the EQCM experiment involves the measurement of the various electrochemical parameters, such as potential, current, and charge, at one of the EQCM electrodes and the simultaneous measurement of the oscillation frequency of the piezoelectric crystal from which, in favourable cases, minute mass changes at the electrode may be inferred.

The interpretation of the poorly resolved voltammogram is aided, however, by simultaneously monitoring the mass changes using an electrochemical quartz crystal microbalance (EQCM). **Figure 3.20** shows the current and mass changes for 1:2 urea/ $\text{CrCl}_3 \cdot 6\text{H}_2\text{O}$ at an unpolished gold electrode on a quartz crystal resonator.

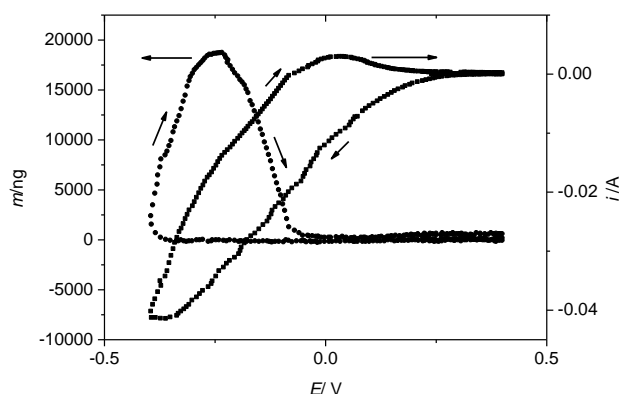


Figure 3.20: Current and mass changes on an unpolished gold crystal for the urea: $2\text{CrCl}_3 \cdot 6\text{H}_2\text{O}$ system.

There is a large cathodic current observed from 0.25 V with respect to the silver wire pseudo-reference electrode. However, mass deposition is only observed from ca. -0.3 V. On the anodic scan the mass still increases significantly showing that the metal nuclei are still growing. The initial current before mass deposition is observed must therefore be caused by the reduction of Cr(III) to Cr(II). Setting the lower scan potential to -0.2 V, an oxidative current is observed on the anodic sweep corresponding to Cr(II) to

Cr(III) confirming this assumption. The mass deposited at -0.4 V is all stripped between -0.2 and 0 V, which shows that the deposition process is electrochemically reversible.

It should however be noted that some of the current may be attributed to side reactions, such as the decomposition of waters of crystallisation. To determine the current efficiency, EQCM studies were carried out at a constant potential of -0.4 V and the mass charge plots (**Figure 3.21**) showed a current efficiency of 74%. This compares with 65% for the $\text{ChCl}: 2\text{CrCl}_3 \cdot 6\text{H}_2\text{O}$ system and about 15% for the aqueous chromic acid.¹

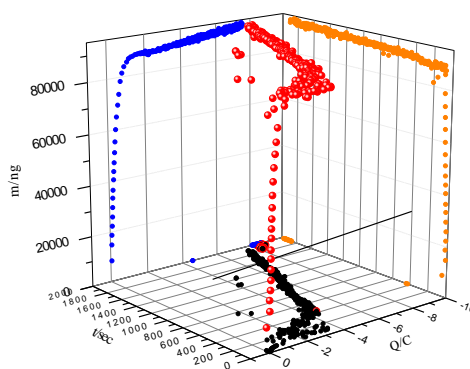


Figure 3.21: 3D plot of $m(Q,t)$ (red circles) for deposition of 1 urea: $2 \text{CrCl}_3 \cdot 6\text{H}_2\text{O}$ on an unpolished Au coated QCM crystal. 2D projections are also shown for clarity, $Q(t)$ (black), $m(t)$ (blue), $m(Q)$ (orange).

The difference in current efficiency between the two eutectic mixtures (type 2 and type 4) could result from the different amounts of chromium being present in the form of a cationic species. Since the electrode will be negative of the potential of zero charge during deposition, the surface concentration of the positively charged chromium species will be high in the urea eutectic, whereas the surface layer may be dominated by choline cations in the $\text{ChCl}:2\text{CrCl}_3 \cdot 6\text{H}_2\text{O}$ system. The high current efficiency suggests that hydrogen embrittlement of the substrate will be less of an issue with this liquid than with aqueous deposition where it is a major problem.

3.9 Bulk deposition

A number of researchers have indicated that the Hull Cell has possibly contributed more to the development of electroplating than any other tool and this is likely true.⁷³ Although it is not nearly as exotic and complex as many of the other analytical tools, the fact that this tool, first demonstrated in 1939 is still viable shows that it has weathered the test of time.⁷⁴

The effect of the current density on deposit morphology was studied using a Hull cell. This enables a range of current densities to be applied to one substrate under otherwise identical conditions. The current density at different positions across the Hull cell was calculated using **Equation 3.24**.

$$J = i(5.1 - 5.24 \log_{10} X) \quad \text{Equation 3.24}$$

where, J is the current density, i is the applied current and X is the distance from high current density end of the panel. It was, however, found that the morphology of the surface layer was dependent on the current density.

Bulk electrodeposition from the 1:2 urea: $\text{CrCl}_3 \cdot 6\text{H}_2\text{O}$ system at 313 K for 2 hours onto a mild steel electrode at an applied voltage of 4 V resulted in an amorphous dark grey deposit of up to 65 μm in thickness (**Figure 3.22**).

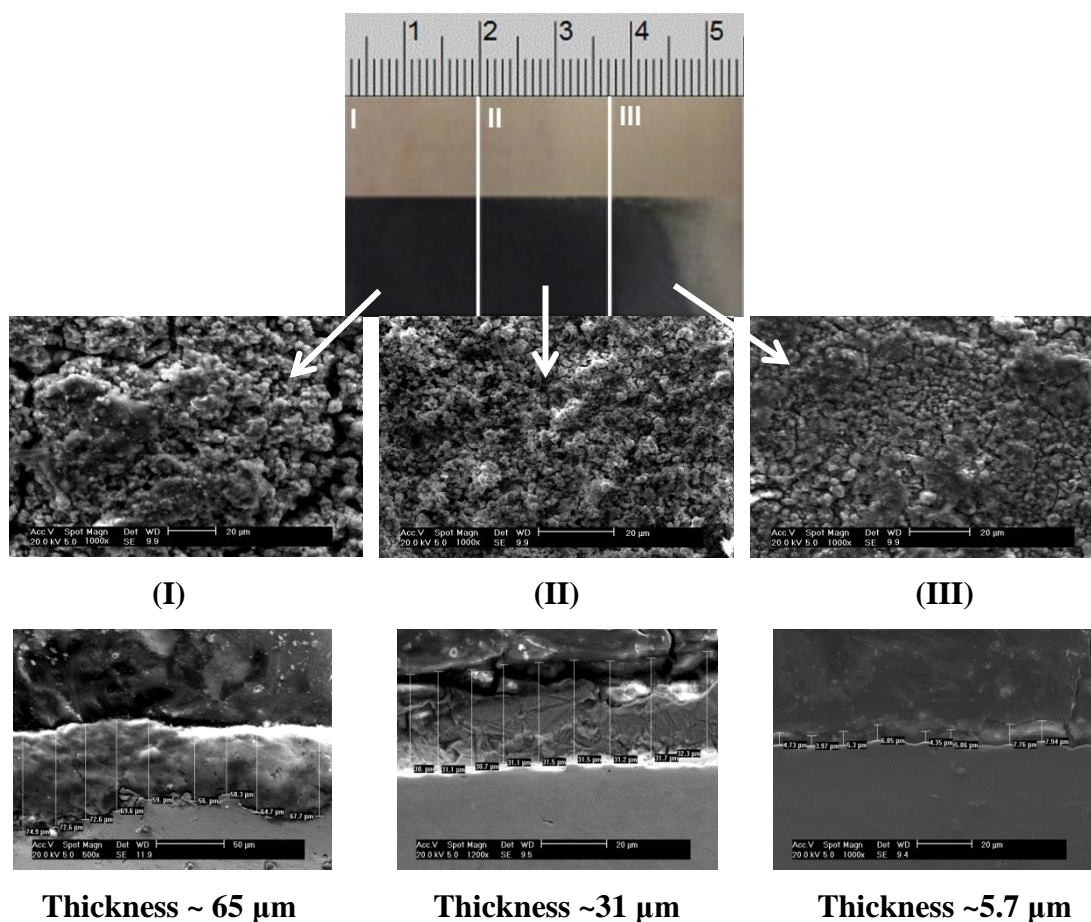


Figure 3.22: Chromium electrodeposit obtained using a Hull cell and the urea: $2\text{CrCl}_3 \cdot 6\text{H}_2\text{O}$ Type 4 DES (Current densities: I= 0.22, II=0.17 and III=0.11 A cm^{-2}) with corresponded thicknesses 65 μm , 31 μm and 5.7 μm respectively.

No significant gas evolution was noticed, verifying that the waters of hydration are less electrochemically active than bulk water. According to SEM the structure of the film is not a macro-crystalline deposit as would be observed with aqueous chromic acid solutions although the surface roughness of the deposit increases as the current density increases. In all cases the deposit is largely crack free, although there may be signs of some micro-cracking occurring at high current densities. EDX shows no presence of oxygen but there is some chloride trapped in the deposit particularly at high current density. In comparison, previous studies into the deposition of chromium from the equivalent Type 2 system at 333 K found that the deposit morphology was amorphous and pale blue/grey in colour,¹⁸ whilst also being very soft and easily removable during wear testing.¹⁰

3.10 Hardness and thickness

Hard chromium plating is typically used to reinstate the original dimensions of worn surfaces of the shafts, pumps and compressors.⁷⁵ However, over the last decade, there has been an increasing anxiety surrounding the processing of chromium coatings utilising electroplating. This is due to environmental, health and safety considerations associated with the handling, storage and disposal of Cr(VI) compounds usually used during the plating process.

Generally, chromium is the hardest of the most commonly deposited metals.⁷⁶ Hard chrome is utilised as a wear resistant coating not only on steel but also on an extensive variety of other metals. Hard chromium varies from decorative chromium not only due to its usage but also due to the difference in deposit thickness. A typical hard chrome deposit is in the range of 10 – 250 μm thick.⁷⁷

The electrochemical equivalent weight of Cr(III) ions is twice larger than that of hexavalent Cr ions. Using aqueous solution thick trivalent chromium deposits cannot be effortlessly obtained.⁷⁸ The maximum chromium thickness achieved from commercial trivalent baths is normally less than 10 μm , making the deposits unsuitable for hard chromium, wear-resistance and other functional applications.^{78, 79}

Hard chrome deposits possess a hardness range from 800 – 1200 HV, depending on the bath type used.⁸⁰ Noticeably, the higher the Vickers number the longer the service life will be provided to the component. Moreover, deposit hardness is a function of the bath chemistry used. Therefore, it is best to utilise a plating process that offers the highest HV value. Decorative chromium deposits possess exactly the same hardness range as

hard chrome. On the other hand, industrial chromium has a tendency to be harder merely due to the greater thickness of deposit. A deposit of at least 50 μm must be utilised before the surface totally reflects the properties of the chromium metal and not the substrate.¹

All hard chrome deposits, however, have a tendency to reduce the fatigue limit of the parts. Shot peening of steels harder than 40 RC (Rockwell scale \approx 400 HV) prior to plating is a common method of minimizing this effect dry prolong the life of the part. The Dura baths deposit is compressive and therefore provides less stress than the standard 100:1 sulfate bath which has a tensile stressed deposit.

Chromium coatings are used for surfaces that endure significant wear *e.g.* hydraulic shafts. An important property of the coatings is therefore their hardness. Chromium deposited using chromic acid has hardness values of typically 800 HV. Previous studies using the $\text{ChCl}/\text{CrCl}_3 \cdot 6\text{H}_2\text{O}$ system produced a coating with a hardness of 242 HV. With proprietary additives it is possible to increase this value to 600 HV.⁸¹ Hardness measurements were carried out on the sample shown in **Figure 3.22** and it was found that the average hardness of the sample was *ca.* 600 \pm 10 HV, which is close to the values required for hard chrome.

3.11 Conclusions

It has been shown that novel Type 4 room-temperature Deep Eutectic Solvents can be formed using urea and hydrated chromium (III) chloride. The eutectic composition occurs at a mole fraction of 0.67 metal salt similarly to many other Type 2, 3 and 4 DESs.

The liquids display high conductivities, despite relatively high viscosities and this is thought to result from chloride being the main charge carrying species. A variety of techniques were used to elucidate the chromium speciation in solution and it is evident that the speciation is different from the analogous $\text{ChCl}/\text{CrCl}_3$ Type 2 system.

In-situ EXAFS has been effectively applied to elucidate dissolved metal structure in a ChCl and urea based DES. The structure of dissolved chromium (III) chloride, until now only poorly understood through destructive ex-situ measurements such as mass spectrometry, has thus been conclusively determined. EXAFS suggests that the main chromium species is the cationic ($[\text{CrCl}_2(\text{OD})_4]^+$) and transport properties can be explained using hole theory.

Electrochemical experiments comprising cyclic voltammetry and chronoamperometry have established that there is an obvious difference in chromium electrodeposition processes in the type 4 and type 2 systems. Chromium electrodeposition proceeds via a 1 electron transfer ($\text{Cr}^{3+/2+}$) followed by a 2 electron reduction to the metal. Deposition onto gold is electrochemically reversible and the reduction process had a high current efficiency despite the hydrate water molecules present. Thick, adherent, non-cracked chromium could be bulk-deposited onto steel and coating hardness values of approximately 600 ± 10 Vickers could be achieved showing that the liquid is able to produce hard chromium coatings.

3.12 References

1. M. Schlesinger and M. Paunovic, *Modern electroplating*, Wiley, New York, 2000.
2. S. B. Wilbur, S. R. Corporation, U. S. A. f. T. Substances and D. Registry, *Toxicological Profile for Chromium*, U.S. Department of Health and Human Services, Public Health Service, Agency for Toxic Substances and Disease Registry, 2000.
3. D. Smart, T. Such and S. Wake, *Trans. Inst. Met. Finish.*, 1983, **61**, 105-110.
4. A. P. Abbott, G. Frisch and K. S. Ryder, *Annu Rev Mater Res*, 2013, **43**, 335-358.
5. Q. Liao, W. R. Pitner, G. Stewart, C. L. Hussey and G. R. Stafford, *J Electrochem Soc*, 1997, **144**, 936-943.
6. S. Zein El Abedin, N. Borissenko and F. Endres, *Electrochemistry communications*, 2004, **6**, 510-514.
7. F. Endres, D. MacFarlane and A. Abbott, *Electrodeposition from ionic liquids*, John Wiley & Sons, 2008.
8. S. Eugenio, C. M. Rangel, R. Vilar and S. Quaresma, *Electrochim Acta*, 2011, **56**, 10347-10352.
9. S. Eugenio, C. M. Rangel, R. Vilar and A. M. B. do Rego, *Thin Solid Films*, 2011, **519**, 1845-1850.
10. A. P. Abbott, G. Capper, D. L. Davies, R. K. Rasheed, J. Archer and C. John, *T I Met Finish*, 2004, **82**, 14-17.
11. A. Abbott, G. Capper, B. Swain and D. Wheeler, *Transactions of the IMF*, 2005, **83**, 51-53.
12. A. P. Abbott, G. Capper, K. J. McKenzie, A. Glidle and K. S. Ryder, *Phys Chem Chem Phys*, 2006, **8**, 4214-4221.
13. A. P. Abbott, J. Griffith, S. Nandhra, C. O'Connor, S. Postlethwaite, K. S. Ryder and E. L. Smith, *Surface and Coatings Technology*, 2008, **202**, 2033-2039.
14. A. P. Abbott, S. Nandhra, S. Postlethwaite, E. L. Smith and K. S. Ryder, *Phys Chem Chem Phys*, 2007, **9**, 3735-3743.
15. H. M. A. Abood, A. P. Abbott, A. D. Ballantyne and K. S. Ryder, *Chem Commun*, 2011, **47**, 3523-3525.
16. N. R. Brooks, S. Schaltin, K. Van Hecke, L. Van Meervelt, K. Binnemans and J. Fransaer, *Chemistry-a European Journal*, 2011, **17**, 5054-5059.
17. A. P. Abbott, K. S. Ryder and U. König, *T I Met Finish*, 2008, **86**, 196-204.

18. A. P. Abbott, G. Capper, D. L. Davies and R. K. Rasheed, *Chemistry – A European Journal*, 2004, **10**, 3769-3774.
19. W. G. McGAVOCK, J. M. Bryant and W. W. Wendlandt, *Science (New York, NY)*, 1956, **123**, 897.
20. P. S. Gentile and L. H. Talley, *Journal of the American Chemical Society*, 1957, **79**, 4296-4297.
21. A. P. Abbott, J. C. Barron, K. S. Ryder and D. Wilson, *Chemistry – A European Journal*, 2007, **13**, 6495-6501.
22. A. P. Abbott, D. Boothby, G. Capper, D. L. Davies and R. K. Rasheed, *Journal of the American Chemical Society*, 2004, **126**, 9142-9147.
23. M. D. Ediger, *Annual review of physical chemistry*, 2000, **51**, 99-128.
24. A. P. Abbott, G. Capper, D. L. Davies, R. K. Rasheed and V. Tambyrajah, *Chem Commun*, 2003, 70-71.
25. J. O. M. Bockris and A. K. N. Reddy, *Volume 1: Modern Electrochemistry: Ionics*, Springer, 1998.
26. L. C. Branco, J. N. Rosa, J. J. Moura Ramos and C. A. Afonso, *Chemistry-a European Journal*, 2002, **8**, 3671-3677.
27. H. Wang, Y. Jing, X. Wang, Y. Yao and Y. Jia, *Journal of Molecular Liquids*, 2011, **163**, 77-82.
28. I. Smallwood, *Handbook of Organic Solvent Properties*, Elsevier Science, 1996.
29. G. J. Janz, *Molten Salts Handbook*, Elsevier Science, 2013.
30. J. G. Huddleston, A. E. Visser, W. M. Reichert, H. D. Willauer, G. A. Broker and R. D. Rogers, *Green Chem*, 2001, **3**, 156-164.
31. A. P. Abbott, R. C. Harris, K. S. Ryder, C. D'Agostino, L. F. Gladden and M. D. Mantle, *Green Chem*, 2011, **13**, 82-90.
32. A. P. Abbott, *Chemphyschem*, 2004, **5**, 1242-1246.
33. P. Wasserscheid and T. Welton, *Ionic liquids in synthesis*, Wiley Online Library, 2008.
34. M. Yoshizawa, W. Xu and C. A. Angell, *Journal of the American Chemical Society*, 2003, **125**, 15411-15419.
35. C. A. Angell, N. Byrne and J.-P. Belieres, *Accounts of chemical research*, 2007, **40**, 1228-1236.
36. W. Xu, E. I. Cooper and C. A. Angell, *The Journal of Physical Chemistry B*, 2003, **107**, 6170-6178.
37. A. P. Abbott, *Chemphyschem*, 2005, **6**, 2502-2505.
38. A. P. Abbott, G. Frisch and K. S. Ryder, *Annual Reports Section "A" (Inorganic Chemistry)*, 2008, **104**, 21-45.
39. A. P. Abbott, J. C. Barron, G. Frisch, S. Gurman, K. S. Ryder and A. F. Silva, *Phys Chem Chem Phys*, 2011, **13**, 10224-10231.
40. A. P. Abbott, G. Capper, K. J. McKenzie and K. S. Ryder, *Journal of Electroanalytical Chemistry*, 2007, **599**, 288-294.
41. C. Hardacre, *Annu. Rev. Mater. Res.*, 2005, **35**, 29-49.
42. H. H. Willard, *Instrumental Methods of Analysis*, Wadsworth Publishing Company, 1988.
43. P. J. Elving and B. Zemel, *Journal of the American Chemical Society*, 1957, **79**, 1281-1285.
44. B. K. Teo, *EXAFS: basic principles and data analysis*, Springer-Verlag, 1986.
45. A. Filipponi, *Journal of Physics: Condensed Matter*, 2001, **13**, R23.
46. J. J. Rehr and R. Albers, *Reviews of Modern Physics*, 2000, **72**, 621.
47. S. Gurman, N. Binsted and I. Ross, *Journal of Physics C: Solid State Physics*, 1986, **19**, 1845.

48. H. G. Moseley, *The London, Edinburgh, and Dublin Philosophical Magazine and Journal of Science*, 1913, **26**, 1024-1034.
49. P. Nockemann, B. Thijs, K. Lunstroot, T. N. Parac-Vogt, C. Görrler-Walrand, K. Binnemans, K. Van Hecke, L. Van Meervelt, S. Nikitenko and J. Daniels, *Chemistry-a European Journal*, 2009, **15**, 1449-1461.
50. J. E. Penner-Hahn, in *eLS*, John Wiley & Sons, Ltd, 2001.
51. J.-D. Grunwaldt and A. Baiker, *Phys Chem Chem Phys*, 2005, **7**, 3526-3539.
52. T. Elsaesser and M. Woerner, *The Journal of Chemical Physics*, 2014, **140**, -.
53. A. P. Abbott, G. Capper, D. L. Davies, K. J. McKenzie and S. U. Obi, *Journal of Chemical & Engineering Data*, 2006, **51**, 1280-1282.
54. A. P. Abbott, K. El Ttaib, G. Frisch, K. J. McKenzie and K. S. Ryder, *Phys Chem Chem Phys*, 2009, **11**, 4269-4277.
55. J. M. Hartley, I. Chung-Man, G. C. H. Forrest, K. Singh, S. J. Gurman, K. S. Ryder, A. P. Abbott and G. Frisch, *Inorganic chemistry*, 2014, **53**, 6280-6288.
56. C. F. Spencer and R. P. Danner, *J Chem Eng Data*, 1972, **17**, 236-241.
57. M. Motin, *Journal of Chemical & Engineering Data*, 2004, **49**, 94-98.
58. A. P. Abbott, R. C. Harris and K. S. Ryder, *The Journal of Physical Chemistry B*, 2007, **111**, 4910-4913.
59. W. D. Harkins and Y. C. Cheng, *Journal of the American Chemical Society*, 1921, **43**, 35-53.
60. A. P. Abbott, G. Capper, D. L. Davies and R. Rasheed, *Inorganic chemistry*, 2004, **43**, 3447-3452.
61. J. M. Bockris and G. Hooper, *Discussions of the Faraday Society*, 1961, **32**, 218-236.
62. K. Izutsu, *Electrochemistry in Nonaqueous Solutions*, Wiley, 2009.
63. K. K. Kanazawa and J. G. Gordon, *Anal Chem*, 1985, **57**, 1770-1771.
64. T. Nomura and O. Hattori, *Analytica Chimica Acta*, 1980, **115**, 323-326.
65. T. Nomura, *Analytica Chimica Acta*, 1981, **124**, 81-84.
66. R. Byrne, P. Lloyd and W. Spencer, *The Journal of the Acoustical Society of America*, 1968, **43**, 232-238.
67. G. Sauerbrey, *Z. Physik*, 1959, **155**, 206-222.
68. S. Wenzel and R. White, *Applied Physics Letters*, 1989, **54**, 1976-1978.
69. C. Lu and A. W. Czanderna, *Applications of Piezoelectric Quartz Crystal Microbalances*, Elsevier Science, 1984.
70. J. P. Mieure and J. L. Jones, *Talanta*, 1969, **16**, 149-150.
71. J. L. Jones and J. P. Mieure, *Anal Chem*, 1969, **41**, 484-490.
72. P. L. Konash and G. J. Bastiaans, *Anal Chem*, 1980, **52**, 1929-1931.
73. C. A. Ogden and D. M. Tench, US Patent no. 4132605 A, 1979.
74. R. O. Hull, US Patent no. 2149344 A, 1939.
75. A. Savarimuthu, H. Taber, I. Megat, J. Shadley, E. Rybicki, W. Cornell, W. Emery, D. Somerville and J. Nuse, *Journal of thermal spray technology*, 2001, **10**, 502-510.
76. C. Chisholm, *Electrodeposition and Surface Treatment*, 1975, **3**, 321-333.
77. S. Komiya, S. Ono and N. Umezumi, *Thin Solid Films*, 1977, **45**, 473-479.
78. Y. Song and D.-T. Chin, *Electrochim Acta*, 2002, **48**, 349-356.
79. N. Mandich, *Plat. Surf. Finish*, 1997, **84**, 108-115.
80. G. Lausmann, *Surface and Coatings Technology*, 1996, **86**, 814-820.
81. E. L. Smith, C. Fullarton, R. C. Harris, S. Saleem, A. P. Abbott and K. S. Ryder, *T I Met Finish*, 2010, **88**, 285-293.

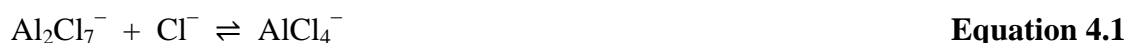
Chapter 4: $[\text{Cr}(\text{en})_3]^{3+}$ based deep eutectic solvents

4.1	Introduction	81
4.2	Ligand field theory	82
4.2.1	Crystal field theory	83
4.3	Colour of transition-metal coordination compounds	88
4.4	Eutectic mixtures based on urea and $[\text{Cr}(\text{en})_3]\text{Cl}_3 \cdot 3\text{H}_2\text{O}$	90
4.5	Physical properties	91
4.5.1	Phase behaviour	91
4.5.2	Viscosity	92
4.5.3	Conductivity	94
4.5.4	Molar conductivity	97
4.6	Solution speciation	99
4.6.1	UV-visible spectrum	99
4.6.2	EXAFS	100
4.7	Density	100
4.8	Molar volume	101
4.9	Cyclic voltammetry	102
4.9.1	Under-potential deposition (upd)	103
4.9.2	The effects of the viscosity on the voltammograms	106
4.10	Bulk deposition	109
4.11	Hardness and thickness	110
4.12	Current efficiency	110
4.13	Conclusion	111
4.14	References	112

4.1 Introduction

In the previous chapter it has been suggested that a variety of species are formed when chromium chloride is mixed with urea. The equilibria between the species can be extreme when local differences in composition occur which is the case close to the electrode surface during electrodeposition.¹

An extreme example of this can be seen with the often studied case of aluminium deposition from a chloroaluminate eutectic mixture. It is known that AlCl_3 forms both AlCl_4^- and Al_2Cl_7^- ions in the liquid. Only Al_2Cl_7^- can be electro-reduced and as aluminium is deposited on the electrode surface the double layer becomes rich in Cl^- ions and the equilibrium



is driven towards AlCl_4^- decreasing the ability for the metal to be reduced.

Of particular interest has been the ability to electro-reduce chromium to circumvent the use of chromic acid for metal deposition.

In aqueous solutions $\text{CrCl}_3 \cdot 6\text{H}_2\text{O}$ undergoes several equilibria:²



In the $\text{ChCl}:\text{CrCl}_3 \cdot 6\text{H}_2\text{O}$ eutectic the anionic complex $[\text{Cr}(\text{H}_2\text{O})_2\text{Cl}_4]^-$ is formed whereas in the urea $\text{CrCl}_3 \cdot 6\text{H}_2\text{O}$ eutectic a variety of complexes of the form $[\text{Cr}(\text{OD})_4\text{Cl}_2]$ where OD is an oxygen donor which could be either water or urea. The equilibria will depend upon the relative concentrations of the three ligands; H_2O , Cl^- and urea. These in turn will be affected by the rate of deposition, the viscosity of the liquid and any agitation of the fluid. It is therefore unsurprising that morphology control in these liquids is difficult. In the current chapter the coordination geometry around a Cr^{III} centre is controlled by making a complex with ethylene diamine, en, to form $[\text{Cr}(\text{en})_3]\text{Cl}_3 \cdot 3\text{H}_2\text{O}$ which is complexed with urea to form a eutectic. The properties of this eutectic are contrasted with those of the urea: $\text{CrCl}_3 \cdot 6\text{H}_2\text{O}$ eutectic (chapter three) where a variety of species are known to form in solution. It is shown that markedly different properties are obtained together with different deposit morphology. This approach could lead to the design of improved DESs and an understanding of how aqueous plating solutions function.

4.2 Ligand field theory

Ligand field theory considers the interaction between a central transition metal atom and its ligand, specifically the part arising from the instant donor atom and their effects on the *d*-orbitals of the metal atom and the electrons which occupy them. Consideration may also be given to more distant parts of the ligand molecules and the presence of orbitals other than *d* on the metal atom.

The first theory, commonly called the crystal field or electrostatic theory, was developed by Bethe³, Van Vleck,⁴ and many others⁵⁻⁷, in connection with studies on magnetism. The second theory, the molecular-orbital theory, was also discussed at an early date by Van Vleck.⁸ More recently each theory has been used to discuss the optical and chemical properties of a variety of compounds. Griffith regards them both as expressing certain aspects of a more complete theory termed ligand-field theory.⁹

Electrostatic considerations could not entirely describe the atomic interactions in the coordination compounds nor clarify an extensive range of magnetic and optical properties of materials. Therefore, in 1929 a novel method of the crystal bounds, based on the quantum mechanics laws was proposed originally by Bequerel.¹⁰ Accordingly, a metal ion placed in a solid is subjected to an electric field. This was formalised into a theory by Bethe³ who examined by means of symmetry considerations how the strength and symmetry of crystal fields affected the electronic energy levels of free ions. Bethe studied the influence of the surrounding ions on the electron distribution within any of the ions in a NaCl-type lattice. These thoughts formed the basis of so-called, crystal field and molecular orbital theories, which aimed to describe the bonds, arising between the atoms or ions in the complex compounds. This was later developed into ligand field theory.

Ligand field theory covers all the features concerned the effect of the nearest neighbours on the physical properties of the atom or ion, placed in the centre of the coordination compound. The key norms of the ligand field theory can be expressed as follows:¹¹

- While considering the orbital energies, the influence of both electrostatic field of ligands and covalence effects should be taken into consideration.
- If the electrons are located on molecular orbitals, analogous to *d*-orbitals, with a rather modified radial term.

Ligand field theory is the theoretical approach utilised in the understanding of the bonding and related electronic properties of transition metal complexes. The valence

theories that are applied to the composites of main group elements can be similarly applied to the transition metal compounds, since the bonding of these compounds are essentially alike. Just as in other cases applying the molecular orbital (MO) theory to transition metal compounds gives convenient results. Nevertheless, two things that make the study of the electronic structures of transition metal compounds dissimilar from the residual body of valance theory are; the presence of partly filled d and f orbitals along with crystal field theory that provides an influential yet simple method of sympathetic and correlating all of the characteristics that ascend from these partially filled orbitals.¹²

4.2.1 Crystal field theory

Crystal field theory (CFT) is a clearly electrostatic approach to the bonding in transition metal complexes. Fundamentally, it was settled to explain spectroscopic characteristics of d -block metal ions in ionic crystals. In crystal field theory, a ligand lone pair is moulded as a point negative charge that keeps away electrons in the d orbitals of the central metal ion. The theory focuses on the resulting splitting of the d orbitals into groups with different energies, and utilises that splitting to justify and associate the optical spectra, thermodynamic equilibrium, and magnetic properties of complexes.

In the existence of an octahedral crystal field, d orbitals are split into a lower energy triply degenerate set (t_{2g}) and a higher energy doubly degenerate set (e_g) separated by an energy Δ_o ; the ligand field splitting factor increases together with a spectrochemical series of ligands and differs with the identity and charge of the metal atom.¹³

Although this theory pays no attention to covalent bonding interactions between ligands and central metal ions in transition metal complexes, it offers a curiously respectable qualitative description of many of their characteristics.

In the model of an octahedral complex utilised in crystal field theory, six point negative charges indicating the ligands are located in an octahedral array around the central metal ion. These charges (in this case ligands) interact strongly with the central metal ion, and the stability of the complex stems in large part from this attractive interaction between opposite charges. On the other hand, there is a much smaller but very significant secondary influence rising from the fact that electrons in different d orbitals interact with the ligands to different ranges. Even though this variance interaction is little more than about 10% of the whole metal-ligand interaction energy, it has major concerns for the characteristics of the complex and is the main attention of this chapter.

Electrons in d_z^2 and $d_{x^2-y^2}$ orbitals, which are of symmetry, type e_g , whereas electrons in d_{xy} , d_{yz} , and d_{zx} orbitals, which are of symmetry type t_{2g} , are concentrated in regions that lie between the ligands (**Figure 4.1**).

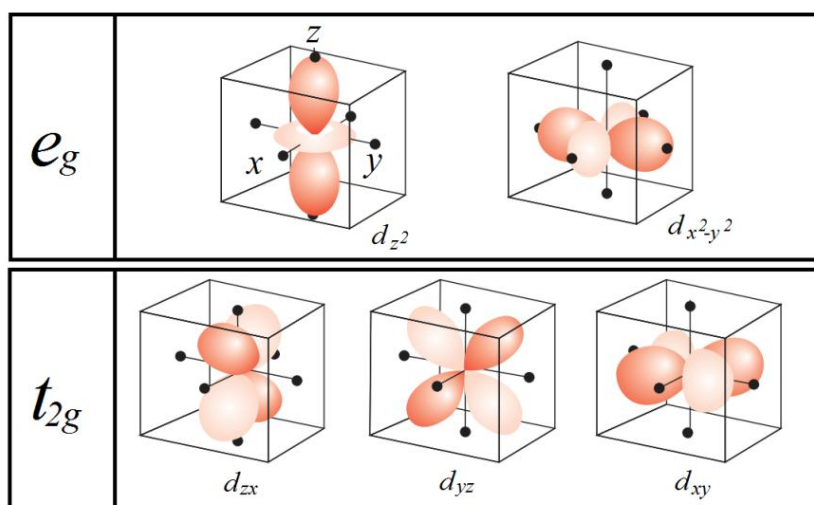


Figure 4.1: The orientation of the five d orbitals regarding the ligands of an octahedral complex: the degenerate e_g and t_{2g} orbitals.¹³

Accordingly, the former are repelled more intensely by the negative charge on the ligands than the latter and place at a higher energy. Group theory shows that the two e_g orbitals have the same energy, this is not willingly obvious from diagrams, and that the three t_{2g} orbitals also possess the equivalent energy. This simple model causes an energy level diagram wherein the three degenerate t_{2g} orbitals lay below the two degenerate e_g orbitals (**Figure 4.2**). The separation of the two sets of orbitals is called the ligand field splitting parameter, Δ_o , where the subscript O indicates an octahedral crystal field.

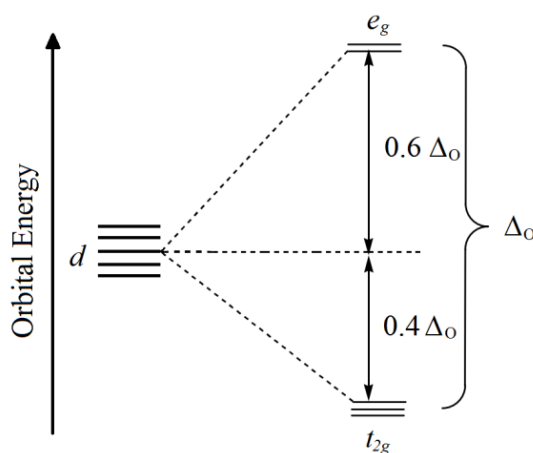
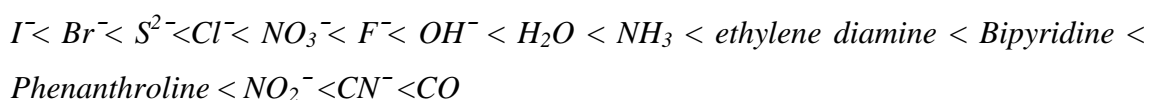


Figure 4.2: Splitting of the d -orbitals by an octahedral field.^{12, 14}

The energy level that relates to the proposed spherically symmetrical environment, wherein the negative charge caused by the ligands is evenly distributed over a sphere rather than being localized at six points, describes the barycentre of the array of levels, with the two e_g orbitals lying at $0.6\Delta_O$ above the barycentre and the three t_{2g} orbitals lying at $0.4\Delta_O$ below it. As in the illustration of the configurations of atoms, a superscript is utilised to point out the number of electrons in each set, for example t_{2g}^2 . It is not so simple to obtain values of Δ_O for complexes with more than one d electron because the energy of a transition then depends not only on orbital energies but also on the electron-electron repulsion energies.

The interaction between a transition metal and ligands coined from the electronic attraction between the metal cation and negative charge on the ligands. Hence, d -orbitals splitting are caused by negative ligands which repel the d -electrons of the metal. Then the d -electrons of the metal closer to the ligands possess a higher energy than those further away. The most dominant type of these complexes is octahedral which is expressed as ML_6 and involves six ligands.

The ligand field splitting parameter differs analytically with the character of the ligand, as shown in **Figure 4.2**. The spectrochemical series places ligands in arrangement of increasing energy of $e_g \rightarrow t_{2g}$ transitions that happen when they are existent in a complex, and exist below for some nominated ligands. Ligands producing a weaker ligand field are to the left in the arrangements and ligands producing a stronger ligand field are to the right:^{13, 15}

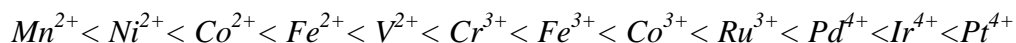


Therefore, strong-field ligands can cause a large splitting (Δ_O) of the d -orbitals. In these complexes, Δ_O is greater than the pairing energy and electrons are dynamically favoured to entirely fill the low energy orbitals before inhabiting higher energy orbitals. These complexes are known as low spin complexes. In contrast, weak-field ligands cause a small splitting (Δ_O) of the d -orbitals and in these complexes, Δ_O is smaller than the pairing energy and electrons fill each of the five d -orbitals before any pairing happens according to Hund's rule. Hund's rule stated that the term with maximum multiplicity has the lowest energy level. Therefore, these complexes are known as high spin complexes.

The OH^- ligand is weaker than H_2O , which might appear abnormal, but this has to do with the fact that the former is superior at making π -bonds which undermines the t_{2g}

orbitals. Electronic characteristics for a complex are closely correlated to its central metal ion and it is not usually likely to state whether a specific ligand provides a large or small ligand field splitting parameter deprived of allowing for the metal ion also. Generally, with increasing oxidation number, Δ increases and increases down a group.

The spectrochemical sequences for some transition metal ions is approximately:^{13, 16, 17}



One reason for this order is that the decrease of ionic radii (**Figure 4.3**) or increase in oxidation number of the metal from left to right in the periodic system causes the bonding between the ligand and the metal central ion to growth in strength. This series is also supposed to reproduce the improved metal-ligand bonding of the more expanded $4d$ and $5d$ orbitals compared to the compact $3d$ orbitals.

A plot of the ionic radii of the di-positive ions for the first transition series displays a general decrease with increasing atomic number, but with a double-bowl shaped profile. This is presented in **Figure 4.3**. As the nuclear charge increases, electrons enter the same sub-shell ($3d$); i.e. the electrons are approximately the same distance from the nucleus. Electrons in the same shell do not screen the positive charge of the nucleus from each other very well. Therefore, the net nuclear charge experienced by the electrons increases as the atomic number increases. This increased charge causes the electrons to move closer to the nucleus, and therefore the ionic radii of the first-row transition elements display an overall decrease across the series.¹⁸

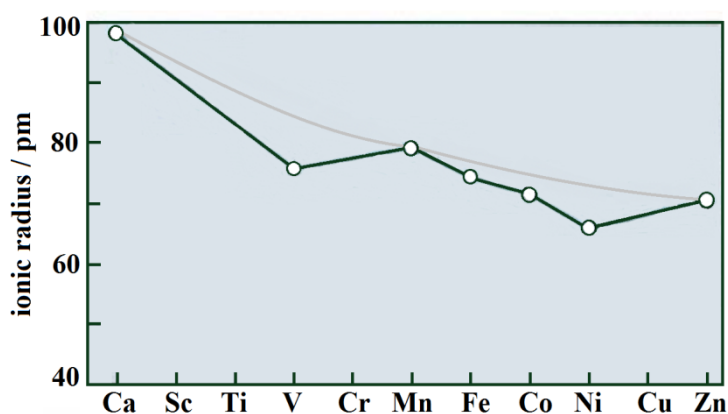


Figure 4.3: Ionic radii of the divalent ions of calcium and the first-row transition metals.¹⁸

Generally, $4d$ and $5d$ metals possess larger Δ_O -values than the $3d$ metals. Therefore, complexes of these metals commonly possess electron configurations typical of strong

ligand fields. **Table 4.1** explains the effect of ligands on the splitting parameters Δ_O of ML_6 complexes.¹³

Table 4.1: Ligand-field splitting parameters Δ_O in cm^{-1} of ML_6 complexes¹⁹

	<i>Ions</i>	<i>Ligands</i>				
		<i>Cl⁻</i>	<i>H₂O</i>	<i>NH₃</i>	<i>en</i>	<i>CN⁻</i>
d^3	<i>Cr³⁺</i>	13 700	17 400	21 500	21 900	26 600
d^5	<i>Mn²⁺</i>	7500	8500		10 100	30 000
	<i>Fe³⁺</i>	11 000	14 300			35 000
d^6	<i>Fe²⁺</i>		10 400			32 800
	<i>Co³⁺</i>		20 700	22 900	23 200	34 800
	<i>Rh³⁺</i>	20 400	27 000	34 000	34 600	45 500
d^8	<i>Ni²⁺</i>	7500	8500	10 800	11 500	

Because the d -orbitals in a complex do not all possess the similar energy, the ground-state electron configuration of a complex is no longer directly obvious. To predict it, the d -orbital energy level illustration shown in **Figure 4.2** is used as a basis for applying the building-up principle. Obviously, the lowest energy configuration bound by the Pauli Exclusion Principle, a maximum of two electrons in an orbital, and if more than one degenerate orbital is obtainable, to the obligation that electrons first occupy separate orbitals and do so with parallel spins.

The strength of the crystal field, as restrained by the value of Δ_O , and the spin-pairing energy, a strong Columbic repulsion, rely on the identity of both the metal and the ligand, so it is impossible to stipulate a general point in the spectrochemical series at which a complex alters from high spin to low spin.

Through a suitable selection of ligands and/or metal ions, such factors as the size, structure, and electric charge and its distribution on the solute surface can be changed methodically. In the conformational analysis of metal chelates, the relatively simple tris ethylenediamine ($NH_2CH_2CH_2NH_2$) complexes have received remarkable attention. In these complexes there are two ways that the carbon-carbon bond of the ethylenediamine ring can bend to reach the unstrained gauche conformation. In the first of these the carbon-carbon bond is nearly parallel to the three-fold axis of the metal complex, and in the second it forms an obtuse angle with this axis. Trisdiamine complexes of chromium (III) have been important from several perspectives. First, the tris-ethylenediamine

complex is valuable as a synthetic intermediate, the action of heat on the chloride salt giving the cis-dichlorobis ethylenediamine complex, and on the thiocyanate salt giving the trans-di-isothiocyanato- complex. Secondly, the cations are resolvable, and studies of their optical activity have been creative.²⁰ A large number of other studies have used these complexes, including kinetic and equilibrium work, which revealed the ready hydrolysis to bis-ethylenediamine complexes. The standard synthetic routes, although chemically simple, are operationally tedious.²¹

4.3 Colour of transition-metal coordination compounds

Transition metal compounds are very often coloured, while the metals and metalloids of the *s* and *p* blocks form colourless compounds. For instance, the nitrate salts of Fe^{3+} , Co^{2+} , Ni^{2+} and Cu^{2+} all form metal aqua complexes of the type $[\text{M}(\text{OH}_2)_n]^{m+}$. Therefore, colour change is a typical characteristic signal of change in the coordination sphere for metal complexes that absorb light in the visible region.

It is not easy to determine accurately the factors which govern the size of Δ_{O} . For octahedral compounds of most first-row transition metal ions, the presence of colour proposes that in some way part of the visible, white, light spectrum is being removed. This can be visualised if the energy gap between the diagonal, t_{2g} , and axial, e_g , levels associates with the visible region, leading to absorption of a nominated part of the visible light that occurs to cause the complex to undergo electron raise from the lower to the higher energy level. Merely by observing the change in colour as ligands are changed, we can determine the energy gap Δ_{O} applying for any ligand set. The stronger the crystal field, the larger Δ_{O} and hence the more energy is required to excite an electron, leading to a higher energy transition, seen experimentally as a shift of the absorbance peak maximum to shorter wavelength. This permits us to rank certain ligands in terms of their ability to separate the diagonal and axial energy levels.

We need to be conscious that the deletion of light of a particular wavelength from incident white light results in the remaining light being apparent as possessing its complementary colour.

Therefore, we only detect colours when one or more of the wavelengths in the visible spectrum have been absorbed, and thus removed, by interaction with some chemical species. When the wavelengths of one or more colours are absorbed, it is the colours on the opposite side of the colour wheel that are transmitted. When light passes through a

solution containing transition metal complexes, we see those wavelengths of light that are transmitted.¹³

Ligand exchange causes strong variations in a complex, as seen when commencing with aqua metal ions. When, for instance, the water ligand is replaced by other ligands (typical donors are halide ions and O-donor, N-donor, S-donor and P-donor groups), in monodentate or polydentate ligands, noticeable physical changes happen. Colour and redox potential change with ligand substitution for instance $[\text{Co}(\text{OH}_2)_6]^{3+}$ is light blue, with a reduction potential E° of +1.8 V (making it unstable in solution, as it oxidizes the solvent slowly); $[\text{Co}(\text{NH}_3)_6]^{3+}$ is yellow, and E° is shifted considerably to 0.0 V (making it stable to reduction in solution). Occasionally, the change of ligand can cause a gross change in molecular shape also; light pink, octahedral $[\text{Co}(\text{OH}_2)_6]^{2+}$ changes to purple, tetrahedral $[\text{CoCl}_4]^{2-}$ when water ligands are substituted entirely by chloride ions.²²

We can see the effect of ligands on the splitting by examining a straight example, the d^3 system. For Cr (III), the difference in colour with ligand type is clearly identified, as complexes absorb in the visible region of the electromagnetic spectrum. The size of Δ_o for d^3 is simply determined from the place of the lowest energy absorption maxima, and follows the trend shown in **Table 4.1**. It is clear that there is a difference with ligand that is rather considerable; additionally, as the charge on the metal ion increases, the size of the splitting increases. Basically, with complex geometry and ligand donor set held constant, the variation with metal ion for a range of ligands is relatively constant and of the order for selected metal ions.²²

It has been stated that the d orbitals and the electron configuration of an isolated central atom (or transition metal ion). For instance, Cr^{3+} has a d^3 electron configuration with three unpaired electrons in three of the five d orbitals. In a compound, the central ion is bounded by ligands; these ligands utilise a ligand field on the central ion and, hence, affect the energy of the d orbitals. Such effects are covered in ligand-field theory. The basis of these phenomena can be expected by considering what happens to the d orbitals when a coordination complex forms. **Figure 4.1** explains the shapes of the five d orbitals and their spatial relation to ligand on the x -, y - and z - axes. The key point here is the orientation of these orbitals. However, the influence on the d orbitals relies on geometry. In the model of an octahedral complex utilised in crystal field theory, six point negative charges demonstrating the ligands are located in an octahedral array around the central metal ion. The crystal- field theory, assumes that there will be important electron-electron repulsion between the electron pair the ligands donate and

any electrons already in the metal d orbitals. This will raise the energy levels of all d orbitals. In a spherical ligand field the d orbitals will stay degenerate, possessing a higher energy associated with those in the free ion. In an octahedral ligand field, a greater repulsion is felt by those d orbitals directed most closely at the ligands. For instance, in the series of compounds $[\text{CoX}(\text{NH}_3)_5]^{n+}$ with $\text{X} = \text{I}^-$, Br^- , Cl^- , H_2O , and NH_3 , the colours range from purple (for $\text{X} = \text{I}^-$) through pink (for Cl^-) to yellow (with NH_3). This order shows that the energy of the lowest energy electronic transition (and therefore Δ_{O}) increases as the ligands are changed along the series. The same order is followed irrespective of the identity of the metal ion.

4.4 Eutectic mixtures based on urea and $[\text{Cr}(\text{en})_3]\text{Cl}_3 \cdot 3\text{H}_2\text{O}$

$[\text{Cr}(\text{en})_3]\text{Cl}_3 \cdot 3\text{H}_2\text{O}$ was prepared according to the method of Rollinson and Bailar.^{23, 24} granular zinc, (1 g) $\text{CrCl}_3 \cdot 6\text{H}_2\text{O}$ (2.66 g), ethylene diamine ($\text{NH}_2\text{CH}_2\text{CH}_2\text{NH}_2$) (10 mL) and methanol (10 mL) were refluxed for one hour. The solution was then cooled to room temperature and the yellow product collected by filtration. The composition was confirmed using x-ray crystallography. The complex is iso-structural and is composed of octahedral $[\text{Cr}(\text{en})_3]^{3+}$ cations and Cl^- ions linked by hydrogen bonds. The waters of hydration are also linked to each other by hydrogen bonds, but no bonds exist between the complex and the H_2O molecules. The octahedron $[\text{Cr}(\text{en})_3]^{3+}$ is more distorted and larger than the $[\text{Co}(\text{en})_3]^{3+}$ cation equivalent.²⁵

The mixture of the novel system can be prepared by mixing the metal salt, $[\text{Cr}(\text{en})_3]\text{Cl}_3 \cdot 3\text{H}_2\text{O}$, with the complexing agent, urea as a hydrogen bond donor. In order to facilitate preparation of the mixture, the components may be heated together at elevated temperature, such as any temperature from 323 K to 333 K. The molar ratio of $\text{CrCl}_3 \cdot 6\text{H}_2\text{O}$ to urea is any value in the range from 1:1 to 4:1 (urea: $[\text{Cr}(\text{en})_3]\text{Cl}_3 \cdot 3\text{H}_2\text{O}$) and 1:2 to 1:3 (urea: $[\text{Cr}(\text{en})_3]\text{Cl}_3 \cdot 3\text{H}_2\text{O}$). The deep eutectic mixture, i.e. the mixture of $2[\text{Cr}(\text{en})_3]\text{Cl}_3 \cdot 3\text{H}_2\text{O}$ and urea) (**Figure 4.4**) having the lowest freezing point. Without wishing to be bound by theory, it is believed that the mixtures of the novel system possess low freezing points (i.e. they are low temperature ionic liquids) due to the unexpected occurrence of a disproportionation process when the metal salt, $[\text{Cr}(\text{en})_3]\text{Cl}_3 \cdot 3\text{H}_2\text{O}$, is contacted with the half molar equivalents of the complexing agent, urea.



Figure 4.4: The DES is formed by mixing the two solids together with moderate heating.

4.5 Physical properties

4.5.1 Phase behaviour

Melting points (T_m) and glass-transition temperatures (T_g) of each examined composition were determined by differential scanning calorimetry (DSC) to establish its binary solid–liquid equilibrium phase diagram. **Figure 4.5** shows the phase diagram for the DES formed between $[\text{Cr}(\text{en})_3] \text{Cl}_3 \cdot 3\text{H}_2\text{O}$ and urea as the HBD. The eutectic composition is formed at 67 mol% $[\text{Cr}(\text{en})_3] \text{Cl}_3 \cdot 3\text{H}_2\text{O}$. Comparing these data with the $\text{CrCl}_3 \cdot 6\text{H}_2\text{O}$ and urea data in the previous chapter and the choline chloride and $\text{CrCl}_3 \cdot 6\text{H}_2\text{O}$ reported previously²⁶ it can be seen that the eutectic point occurred at the same Cr composition i.e. 67 mol%. All three systems have eutectic freezing points in the region of 282–285 K (9 to 12 °C).

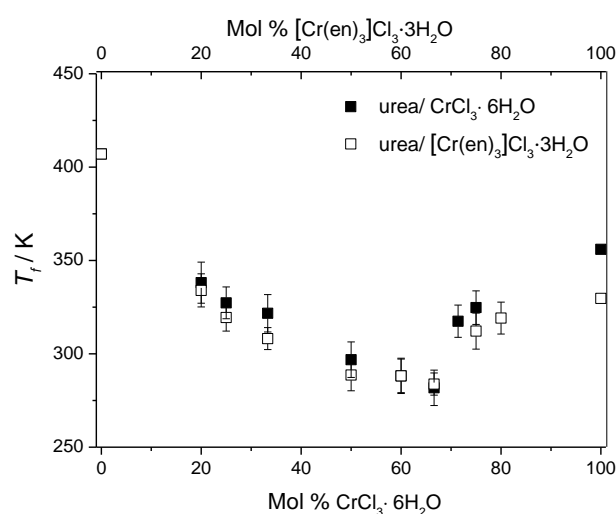


Figure 4.5: Melting points of urea: $[\text{Cr}(\text{en})_3] \text{Cl}_3 \cdot 3\text{H}_2\text{O}$ as a function of composition together with those for the urea: $\text{CrCl}_3 \cdot 6\text{H}_2\text{O}$ system for comparison.

In all systems, the original reduction in the melting points up to the eutectic compositions is caused not only by the interaction between the components, but also the formation of the complex ions that are the basis of the DES. At the eutectic composition, the species have the smallest degree of interaction between the cation and anion and thus the lowest melting point.

4.5.2 Viscosity

As it has been stated that DESs are, in general, relatively viscous compared with molecular liquids.²⁷ **Figure 4.6** shows viscosity of the urea: $[\text{Cr}(\text{en})_3]\text{Cl}_3 \cdot 3\text{H}_2\text{O}$ mixtures as a function of composition and temperature. Unlike the $\text{ChCl}:\text{CrCl}_3 \cdot 6\text{H}_2\text{O}$ mixtures where the maximum conductivity and minimum viscosity occur at the eutectic composition when the $[\text{Cr}(\text{en})_3]\text{Cl}_3 \cdot 3\text{H}_2\text{O}$ complex is used the maximum conductivity and minimum viscosity occur at the lowest metal complex content. This is unusual as this is also when there are the least charge carriers in the system. It is often the case with these types of liquids that conductivity is unrelated to the number of charge carriers but rather it is controlled by the mobility of the charge carriers. This behaviour has previously been discussed in terms of hole theory i.e. the ability of the free space in the liquid to move.^{28, 29}

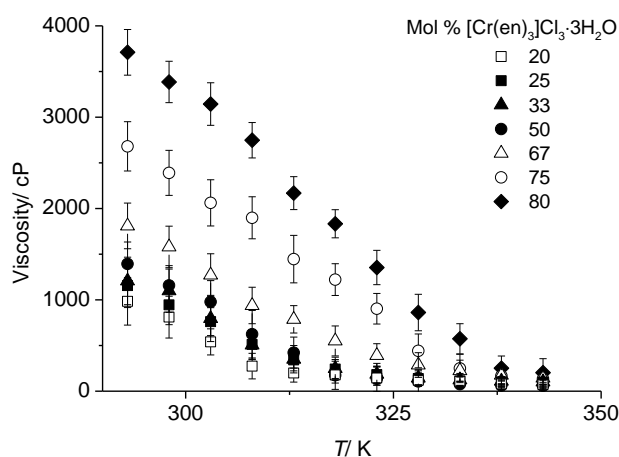


Figure 4.6: Viscosity of urea: $[\text{Cr}(\text{en})_3]\text{Cl}_3 \cdot 3\text{H}_2\text{O}$ as a function of temperature and composition

For a wide range of DESs, viscosity decreases in an exponential manner with increasing temperature.²⁷ However, this is not the case for the majority of the compositions described here and especially not for the mixtures with high chromium salt content, as shown in **Figure 4.6**.

The viscosity of the medium is reduced as the mole fraction of $[\text{Cr}(\text{en})_3]\text{Cl}_3 \cdot 3\text{H}_2\text{O}$ decreases. The minimum viscosity is not observed at the eutectic composition, which is what is observed for all other DESs systems studied to date.³⁰⁻³² It should however be noted that the viscosity of these Type 4 eutectics is considerably lower compared to Type 2 DESs, *e.g.* $\text{ChCl} : \text{CrCl}_3 \cdot 6\text{H}_2\text{O}$,²⁶ and Type 4 DESs, *e.g.* $\text{urea} : \text{CrCl}_3 \cdot 6\text{H}_2\text{O}$ and $\text{urea} : \text{ZnCl}_2$, previously reported.^{30, 32} At 293 K the viscosity of the **ChCl**: $\text{CrCl}_3 \cdot 6\text{H}_2\text{O}$ system at the eutectic composition (1:2) is 4800 cP and the **urea**: $\text{CrCl}_3 \cdot 6\text{H}_2\text{O}$ is 2602 cP (1:2) while the **urea**: $[\text{Cr}(\text{en})_3] \text{Cl}_3 \cdot 3\text{H}_2\text{O}$ is 1394 cP (1:2). This reduction in viscosity means improved mass transport and should cause an increase in electrical conductivity. The change in viscosity, η with temperature can be described **Equation 3.2** in previous chapter.

Applying **Equation 3.2** to the data in **Figure 4.6** the E_η were calculated and are shown in **Table 4.2**. The obtained data compared with analogues $\text{urea} : \text{CrCl}_3 \cdot 6\text{H}_2\text{O}$ system. Earlier studies have shown that the E_η values for ionic liquids are noticeably larger than traditional liquids and high temperature molten salts.²⁷ This is caused by the large ion to hole radius ratio in ionic solvents. It has been shown empirically that E_η values are related to the melting point of liquids (T_m) by **Equation 3.3**.³³

This has been found to be accurate for a range of molecular liquids and high-temperature molten salts.³³ This would propose an E_η value of approximately 10 kJmol^{-1} for the $\text{urea} : [\text{Cr}(\text{en})_3]\text{Cl}_3 \cdot 3\text{H}_2\text{O}$ mixtures, which is significantly smaller than that shown in **Table 4.2**. The values for the chromium containing liquid are, however, similar to other room-temperature ionic liquids. Branco *et al.*³⁴ described the viscosity of a variety of imidazolium salts and through these data the energy for activation of viscous flow was found to range from 37.2 (C_4mimBF_4) to 59.7 kJmol^{-1} ($\text{C}_5\text{O}_2\text{mimCl}$).

The Abbott group²⁶ showed that the empirical relationship observed in **Equation 3.3** for molecular liquids and high temperature molten salts, is not valid for ambient temperature ionic liquids and may result from the large size of the solvent ions found in the latter.

Table 4.2: Activation energies for viscous flow (E_η) and conductivity (E_A) as a function of liquid composition for the novel system compared with other DES systems. Coefficients of correlation (r) for the fits to **Equations 4.1** and **4.3**.

DESs	E_η [kJ·mol ⁻¹]	r	E_A [kJ·mol ⁻¹]	$-r$
urea: [Cr(en) ₃]Cl ₃ ·3H ₂ O				
1:4	49.2	0.962	23.5	0.975
1:3	53.0	0.903	20.2	0.953
1:2	60.9	0.976	18.8	0.964
1:1	45.1	0.992	19.4	0.958
2:1	46.3	0.982	20.3	0.974
3:1	44.7	0.967	19.2	0.975
4:1	46.2	0.984	18.4	0.967
urea: CrCl ₃ ·6H ₂ O ³²				
1:3	53.4	0.973	18.2	0.990
1:2	57.3	0.986	13.7	0.994
3:1	45.2	0.991	18.3	0.995
4:1	46.8	0.964	17.5	0.987

4.5.3 Conductivity

Figure 4.7 shows the conductivity of the urea: [Cr(en)₃]Cl₃·3H₂O system as a function of temperature and composition. Conductivity increases with temperature in a linear fashion for all compositions, whilst in most other DESs the conductivity increases exponentially with temperature.²⁷ Unlike viscosity, conductivity does not change regularly as the mole fraction of [Cr(en)₃]Cl₃·3H₂O increases. The highest conductivity is observed for the 4:1 urea: [Cr(en)₃]Cl₃·3H₂O composition, which is also the least viscous. This indicates that ionic mobility rather than the concentration of charge carriers is most important in controlling conductivity. This is common to other eutectic mixtures³² and ionic liquids and a strong indication for the applicability of hole-theory to describe transport properties.^{28, 35}

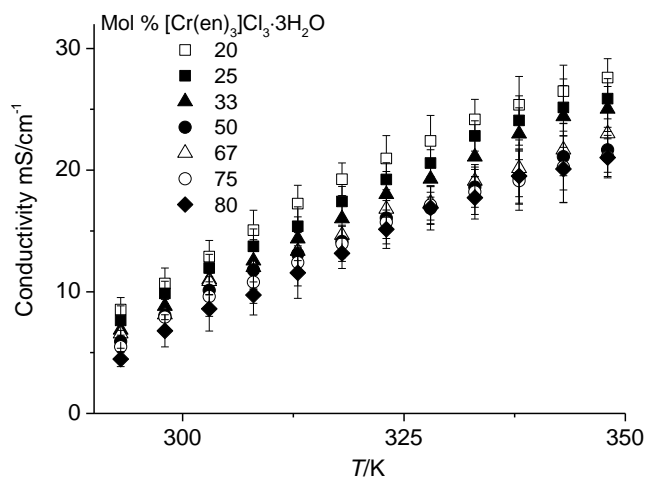


Figure 4.7: Conductivity of urea: $[\text{Cr}(\text{en})_3]\text{Cl}_3 \cdot 3\text{H}_2\text{O}$ as a function of temperature and composition.

It should be noted that, as it is shown in **Figure 4.8**, the magnitude of the conductivity is higher than any other DES reported to date. At 313 K (40°C) for example, conductivities of the urea: $[\text{Cr}(\text{en})_3]\text{Cl}_3 \cdot 3\text{H}_2\text{O}$ are twice those of the urea: $\text{CrCl}_3 \cdot 6\text{H}_2\text{O}$ system (5 mS cm^{-1}) and an order of magnitude larger than those of the analogous $\text{ChCl}:\text{CrCl}_3 \cdot 6\text{H}_2\text{O}$ (0.4 mS cm^{-1}).^{26, 32} This is surprising given the smaller number of waters of hydration and the larger cationic species. It should, however be noted that the cationic species clearly has a 3+ charge and none of the halide anions are complexed with the chromium centre so there are more charge carriers per mole of chromium. It is probably for this reason that the viscosity increases as the concentration of $[\text{Cr}(\text{en})_3]\text{Cl}_3 \cdot 3\text{H}_2\text{O}$ increases since the high cationic charge will cause increased ionic interactions. This is, to our knowledge, the first time that a tricationic species has been reported in this type of fluid. Binnemans *et al.* have however reported a eutectic formed between copper (II) bistriflamide and acetonitrile forming the complex dication $[\text{Cu}(\text{ACN})_4]^{2+}$.³⁶

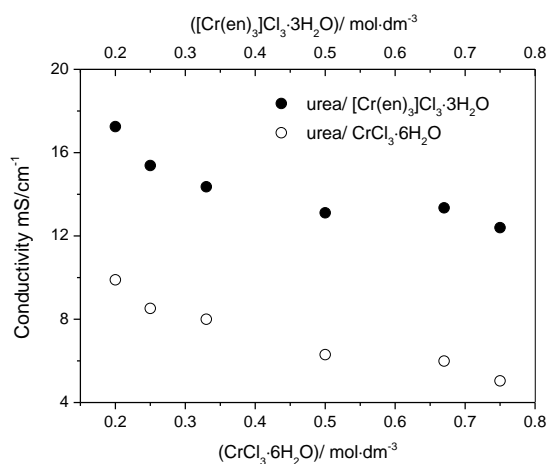


Figure 4.8: The conductivity of $[\text{Cr}(\text{en})_3]\text{Cl}_3\cdot 3\text{H}_2\text{O}$ based DES and $\text{CrCl}_3\cdot 6\text{H}_2\text{O}$ based DES as a function of $[\text{Cr}(\text{en})_3]\text{Cl}_3\cdot 3\text{H}_2\text{O}$ and $\text{CrCl}_3\cdot 6\text{H}_2\text{O}$ concentration, at 313K.

An equivalent expression to **Equation 3.2** has been shown to valid for the variation of conductivity, σ , with temperature (i.e. **Equation 3.4**).³³

The activation energy for conduction (E_A) is listed in **Table 4.2** as a function of composition. Similar to the E_η values, they are to some extent larger than the analogues urea: $\text{CrCl}_3\cdot 6\text{H}_2\text{O}$ ³² system and they are considerably larger than high-temperature molten salts (usually group I halides have values of 5 to 20 $\text{kJ}\cdot\text{mol}^{-1}$).³⁷

For ionic fluids, the conductivity is normally controlled by the mobility of the charge carriers. Therefore a plot of conductivity versus fluidity must be linear for a certain charge carrier. Although the case of chromium, is to some extent complex, because of the different ligand arrangements, that are conceivable.

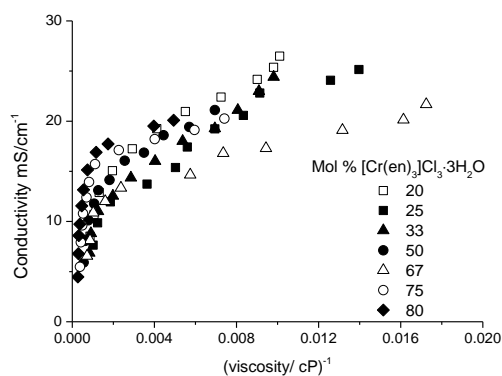


Figure 4.9: Conductivity as a function of $1/\text{viscosity}$ for the data in Figures 3.3 and 3.4a

Figure 4.9 shows a complex relationship between conductivity and the reciprocal of viscosity (i.e. fluidity) and to investigate this further it is more informative to analyse the molar conductivity as a function of fluidity.

4.5.4 Molar conductivity

The Walden rule $\Lambda\eta = \text{constant}$ is frequently applied to ILs, and has been used to analyse ion pairing issues. If the viscosity and conductivity of the electrolyte follows Walden's rule, the ionic conductivity is linked to viscosity using the qualitative method of Angell.³⁸

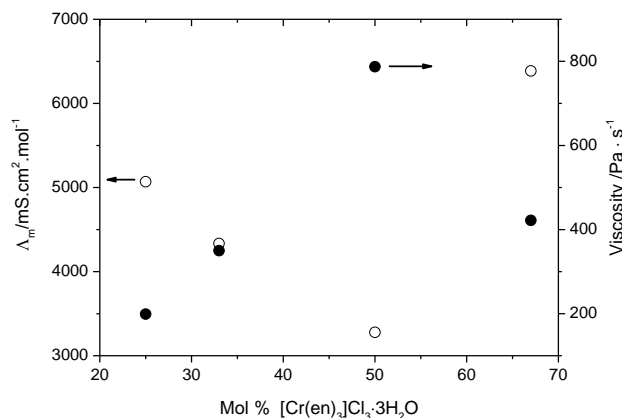


Figure 4.10: Molar conductivity and viscosity as a function of composition for the urea: $[\text{Cr}(\text{en})_3] \text{Cl}_3 \cdot 3\text{H}_2\text{O}$ system at 313 K.

In aqueous solutions molar conductivity is usually observed to decrease, because of ionic atmosphere and ion pairing effects, as the electrolyte concentration is increased.³³

We have seen in the case of viscosity, **Figure 4.6**, an increase in the viscosities as more $[\text{Cr}(\text{en})_3] \text{Cl}_3 \cdot 3\text{H}_2\text{O}$ was added. While the inverse trend could be seen in the case of conductivity, this would be expected since more charge carrying species are being added to the system. Perhaps this can be seen more clearly in **Figure 4.10** by simply plotting the data at 313 K.

This is thought to be because of the effect of viscosity being greater than the effect of conductivity on the system after more than 33 % $[\text{Cr}(\text{en})_3] \text{Cl}_3 \cdot 3\text{H}_2\text{O}$ is added. Although there are more charge carrying species ($[\text{Cr}(\text{en})_3] \text{Cl}_3 \cdot 3\text{H}_2\text{O}$) in the system, the viscosity of the system slows down the flow of ions through the system. This proposes that the motion of ions in these liquids may be different to other eutectic solvents.

These share the high metal concentrations of type 2 eutectics but have the technological advantage of much lower viscosities. Deposition from these liquids is only possible for certain compositions (e.g. urea: $[\text{Cr}(\text{en})_3] \text{Cl}_3 \cdot 3\text{H}_2\text{O} > 1:1$) and these coincide with a changes in important physical properties like conductivity or viscosity (**Figure 4.10**).

The viscosity and conductivity of ionic liquids are main part physical properties which can be measured to result from the relative mobility of the ionic species present.

Nevertheless, few efforts have been made to precisely model the mass transport properties of ionic liquids at ambient temperatures. Research into this area has been slowed down by the complexity of the ionic interactions in ionic liquids.³⁹

Figure 4.11 shows the molar conductivity as a function of fluidity for both the urea: $\text{CrCl}_3 \cdot 6\text{H}_2\text{O}$ and urea: $[\text{Cr}(\text{en})_3]\text{Cl}_3 \cdot 3\text{H}_2\text{O}$ systems. There are several points of note from this figure; the decrease in molar conductivity with decreasing fluidity is not as marked as that observed in ionic liquids with discrete anions.⁴⁰ It is noteworthy not only that the molar conductivity for the $[\text{Cr}(\text{en})_3]^{3+}$ system is higher than that for the CrCl_3 system but also comparing the higher chromium content systems the value for the former is approximately three times the latter which corresponds to the relative charges on the cations. It has previously been shown that the conductivity of ionic liquids can be assumed to follow the Nernst-Einstein equation because charge mobility is limited by the number of suitably sized holes and these are effectively at zero concentration (**Equation 3.5**).²⁹

Using this approach the predicted molar conductivities of urea: $3[\text{Cr}(\text{en})_3]\text{Cl}_3 \cdot 3\text{H}_2\text{O}$ and urea: $3\text{CrCl}_3 \cdot 6\text{H}_2\text{O}$ at 298 K are 4.82 and $1.49 \text{ Scm}^2\text{mol}^{-1}$ compared to the measured values of 5.27 and $1.81 \text{ Scm}^2\text{mol}^{-1}$. This shows that both systems follow the Nernst-Einstein model and the high molar conductivity results from the high cationic charge. In these calculations the radii of the various charge carrying species were determined by the same method as that applied previously⁴¹ $\text{Cr}(\text{en})_3^{3+} = 3.67 \text{ \AA}$, $\text{Cl}^- = 1.81 \text{ \AA}$ and for the purposes of fitting the OD was assumed to be water yielding a radius of $[\text{CrCl}_2(\text{H}_2\text{O})_4]^+$ of 3.12 \AA .

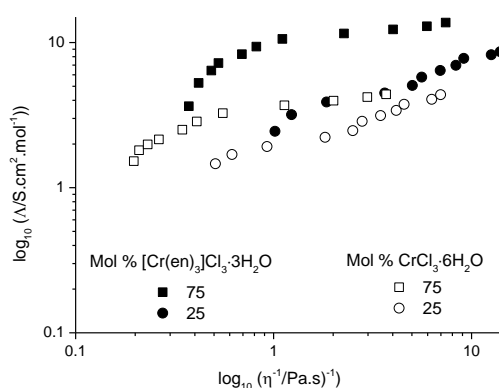


Figure 4.11: Molar conductivity as a function of fluidity for the urea: $\text{CrCl}_3 \cdot 6\text{H}_2\text{O}$ and urea: $[\text{Cr}(\text{en})_3]\text{Cl}_3 \cdot 3\text{H}_2\text{O}$ systems.

4.6 Solution speciation

In order to understand the behaviour of the eutectics it is important to have an sympathetic of the metal species present in the system.

The liquids are highly conducting and, since chromium and chloride ions are the only charge carriers, the conducting species must originate from $[\text{Cr}(\text{en})_3]\text{Cl}_3 \cdot 3\text{H}_2\text{O}$.

4.6.1 UV-visible spectrum

When $[\text{Cr}(\text{en})_3]\text{Cl}_3 \cdot 3\text{H}_2\text{O}$ was mixed with urea an intense red/brown coloured liquid forms slowly. This is somewhat surprising because $[\text{Cr}(\text{en})_3]\text{Cl}_3 \cdot 3\text{H}_2\text{O}$ is a bright-yellow crystalline solid and urea a white crystalline solid. The visible appearance and uv-visible spectra of the liquid is shown in **Figure 4.12**. The intense colour of the urea: $[\text{Cr}(\text{en})_3]\text{Cl}_3 \cdot 3\text{H}_2\text{O}$ mixtures is unusual because $[\text{Cr}(\text{en})_3]\text{Cl}_3 \cdot 3\text{H}_2\text{O}$ forms yellow solutions when dissolved in water or polar organic solvents as shown in **Figure 4.12**.

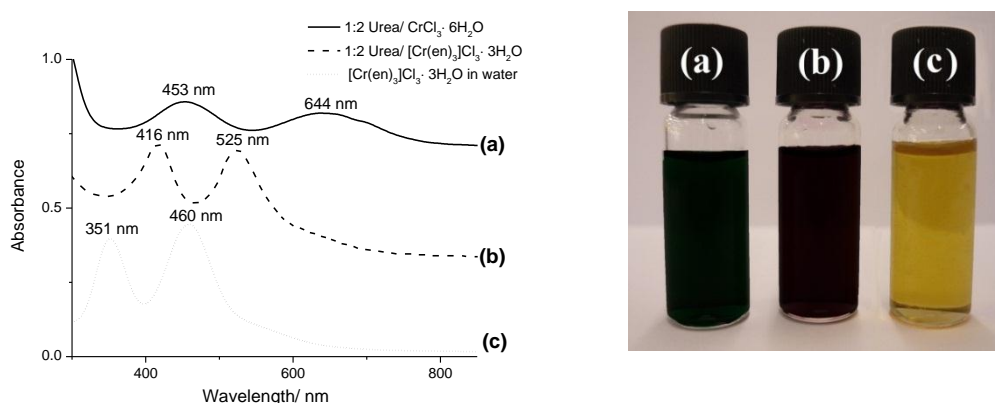


Figure 4.12: *UV-vis spectra of (a) 2:1 urea: $\text{CrCl}_3 \cdot 6\text{H}_2\text{O}$, (b) 2:1 urea: $[\text{Cr}(\text{en})_3]\text{Cl}_3 \cdot 3\text{H}_2\text{O}$ and (c) 10mg $[\text{Cr}(\text{en})_3]\text{Cl}_3 \cdot 3\text{H}_2\text{O}$ in 3ml H_2O*

Comparing the absorbance spectrum of 2 urea: 1 $[\text{Cr}(\text{en})_3]\text{Cl}_3 \cdot 3\text{H}_2\text{O}$ to that without the **en** ligand (**Figure 4.12**) it can be seen that both have two absorbance maxima but they are both shifted by approximately 60 nm. **Figure 4.12** also shows that the absorbance maxima for the $[\text{Cr}(\text{en})_3]\text{Cl}_3 \cdot 3\text{H}_2\text{O}$: 2 urea mixture are much sharper than the corresponding mixture without ethylene diamine as a ligand and this is because the latter system is known to have a variety of chromium species with different amounts of urea, water and chloride bound to the metal centre.

It is suggested that the big shift in absorbance maxima arises from hydrogen bonding between the chloride counter-ions and the ethylene diamine moiety decreasing charge density on the nitrogen. To test this idea a eutectic was made between

$[\text{Cr}(\text{en})_3]\text{Cl}_3 \cdot 3\text{H}_2\text{O}$ and 2 mole equivalents of glycerol as the HBD. This was also intensely brown but as more glycerol was added the liquid turned yellow (**Figure 4.13**).

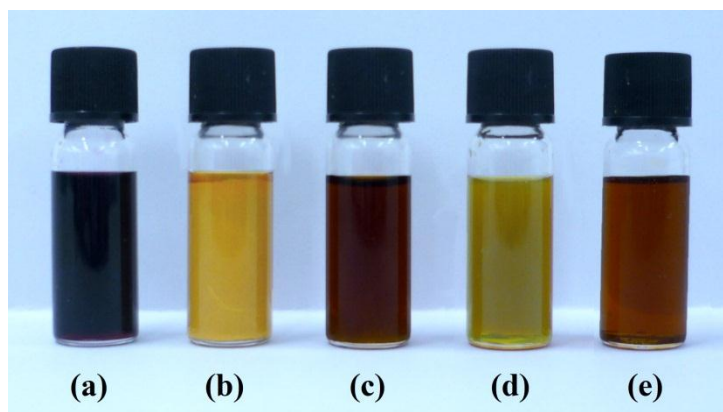


Figure 4.13: (a) 2:1 Urea/ $[\text{Cr}(\text{en})_3]\text{Cl}_3 \cdot 3\text{H}_2\text{O}$, (b) diluted $[\text{Cr}(\text{en})_3]\text{Cl}_3 \cdot 3\text{H}_2\text{O}$ in H_2O , (c) adding HCl to (b), (d) diluted $[\text{Cr}(\text{en})_3]\text{Cl}_3 \cdot 3\text{H}_2\text{O}$ in glycerol (e) adding ChCl to (d)

The addition of choline chloride, (ChCl , $\text{HOC}_2\text{H}_4\text{N}^+(\text{CH}_3)_3\text{Cl}$) to the liquid caused it to turn red/ brown again (**Figure 4.13e**). This was also confirmed by adding concentrated HCl to an aqueous solution of $[\text{Cr}(\text{en})_3]\text{Cl}_3 \cdot 3\text{H}_2\text{O}$ as can be seen from **Figure 4.13b** and **c**. This is a novel solvatochromic shift that we are unaware of in the literature and demonstrates the change in Lewis basicity of the liquid.

4.6.2 EXAFS

EXAFS analysis of the $[\text{Cr}(\text{en})_3]\text{Cl}_3 \cdot 3\text{H}_2\text{O}$: urea systems in the mole ratio 1:2 and 2:1 show what appears to be ethylene diamine coordination with 6 nitrogen and 6 near neighbour carbon atoms. The EXAFS spectra are almost identical at both compositions and show no evidence of chloride ligands being present in the chromium coordination shell. This underpins the origin of the colour change as being a hydrogen bond acceptor issue.

4.7 Density

Unsurprisingly these liquids have extremely high densities which are even higher than the urea: $\text{CrCl}_3 \cdot 6\text{H}_2\text{O}$ system (**Figure 4.14b**).³² In an endeavour to understand the change in conductivity with concentration shown in **Figure 4.7** it is useful to calculate the change in molar volume, or its inverse, molar concentration.

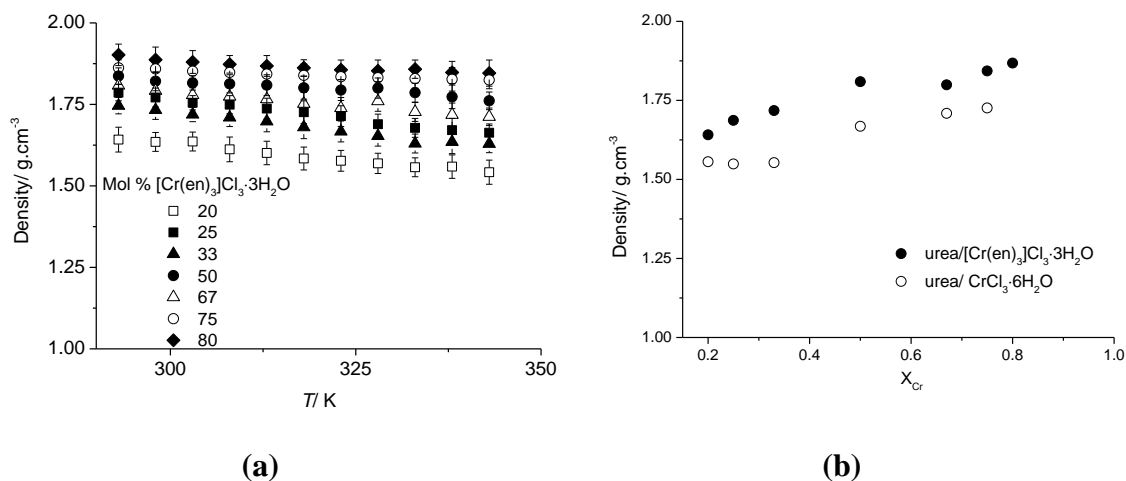


Figure 4.14: (a) Density of the urea: $[\text{Cr}(\text{en})_3]\text{Cl}_3 \cdot 3\text{H}_2\text{O}$ system as a function of temperature and composition. (b) Density of the urea: $[\text{Cr}(\text{en})_3]\text{Cl}_3 \cdot 3\text{H}_2\text{O}$ and urea: $\text{CrCl}_3 \cdot 6\text{H}_2\text{O}$ systems at 313 K as a function of composition.

4.8 Molar volume

The influence of the salt upon the structure of the liquid can be obviously seen by measuring the liquid density. The amount of free volume can be determined using a hard sphere model. Using this approach the fractional molar free volume can be obtained using **Equation 3.17**.

Using the density data shown in **Figure 4.14a** the molar volume V_m can be calculated using **Equation 3.14** and **Equation 3.15**.

Figure 4.15 shows the change in molar volume as a function of composition and it is immediately evident that although the chromium content and hence the number of charge carriers increases the number of charged species per unit volume decrease. This may naturally be expected but it is the extent of this change which is surprising *viz.* the molar volume doubles (and the molar concentration halves) in the concentration range studied.

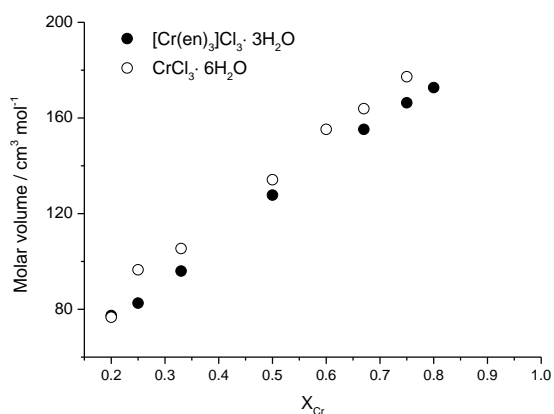


Figure 4.15: Relative changes in liquid molar volume as a function of composition

4.9 Cyclic voltammetry

Figure 4.16 shows the cyclic voltammogram for the urea: $[\text{Cr}(\text{en})_3]\text{Cl}_3 \cdot 3\text{H}_2\text{O}$ system as a function of composition. As the chromium content increases both the anodic and cathodic charge decrease which is counter intuitive as there is more electroactive species in the liquid.

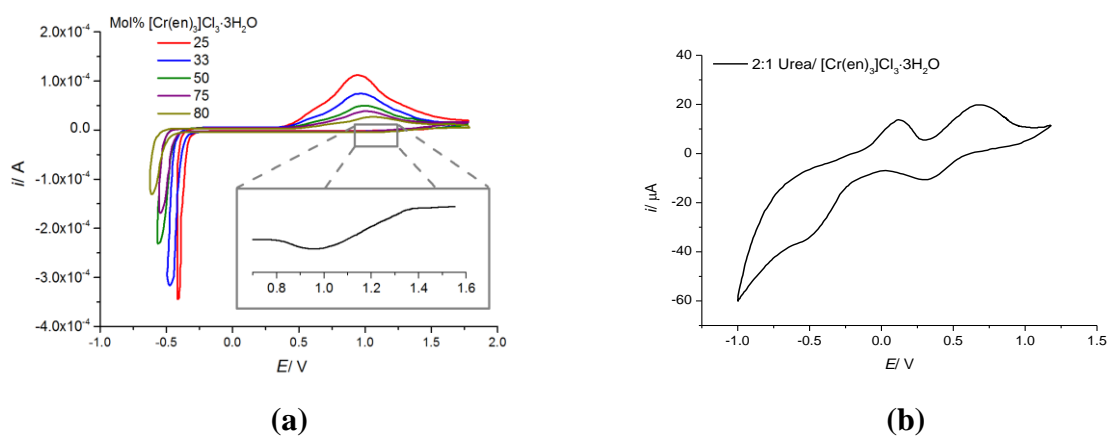


Figure 4.16: (a) Cyclic voltammogram for the urea: $[\text{Cr}(\text{en})_3]\text{Cl}_3 \cdot 3\text{H}_2\text{O}$ system at 40°C on a Pt microelectrode, at a sweep rate of 20 mV s^{-1} for different compositions, and (b) corresponding cv on a GC electrode ($r=1.5\text{ mm}$), at a sweep rate of 10 mV s^{-1}

From the previous discussion this is clearly due to the change in liquid viscosity and hence material growth becomes diffusion controlled. To prove this **Figure 4.18** shows a plot of charge vs $(1/\eta)^{1/2}$ which is clearly linear confirming this idea. The form of the voltammogram in **Figure 4.16a** shows a quasi-reversible deposition process where reduction of the metal complex occurs from Cr^{III} to the metal.

4.9.1 Under-potential deposition (upd)

The understanding of upd metal monolayers is based essentially on two general models, i.e. adsorption models which consider particle-substrate interactions,^{42,43} and two-dimensional (2D) nucleation and growth models leading to phase formation.⁴⁴ Equally, both models were utilised to explain the controlling-rate phase for metal upd at different foreign substrates under distinct electrochemical perturbations. The kinetics of metal upd, on the other hand, frequently appear under a mixed control comprising mass transport, surface adsorption and charge transfer contributions, as shown through rotating ring-disk electrode studies.⁴⁵ The whole process may become even more complex if the upd process involves adsorbate-substrate interactions adequately strong to relocate atoms of the substrate and incite surface rearrangement. Then the slanted metal surface structure eases the penetration of the adsorbate beneath the substrate surface. This can cause a significant change in the electrocatalytic properties of the electrode and ultimately to surface alloy formation. In this case, upd of metal atoms at foreign substrates can cause metastable systems undergoing slow changes of their structure, which can be redirected through their own electrochemical properties, for example through a time-dependent voltammetric response.⁴⁵

The adsorption of metal ions on a foreign metal substrate can have two forms: The Gibbs energy of interaction of the adsorbate with the substrate can be weaker or stronger than the adsorbate-adsorbate interaction. In the first case, weak Gibbs energy, the adsorbate will be deposited at potentials lower than the equilibrium potential ϕ_{00} for bulk deposition and dissolution, and will often form three-dimensional clusters from the start. In the latter case, strong Gibbs energy, the adsorbate can be deposited on the foreign substrate at potentials above ϕ_{00} . This case is recognized as underpotential deposition (upd). In general, up to a monolayer can be formed in this way; in a few cases the adsorbate-substrate interaction is sufficiently strong to allow the deposition of a second layer at potentials slightly above ϕ_{00} .⁴⁶

The energetic features of underpotential deposition can be investigated by a slow potential scan starting, a few mV/sec, at a potential where no adsorption occurs. As the potential is lowered, one or more current peaks are observed, which are caused by the adsorption of the metal ions. Additional peaks may possibly be due to different adsorption sites, or to different structures of the adsorbate layer. If the potential is scanned further past the equilibrium potential ϕ_{00} , the usual bulk deposition is observed.

More willingly than performing a single potential scan, it is common to reverse the direction of the scan at the beginning of the bulk deposition, and to observe the desorption of the adatoms, which gives rise to positive current peaks. The sweep direction is then reversed again at a potential well positive of the desorption, and this process is repeated several times. Consecutive sweeps give identical curves if the reactions that occur in this range are reversible.

The difference between the potential of the current peak for the desorption and the bulk deposition potential is known as the underpotential shift ϕ_{upd} . For simple systems the value of ϕ_{upd} is independent of the concentration of ions in the bulk of the solution, since the Gibbs energies of adsorption and deposition shift both according to the Nernst equation. Deviations from this behaviour may indicate coadsorption of other ions.

During the 1960s and 1970s, before the preparation of single crystal electrodes was well established, many cases of upd were investigated on polycrystalline metals. Remarkably large upd shifts, up to 1 V in aqueous and even higher in non-aqueous solutions, were observed, which correlated quite well with the difference in the work functions of the two metals involved.⁴⁷ No such correlation holds for single crystals, and the data in non-aqueous solvents were found to be incorrect. Further investigations with STM and with x-ray techniques revealed, that several systems that had been thought to be pure metal adsorbate layers really consisted of co-adsorbed metal and anions, structures similar to two-dimensional salts. Consequently, the correlation between the upd shift and the work function on polycrystalline metals is doubtful.

The expression underpotential deposition (upd) represents the deposition of metal ions with a charge of $+ze$ (Me_A^{z+}) on a substrate of a different material, typically another metal Me_S . If the equilibrium potential at which this deposition happens is positive of the equilibrium potential for the formation of the solid phase of the deposited metal, then this phenomenon is named underpotential deposition and the analogical difference is the upd-shift. The cause for the presence of upd is the same as for the filling of a first monolayer (or the chronological filling of more layers) of a rare-gas on a substrate at a pressure beneath the equilibrium pressure of its solid phase. The binding energy between the rare-gas atoms and the substrate is larger than the binding energy in a kink site of the crystalline phase of the rare-gas. For rare-gas/solid interactions, the difference in the binding energy might amount to a factor of two. For metal-on-metal deposition, the modifications are smaller. Due to this smallness, other parameters such as the structure of the upd-layer as a function of the density, or a probable stabilization

of the layer by ions from the electrolyte play a significant role for the size of the upd-shift and as to whether upd take place at all.⁴⁸

The procedures, which are associated, are demonstrated in **Figure 4.17**. The equilibrium between the solid phase and the electrolyte concerns the equilibrium between a metal atom at a Halbkristallage, kink site in half crystal position, and the metal-ion in the electrolyte (**Figure 4.17a**). The reaction between the two states of the metal atom can be written as:



The energies participated in the reaction are the coherent energy, the require energy to remove an electron from the bare atom, the energy to bring the electron from the vacuum level into the solid, and the solvation energy of the metal ion. The electrode potential at which this reaction is in equilibrium is the Nernst-potential.⁴⁸

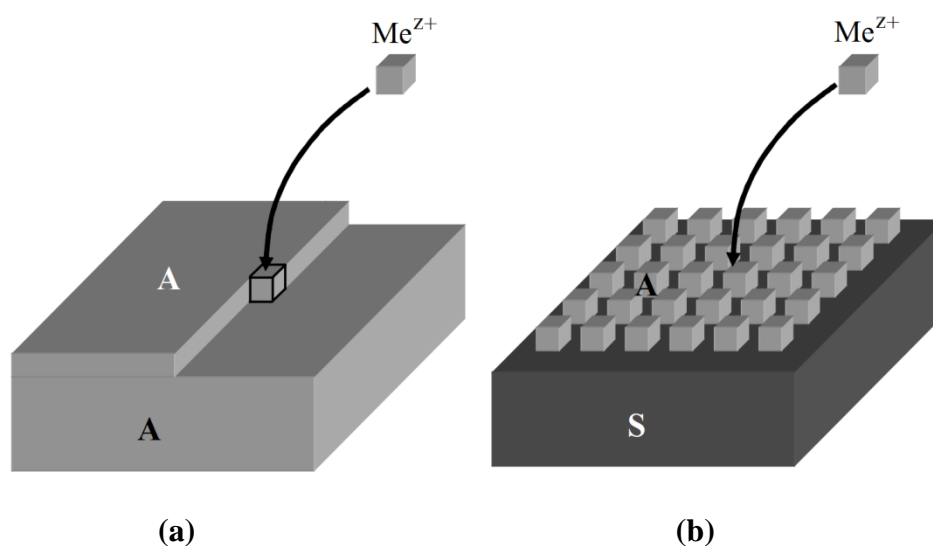


Figure 4.17: (a) *Electrochemical deposition of bulk material A and (b) of a layer of the material A on a substrate S of a different material.*⁴⁸

When **Figure 4.17b** occurs at a potential that is positive of the Nernst-potential of material A it is termed underpotential deposition (upd). The upd-layer is stable in the potential range between the upd-potential and the Nernst potential. Underpotential deposition requires that the mean binding energy for an atom in the upd-layer of material A is larger than the coherent energy (the binding energy to a kink site) of material A.

Therefore, The upd-reaction can be written as:



The equilibrium electrode potential relies on the structure of the substrate and the adsorbed layer. Due to the lateral interactions in the upd-layer, the equilibrium potential also relies on the coverage. Phase transitions in the upd-layer affect the upd-potential in addition to the possible co-adsorption of anions from the electrolyte and the formation of a compound structure with these anions. In other words, upd-layers are even more complex than the usual adsorbate layers. Nevertheless, just as for adsorbate in vacuum one does not need to have the full sympathetic of the difficulty of upd-layers to achieve a qualitative representation of the behaviour of isotherms.

The form of the voltammogram in **Figure 4.16a** shows a quasi-reversible deposition process where reduction of the metal complex occurs from Cr^{III} to the metal. Close inspection shows a small cathodic peak at +1 V corresponding to under-potential deposition (upd) which blocks the electrode such that the Cr^{II} intermediate is not observed. Repeating the experiment for the 2urea: $[\text{Cr}(\text{en})_3] \text{Cl}_3 \cdot 3\text{H}_2\text{O}$ system on a glassy carbon electrode, where upd does not occur, reveals a markedly different voltammogram with two reversible signals corresponding to Cr^{III} reduction to Cr^{II} followed by Cr^{II} reduction to Cr^0 (**Figure 4.16b**).

4.9.2 The effects of the viscosity on the voltammograms

Voltammograms are often affected by the viscosity of the liquid as many processes are diffusion-controlled. Voltammetric peak currents in relatively viscous liquids are proportional to the square-root of the fluidity.

Generally, fluids composed widely of ions are found to be relatively viscous when compared to molecular solvents and conductivity in ionic liquids is found to be relatively low. Studies have shown that there is a linear correlation between the molar conductivity (Λ_m) and the fluidity (η^{-1}) of ionic liquids. Some groups have invoked the empirical Walden rule where for a given electrolyte⁴⁹⁻⁵¹

$$\Lambda_m^0 \eta^0 = \text{constant} \quad \text{Equation 4.4}$$

where Λ_m^0 is the limiting molar conductivity and η^0 is the viscosity. Deviations from

this behaviour have been described in terms of sub-ionic or super-ionic behaviour⁵¹ which arise from ionic association. **Equation 4.4** has its origin in the Nernst–Einstein relation of an electrolyte, which relates the limiting molar conductivity to the diffusion coefficients of its constituent ions.

$$\Lambda_m^0 = \left(\frac{z^2 F^2}{RT}\right)(D_+^0 + D_-^0) \quad \text{Equation 4.5}$$

where z is the charge of the ion, F is the Faraday constant, R is the gas constant, D^0 is the diffusion coefficient of the ions and T the absolute temperature. The Stokes–Einstein relation is typically used to relate the diffusion coefficient to the radius of the diffusing species, r , and the viscosity of the medium,

$$D^0 = \frac{k_B T}{6\pi\eta r_0} \quad \text{Equation 4.6}$$

where r_0 is the hydrodynamic radius of the spherical diffusing particle, and k_B is the Boltzmann constant. **Equation 4.6** has been obtained from the concept that thermal motion of a particle is compensated with the viscous friction.

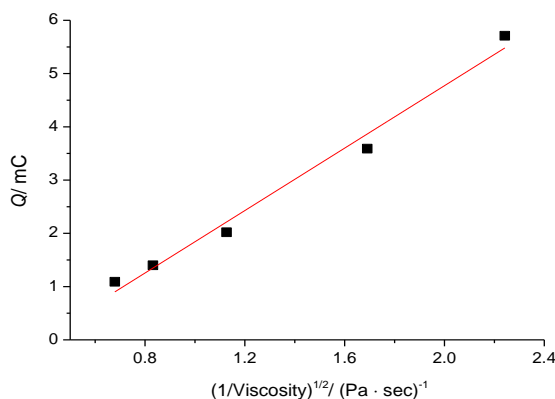


Figure 4.18: Cathodic charge vs $(1/\eta)^{1/2}$ for the data in Figure 4.16a

Figure 4.18 shows a plot of charge vs $(1/\eta)^{1/2}$ for the data in Figure 4.17. The correlation is clearly linear confirming that the process is diffusion controlled.

Combining **Equation 4.5** and **Equation 4.6** yields **Equation 3.5**.

The above equations are resultant for spherical species at infinite dilution in a structureless dielectric or in a medium where the size of the diffusing species is much larger than that of the solvent molecules. Obviously, in an ionic liquid the ions are not at

infinite dilution and hence the validity of any of the above equations can be interrogated. Abbott has recently shown that ion transport in ionic liquids is limited by the availability of holes of suitable size within the structure of ionic liquids.^{28, 29} It is these holes that are at infinite dilution and this is the reason that the behaviour of ionic liquids approximates those defined by **Equation 3.5**.

It has recently been shown that many of the deviations observed from **Equation 4.4** can be accounted for by using **Equation 3.5**. However, studies of the transport behaviour of the constituent ionic liquid ions and both ionic and neutral solutes have shown that translational motion in ionic liquids does not obey the Stokes–Einstein equation.⁵²⁻⁵⁶

If solutions of $[\text{Cr}(\text{en})_3]^{3+}$ in these DESs obey the Stokes–Einstein relationship, then the product $D\eta$ should be constant and a plot of D vs. $1/\eta$ should place each of the data points on a straight line. **Figure 4.19** shows plots of D vs. $1/\eta$, and the relatively good correlation suggests Stokesian behaviour.

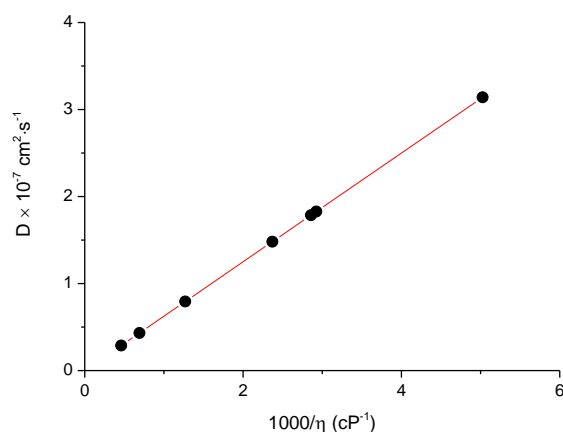


Figure 4.19: Diffusion of $[\text{Cr}(\text{en})_3]^{3+}$ in DES, vs. $1/\eta$ at 313K for the selected composition in Figure 4.16a

The distance term, r_0 , in **Equation 4.13** should strictly be the correlation length, ζ , and this is only equivalent to the radius of the diffusing species when the solvent particles are much smaller than the diffusing species.⁵⁷

Values for the correlation length, ζ , were calculated using:

$$\xi = \frac{k_B T}{6\pi\eta D} \quad \text{Equation 4.7}$$

Measured diffusion coefficient data was used to determine correlation length in the ionic liquid. It is shown that the correlation length yielded by the Stokes–Einstein equation gives information about the structure of an ionic liquid and correlates to the void volume of the liquid, suggesting that mass transport proceeds by a series of jumps between voids of suitable dimensions.⁵⁸

This equates to a hole radius of approximately 4 Å, which is almost exactly the correlation length for $[\text{Cr}(\text{en})_3]^{3+}$ at that temperature. We have shown that we can correlate with the average size of holes, or voids, within the ionic liquid. This interpretation suggests that a model by which a migrating species can jump between voids or holes within the liquid is highly appropriate and is consistent with the observed behaviour measured across a range of temperatures.

4.10 Bulk deposition

For the $\text{ChCl}:\text{CrCl}_3\cdot 6\text{H}_2\text{O}$ and urea: $\text{CrCl}_3\cdot 6\text{H}_2\text{O}$ systems the speciation is dynamic and strongly dependent upon the composition of the surrounding environment.^{26, 32} The speciation in these liquids will change during deposition which will lead to changes in morphology and it is suggested that this is the reason for the black, non-crystalline deposits observed during bulk deposition. In the 2 urea: $[\text{Cr}(\text{en})_3]\text{Cl}_3\cdot 3\text{H}_2\text{O}$ system as the metal is reduced onto the electrode surface en ligands are released into the double layer but these will not affect the speciation of the chromium as it is already completely surrounded by en ligands.

Bulk deposition was carried out using the 2 urea: $[\text{Cr}(\text{en})_3]\text{Cl}_3\cdot 3\text{H}_2\text{O}$ system on a copper substrate using a current density =100 mAcm⁻² for 1 hour at 313 K and the result is shown in **Figure 4.20**. It can clearly be seen that a bright metallic deposit was obtained with a nodular morphology which contrasts strongly with those obtained from the other DESs.

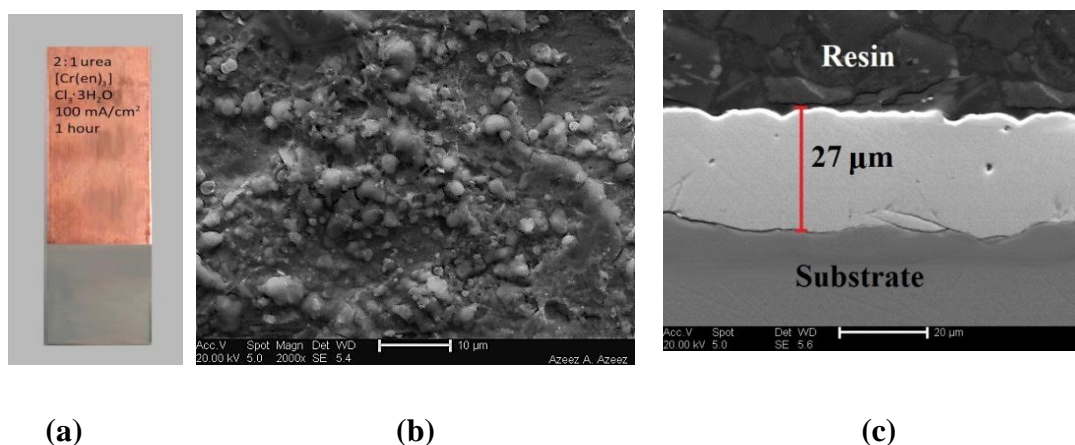


Figure 4.20: (a) Optical photograph and (b) SEM image of chromium deposit (c) cross section obtained from the electroreduction of 2:1 urea: $[Cr(en)_3]Cl_3 \cdot 3H_2O$ on a copper substrate (Current density = 100 mAcm^{-2} for 1 hour at 313 K)

4.11 Hardness and thickness

Hard chromium plate is a deceptive description of the deposit, as the metal deposited is typically no harder than that in bright chromium plate, both being produced under similar conditions. The difference between the two types lies in the thickness of the chromium layer and the purposes for its thickness. While bright chromium has a primarily decorative purpose, the very much thicker hard chromium layer (20 - 100 μm) is directly deposited onto the component substrate and is utilised to improve the mechanical properties to the surface.

The film shown in **Figure 4.20** had an average thickness of 27 μm and a Vickers hardness of $710 \pm 10 \text{ HV}$ which is close to the 800 HV obtained by the conventional aqueous chromic acid process. Commercially produced chromium plate possess harnesses in the range 800- 1100 HV, and is therefore, significantly harder than any other electrolytically deposited metal.⁵⁹ The deposit morphology also contributes to the increase in hardness compared to that obtained using urea: $CrCl_3 \cdot 6H_2O$ systems ($600 \pm 10 \text{ HV}$).³² The sample is not micro-cracked and is very adherent.

4.12 Current efficiency

An electrochemical quartz crystal microbalance, EQCM, was used to determine charge / mass balance for Cr deposition. The current efficiency can be obtained from the slope of the mass *versus* charge plot by comparison with the theoretical value calculated from Faraday's law according to the following equation:

$$\frac{d(\Delta m)}{dq} = \frac{r.a.m}{nF}$$

Equation 4.8

Where, Δm is the change in mass, dq the change in charge $r.a.m$ the relative atomic mass, n is the number of electrons involved in the process and F the Faraday constant. The current efficiency was found to be 98% at a deposition potential of - 0.4 V *versus* a Ag wire quasi-reference electrode. This is considerably higher than that reported for other DESs (typically 65-74%) and contrasts strongly with aqueous chromic acid solutions where current efficiencies are typically 15%.^{26, 32, 60}

4.13 Conclusions

This study has shown that controlling the speciation of a metal ion during electrodeposition can significantly affect the morphology and properties of the metallic film. A trivalent cationic chromium species was produced for a DES for the first time and this had a higher conductivity than any similar liquid previously described. The unusual conductivity as a function of composition was explained in terms of the change in molar volume. Using this liquid bright, adherent, hard chromium was obtained by electroreduction which contrasted with softer, black, less crystalline deposits which were obtained when speciation was less well defined.

4.14 References

1. A. P. Abbott, G. Frisch and K. S. Ryder, *Annu Rev Mater Res*, 2013, **43**, 335-358.
2. P. J. Elving and B. Zemel, *Journal of the American Chemical Society*, 1957, **79**, 1281-1285.
3. H. A. Bethe, *Ann. Phys. LPZ*, 1929, **3**.
4. J. Van Vleck, *Physical Review*, 1932, **41**, 208.
5. R. Schlapp and W. G. Penney, *Physical Review*, 1932, **42**, 666.
6. O. Jordahl, *Physical Review*, 1934, **45**, 87.
7. J. Howard, *The Journal of Chemical Physics*, 1935, **3**, 813-817.
8. J. Van Vleck, *The Journal of Chemical Physics*, 1935, **3**, 807-813.
9. J. Griffith and L. Orgel, *Q. Rev. Chem. Soc.*, 1957, **11**, 381-393.
10. J. Becquerel, *Zeitschrift für Physik A Hadrons and Nuclei*, 1929, **58**, 205-216.
11. D. O. Hayward, *Quantum Mechanics for Chemists*, Royal Society of Chemistry, 2002.
12. P. L. G. F. Albert Cotton, Sir Geoffrey Wilkinson, *BASIC INORGANIC CHEMISTRY, 3RD ED*, Wiley India Pvt. Limited, 2007.
13. P. Atkins, *Shriver and Atkins' Inorganic Chemistry*, OUP Oxford, 2010.
14. J. E. Huheey, E. A. Keiter, R. L. Keiter and O. K. Medhi, *Inorganic Chemistry: Principles of Structure and Reactivity*, Pearson Education, 2006.
15. I. B. Bersuker, *Electronic Structure and Properties of Transition Metal Compounds: Introduction to the Theory*, Wiley, 2010.
16. D. F. Shriver and P. W. Atkins, *Inorganic Chemistry*, W.H. Freeman and Company, 1999.
17. R. G. Burns, *Mineralogical Applications of Crystal Field Theory*, Cambridge University Press, 1993.
18. R. Janes and E. A. Moore, *Metal-ligand Bonding*, Royal Society of Chemistry, 2004.
19. H. B. Gray, *Electrons and chemical bonding*, W. A. Benjamin, 1964.
20. C. Rollinson and J. Bailar, *Vol. 2 McGraw-Hill, New York*, 1946, 196-202.
21. K. N. Raymond, P. W. R. Corfield and J. A. Ibers, *Inorganic chemistry*, 1968, **7**, 842-844.
22. G. A. Lawrance, *Introduction to Coordination Chemistry*, Wiley, 2013.
23. C. L. Rollinson and J. C. Bailar Jr, *Journal of the American Chemical Society*, 1943, **65**, 250-254.
24. H. Gutowsky, *The Journal of Chemical Physics*, 1949, **17**, 128-138.
25. A. Whuler, C. Brouty, P. Spinat and P. Herpin, *Acta Crystallographica Section B: Structural Crystallography and Crystal Chemistry*, 1975, **31**, 2069-2076.
26. A. P. Abbott, G. Capper, D. L. Davies and R. K. Rasheed, *Chemistry – A European Journal*, 2004, **10**, 3769-3774.
27. A. P. Abbott, D. Boothby, G. Capper, D. L. Davies and R. K. Rasheed, *Journal of the American Chemical Society*, 2004, **126**, 9142-9147.
28. A. P. Abbott, *Chemphyschem*, 2004, **5**, 1242-1246.
29. A. P. Abbott, *Chemphyschem*, 2005, **6**, 2502-2505.
30. A. P. Abbott, J. C. Barron, K. S. Ryder and D. Wilson, *Chemistry – A European Journal*, 2007, **13**, 6495-6501.
31. A. P. Abbott, G. Capper, D. L. Davies, R. K. Rasheed and V. Tambyrajah, *Chem Commun*, 2003, 70-71.
32. A. P. Abbott, A. A. Al-Barzinjy, P. D. Abbott, G. Frisch, R. C. Harris, J. Hartley and K. S. Ryder, *Phys Chem Chem Phys*, 2014, **16**, 9047-9055.

33. J. O. M. Bockris and A. K. N. Reddy, *Volume 1: Modern Electrochemistry: Ionics*, Springer, 1998.
34. L. C. Branco, J. N. Rosa, J. J. Moura Ramos and C. A. Afonso, *Chemistry-a European Journal*, 2002, **8**, 3671-3677.
35. A. P. Abbott, R. C. Harris, K. S. Ryder, C. D'Agostino, L. F. Gladden and M. D. Mantle, *Green Chem*, 2011, **13**, 82-90.
36. N. R. Brooks, S. Schaltin, K. Van Hecke, L. Van Meervelt, K. Binnemans and J. Fransaer, *Chemistry-a European Journal*, 2011, **17**, 5054-5059.
37. G. J. Janz, *Molten Salts Handbook*, Elsevier Science, 2013.
38. M. Yoshizawa, W. Xu and C. A. Angell, *Journal of the American Chemical Society*, 2003, **125**, 15411-15419.
39. P. Wasserscheid and T. Welton, *Ionic liquids in synthesis*, Wiley Online Library, 2008.
40. D. R. MacFarlane, M. Forsyth, E. I. Izgorodina, A. P. Abbott, G. Annat and K. Fraser, *Phys Chem Chem Phys*, 2009, **11**, 4962-4967.
41. A. P. Abbott, R. C. Harris and K. S. Ryder, *The Journal of Physical Chemistry B*, 2007, **111**, 4910-4913.
42. W. Lorenz, H. Hermann, N. Wüthrich and F. Hilbert, *J Electrochem Soc*, 1974, **121**, 1167-1177.
43. K. Engelsmann, W. Lorenz and E. Schmidt, *Journal of Electroanalytical Chemistry and Interfacial Electrochemistry*, 1980, **114**, 1-10.
44. A. Bewick and B. Thomas, *Journal of Electroanalytical Chemistry and Interfacial Electrochemistry*, 1977, **85**, 329-337.
45. S. Swathirajan and S. Bruckenstein, *J Electrochem Soc*, 1982, **129**, 1202-1210.
46. W. Schmickler and E. Santos, *Interfacial Electrochemistry*, Springer, 2010.
47. H. Gerischer and C. W. Tobias, *Advances in Electrochemistry and Electrochemical Engineering*, John Wiley & Sons, 1984.
48. H. Ibach, *Physics of Surfaces and Interfaces*, Springer, 2006.
49. C. A. Angell, N. Byrne and J.-P. Belieres, *Accounts of chemical research*, 2007, **40**, 1228-1236.
50. W. Xu, E. I. Cooper and C. A. Angell, *The Journal of Physical Chemistry B*, 2003, **107**, 6170-6178.
51. W. Xu and C. A. Angell, *Science*, 2003, **302**, 422-425.
52. H. Tokuda, K. Hayamizu, K. Ishii, M. A. B. H. Susan and M. Watanabe, *The Journal of Physical Chemistry B*, 2005, **109**, 6103-6110.
53. H. Tokuda, K. Hayamizu, K. Ishii, M. A. B. H. Susan and M. Watanabe, *The Journal of Physical Chemistry B*, 2004, **108**, 16593-16600.
54. T. Köddermann, R. Ludwig and D. Paschek, *Chemphyschem*, 2008, **9**, 1851-1858.
55. M. A. Vorotyntsev, V. A. Zinovyeva and M. Picquet, *Electrochim Acta*, 2010, **55**, 5063-5070.
56. D. Jeong, M. Choi, H. J. Kim and Y. Jung, *Phys Chem Chem Phys*, 2010, **12**, 2001-2010.
57. F. H. Stillinger and J. A. Hodgdon, *Physical review E*, 1994, **50**, 2064.
58. A. P. Abbott, P. Licence and A. W. Taylor, *Phys Chem Chem Phys*, 2011, **13**, 10147-10154.
59. P. Morisset, J. Oswald, C. Draper, R. Pinner and R. Ehrhardt, *J Electrochem Soc*, 1955, **102**, 143C-144C.
60. M. Schlesinger and M. Paunovic, *Modern electroplating*, Wiley, New York, 2000.

Chapter 5: Cr alum based deep eutectic solvents

5.1	Introduction	115
5.2	Eutectic mixtures based on urea and chrome alum	115
5.3	Physical properties	115
5.3.1	Phase behaviour	115
5.3.2	Viscosity	116
5.3.3	Conductivity	119
5.3.4	Molar conductivity	122
5.4	Solution speciation	124
5.4.1	UV-visible spectrum	124
5.4.2	EXAFS	125
5.5	Density	126
5.6	Molar volume	127
5.7	Cyclic voltammetry	128
5.8	Bulk deposition	128
5.9	Hardness and thickness	130
5.10	Current efficiency	130
5.11	Conclusion	131
5.12	References	132

5.1 Introduction

After using a strong ligand, en, in chapter four the aim of this short study was to remove strong ligands such as chloride and form the first deep eutectic solvents without a chloride anion. Eutectic mixtures did not form between chromium sulfate and urea but they were found to form with the double salt $\text{KCr}(\text{SO}_4)_2 \cdot 12\text{H}_2\text{O}$. This is a very common salt which was used extensively for applications such as leather tanning.

5.2 Eutectic mixtures based on urea and chrome alum

The present chapter was designed to investigate what effects would be seen in the chromium electrodeposition and physical properties if the chrome alum was replaced by chromium chloride. The mixture of the novel system can be prepared by mixing the metal salt, $\text{KCr}(\text{SO}_4)_2 \cdot 12\text{H}_2\text{O}$, with the complexing agent, urea as a hydrogen bond donor. In order to facilitate preparation of the mixture, the components may be heated together at elevated temperature, such as any temperature from 323 to 333 K. The molar ratio of $\text{KCr}(\text{SO}_4)_2 \cdot 12\text{H}_2\text{O}$ to urea is any value in the range 4:1 to 1:3 (**Figure 5.1**).



Figure 5.1: The DES formed by mixing the two solids together

5.3 Physical properties

5.3.1 Phase behaviour

We have previously reported the preparation of two novel, type 4, deep eutectic solvents by using *Cl* and *en* based chromium salts and urea as a hydrogen bond donor. Here we examine the nature of the weak ligand, SO_4^{2-} , in the chrome alum salt.

Figure 5.2 shows the melting points of urea: $\text{KCr}(\text{SO}_4)_2 \cdot 12\text{H}_2\text{O}$ mixtures as a function of composition and it can be seen that the eutectic is formed at a composition of 1:1 urea: $\text{KCr}(\text{SO}_4)_2 \cdot 12\text{H}_2\text{O}$. The melting temperature of the eutectic composition is *c.a.*

285 K (12 °C), producing a melting point depression of 375 K (102 °C), with respect to the weighted average of the pure components.

Unlike the urea: $\text{CrCl}_3 \cdot 6\text{H}_2\text{O}^1$ and urea: $[\text{Cr}(\text{en})_3]\text{Cl}_3 \cdot 3\text{H}_2\text{O}$ systems the eutectic composition formed with 50% of both $\text{KCr}(\text{SO}_4)_2 \cdot 12\text{H}_2\text{O}$ and urea. It is interesting to note the melting point of the alum mixtures are almost always lower than the chloride of en systems despite the melting point of the pure chrome alum being higher than the other two salts. (**Figure 5.2**).

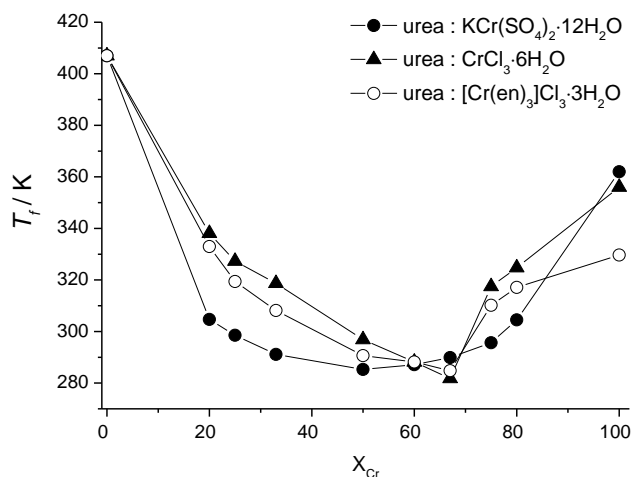


Figure 5.2: Melting points of urea: $\text{KCr}(\text{SO}_4)_2 \cdot 12\text{H}_2\text{O}$, urea: $\text{CrCl}_3 \cdot 6\text{H}_2\text{O}$ and urea: $[\text{Cr}(\text{en})_3]\text{Cl}_3 \cdot 3\text{H}_2\text{O}$ systems as a function of compositions

The depression of freezing point is usually related to the strength of the interaction between the metal centre and the complexing ligand. This will be discussed later in terms of the speciation in the liquid.

5.3.2 Viscosity

Figure 5.3 shows the viscosity of urea: $\text{KCr}(\text{SO}_4)_2 \cdot 12\text{H}_2\text{O}$ mixtures as a function of temperature and composition. For a wide range of DESs, viscosity decreases in an exponential manner with increasing temperature.²³ This is, however, not the case for the majority of the compositions described here and especially not for the mixtures with high chromium salt. The viscosity of the medium is reduced as the mole fraction of $\text{KCr}(\text{SO}_4)_2 \cdot 12\text{H}_2\text{O}$ decreases. The minimum viscosity is not observed at the eutectic composition (1:1 urea: $\text{KCr}(\text{SO}_4)_2 \cdot 12\text{H}_2\text{O}$), which is what is observed for all other DESs systems studied to date.^{24, 25} It should however be noted that the viscosity of these Type 4 eutectics is significantly lower compared to Type 2 DESs, e.g. $\text{ChCl}:\text{CrCl}_3 \cdot 6\text{H}_2\text{O}$,²⁶ $[\text{Cr}(\text{en})_3]\text{Cl}_3 \cdot 3\text{H}_2\text{O}$ and $\text{CrCl}_3 \cdot 6\text{H}_2\text{O}^1$ based Type 4 DESs, anhydrous Type 4 DESs, e.g.

urea: ZnCl_2 , previously reported.²⁴ At 293 K (20° C) the viscosity of the $\text{ChCl}:\text{CrCl}_3\cdot 6\text{H}_2\text{O}$ system at the eutectic composition (1:2) is 4800 cP, the urea: $\text{CrCl}_3\cdot 6\text{H}_2\text{O}$ is 2602 cP (1:2) and the urea: $[\text{Cr}(\text{en})_3]\text{Cl}_3\cdot 3\text{H}_2\text{O}$ is 1394 cP (1:2) while urea: $\text{KCr}(\text{SO}_4)_2\cdot 12\text{H}_2\text{O}$ is 441 cP.

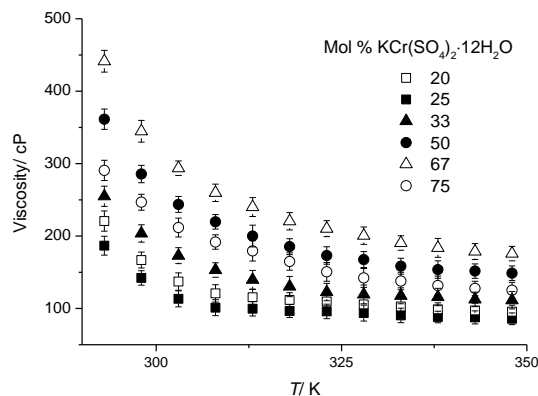


Figure 5.3: Viscosity of urea: $\text{KCr}(\text{SO}_4)_2\cdot 12\text{H}_2\text{O}$ as a function of temperature and composition.

However, ionic liquids are in general tens and even hundreds of times more viscous than the traditional organic solvents. The novel DES is less viscous than any reported previously. This again is probably due to the increase in number of hydration water. Moreover, high viscosity not only decreases the likelihood of its applications, such as heterogeneous catalysis and supporting electrolytes, in these fields that require fast mass and ion transport, but also leads to operational difficulties in filtration, extraction and decantation. Consequently, in most cases, the required viscosity of ionic liquids should be as low as possible. In general, a low-viscosity ionic liquids is characteristic of well-delocalized positive and negative charges,²⁷ low-symmetry ions²⁸ and highly flexible side chains.²⁹ These structural features are relevant to weak Coulomb interactions and low effective packing between ions, thereby leading to low viscosity.³⁰

This reduction in viscosity means improved mass transport and should cause an increase in electrical conductivity. The change in viscosity, η with temperature can be described by the **Equation 3.2**.

Applying **Equation 3.2** to the data in **Figure 5.3** the E_η were calculated and are shown in **Table 5.2**. The obtained data compared with analogues urea: $\text{CrCl}_3\cdot 6\text{H}_2\text{O}$ and urea : $[\text{Cr}(\text{en})_3]\text{Cl}_3\cdot 3\text{H}_2\text{O}$ systems. Earlier studies have shown that the E_η values for ionic liquids are noticeably larger than traditional liquids and high temperature molten salts.³¹ This is caused by the large ion to hole radius ratio in ionic solvents.

Table 5.2: Activation energies for viscous flow (E_η) and conductivity (E_A) as a function of liquid composition for the novel system compared with other DES systems. Coefficients of correlation (r) for the fits to **Equations 5.1** and **5.3** are also given.

DESs	E_η [kJ·mol ⁻¹]	r	E_A [kJ·mol ⁻¹]	$-r$
urea : KCr(SO ₄) ₂ ·12H ₂ O				
1:3	12.6	0.902	18.2	0.901
1:2	12.9	0.957	25.6	0.914
1:1	12.6	0.914	24.9	0.924
2:1	11.5	0.904	29.0	0.904
3:1	9.36	0.916	20.9	0.915
4:1	10.6	0.952	19.9	0.931
urea : [Cr(en) ₃] Cl ₃ ·3H ₂ O				
1:4	49.2	0.962	23.5	0.975
1:3	53.1	0.903	20.2	0.953
1:2	60.9	0.976	18.8	0.964
1:1	45.1	0.992	19.4	0.958
2:1	46.3	0.982	20.2	0.974
3:1	44.7	0.967	19.2	0.975
4:1	46.2	0.984	18.4	0.967
urea : CrCl ₃ ·6H ₂ O ¹				
1:3	53.4	0.973	18.2	0.990
1:2	57.3	0.986	13.7	0.994
3:1	45.2	0.991	18.3	0.995
4:1	46.8	0.964	17.5	0.987

It has been shown empirically that E_η values are related to the melting point of liquids (T_m) by **Equation 3.3**.³²

This has been found to be accurate for a range of molecular liquids and high-temperature molten salts.³² This would propose an average E_η value of approximately 9.18 kJmol⁻¹ for the urea: KCr(SO₄)₂·12H₂O mixtures, which is comparable with the data shown in **Table 5.3**. These values are different than the other systems (urea: [Cr(en)₃] Cl₃·3H₂O and urea: CrCl₃·6H₂O).¹

The values for the chromium containing liquid are, however, similar to other room-temperature ionic liquids. Branco *et al.*³³ described the viscosity of a variety of imidazolium salts and through these data the energy for activation of viscous flow was found to range from 37.2 (C₄mimBF₄) to 59.7 kJmol⁻¹ (C₅O₂mimCl).

Table 5.3: Activation energies for viscous flow (E_η) as a function of liquid composition for the novel system compared with data obtained from $E_\eta = 3.74 RT_m$ equation.

urea: $\text{KCr}(\text{SO}_4)_2 \cdot 12\text{H}_2\text{O}$	$E_\eta = 3.74 RT_m$	E_η [$\text{kJ} \cdot \text{mol}^{-1}$]
1:3	9.46	12.6
1:2	9.01	12.9
1:1	8.87	12.6
2:1	9.05	11.6
3:1	9.28	9.36
4:1	9.47	10.6

Latter, Abbott³⁴ showed that the empirical relationship observed in **Equation 5.3** for molecular liquids and high temperature molten salts, is not valid for ambient-temperature ionic liquids and may result from the large size of the solvent ions found in the latter. Perhaps, it's suitable for less viscous liquids such as urea: $\text{KCr}(\text{SO}_4)_2 \cdot 12\text{H}_2\text{O}$ mixtures.

5.3.3 Conductivity

Figure 5.4 shows the conductivity of the urea: $\text{KCr}(\text{SO}_4)_2 \cdot 12\text{H}_2\text{O}$ system as a function of temperature and composition. Conductivity increases with temperature in a linear fashion for all compositions, whilst in most other DESs the conductivity increases exponentially with temperature.²³ Similarly to viscosity, conductivity does not change regularly as the mole fraction of $\text{KCr}(\text{SO}_4)_2 \cdot 12\text{H}_2\text{O}$ increases. The highest conductivity is observed for the 1:3 urea: $\text{KCr}(\text{SO}_4)_2 \cdot 12\text{H}_2\text{O}$ composition, while the 1:2 urea: $\text{KCr}(\text{SO}_4)_2 \cdot 12\text{H}_2\text{O}$ is the least viscous composition. This indicates that ionic mobility rather than the concentration of charge carriers is most important in controlling conductivity. This is common to other eutectic mixtures and ionic liquids and a strong indication for the applicability of hole-theory to describe transport properties.^{35,36}

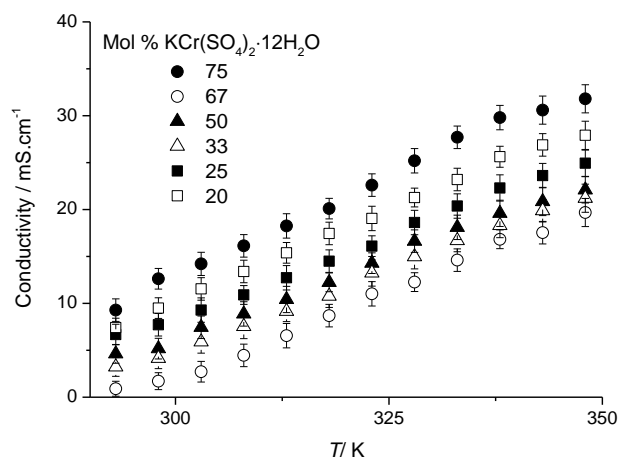


Figure 5.4: Conductivity of urea: $KCr(SO_4)_2 \cdot 12H_2O$ as a function of temperature and composition.

Generally, apart from urea: $[Cr(en)_3]Cl_3 \cdot 3H_2O$ system, the conductivities observed for the Chrome alum systems are much higher than any other DES previously reported (**Figure 5.5**).¹ At 303 K for example, conductivities of the 1:3 urea: $KCr(SO_4)_2 \cdot 12H_2O$ system are close to the analogous urea: $[Cr(en)_3]Cl_3 \cdot 3H_2O$ system and it is three times larger (10 mS cm^{-1}) than those of the analogous urea: $CrCl_3 \cdot 6H_2O$ system (3 mS cm^{-1}) and 20 times larger than those of the analogous $ChCl:CrCl_3 \cdot 6H_2O$ system (0.5 mS cm^{-1}).^{1,26}

This can be partly associated to the viscosity of the ionic liquids, but may also be due to the change in the type of charge carrier. These values are also comparable to some of the highest conductivities reported for room temperature ionic liquids with discrete anions.³⁷

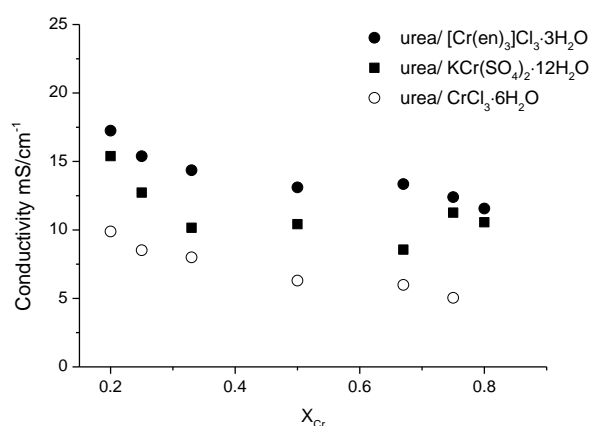


Figure 5.5: The conductivity of urea: $KCr(SO_4)_2 \cdot 12H_2O$, $[Cr(en)_3] Cl_3 \cdot 3H_2O$ based DES and $CrCl_3 \cdot 6H_2O$ based DES as a function of Cr concentration, at 313 K.

An equivalent expression to **Equation 3.2** has been shown to valid for the variation of conductivity, σ , with temperature (i.e. **Equation 3.4**).³²

The activation energy for conduction (E_a) is listed in **Table 5.2** as a function of composition. Similar to the E_η values, they are to some extent larger than the analogues urea: $[\text{Cr}(\text{en})_3]\text{Cl}_3 \cdot 3\text{H}_2\text{O}$ and urea: $\text{CrCl}_3 \cdot 6\text{H}_2\text{O}^1$ system and they are considerably larger than high-temperature molten salts (usually group I halides have values of 5 to 20 $\text{kJ} \cdot \text{mol}^{-1}$).³⁸

For ionic fluids, the conductivity is normally controlled by the mobility of the charge carriers. Therefore a plot of conductivity versus fluidity must be linear for a certain charge carrier. Although the case of chromium chloride, is to some extent complex, because of the different ligand arrangements, that are conceivable.

The current study focusses on urea as a hydrogen bond donor (HBD) although other HBDs also form eutectic mixtures with hydrated metal salts. **Figure 5.6** compares the conductivity for different Type 4 DESs. Ethylene glycol and glycerol have been shown to form good hydrogen bond donors (HBDs) forming eutectic mixtures with choline chloride (Type 3 DES).³⁵ As it has been shown that in the urea: $\text{CrCl}_3 \cdot 6\text{H}_2\text{O}$ system, in the Type 4 DESs with $\text{KCr}(\text{SO}_4)_2 \cdot 12\text{H}_2\text{O}$, the urea system exhibits the highest conductivity.

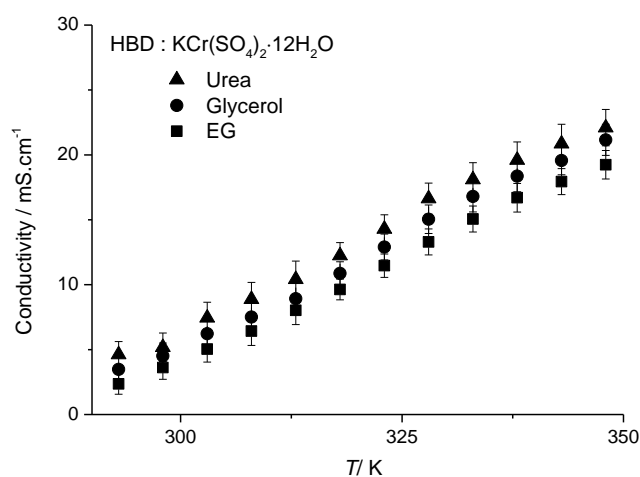


Figure 5.6: Conductivity of HBD: $\text{KCr}(\text{SO}_4)_2 \cdot 12\text{H}_2\text{O}$ (1:1) as a function of temperature.

Figure 5.7 shows a strong linear relationship between conductivity and the reciprocal of viscosity (i.e. fluidity) which displays that the ionic mobility is controlling the conductivity of the liquid. It also shows that since the slope is approximately constant at most compositions, the charge-carrying type is controlled by one species.

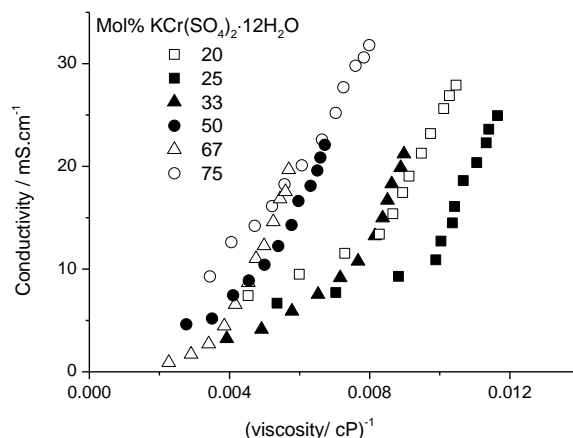


Figure 5.7: Conductivity as a function of $1/\text{viscosity}$ for the data in Figures 5.3 and 5.4

5.3.4 Molar conductivity

Recently, it has been stated that the Walden rule is approximately valid in ILs, and is a suitable extent for analysis of the ion pairing issue in electrolyte solution. If the viscosity and conductivity of the electrolyte follows Walden's rule, the ionic conductivity is linked to viscosity using the qualitative method of Angell.³⁹

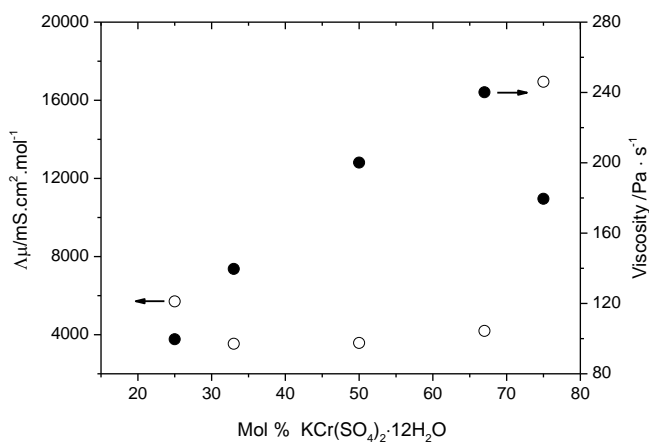


Figure 5.8: Molar conductivity and viscosity as a function of composition for the urea: $KCr(SO_4)_2 \cdot 12H_2O$ system at 313 K.

In aqueous solutions molar conductivity is usually observed to decrease, because of ionic atmosphere and ion pairing effects, as the electrolyte concentration is increased.³²

We have seen in the case of viscosity, **Figure 5.3**, an increase in the viscosities as more $KCr(SO_4)_2 \cdot 12H_2O$ was added. While the inverse trend could be seen in the case of conductivity, this would be expected since more charge carrying species are being

added to the system. Perhaps this can be seen more clearly in **Figure 5.8** by simply plotting the data at 313 K.

This is thought to be because of the effect of viscosity being greater than the effect of conductivity on the system after more than 33 % $\text{KCr}(\text{SO}_4)_2 \cdot 12\text{H}_2\text{O}$ is added. Although there are more charge carrying species ($\text{KCr}(\text{SO}_4)_2 \cdot 12\text{H}_2\text{O}$) in the system, the viscosity of the system slows down the flow of ions through the system. This proposes that the motion of ions in these liquids may be different to other eutectic solvents.

These share the high metal concentrations of type 2 eutectics but have the technological advantage of much lower viscosities. Deposition from these liquids is only possible for certain compositions (e.g. urea: $\text{KCr}(\text{SO}_4)_2 \cdot 12\text{H}_2\text{O} > 1:1$) and these coincide with a changes in important physical properties like conductivity or viscosity (**Figure 5.8**).

The viscosity and conductivity of ionic liquids are main part physical properties which can be measured to result from the relative mobility of the ionic species present. Nevertheless, few efforts have been made to precisely model the mass transport properties of ionic liquids at ambient temperatures. Research into this area has been slowed down by the complexity of the ionic interactions in ionic liquids.⁴⁰

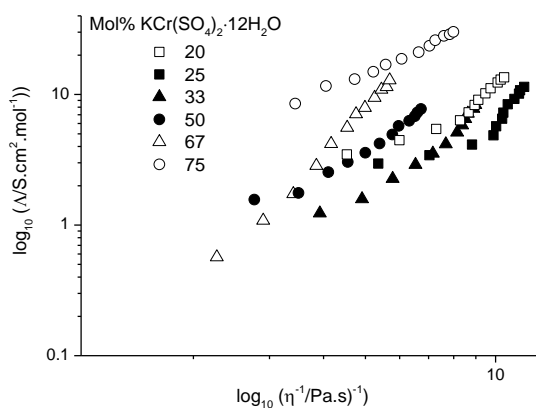


Figure 5.9: Molar conductivity as a function of fluidity for the urea: $\text{KCr}(\text{SO}_4)_2 \cdot 12\text{H}_2\text{O}$ systems.

Figure 5.9 shows the molar conductivity as a function of fluidity for the urea: $\text{KCr}(\text{SO}_4)_2 \cdot 12\text{H}_2\text{O}$ systems. There are several points of note from this figure; the decrease in molar conductivity with decreasing fluidity is not as marked as that observed in ionic liquids with discrete anions.⁴¹ It is noteworthy not only that the molar conductivity for the Cr alum system is higher than that for the $[\text{Cr}(\text{en})_3]^{3+}$ and CrCl_3 system but also comparing the higher chromium content systems the value for the

former is approximately three times the latter which corresponds to the relative charges on the cations. It has previously been shown that the conductivity of ionic liquids can be assumed to follow the Nernst-Einstein equation because charge mobility is limited by the number of suitably sized holes and these are effectively at zero concentration (Equation 3.5).⁴²

5.4 Solution speciation

In order to understand the behaviour of the eutectics it is important to have a sympathetic of the metal species present in the system. The liquids are highly conducting and, since chromium and chloride ions are the only charge carriers, the conducting species must originate from $\text{KCr}(\text{SO}_4)_2 \cdot 12\text{H}_2\text{O}$.

5.4.1 UV-visible spectrum

When organic compounds absorb UV radiation, the UV light induces transitions of electrons between different energy levels. The transitions of interest in the present context are mainly from ground-state π -orbitals to unoccupied π -orbitals of higher energy. The latter are termed antibonding π -orbitals, and are designated by the symbol π^* . After undergoing this transition by the absorption of a photon of appropriate energy, the molecule is said to be in the excited state.

Chromium (III) is a common example of a d^3 ion, and its electronic spectra have been extensively studied. In this experiment the visible spectra of several complexes of Cr^{3+} will be studied in order to observe the spectral changes produced by changing the ligands in the complexes. Some typical values of Δ_0 , the crystal field splitting parameter, for a series of octahedral Cr^{3+} complexes will be determined.

Elving and Zemel showed that the number of chloride and water ligands bound to the metal affected the UV-visible spectrum of the chromium species⁴³. They indicated two bands varying from 407 to 475 nm ($4\text{T}_{1g} \leftarrow 4\text{A}_{2g}$) for the first and from 575 to 665 nm ($4\text{T}_{2g} \leftarrow 4\text{A}_{2g}$) for the second band. For each band the lower end of the wavelength absorbance was assigned to the hexaaqua complex and the upper end to the trichloro species. The addition of each chloride ligand moves the wavelength of each band by about 20 to 30 nm. In a neutral aqueous solution, the hexaaqua species dominates but the trichloro species dominates in 12 mol dm^{-3} HCl.

UV-Vis measurements in aqueous solution indicate that the solid resulting from the rapid precipitation of chrome alum solutions with NaOH is monomeric in nature because its dissolution in acidic media regenerates the mononuclear.⁴⁴

Figure 5.10 shows the difference between the 1:2 urea: $\text{CrCl}_3 \cdot 6\text{H}_2\text{O}$ system and the 1:2 urea: $\text{KCr}(\text{SO}_4)_2 \cdot 12\text{H}_2\text{O}$ mixture. While these spectra are indicative of more than one complex co-existing in solution, the maxima of the two bands are both shifted by about 39 nm suggesting that, on average, the 1:2 urea: $\text{KCr}(\text{SO}_4)_2 \cdot 12\text{H}_2\text{O}$ system contains 1 chloride than the 1:2 urea: $\text{CrCl}_3 \cdot 6\text{H}_2\text{O}$ mixture.

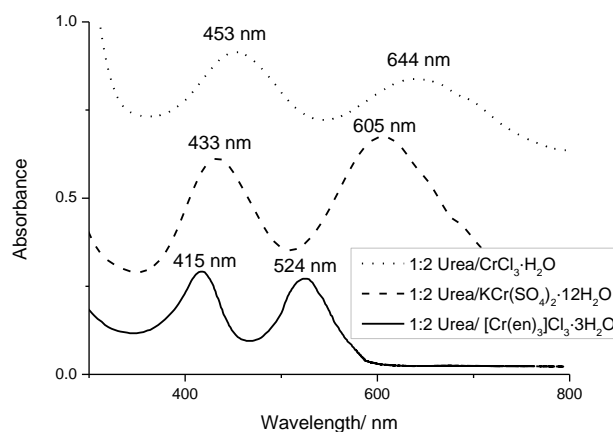


Figure 5.10: UV-Vis spectra of 1: 2 urea: $\text{CrCl}_3 \cdot 6\text{H}_2\text{O}$ and 1: 2 urea: $\text{KCr}(\text{SO}_4)_2 \cdot 12\text{H}_2\text{O}$.

5.4.2 EXAFS

EXAFS was recorded to elucidate the nature of the chromium species, in particular with respect to their overall charge. **Figure 5.11** shows Fourier transforms of the EXAFS data for all chrome alum samples, O-coordination seems the most reasonable. The CrCl_3 -based sample may have solidified at some point either during or immediately after EXAFS, but the acquired EXAFS spectrum does not match that of the solid reference sample. Potential sources of O-coordination could be water, urea, or sulfate. Signal between 3-5 Å suggests at least part of this coordination is due to urea or sulfate. As Bacon and Gardner stated that, in the solid state, the coordination at Cr for the alum complex is hexaaqua coordinated.⁴⁵ This could possibly suggest that urea is the more likely source of O-coordination in the urea-based systems.

The Cr-O bond lengths obtained here are perhaps a little on the short side, compared to those in the other chromium paper (although saying that, the 1:4 Cr: urea sample has similar values). If any N-coordination is present, it would not be readily distinguishable from the O-coordination (**Table 5.4**).

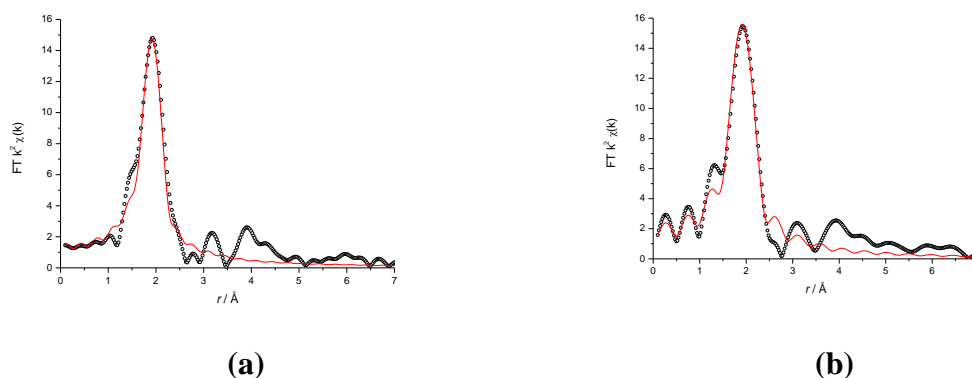


Figure 5.11: Fourier transforms of the EXAFS data (black circles) and fits (red line) for (a) 1:2 Cr-alum:urea and (b) 2:1 Cr-alum:urea.

Table 5.4: EXAFS fit parameters of chrome-alum liquids

Chrome alum: urea	Coordinating atom	Number of atoms, N	Distance from Cr $r/\text{Å}$	Debye-Waller factor, $a/\text{Å}^2$	Fit index, $R1/\%$
1:2	O	5.4(4)	1.958(7)	0.006(2)	7.0 %
2:1	O	5.2(5)	1.971(9)	0.004(3)	7.6 %

5.5 Density

The variation of density as a function of temperature and composition are shown in **Figure 5.12**. The densities for all compositions decrease with increasing temperature, as expected. The densities of the liquids are lower than those of the solid state components (density urea = $1.32 \text{ g}\cdot\text{cm}^{-3}$, $\text{KCr}(\text{SO}_4)_2\cdot 12\text{H}_2\text{O} = 1.85 \text{ g}\cdot\text{cm}^{-3}$). In general, these liquids have relatively high densities but not higher than the urea: $[\text{Cr}(\text{en})_3]\text{Cl}_3\cdot 3\text{H}_2\text{O}$ and the urea: $\text{CrCl}_3\cdot 6\text{H}_2\text{O}$ system¹ (**Figure 5.12b**).

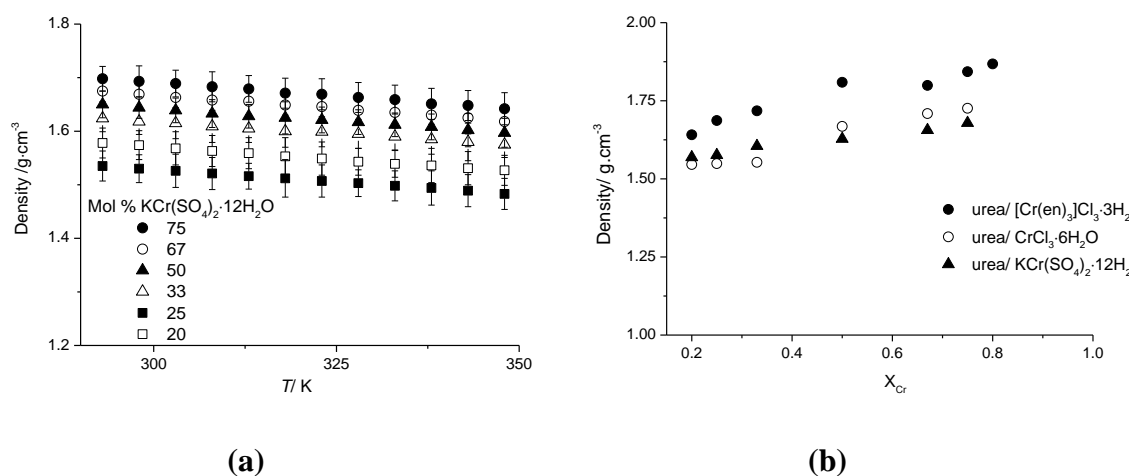


Figure 5.12: Density of the (a) urea: $\text{KCr}(\text{SO}_4)_2\cdot 12\text{H}_2\text{O}$ and (b) density of all urea: chromium systems at 313 K as a function of composition.

5.6 Molar volume

The influence of the salt upon the structure of the liquid can be obviously seen by measuring the liquid density. The amount of free volume can be determined using a hard sphere model. Using this approach the fractional molar free volume can be obtained using **Equation 3.17**.

Using the density data shown in **Figure 4.15a** the molar volume V_m can be calculated using **Equation 3.14** and **Equation 3.15**.

Figure 5.13 shows the change in molar volume as a function of composition and it is immediately evident that although the chromium content and hence the number of charge carriers increases the number of charged species per unit volume decrease. This may naturally be expected but it is the extent of this change which is surprising *viz.* the molar volume doubles (and the molar concentration halves).

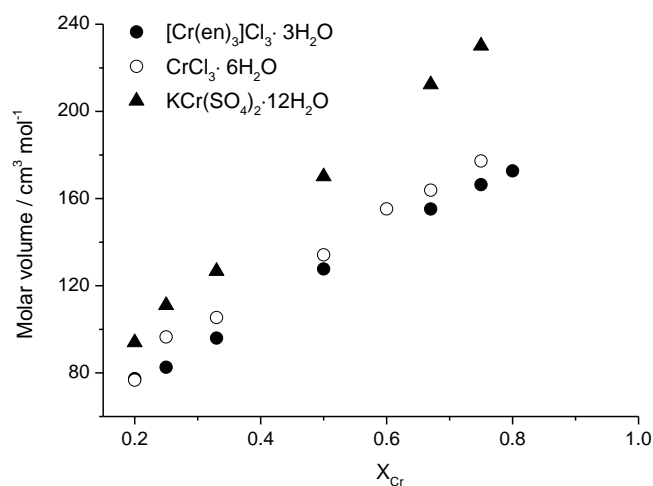


Figure 5.13: Change in volume as a function of composition at 298 K.

5.7 Cyclic voltammetry

Figure 5.14 shows the cyclic voltammogram for the urea: $[\text{Cr}(\text{en})_3]\text{Cl}_3 \cdot 3\text{H}_2\text{O}$ system as a function of composition. As the chromium content increases both the anodic and cathodic charge decrease which is counter intuitive as there is more electroactive species in the liquid.

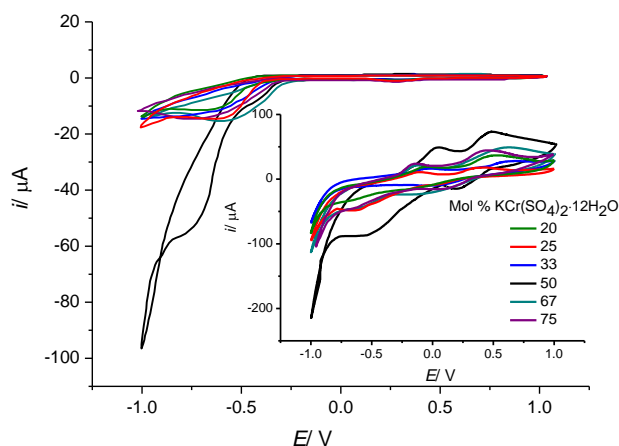


Figure 5.14: Cyclic voltammogram for the urea: $\text{KCr}(\text{SO}_4)_2 \cdot 12\text{H}_2\text{O}$ system at 313 K on a Pt electrode (area= $7.85 \times 10^{-3} \text{ cm}^2$), inset :on a GC electrode (area= $7.06 \times 10^{-2} \text{ cm}^2$) at a sweep rate of 20 mV s^{-1} for different compositions.

The form of the voltammogram in **Figure 5.14** shows a quasi-reversible deposition process where reduction of the metal complex occurs from Cr^{III} to the metal. Close inspection shows a small cathodic peak at +0.5 V corresponding to under-potential deposition (upd) which blocks the electrode such that the Cr^{II} intermediate is not observed. Repeating the experiment for the urea $\text{KCr}(\text{SO}_4)_2 \cdot 12\text{H}_2\text{O}$ systems on a glassy carbon electrode, where upd does not occur, reveals a markedly different voltammogram with two reversible signals corresponding to Cr^{III} reduction to Cr^{II} followed by Cr^{II} reduction to Cr^0 (**Figure 5.14 inset**).

5.8 Bulk deposition

Importantly for the 2 urea $\text{KCr}(\text{SO}_4)_2 \cdot 12\text{H}_2\text{O}$ system as the metal is reduced onto the electrode surface $(\text{SO}_4)^{2-}$ ligands are reduced into the double layer but these will not affect the speciation of the chromium as it is already completely surrounded by $(\text{SO}_4)^{2-}$ ligands. This can be contrasted with the $\text{ChCl} : \text{CrCl}_3 \cdot 6\text{H}_2\text{O}$ and urea: $\text{CrCl}_3 \cdot 6\text{H}_2\text{O}$ systems where speciation is dynamic and strongly dependent upon the composition of

the surrounding environment.^{1, 34} It can therefore be seen that speciation in these liquids will change during deposition which will lead to changes in morphology and it is suggested that this is the reason for the black, non-crystalline deposits observed during bulk deposition.

Bulk deposition was carried out using the 2 urea: $\text{KCr}(\text{SO}_4)_2 \cdot 12\text{H}_2\text{O}$ system on a mild-steel substrate using a current density = $150 \text{ mA} \cdot \text{cm}^{-2}$ for 1 hour at 40°C and the result is shown in **Figure 5.15**. It can clearly be seen that a black, metallic deposit was obtained with a nodular morphology which contrasts strongly with those obtained from the other DESs.

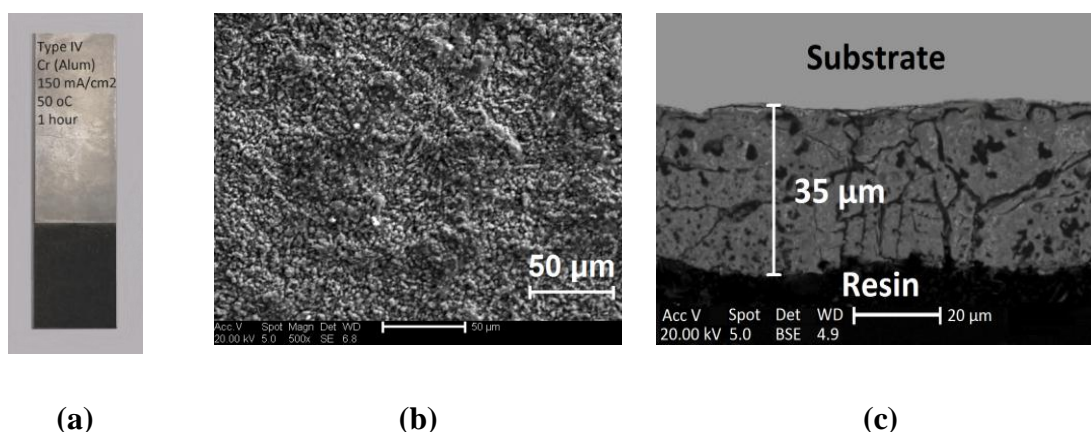


Figure 5.15: (a) Optical photograph and (b) SEM image of chromium deposit (c) cross section obtained from the electroreduction of 2:1 urea: $\text{KCr}(\text{SO}_4)_2 \cdot 12\text{H}_2\text{O}$ on a mild-steel (Current density = 150 mAcm^{-2} for 1 hour at 313 K)

A closer inspection of **Figure 5.15b** indicates that the morphology is nano-particles. At different SEM magnification particle formed were observed spherical in shape **Figure 5.16**. Similar results in the shape of the Cr nanoparticle were reported in the previous studies in the Cr nanoparticle using the chemical method.⁴⁶

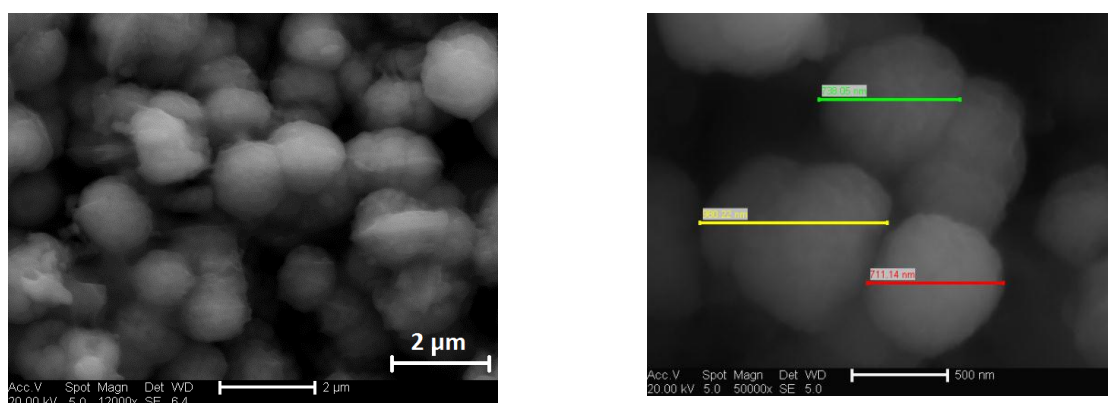


Figure 5.16: High magnification SEM of the sample in Figure 5.18.

5.9 Hardness and thickness

The film had an average thickness of 35 μm and a Vickers hardness of 680 ± 10 HV which is close to the 800 HV obtained by the conventional aqueous chromic acid process. Commercially produced chromium plate possess harnesses in the range 800-1100 HV, and is therefore, significantly harder than any other electrolytically deposited metal.⁴⁷ The deposit morphology also contributes to the increase in hardness compared to that obtained using urea: $\text{CrCl}_3 \cdot 6\text{H}_2\text{O}$ systems (600 ± 10 HV).¹ The sample is not micro-cracked and is very adherent.

5.10 Current efficiency

An electrochemical quartz crystal microbalance, EQCM, was used to determine charge / mass balance for Cr deposition and a representative data set is presented in **Figure 5.17**. The current efficiency can be easily obtained from the slope of the mass *versus* charge plot by comparison with the theoretical value calculated from Faraday's law according to the **Equation 4.8**.

In this case equivalent to $51.99/3F = 17.96 \times 10^{-5} \text{g} \cdot \text{C}^{-1}$. The slope of the graph shown in **Figure 5.17** ($16.60 \times 10^{-5} \text{g} \cdot \text{C}^{-1}$) corresponds to a current efficiency of *c.a.* 92% at a deposition potential of -0.7 V *versus* Ag wire quasi-reference.

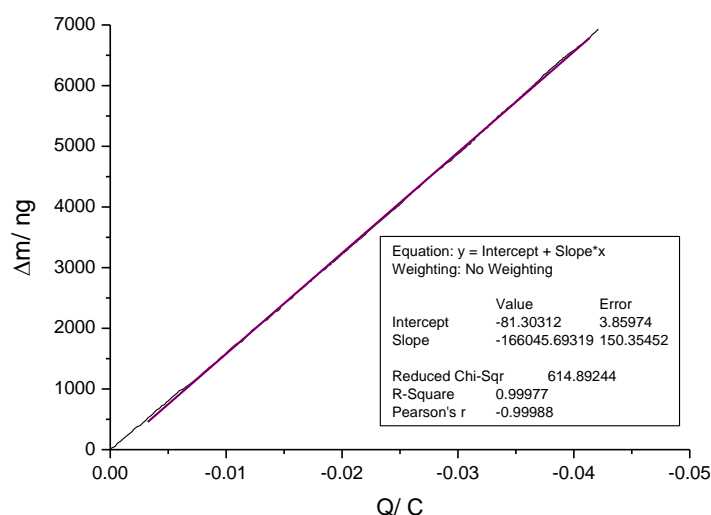


Figure 5.17: Mass-charge plot for the deposition of Cr on a Platinum electrode (0.23 cm^2 QCM crystal) at an applied potential of -0.7 V from 2:1 urea: $\text{KCr}(\text{SO}_4)_2 \cdot 12\text{H}_2\text{O}$. Linear regression gives a slope, $dm/dQ = 16.60 \times 10^{-5} \text{g} \cdot \text{C}^{-1}$.

5.11 Conclusions

This chapter has shown that controlling the speciation of a metal ion during electrodeposition can significantly affect the morphology and properties of the metallic film. This is the first DES to be produced with a non-chloride anion. The chrome alum DES exhibits a higher conductivity than any similar liquid previously described. The unusual conductivity as a function of composition was explained in terms of the change in molar volume. Using this liquid black, adherent, hard chromium was obtained by electroreduction which contrasted with softer, black, less crystalline deposits which were obtained when chloride was the counter-ion in Chapter 3.

5.12 References

1. A. P. Abbott, A. A. Al-Barzinjy, P. D. Abbott, G. Frisch, R. C. Harris, J. Hartley and K. S. Ryder, *Phys Chem Chem Phys*, 2014, **16**, 9047-9055.
2. B. V. L'vov, *Thermal Decomposition of Solids and Melts: New Thermochemical Approach to the Mechanism, Kinetics and Methodology*, Springer, 2007.
3. J. W. Mellor, *A Comprehensive Treatise on Inorganic and Theoretical Chemistry*, Longmans, Green, 1948.
4. F. Ullmann, W. Gerhartz, Y. S. Yamamoto, F. T. Campbell, R. Pfefferkorn and J. F. Rounsaville, *Ullmann's Encyclopedia of industrial chemistry*, VCH, 1986.
5. J. Eisenstein, *Reviews of Modern Physics*, 1952, **24**, 74.
6. A. D. Covington and T. Covington, *Tanning Chemistry: The Science of Leather*, Royal Society of Chemistry, 2009.
7. N. N. Greenwood and A. Earnshaw, *Chemistry of the Elements*, Elsevier Science, 1997.
8. B. J. Marshall, D. O. Pederson and W. E. Bailey, *Journal of Applied Physics*, 1967, **38**, 2116-2120.
9. A. Biswas, *Encyclopaedia of Chemistry*, Anmol Publications Pvt. Limited, 2006.
10. B. Bodger, R. McGrann and D. Somerville, *Plating and surface finishing*, 1997, **84**, 28-31.
11. J. Tyler, *Metal Finishing*, 1995, **93**, 11-14.
12. J. K. Dennis and T. E. Such, *Nickel and Chromium Plating*, Woodhead Publishing, 1993.
13. D. W. Hardesty, *J Electrochem Soc*, 1969, **116**, 1194-1197.
14. B. O. Seraphin, in *Solar Energy Conversion*, ed. B. Seraphin, Springer Berlin Heidelberg, 1979, vol. 31, ch. 2, pp. 5-55.
15. G. E. McDonald, *Solar Energy*, 1975, **17**, 119-122.
16. D. D. Allred, M. R. Jacobson and E. E. Chain, *Solar Energy Materials*, 1985, **12**, 87-129.
17. C. M. Lampert, I. E. A. S. Heating, C. Program, I. E. A. S. Heating, C. P. T. X. S. M. R and D., *Failure and Degradation Modes in Selected Solar Materials: A Review*, International Energy Agency, 1989.
18. M. Selvam, K. Srinivasan, N. Shanmugam, S. John and B. Shenoi, *Metal Finishing*, 1982, **80**, 107-112.
19. A. P. Abbott, G. Capper, D. L. Davies, R. K. Rasheed, J. Archer and C. John, *T I Met Finish*, 2004, **82**, 14-17.
20. Z. A. Hamid, *Surface and Coatings Technology*, 2009, **203**, 3442-3449.
21. F. Endres, D. MacFarlane and A. Abbott, *Electrodeposition from ionic liquids*, John Wiley & Sons, 2008.
22. A. P. Abbott and K. J. McKenzie, *Phys Chem Chem Phys*, 2006, **8**, 4265-4279.
23. A. P. Abbott, D. Boothby, G. Capper, D. L. Davies and R. K. Rasheed, *J Am Chem Soc*, 2004, **126**, 9142-9147.
24. A. P. Abbott, J. C. Barron, K. S. Ryder and D. Wilson, *Chemistry – A European Journal*, 2007, **13**, 6495-6501.
25. A. P. Abbott, G. Capper, D. L. Davies, R. K. Rasheed and V. Tambyrajah, *Chem Commun*, 2003, 70-71.
26. A. P. Abbott, G. Capper, D. L. Davies and R. K. Rasheed, *Chemistry*, 2004, **10**, 3769-3774.
27. Y. Fukaya, Y. Iizuka, K. Sekikawa and H. Ohno, *Green Chem*, 2007, **9**, 1155-1157.
28. O. J. Curnow, D. R. MacFarlane and K. J. Walst, *Chem Commun*, 2011, **47**, 10248-10250.

29. L. J. Siqueira and M. C. Ribeiro, *The Journal of Physical Chemistry B*, 2009, **113**, 1074-1079.
30. Z. J. Chen, T. Xue and J.-M. Lee, *RSC Advances*, 2012, **2**, 10564-10574.
31. A. P. Abbott, D. Boothby, G. Capper, D. L. Davies and R. K. Rasheed, *Journal of the American Chemical Society*, 2004, **126**, 9142-9147.
32. J. O. M. Bockris and A. K. N. Reddy, *Volume 1: Modern Electrochemistry: Ionics*, Springer, 1998.
33. L. C. Branco, J. N. Rosa, J. J. Moura Ramos and C. A. Afonso, *Chemistry-a European Journal*, 2002, **8**, 3671-3677.
34. A. P. Abbott, G. Capper, D. L. Davies and R. K. Rasheed, *Chemistry – A European Journal*, 2004, **10**, 3769-3774.
35. A. P. Abbott, R. C. Harris, K. S. Ryder, C. D'Agostino, L. F. Gladden and M. D. Mantle, *Green Chem*, 2011, **13**, 82-90.
36. A. P. Abbott, *Chemphyschem : a European journal of chemical physics and physical chemistry*, 2004, **5**, 1242-1246.
37. P. Wasserscheid and T. Welton, *Ionic Liquids in Synthesis*, Wiley-VCH, 2008.
38. G. J. Janz, *Molten Salts Handbook*, Elsevier Science, 2013.
39. M. Yoshizawa, W. Xu and C. A. Angell, *Journal of the American Chemical Society*, 2003, **125**, 15411-15419.
40. P. Wasserscheid and T. Welton, *Ionic liquids in synthesis*, Wiley Online Library, 2008.
41. D. R. MacFarlane, M. Forsyth, E. I. Izgorodina, A. P. Abbott, G. Annat and K. Fraser, *Phys Chem Chem Phys*, 2009, **11**, 4962-4967.
42. A. P. Abbott, *Chemphyschem*, 2005, **6**, 2502-2505.
43. P. J. Elving and B. Zemel, *Journal of the American Chemical Society*, 1957, **79**, 1281-1285.
44. M. J. Avena, C. E. Giacomelli and C. P. De Pauli, *Journal of Colloid and Interface Science*, 1996, **180**, 428-435.
45. G. Bacon and W. Gardner, *Proceedings of the Royal Society of London. Series A. Mathematical and Physical Sciences*, 1958, **246**, 78-90.
46. S. Khamlich, O. Nemraoui, N. Mongwaketsi, R. McCrindle, N. Cingo and M. Maaza, *Physica B: Condensed Matter*, 2012, **407**, 1509-1512.
47. P. Morisset, J. Oswald, C. Draper, R. Pinner and R. Ehrhardt, *J Electrochem Soc*, 1955, **102**, 143C-144C.

Chapter 6: The role of additives in the electrodeposition of chromium

6.1	Introduction	135
6.2	Levelling and brightening	135
6.3	Effect of brighteners on the morphology	137
6.4	Use of additives for electrodeposition from ionic liquids	139
6.5	Results and discussion	142
6.6	Effect of additives on bulk deposition	142
6.7	Viscosity and conductivity	146
6.8	Solution speciation	149
6.9	Cyclic voltammetry	151
6.10	Hardness and thickness	153
6.11	X-ray diffraction	154
6.12	Conclusions	155
6.13	References	157

6.1 Introduction

Electrodeposited chromium has a high degree of hardness (800–1100 HV) and possess a high level of brightness.¹ X-ray diffraction studies on the deposit show a high degree of preferred orientation which have a tendency to produce a great level of tensile stress within the deposit leading to unprompted cracking of thicker deposits.² This cracked deposit can be useful for oil retention for thicker deposits which helps with lubricated wear resistance. In thinner coatings micro-discontinuous chromium deposits can distribute the corrosion current in a corrosive environment and improve corrosion resistance.¹

Many studies have focused on complexants with trivalent chromium ions and the role of organic brighteners however the mechanism is not fully understood.³⁻⁹ Previous studies¹⁰⁻¹² have suggested that electrodeposition of chromium from trivalent baths involves two consecutive reduction steps:



The formation of Cr(II) ions during the metal deposition from trivalent chromium baths is important.^{13, 14} Characteristics of electroreduction of Cr³⁺ and Cr²⁺ ions were reviewed by Korshunov et al.¹⁵ Much of the effort on mechanisms of action of additives in electrodeposition has focused on their ability to modify the crystallization of the metal.¹⁶⁻¹⁸ Some of these mechanisms have previously been summarized by Loshkarev.¹⁹⁻²¹

6.2 Levelling and brightening

A complex mixture of additives which act as brighteners, levellers, structural modifiers and wetting agents are generally added to the electroplating bath with the intention of improving deposition efficiency and controlling deposit morphology. Brightening enable the electroplating solution to produce fine deposits with crystallites smaller than the wavelengths of visible light, specifically smaller than 0.4 μm^{22, 23} and having oriented grain structure.²⁴ It has been found that the brightness influenced by the degree to which morphological elements of the surface of electrodeposits are in the same plane.²⁵ Some additives may possibly act at the same time as levellers and brighteners, such as thiourea in Watts-type nickel electroplating baths.²⁶ Watson and Edwards²⁷ have presented that, as a function of its concentration, coumarin used as additive in a nickel plating bath might produce maximum levelling and milky brightness at 0.34 mmol dm⁻³,

less levelled but fully bright deposits at $0.001 \text{ mol dm}^{-3}$ and deposits entirely without brightness and only geometrically levelled at $0.005 \text{ mol dm}^{-3}$. An acceptable clarification for this performance has not yet been found. In a lot of circumstances, to fulfil both conditions, mixtures of levelling and brightening agents are utilised. The particular act of specific agents in certain baths is one of the features that are not easy to clarify. It is well recognized that some small differences in the structure of a brightener can loss its brightening capability and there are few probabilities to use one and the similar agent in different baths.²⁸

For a deposit to be bright, the microscopic roughness of the deposit must be low compared with the wavelength of the incident light so that it is reflected rather than scattered. Brighteners are normally used in relatively high concentration (several g.dm^{-3}) and may result in considerable organic matter in the deposit. They generally cause the formation of an even, fine-grained deposit and, therefore, may act by variation of the nucleation process. While levellers produce a level deposit on a more macroscopic scale and act by adsorption at points where otherwise there would be rapid deposition of metal. Therefore, adsorption of additives occurs especially at dislocations because of a higher free energy of adsorption and at peaks because the rate of their diffusion to such points is improved. Usually the adsorbed additive will reduce the rate of electron transfer.

Levelling and brightening phenomena are essentially associated with those parameters which determine the current distribution and the processes of crystal growth on an electrode. This is because, broadly speaking, the current distribution at the surface will control the local growth rates of the electrodeposit. The current distribution which would result if polarisation were considered to be absent at a metallic electrode is known as the primary current distribution.²⁹

Additives can be characterised by their main function, as brighteners of the first and second class, levellers, stress relievers, depolarisers and wetting agents. Certain chemicals can deliver more than one function. For instance, an additive introduced to help relieve stress in the deposit can also help with the brightness, consequently improving the appearance of the deposit.¹ In practice, many addition agents act as both brighteners and levellers.³⁰

The diffusion-controlled leveling theory may be suitable for rough surfaces but becomes inappropriate on smooth surfaces or on the continued growth of bright deposits. It

appears likely that the “trial and error” method of selecting brightening agents is the only truly operative method for the near future.³¹⁻³³ Moreover, the quantity of additive required is unpredictable. Similarly, the number of these additives utilised in electroplating is very large and it is difficult to classify them. However, a temporary classification can be made as given in **Table 6.1**.^{23 34} Classic additives include wetting agents, brightening agents, leveling agents, carriers, ductility agents, and others.

Table 6.1: *Classification of additives used in the electrodeposition of metals*

Properties	Classification
Chemical nature	Organic compounds Inorganic compounds
Interfacial activity	Surfactants: - anionic - cationic - nonionic Tensioinactive substances
Dimensions of particles	Molecular solutions Colloids
Mechanism of adsorption on the cathode ²³	Rapid adsorption-desorption Class 1 Brighteners (carriers, control agents) Specific adsorption Class 2 Brighteners (levellers, polarizers)
Effect on the deposit	Levelling agents Brightening agents

6.3 Effect of brighteners on the morphology

The prediction of brightener efficacy depends very much on empirical observations for instance molecules with C-S bonds tend to function for silver plating, whereas alkynes are useful brighteners in nickel electroplating.²³

The brightness of a surface is defined as the optical reflecting power of the surface. It is measured by the amount of light noticeably reflected. Weil and Paquin²⁵ showed a linear correlation between the logarithm of the amount of light peculiarly reflected by a surface and the fraction of the surface possessing roughness of less than deposition: (a) diffusion-controlled levelling, (b) grain refining, and (c) randomization of crystal growing. Some essential characteristics of brightening and levelling are described by Oniciu and Muresan.²³

Four key effects of additives on the cathodic process may be considered for the additives in electrodeposition process:¹⁶

- (1) Poisoning of the surface (therefore, motivate the reaction overpotential).
- (2) Concurrent reduction of additives, which decrease net current of the reduction of metal ions.
- (3) Modification in the microstructure and crystallographic texture.
- (4) Change in the value of the overpotential of the deposition such as the charge transfer overpotential, the diffusion overpotential, the reaction overpotential, the crystallization overpotential, and the true resistance overpotential.

Winand discussed the mechanism of additive effects on electrodeposition as follows:³⁵

Organic additives

The organic additives in the solution have several effects:

- (1) if they adsorb at the surface of metal and have no affinity for water, they act as a strong inhibitors;
- (2) if they adsorb at the surface of metal and have affinity for water, they slightly inhibit the deposition or activate the deposition;
- (3) if they do not adsorb at the surface of metal and possess affinity for water, they slightly accelerate the deposition;
- (4) if they do not adsorb at the surface of metal and possess no affinity for water, they have no influence.

Inorganic additives

Inorganic anions can change the structure of the double layer and, thus, influence the charge transfer overpotential. The activation anions are: Cl^- , Br^- , I^- ; Intermediate ions are: NO_3^- , SO_4^{2-} ; and the inhibiting anions are: BF_4^- , $\text{NH}_2\text{SO}_2^{2-}$, ClO_4^- .

The anodic and cathodic reactions involve an electronic transfer between the solid electrode and ionic species in the electrolyte. Both electronic transfers can be used for oxidation. A direct oxidation can be used on the anodic side, while an indirect cathodic oxidation via an electro-Fenton reaction occurs. Therefore, from a macroscopic point of view the overall rate of an electrochemical reaction is the difference between the rates of oxidation (the anodic reaction) and reduction (the cathodic reaction).

The lattice structure of electrodeposited hard chromium is mainly reliant upon plating variables, but conventional plate consists of bcc crystals with a cell parameter of 288 pm. Variable proportions of a hexagonal close-packed structure are also sometimes

detected, depending upon the electrolytic circumstances under which the chromium is deposited.³⁶

6.4 Use of additives for electrodeposition from ionic liquids

Only a small amount of work has been carried out into brighteners in ionic liquids and few conclusions can as yet be drawn. Brighteners which depend on electrostatic or hydrophobic connections may function in ionic liquids but their efficiency is likely to be surface and (ionic liquid) cation/anion specific. So far all systems that possess bright metallic finishes have been found to have a nano-crystalline structure due possibly because of a progressive nucleation mechanism.

In aqueous solutions a variety of compounds are regularly added to act as brighteners. These are supposed to work by either shifting the redox potential of the metal through complexation or by impeding metal nucleation and progress at the electrode surface.³⁷ The addition of complexing agents such as ethylene diamine and EDTA can affect redox potentials where the position of stripping potentials can be shifted by over 250 mV. The complexing agents make it harder to reduce the metal and impede nucleation, which leads to less nuclei initiating and allows the crystals to grow larger before they meet a neighbouring grain. Bulk deposition from an ionic liquid having just CuCl_2 yields black, powdery deposits while adding a complexing agent can produce lustrous metallic deposits.³⁸ Adding of strong complexing agents to ionic liquids may not be unimportant, though, as it will similarly affect the charge on the metal centre and the interaction between the metal centre and the halide anion of the ammonium salt, affect viscosity and the phase behaviour. In Type 3 eutectics the probability exists to choose a Brønsted acid that might act as a built in brightener.

Abbott *et al.* carried out studies using commercial brighteners for zinc plating from Type 3 eutectics but to date none of these have shown any improved surface finishes.³⁷

³⁹ Some success has been achieved using complexing agents for instance ethylenediamine and acetonitrile and these are thought to function by complexing the chloride ions which adsorb on the electrode surface and lead to platelet morphologies for the deposits.

Endres⁴⁰ studied the use of nicotinic acid for the deposition of Pd and Al/Mn alloys from an AlCl_3 -1-butyl-3-methylimidazolium chloride ionic liquid and showed that, in

difference to producing a brighter surface finish, it assisted the formation of nano-crystalline deposits.

Brighteners that include a complexation with a solution-based species will rely upon the relative strength of the ligand–metal interactions. It would be logical to understand that ionic liquids with discrete, poorly coordinating anions should allow the direct use of brighteners utilised in aqueous solutions, as the interaction between the metal salt and the anion will be significantly weaker than those between the metal salt and the brightener. In eutectic-based ionic liquids the chloride anions act as strong Lewis bases and could reduce the relative interaction between the metal salt and the brightener. Brighteners which depend on electrostatic or hydrophobic interactions might function in ionic liquids but their efficacy is about to be surface and cation/anion specific. As with other solutes in ionic liquids, the overall rule of like dissolving like is valid i.e. ionic species will usually be soluble as will species capable to act together with the anion. Aromatic species have a tendency to show poor solubility in ionic liquids consisting of aliphatic cations and vice versa.

Ionic liquids themselves can be used as additives during plating from aqueous electrolytes, such as for grain refining.⁴¹⁻⁴³ Some investigations have investigated which additives enhance the properties of electrodeposited layers in ILs. Fedorov and Ivaništšev, Borisenko, Atkin, and Endres have studied the structure and dynamics of the IL/electrode interface.⁴² One significant fact discussed in those contributions is that the double layer in ILs is not the same from that in aqueous solutions. The current model involves a structure of alternating anions and cations radiating from the electrode surface which is probably quite rigid for at least 5 ion pair dimensions from the electrode surface. In the absence of additives, the cations of an IL will concentrate at the electrode surface when it is negatively polarized. The reduction of metal cations is anticipated to happen gradually, through the adsorbed layer of cations (e.g., 1-butyl-1-methylpyrrolidinium cation, [BMP]⁺). Consequently, the reduction of the metal ions is slowed down.⁴²

In the presence of additives, a cationic complex of the metal ions with the additive can be formed, and this can relatively compensate for the electrostatic barrier at the interface by enabling charge transfer to the metal ions. Further mechanisms can be based on the adsorption of the additives on the electrode surface. Via substituting some of the bulky adsorbed IL cations, the additive molecules can induce a more facile electrode reaction.

Hence, a smoother and shinier surface could be obtained in the presence of additives (e.g. acetonitrile, coumarin, thiourea, benzotriazole or acetone)⁴⁴⁻⁴⁶ with better adhesion on the substrate also observed in the case of coumarin.^{47, 48} For instance, acetonitrile has been added as an additive during Fe deposition from 1-butyl-1-methylpyrrolidinium bis(tri-fluoromethylsulfonyl) amide, [BMP][TFSA], containing $\text{Fe}(\text{TFSA})_2$ ⁴⁷. Acetone,^{45, 46} coumarin⁴⁸ and thiourea^{46, 48} have been added during Co and Ni electrodeposition from [BMP][TFSA], containing $\text{Co}(\text{TFSA})_2$ or $\text{Ni}(\text{TFSA})_2$. Variations in the coordination chemistry has been noted with the use of thiourea,⁴⁸ acetonitrile and acetone are greater because the coordination number of acetonitrile or acetone is 14 associated to those induced by the [TFSA]-anion (coordination number 7).⁴⁷

The variations in the coordination surroundings showed the creation of a complex product between the metal ions and the additives, which might simplify the reduction of the Co^{2+} . Nevertheless, the coordination was not affected when coumarin was used in Co deposition from [BMP][TFSA] ILs containing $\text{Co}(\text{TFSA})_2$ ⁴⁸ proposing that no complex of Co^{2+} ions with coumarin was made. The reduction of cobalt happened from the divalent cobalt species $[\text{Co}(\text{TFSA})_3]^-$.

Nicotinamide has been used as an additive during Al electrodeposition from AlCl_3 in 1-butyl-3-methylimidazolium chloride⁴⁹ which resulted in a smooth surface finish. Zinc electrodeposition from Reline (1:2 choline chloride: urea) and Ethaline (1:2 choline chloride: ethylene glycol) in the presence of acetonitrile, ethylene diamine and ammonia has been studied by the Abbott group.³⁹ The use of ammonia encouraged mass transport, improved deposition rates and produced a smooth surface morphology. The addition of ethylene diamine slowed the reduction of Ni but favoured the reduction of Zn. Brighter deposits might be obtained in the presence of either ethylene amine or ammonia. Acetonitrile had an insignificant effect on the electrochemical deposition of Zn from ILs. LiCl has been used in Al electrodeposition⁵⁰ and LiF in Ta electrodeposition.⁵¹ In all cited studies, it was shown that the grain size and morphology of the deposits, and the electrochemical behaviour might be changed by the lithium cations which are thought to adsorb preferentially at the electrode interface due to their high charge density. This can change the charge density at the electrode-liquid interface and modify the nucleation mechanism.

The role of brighteners is an important topic and one that is being further investigated in the group.

6.5 Results and discussion

The appearance, structure and properties of hard chromium are highly sensitive to plating conditions in a typical plating bath, and substantial work has been carried out in establishing ranges (in terms of plating variables) in which acceptable deposits may be obtained. The ranges in which bright hard chromium deposits (corresponding to optimum physical properties, in general) are produced from standard solutions are narrow and poorly understood. Structure of the substrate is only important in controlling the deposit structure where the deposit is thin. Therefore, the substrate initially nucleates with lateral, epitaxial growth,¹ but finally loses its effect, with subsequent growth being controlled completely by plating conditions such as voltage, current, temperature and concentration.

In previous chapters the role of conductivity and viscosity were studied. This was seen to be improved through the incorporation of more waters of hydration and group 1 cations such as potassium. In Chapter 4 the complexation of the chromium centre was studied with ethylene diamine and it was seen that maintaining constant speciation was important in obtaining bright, hard deposits. The aim of the current chapter is to investigate the role of these three aspects using three types of additives;

- (a) Water
- (b) Complexing agents (boric acid)
- (c) A catalyst for the anodic reaction (sodium bromide).

In the following sections the effect of the selected classical additives on the deposit morphology and properties will be determined for the following systems:

- i. 2 Urea: $\text{CrCl}_3 \cdot 6\text{H}_2\text{O}$
- ii. 2 Urea: $\text{KCr}(\text{SO}_4)_2 \cdot 12\text{H}_2\text{O}$

Initially the effect on morphology will be determined in a phenomenological manner and then conductivity, viscosity and speciation data will be obtained in an endeavour to explain the observed deposit morphology.

6.6 Effect of additives on bulk deposition

Table 6.2 shows the deposits obtained from the electrolysis of 2 urea: $\text{CrCl}_3 \cdot 6\text{H}_2\text{O}$ with and without various additives at specified current densities. It also shows the deposit morphology in plan and cross section obtained from SEM and the hardness of the films

obtained on mild steel. The system without additives produces a dense, black film with relatively good hardness. The addition of water does not change the appearance but it does increase the thickness and hardness of the film despite the lower current density.

Boric acid is a common brightener used in aqueous chromium plating and when added to the 2 urea: $\text{CrCl}_3 \cdot 6\text{H}_2\text{O}$ liquid little difference in appearance deposit morphology and hardness are observed compared to the neat liquid. Sodium bromide has been found within the group, to act as a brightener and it is thought to function by increasing the rate of the anodic reaction. It has been shown that for most electrodeposition processes the rate of the anodic reaction is the determining step.⁵² The addition of NaBr allows an increase in the current density and changes the appearance, morphology and thickness but the deposit is softer than without the additive. It is thought that the bromide is easily oxidised to bromine which complexes with the excess of chloride ions and produces Br_2Cl^- which is quite stable in solution. The incorporation of metal powder, in this case chromium should enable the oxidation of the chromium and the regeneration of the bromide ions.

The addition of boric acid and water causes the most significant change in appearance, morphology and hardness. Presumably the water encourages greater dissociation of the acid. Boric acid could function as an interfacial modifier or as a complexing agent changing the speciation. The final additive combination tested was NaBr plus water. It does permit a higher current density to be applied compared with just water although there is as yet insufficient evidence to show this is because the anodic process is catalysed. There is a clear difference in the appearance of the deposited film although it is not as bright as the corresponding liquid with boric acid in it. The hardness is comparable to the liquid with just water as an additive but the microstructure is finer which results in a dull but metallic looking coating.

The same experiments were repeated using the 2 urea: $\text{KCr}(\text{SO}_4)_2 \cdot 12\text{H}_2\text{O}$ eutectic and the resulting films are shown in **Table 6.3**. At first glance the results are remarkably similar to those seen in **Table 6.2** showing that that the additives have a similar effect on current density and film hardness irrespective of the liquid viscosity, conductivity or chromium speciation. Each of these variables will be studied in depth below. It is clear however that boric acid has the most significant effect on surface morphology and properties. The deposits obtained from bulk deposition have the highest hardness values.

Table 6.2: Optical photograph, SEM image, thickness cross section and plating conditions of chromium deposit obtained from the electroreduction of **2 urea**: $\text{CrCl}_3 \cdot 6\text{H}_2\text{O}$ with and without additives, for 1 hour at 313 K and ~ 5 V.

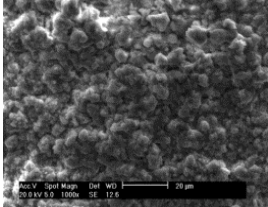
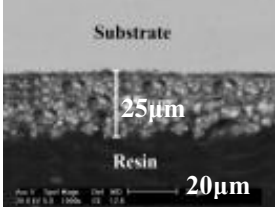
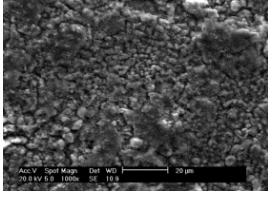
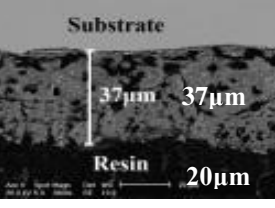
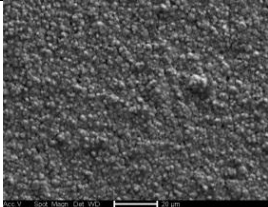
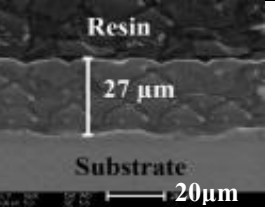
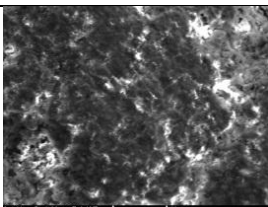
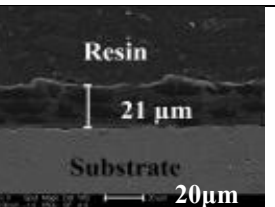
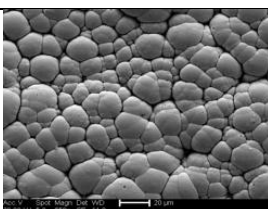
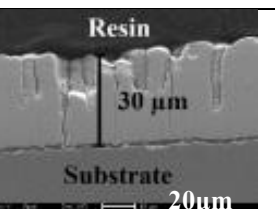
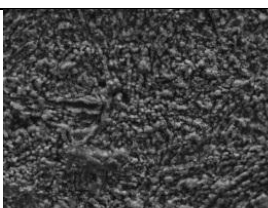
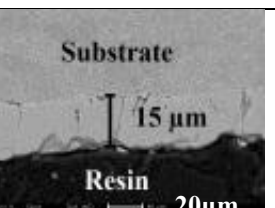
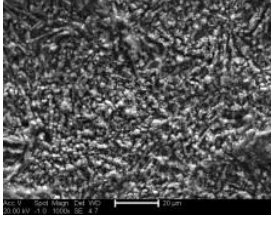
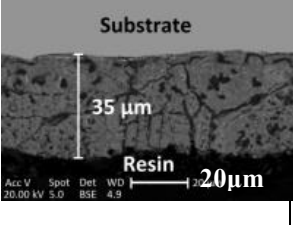
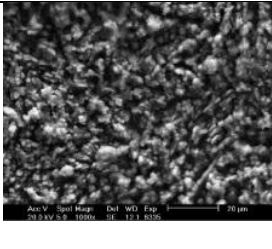
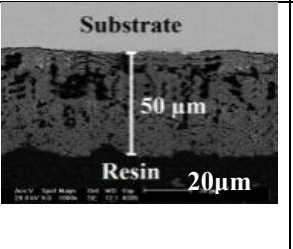
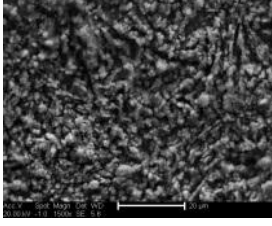
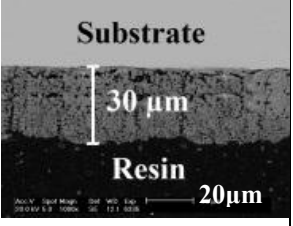
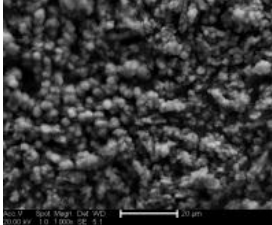
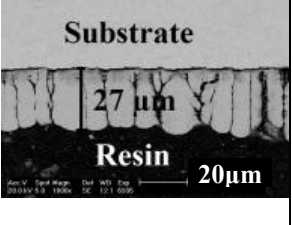
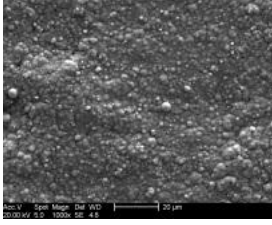
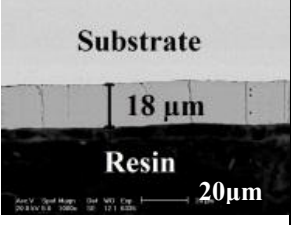
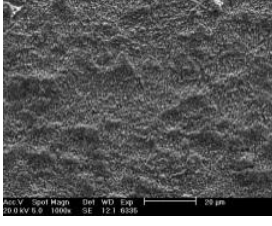
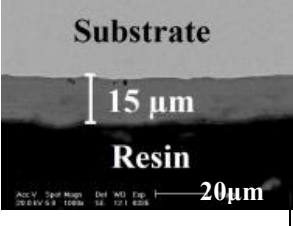
DES + (Current density/ $\text{mA} \cdot \text{cm}^{-2}$)	Optical image	SEM image	Cross section thickness	Hardness/ HV
2urea: $\text{CrCl}_3 \cdot 6\text{H}_2\text{O}$ (200)				650 ± 10
DES + 20% H_2O (122)				715 ± 10
DES + 0.1 M boric acid (250)				610 ± 10
DES + 0.1 M NaBr (250)				600 ± 10
DES + 20% H_2O + 0.1 M boric acid (150)				850 ± 10
DES + 20% H_2O + 0.1 M NaBr (180)				700 ± 10

Table 6.3: Optical photograph, SEM image, thickness cross section and plating conditions of chromium deposit obtained from the electroreduction of 2 urea: $KCr(SO_4)_2 \cdot 12H_2O$ with and without additives, for 1 hour at 313 K and ~ 4 V.

<i>DES + (Current density/ $mAcm^{-2}$)</i>	<i>Optical image</i>	<i>SEM image</i>	<i>Cross section thickness</i>	<i>Hardness/ HV</i>
2urea: $KCr(SO_4)_2 \cdot 12H_2O$ (150)				680 ± 10
DES + 20% H_2O (125)				700 ± 10
DES + 0.1 M boric acid (150)				680 ± 10
DES + 0.1 M NaBr (150)				650 ± 10
DES + 20% H_2O + 0.1 M boric acid (130)				800 ± 10
DES + 20% H_2O + 0.1 M NaBr (120)				780 ± 10

6.7 Viscosity and conductivity

Table 6.4 shows the conductivity and viscosity of the urea: $\text{CrCl}_3 \cdot 6\text{H}_2\text{O}$ and the urea: $\text{KCr}(\text{SO}_4)_2 \cdot 12\text{H}_2\text{O}$ systems with added water, NaBr and boric acid (BA) (Full data as a function of temperature are in chapter 8). It can clearly be seen that water has the most significant effect upon conductivity and viscosity and the other additives have a negligible effect.

Interestingly the addition of both boric acid and sodium bromide both decrease the conductivity slightly despite adding more charge carriers and this is due to the associated increase in viscosity. In all cases an increase in conductivity is associated with a decrease in viscosity

Table 6.4: Conductivity and viscosity at 323 K of the urea: $\text{CrCl}_3 \cdot 6\text{H}_2\text{O}$ and the urea: $\text{KCr}(\text{SO}_4)_2 \cdot 12\text{H}_2\text{O}$ systems with added water, NaBr and boric acid (BA)

DES = 2urea: $\text{CrCl}_3 \cdot 6\text{H}_2\text{O}$						
	No additive	20 wt% H_2O	0.1M BA	0.1M NaBr	20wt% H_2O +0.1M BA	20wt% H_2O +0.1M NaBr
Conductivity mS.cm^{-1}	9.81	28.20	7.35	5.39	23.62	18.68
Viscosity cP	371.9	26.51	409.1	446.3	29.81	44.71
DES = 2urea: $\text{KCr}(\text{SO}_4)_2 \cdot 12\text{H}_2\text{O}$						
	No additive	20wt% H_2O	0.1M BA	0.1M NaBr	20wt% H_2O +0.1M BA	20wt% H_2O +0.1M NaBr
Conductivity mS.cm^{-1}	13.24	43.20	11.25	8.21	34.12	20.47
Viscosity cP	122.7	16.62	135.0	146.0	28.25	33.90

Although 20 wt% of water may seem like a large amount of additive it equates to about 5 mole equivalents for each chromium complex in the liquid and it results in an increase in viscosity by a factor of between two and three times. The decrease in viscosity is considerably greater. The effect of the additives on viscosity and conductivity can be more clearly seen in **Figure 6.1** for the 2 urea: $\text{CrCl}_3 \cdot 6\text{H}_2\text{O}$ and 2 urea: $\text{KCr}(\text{SO}_4)_2 \cdot 12\text{H}_2\text{O}$ mixtures with different additives. While boric acid and sodium bromide change the conductivity and conductivity of the liquid slightly the slopes are the same showing that it is the same charge carrying species i.e. the smaller proton and sodium ions do not increase ionic mobility. It is also clear that the addition of water increases the conductivity but the slope of conductivity/fluidity actually decreases.

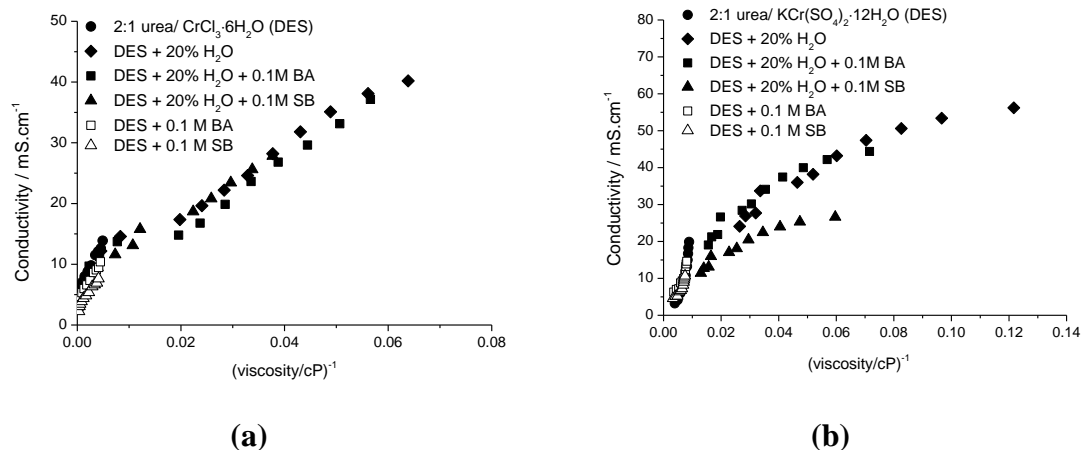


Figure 6.1: Conductivity as a function of fluidity for the (a) 2 urea: CrCl₃·6H₂O and (b) 2 urea: KCr(SO₄)₂·12H₂O systems with different additives

To probe this more clearly it is useful to show the data in a Walden plot by converting the conductivity data to molar conductivity and this is shown for the pure liquids and those with water as an additive in **Figure 6.2**. It can be seen that there is a relatively modest increase in molar conductivity despite a significant increase in fluidity. While this needs significantly more in depth study it could be proposed that this is due to a difference in the mechanism of conductivity when water is added. It has been postulated that in ionic liquids and DESs the conductivity is limited by the availability of suitably sized holes for ions to move via. When water is added there is an increase in the ions being able to move but the ions are now not independent but they are associated and so although there are more charge carriers their mobility is restricted due to association. It might be expected that the higher conductivity may lead to an increase in the current density for deposition but this is not the case and there is also no correlation between the current density and the deposit thickness or deposit hardness.

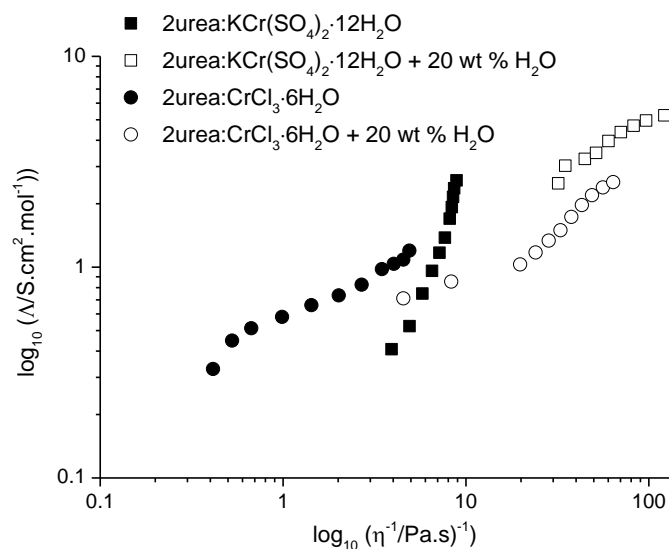


Figure 6.2: Molar conductivity as a function of $1/\text{viscosity}$ for the 2urea: $\text{CrCl}_3 \cdot 6\text{H}_2\text{O}$ and 2urea: $\text{KCr}(\text{SO}_4)_2 \cdot 12\text{H}_2\text{O}$ systems with and without the addition of 20 wt% water.

To determine whether there was a change in the properties of the liquid when water was added the viscosity of the $\text{CrCl}_3 \cdot 6\text{H}_2\text{O} : 4\text{urea}$ as a function of spindle speed. **Figure 6.3** shows a steady decrease in viscosity with shear rate suggesting that the liquid behaves in a non-Newtonian manner. Newtonian fluids should have a constant viscosity with shear rate and this is clearly not the case with the chrome alum eutectic. A decrease in viscosity with shear rate means that at low rotation speed the interionic and intermolecular forces are large and resist the motion of the spindle. At higher rotation speeds the ions do not have sufficient time to reform their interactions and so the viscosity decreases. This is a characteristic for pseudo-plastic fluids. The addition of water to the eutectic decreases the change of viscosity with shear rate but it still decreases showing that non-Newtonian behaviour exists. This is very important as the standard solution models which are traditionally used for ionic liquids such as Fickian diffusion are no longer valid and it may also help to explain why previous studies of diffusion have found that the Stokes-Einstein equation is not valid in a range of standard ionic liquids.

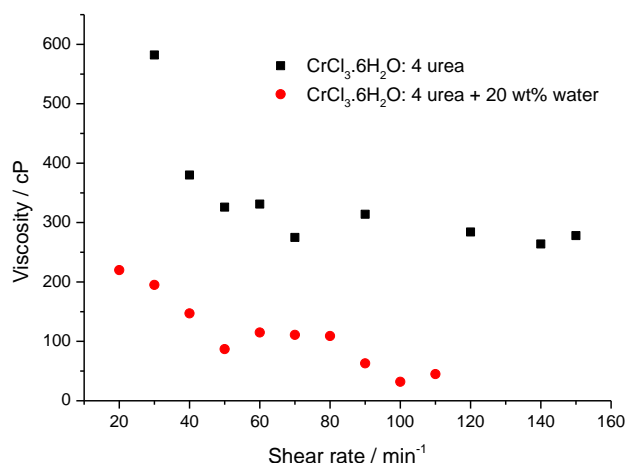


Figure 6.3: Viscosity for the 4urea: $\text{CrCl}_3 \cdot 6\text{H}_2\text{O}$ system with and without 20 wt% water as a function of shear rate.

6.8 Solution speciation

To understand the role of the brighteners it is important to determine the difference in speciation in the liquids. **Figure 6.4** shows the UV-Vis spectra for the systems shown in **Tables 6.2** and **6.3**. The absorbance maxima of the peaks are listed in **Table 6.5**. The spectra are very comparable for all of the liquids showing that speciation remains similar. It is however noticeable that for both systems the peak at 600 to 620 nm develop a shoulder at 680 to 700 nm on the addition of water.

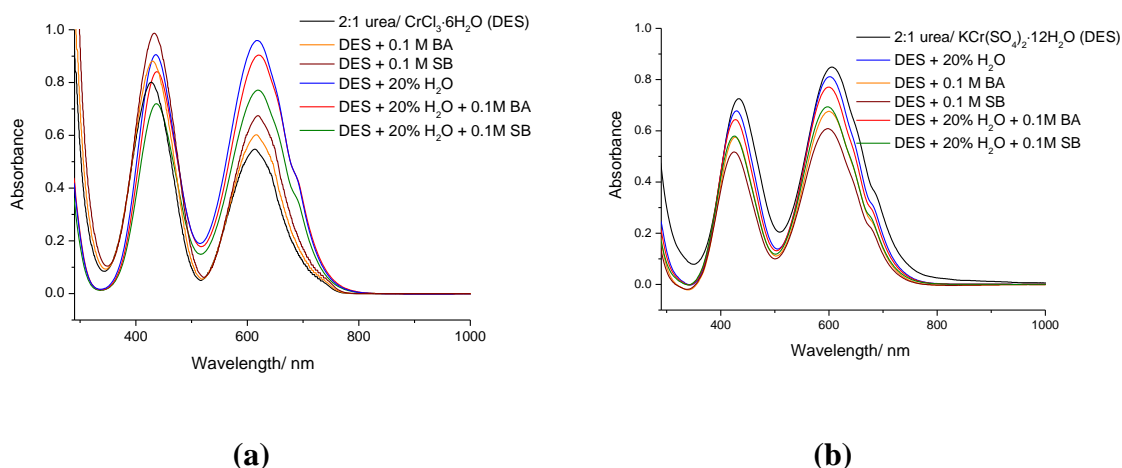


Figure 6.4: UV-Vis spectra of (a) 2 urea: $\text{CrCl}_3 \cdot 6\text{H}_2\text{O}$ and (b) 2 urea: $\text{KCr}(\text{SO}_4)_2 \cdot 12\text{H}_2\text{O}$ systems with and without additives

Table 6.5: The positions of the absorption maximum (nm) of Cr(III) complexes in both DESs shown in Figure 6.2.

System	2urea: CrCl ₃ ·6H ₂ O peak maxima/ nm		2urea: KCr(SO ₄) ₂ ·12H ₂ O peak maxima/ nm	
No additive	426	613	433	605
DES + 0.1 M boric acid	430	617	427	600
DES + 0.1 M sodium bromide	433	617	425	598
DES + 20% H ₂ O	436	617	430	603
DES + 20% H ₂ O + 0.1 M boric acid	438	622	426	599
DES + 20% H ₂ O + 0.1 M sodium bromide	437	619	425	597

Elving and Zemel⁵³ studied the CrCl₃·6H₂O in water system⁵⁴ and found that the number of chloride and water ligands bound to the metal affected the UV-visible spectrum of the chromium species. They found two bands varying from 407 to 475 nm (4T_{1g} ← 4A_{2g}) for the first and from 575 to 665 nm (4T_{2g} ← 4A_{2g}) for the second band. For each band the lower end of the wavelength absorbance was assigned to the hexaqua complex and the upper end to the tri-chloro species. The addition of each chloride ligand moves the wavelength of each band by about 20 to 30 nm. In a neutral aqueous solution, the hexa-aqua species dominates but the tri-chloro species dominates in 12 mol dm⁻³ HCl. The literature assignments are listed in **Table 6.6**. Comparison of the data in **Tables 6.5** and **6.6** suggests that [Cr(H₂O)₅Cl]²⁺Cl₂·H₂O is the dominant chromium species in all the CrCl₃ liquids and a similar penta-aqua species probably dominates in the chrome alum liquid as well.

Table 6.6: The literature data⁵³ on the positions of the absorption maximum (nm) of Cr(III) complexes

CrCl ₃ ·6H ₂ O complexes	1 st absorption peak/ nm	2 nd absorption peak/ nm
[Cr(H ₂ O) ₆] ³⁺ Cl ₃	407	575
[Cr(H ₂ O) ₅ Cl] ²⁺ Cl ₂ ·H ₂ O	430	605
[Cr(H ₂ O) ₄ Cl ₂] ⁺ Cl·2H ₂ O	450	635
[Cr(H ₂ O) ₃ Cl ₃].3H ₂ O	475	665

The shoulder formed on the addition of water is surprisingly not from the hexa-aqua species. The origin of the shoulder at 680 to 700 nm formed on the addition of water is not clear from this study but it is important to highlight that the addition of boric acid and sodium bromide do not lead to a significant change in speciation and therefore it must be concluded that these probably function by modifying the double layer properties close to the electrode surface.

6.9 Cyclic voltammetry

Figure 6.5 shows cyclic voltammograms for the 2 urea: $\text{CrCl}_3 \cdot 6\text{H}_2\text{O}$ and 2 urea: $\text{KCr}(\text{SO}_4)_2 \cdot 12\text{H}_2\text{O}$ systems at different compositions, recorded at 313 K on a Pt disc electrode with a sweep rate of 20 mV s^{-1} .

Analysing first the systems without added water; for the 2urea: $\text{CrCl}_3 \cdot 6\text{H}_2\text{O}$ system on Pt (**Figure 6.5a**) there is a quasi-reversible reduction process with an onset potential of -0.5 V. There are, however smaller signals probably corresponding to under-potential deposition centred on 0.6 V. On a graphite electrode (**Figure 6.5b**) the $\text{Cr}^{\text{III/II}}$ redox couple can be seen more clearly at +0.6 V and the $\text{Cr}^{\text{II/0}}$ couples are better defined at -0.45 V. The addition of boric acid decreases the reduction current and the addition of sodium bromide decreases it still further. This could be an interfacial phenomenon but the data in **Table 6.4** suggest that it is possibly just a mass transport effect as the viscosity increases in the order no additive < boric acid < sodium bromide.

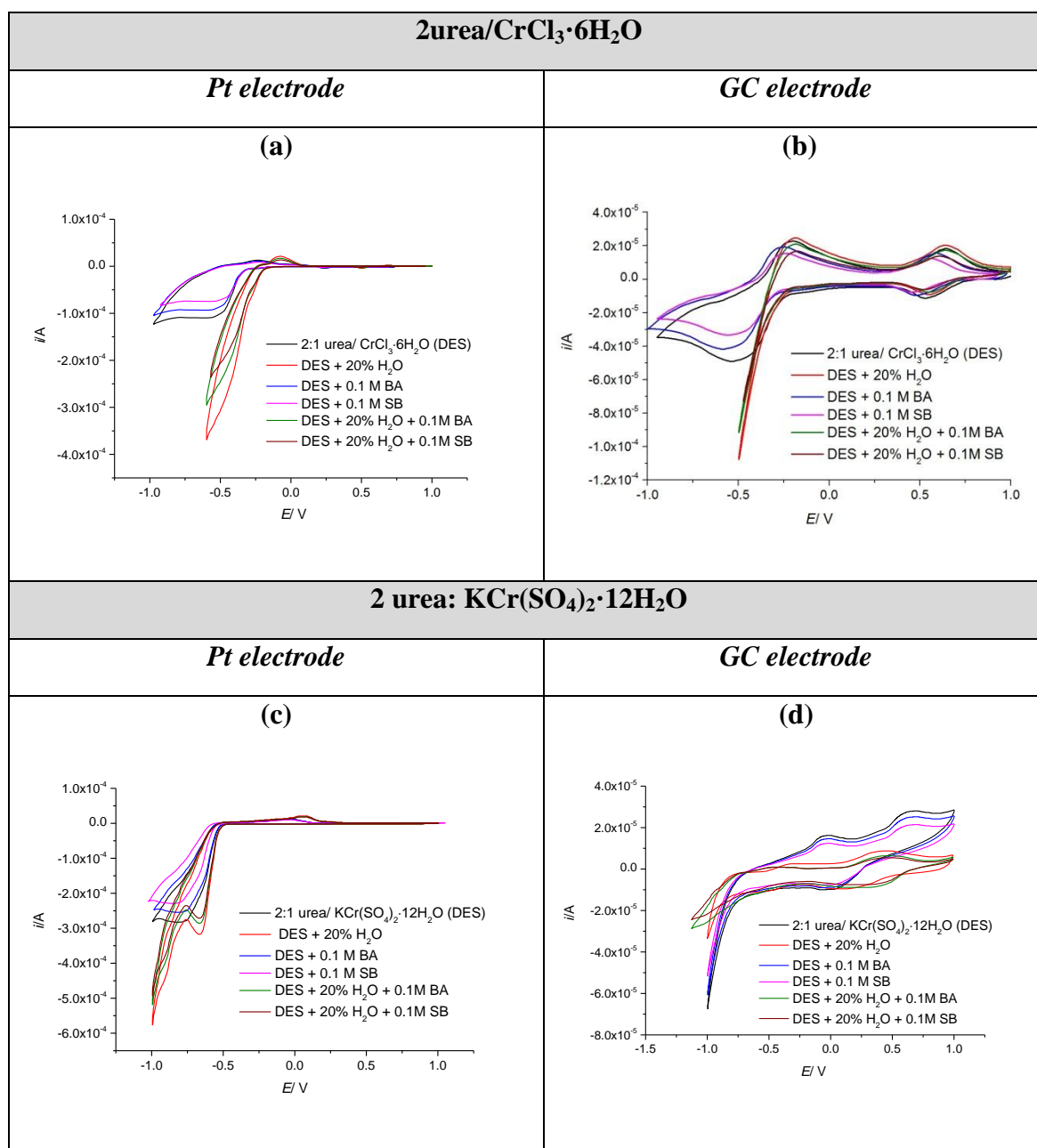


Figure 6.5: Cyclic voltammogram for the 2 urea: $\text{CrCl}_3 \cdot 6\text{H}_2\text{O}$ and 2 urea: $\text{KCr}(\text{SO}_4)_2 \cdot 12\text{H}_2\text{O}$ systems as a function of additives at 313 K on a Pt electrode (area = $7.85 \times 10^{-3} \text{ cm}^2$) and a GC electrode (area = $4.90 \times 10^{-2} \text{ cm}^2$) at a sweep rate of 20 mV s^{-1}

For the 2 urea: $\text{KCr}(\text{SO}_4)_2 \cdot 12\text{H}_2\text{O}$ system on Pt (**Figure 6.5c**) the same trend is observed in the absence of added water although the currents are larger and again these scale with the viscosity of the liquids shown in **Table 6.4** confirming the supposition that the process is mass transport controlled. On a graphite electrode (**Figure 6.5d**) the $\text{Cr}^{\text{III/II}}$ redox couple is markedly less reversible and less affected by additives.

Comparing the data for the liquids with added water it can be seen that for the 2 urea: $\text{CrCl}_3 \cdot 6\text{H}_2\text{O}$ system on Pt (**Figure 6.5a**) the onset potential for reduction of Cr^{III} is shifted to less negative values. The reduction current increases significantly which

could be due to water reduction although there is negligible gassing even during bulk electrolysis. On the other hand, increases the conductivity and fluidity could also be responsible for increases the cathodic current. The observation that the current decreases when boric acid is added supports the idea that hydrogen evolution is negligible and the current scales with viscosity. The same trends are observed on graphite.

EQCM studies were carried out on the 2 urea:CrCl₃·6H₂O with 20 wt% H₂O and 0.1 mol dm⁻³ boric acid system and it was found that the current efficiency was 63% while for the 2 urea: Cr alum with 20% H₂O and 0.1 mol dm⁻³ boric acid is it was found to be 70%. This shows that there is some decrease in current efficiency and by inference some hydrogen evolution but the values are considerably higher than the current efficiency in aqueous solutions.

The addition of water to the chrome alum system has a less significant effect upon the onset potential and reduction current for chromium reduction but water also has only a small effect on liquid viscosity which would correlate well with the data in **Figure 6.5c**. These data suggest that voltammetric currents correlate well with viscosity showing that nucleation is mass transport controlled but deposit thicknesses are not related to viscosity showing that growth has a different mechanism. This is a common observation within the group and one that is currently undergoing further investigation.

6.10 Hardness and thickness

Chromium coatings are used for surfaces that endure significant wear *e.g.* hydraulic shafts. An important property of the coatings is therefore their hardness. Generally, chromium is the hardest of the most commonly deposited metals.⁵⁵ Chromium deposited using chromic acid has hardness values of typically 800 HV. Previous studies using the ChCl/CrCl₃·6H₂O system produced a coating with a hardness of 242 Vickers. In aqueous commercial trivalent baths the maximum chromium thickness achieved is normally less than 10 μm. These coatings are not hard as they display too many of the characteristics of the softer substrate, making the deposits unsuitable for wear-resistant applications.^{56, 57} The systems in **Table 6.2** and **6.3** all have thicknesses between 15 and 50 μm which means that the indentation of the measuring method will not perturb the substrate giving a true measurement of hardness. It is evident that the systems which have water added to them produce films which are more compact when viewed in cross-

section. For both DESs the systems without water have a higher density of micro-cracks which are evidently affecting film hardness. The hardest coatings appear to be those which are most homogeneous in cross-section and there seems little correlation with the surface morphology.

The coatings produced using both boric acid and water had the hardest surfaces with hardness values of 800-850 HV. This is at least as hard as aqueous chromic acid and the thicknesses obtained are significantly in excess of those possible using aqueous trivalent chromium electrolytes.

6.11 X-ray diffraction

The X-ray diffraction spectrum of an electrodeposited metallic coating is usually different from that of the metal in a normal annealed state and the same is true for physical properties as the hardness. The crystal structure of the deposits can affect the properties of the film and to determine the effect of additives on crystal structure powder x-ray diffraction was carried out on the coatings.

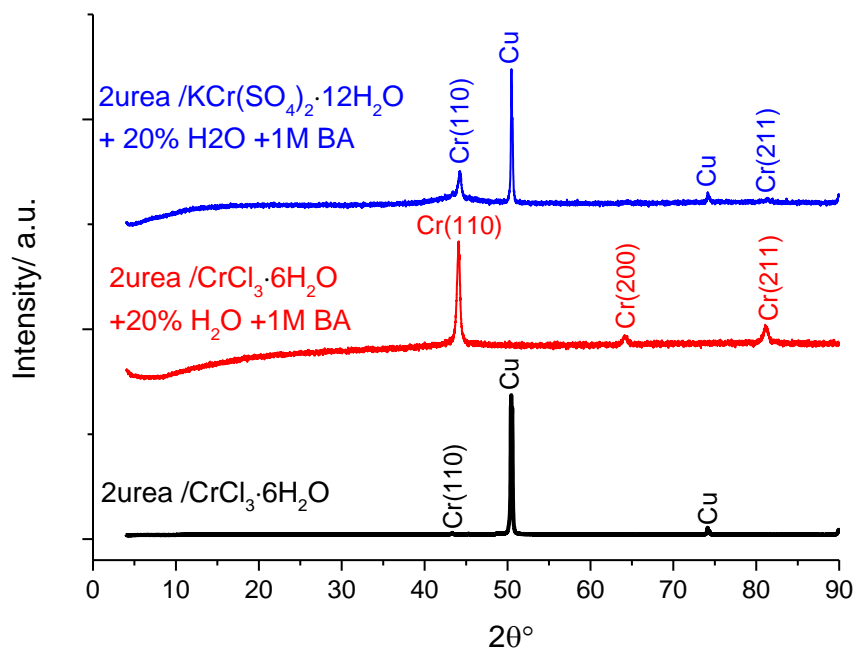


Figure 6.6: XRD patterns of the chromium coatings prepared from the selected electrolyte separately.

X-ray diffraction (XRD) studies were done to determine the crystallite size and crystal structure of the coatings employing Cu K_{α} radiation of wavelength 0.154 nm. The crystallite size was determined with reference to the (200) reflection applying line broadening technique using Scherrer equation,⁵⁸

$$d = \frac{K\lambda}{\beta \cos\theta} \quad \text{Equation 6.2}$$

where, K is the Scherrer factor ≈ 1 , d the crystallite size, λ is the wavelength of the X-rays (0.154 nm for Cu K_{α} radiation) and θ is the Bragg diffraction angle. β is the full width at half maximum height of the peak. Using **Equation 6.2** the particle size of the crystallites is in the range 40.8 to 90.1 nm. This appears to be the same irrespective of the DES used.

The orientation of the deposit has been shown to be reliant upon the nature of the substrate, plating conditions, and the plate thickness and epitaxial effects are normally limited to those layers of the deposit immediately adjacent to the substrate. It may therefore be concluded that structure and properties of chromium plate is only substrate-sensitive where the deposit is thin. Regardless of substrate effects, the brightest chromium deposits have been shown when the (111) orientation dominates⁵⁹ at a thickness of 1 μm , which does not vary with deposit thickness. In less bright deposits, the variation of texture with thickness is more marked.⁵⁹ In the data from **Figure 6.6** it can be seen that the (110) orientation dominates with a smaller signal from the (211) orientation. In the urea: $\text{CrCl}_3 \cdot 6\text{H}_2\text{O}$ systems there is some signal for the (200) structure which is not observed with the chrome alum eutectic.

6.12 Conclusions

This chapter has studied the effect of additives on the morphology and hardness of chromium films. It has been shown that additives such as boric acid and sodium bromide lead to less dense films but the addition of 20 wt% water significantly improves deposit homogeneity and particularly when water is combined with boric acid or sodium bromide then bright, hard, and most importantly thick chromium films can be obtained. This is the first time that trivalent chromium containing liquids have been able to be used to obtain these specifications. Thicknesses of up to 50 μm have been obtained

and a hardness of 850 HV is sufficient for use in anti-wear coatings. There is potential to further improve the hardness by heat treating the materials.

These brighteners have been shown to be effective for both chromium-based eutectic and it is shown that the additives do not significantly affect speciation but rather they appear to function by modifying interfacial properties. Both boric acid and sodium bromide increase the viscosity of the DES but water significantly increases the fluidity of the liquids. The cathodic currents ascribed the chromium reduction appear to scale with the viscosity of the liquid showing that nucleation is mass transport controlled. Growth, however, does not appear to follow this behaviour and the mechanism for sustained growth is a topic that requires further study.

6.13 References

1. J. K. Dennis and T. E. Such, *Nickel and Chromium Plating*, Woodhead Publishing, 1993.
2. W. An and P. N. Pintauro, *Industrial Electrochemistry and Electrochemical Engineering (General) - 215th ECS Meeting*, Electrochemical Society, 2009.
3. Y. Song and D.-T. Chin, *Plating and surface finishing*, 2000, **87**, 80-87.
4. F. Danilov, V. Protsenko, T. Butyrina, E. Vasil'eva and A. Baskevich, *Protection of metals*, 2006, **42**, 560-569.
5. Z. Zeng, Y. Sun and J. Zhang, *Electrochemistry communications*, 2009, **11**, 331-334.
6. S. Survilienė, V. Jasulaitienė, O. Nivinskienė and A. Češūnienė, *Applied surface science*, 2007, **253**, 6738-6743.
7. J.-Y. Hwang, *Plating and surface finishing*, 1991, **78**, 118-125.
8. J. McDougall, M. El-Sharif and S. Ma, *J Appl Electrochem*, 1998, **28**, 929-934.
9. I. Drela, J. Szykarczuk and J. Kubicki, *J Appl Electrochem*, 1989, **19**, 933-936.
10. S. White and U. Twardoch, *J Appl Electrochem*, 1987, **17**, 225-242.
11. V. Protsenko, T. Butyrina and F. Danilov, *Protection of metals*, 2007, **43**, 398-406.
12. I. M. Kolthoff and J. J. Lingane, *Polarography: Polarographic Analysis and Voltammetry, Amperometric Titrations*, Interscience Publishers, 1946.
13. J. Szykarczuk, I. Drela and J. Kubicki, *Electrochim Acta*, 1989, **34**, 399-403.
14. A. Edigaryan and Y. M. Polukarov, *Protection of metals*, 1998, **34**, 95-100.
15. V. Korshunov, V. Safonov and L. Vykhodtseva, *Russian Journal of Electrochemistry*, 2008, **44**, 255-264.
16. H. Fischer, *Electrodeposition and Surface Treatment*, 1973, **1**, 319-337.
17. H. Fischer, *Electrodeposition and Surface Treatment*, 1973, **1**, 239-251.
18. M. Fleischmann, H. Thirsk and P. Delahay, *Vol. 3 Interscience, New York*, 1963, 123.
19. Y. Loshkarev, *Zashchita Metallov*, 1972, **8**, 163-169.
20. T. Franklin, *Surface and Coatings Technology*, 1987, **30**, 415-428.
21. M. A. Loshkaryov and Y. M. Loshkaryov, *Surface Technology*, 1978, **6**, 397-408.
22. M. Nuñez, *Metal Electrodeposition*, Nova Science Publishers, 2005.
23. L. Oniciu and L. Mureşan, *J Appl Electrochem*, 1991, **21**, 565-574.
24. W. Blum, A. Beckman and W. R. Meyer, *Transactions of The Electrochemical Society*, 1941, **80**, 249-299.
25. R. Weil and R. Paquin, *J Electrochem Soc*, 1960, **107**, 87-91.
26. G. T. Rogers, M. J. Ware and R. V. Fellows, *J Electrochem Soc*, 1960, **107**, 677-682.
27. J. O. Dukovic and C. W. Tobias, *J Electrochem Soc*, 1990, **137**, 3748-3755.
28. S. Barnes, *Electrochim Acta*, 1961, **5**, 79-86.
29. H. Gerischer and C. W. Tobias, *Advances in Electrochemistry and Electrochemical Engineering*, John Wiley & Sons, 1984.
30. G. P. P. N. P. W. An, *Industrial Electrochemistry and Electrochemical Engineering (General) - 215th ECS Meeting*, Electrochemical Society, 2009.
31. A. Vagramyan, Z. Solov'Eva and S. Senderoff, *J Electrochem Soc*, 1963, **110**, 122C-122C.
32. E. Raub and K. Muller, 1967, 268 P. ELSEVIER PUBLISHING CO., NEW YORK, 1967.

33. M. Schwartz, *Handbook of Deposition Technologies for Films and Coatings—Science, Technology and Applications*, William Andrew Publishing, Noyes, 1994, 506.
34. Y. D. Gamburg and G. Zangari, *Theory and Practice of Metal Electrodeposition*, Springer, 2011.
35. R. Winand, *Hydrometallurgy*, 1992, **29**, 567-598.
36. C. A. Snavely, *Transactions of The Electrochemical Society*, 1947, **92**, 537-577.
37. F. Endres, D. MacFarlane and A. Abbott, *Electrodeposition from ionic liquids*, John Wiley & Sons, 2008.
38. A. P. Abbott and K. J. McKenzie, *Phys Chem Chem Phys*, 2006, **8**, 4265-4279.
39. A. P. Abbott, J. C. Barron, G. Frisch, K. S. Ryder and A. F. Silva, *Electrochim Acta*, 2011, **56**, 5272-5279.
40. F. Endres, M. Bukowski, R. Hempelmann and H. Natter, *Angewandte Chemie International Edition*, 2003, **42**, 3428-3430.
41. V. Vidhya, J. V. Rani, A. R. Kumar, R. Thangamuthu, K. Murali and M. Jayachandran, *Journal of Materials Science: Materials in Electronics*, 2011, **22**, 1460-1465.
42. A. Ispas and A. Bund, *Electrochemical Society Interface*, 2014, 47.
43. M. Allahyarzadeh, B. Roozbehani, A. Ashrafi, S. Shadizadeh, A. Seddighian and E. Kheradmand, *J Electrochem Soc*, 2012, **159**, D473-D478.
44. S. Schaltin, N. R. Brooks, L. Stappers, K. Van Hecke, L. Van Meervelt, K. Binnemans and J. Fransaer, *Phys Chem Chem Phys*, 2012, **14**, 1706-1715.
45. Y. Katayama, R. Fukui and T. Miura, *J Electrochem Soc*, 2007, **154**, D534-D537.
46. Y.-L. Zhu, Y. Katayama and T. Miura, *Electrochim Acta*, 2012, **85**, 622-627.
47. Y.-l. Zhu, Y. Katayama and T. Miura, *J Electrochem Soc*, 2012, **159**, D699-D704.
48. R. Fukui, Y. Katayama and T. Miura, *Electrochim Acta*, 2011, **56**, 1190-1196.
49. Q. Zhang, Q. Wang, S. Zhang and X. Lu, *Journal of Solid State Electrochemistry*, 2014, **18**, 257-267.
50. A. P. Abbott, F. Qiu, H. M. Abood, M. R. Ali and K. S. Ryder, *Phys Chem Chem Phys*, 2010, **12**, 1862-1872.
51. S. Zein El Abedin, U. Welz-Biermann and F. Endres, *Electrochemistry communications*, 2005, **7**, 941-946.
52. A. P. Abbott, R. C. Harris, Y.-T. Hsieh, K. S. Ryder and I. W. Sun, *Phys Chem Chem Phys*, 2014, **16**, 14675-14681.
53. P. J. Elving and B. Zemel, *Journal of the American Chemical Society*, 1957, **79**, 1281-1285.
54. A. P. Abbott, G. Capper, D. L. Davies and R. K. Rasheed, *Chemistry – A European Journal*, 2004, **10**, 3769-3774.
55. C. Chisholm, *Electrodeposition and Surface Treatment*, 1975, **3**, 321-333.
56. Y. Song and D.-T. Chin, *Electrochim Acta*, 2002, **48**, 349-356.
57. N. Mandich, *Plat. Surf. Finish*, 1997, **84**, 108-115.
58. H. P. Klug and L. E. Alexander, *X-Ray Diffraction Procedures: For Polycrystalline and Amorphous Materials, 2nd Edition*, by Harold P. Klug, Leroy E. Alexander, pp. 992. ISBN 0-471-49369-4. Wiley-VCH, May 1974., 1974, **1**.
59. W. Hume-Rothery and M. R. J. Wyllie, *Proceedings of the Royal Society of London. Series A. Mathematical and Physical Sciences*, 1943, **181**, 331-344.

Chapter 7: Summary and future directions

7.1	Summary	160
	7.1.1 Cr electrodeposition from deep eutectic solvents	160
	7.1.2 The effect of ligands exchange	161
	7.1.3 The effect of additives on the Cr electrodeposition	162
7.2	Future directions	163
7.3	References	164

7.1 Summary

The current electrodeposition baths are based on aqueous chromic acid and are under legislative pressure due to the toxicity of the components. Ionic liquids are a potential alternative electrodeposition medium because of their tuneable solvent properties. While ionic liquids have been used for the deposition of most metals very few have been studied in detail and almost nothing has been carried out in the area of chromium deposition.

The aim of this thesis was to focus on chromium and develop a novel range of eutectic mixtures which could control the speciation of the chromium ion. To this end three novel eutectic systems were developed

- urea: $\text{CrCl}_3 \cdot 6\text{H}_2\text{O}$,
- urea: $[\text{Cr}(\text{en})_3]\text{Cl}_3 \cdot 3\text{H}_2\text{O}$ and
- urea: $\text{KCr}(\text{SO}_4)_2 \cdot 12\text{H}_2\text{O}$.

The results contained within this thesis represent the first comprehensive study of chromium deposition from the Cr(III) based deep eutectic solvents.

7.1.1 Cr electrodeposition from deep eutectic solvents

The physical properties, speciation, concentration effects, electrochemical behaviour of the above systems were studied and their effects upon the morphology of Cr deposits obtained were determined. It was found that all three systems behaved very differently. It has been shown that the novel Type 4 deep eutectic solvents can be formed using urea and different chromium salts. In both urea: $\text{CrCl}_3 \cdot 6\text{H}_2\text{O}$ and urea: $[\text{Cr}(\text{en})_3]\text{Cl}_3 \cdot 3\text{H}_2\text{O}$ systems the eutectic composition occurs at a mole fraction of 0.67 metal salt, similarly to many other Type 2, 3 and 4 DESs. While in the urea: $\text{KCr}(\text{SO}_4)_2 \cdot 12\text{H}_2\text{O}$ system the eutectic composition occurs at a mole fraction of 0.5 metal salt.

In general, these liquids display high conductivities, with relatively low viscosities. Numerous techniques, applied to the *in-situ* liquid phase, such as; EXAFS, UV-visible and FAB-MS were applied to the metal speciation in the selected systems. These techniques provided independent and mutually supportive evidence for the behaviour observed in distinct experiments.

Analysis of cyclic voltammetry, chronoamperometry and electrogravimetry conducted in the all systems indicated differences in the reactivity and mobility of species in solution which affected the growth mechanism and resulted in changes in deposit morphology after bulk electrolysis. Deposit morphology affected the appearance and

hardness of the chromium films. Thick, adherent, non-cracked chromium could be bulk-deposited onto steel and coating hardness values showing that these liquids are able to produce hard chromium coatings.

7.1.2 The effect of ligands exchange

A variety of species are formed when chromium chloride is mixed with urea (urea: $\text{CrCl}_3 \cdot 6\text{H}_2\text{O}$ system). The equilibria between the species can be extreme when local differences in composition occur which is the case close to the electrode surface during electrodeposition. The equilibria will depend upon the relative concentrations of the three ligands; H_2O , Cl^- and urea. These in turn will be affected by the rate of deposition, the viscosity of the liquid and any agitation of the fluid. It is therefore unsurprising that morphology control in these liquids is difficult.

A trivalent cationic chromium species was produced for a DES for the first time and this had a higher conductivity than any similar liquid previously described. The coordination geometry around a Cr^{III} centre is controlled by making a complex with ethylene diamine, en, as a strong ligand to form $[\text{Cr}(\text{en})_3]\text{Cl}_3 \cdot 3\text{H}_2\text{O}$ which is complexed with urea to form a eutectic. The properties of this eutectic are contrasted with those of the urea: $\text{CrCl}_3 \cdot 6\text{H}_2\text{O}$ eutectic where a variety of species are known to form in solution. It is shown that markedly different properties are obtained together with different deposit morphology. Using this liquid bright, adherent, hard chromium was obtained by electroreduction which contrasted with softer, black, less crystalline deposits which were obtained when speciation was less well defined. This indicates that controlling the speciation of a metal ion during electrodeposition can significantly affect the morphology and properties of the metallic film.

EXAFS was applied to these systems to identify the metal species present in solution. This technique conclusively proved that Cr was present as $[\text{CrCl}_2(\text{OD})_4]^+$ in urea: $\text{CrCl}_3 \cdot 6\text{H}_2\text{O}$ system. Where, OD is an oxygen donor which could be either water or urea. The equilibria will depend upon the relative concentrations of the three ligands; H_2O , Cl^- and urea. These in turn will be affected by the rate of deposition, the viscosity of the liquid and any agitation of the fluid. It is therefore unsurprising that morphology control in these liquids is difficult

Whereas EXAFS analysis of the $[\text{Cr}(\text{en})_3]\text{Cl}_3 \cdot 3\text{H}_2\text{O}$: urea systems in the mole ratio 1:2 and 2:1 show what appears to be ethylene diamine coordination with 6 nitrogen and 6 near neighbour carbon atoms. The EXAFS spectra are almost identical at both

compositions and show no evidence of chloride ligands being present in the chromium coordination shell. This underpins the origin of the colour change as being a hydrogen bond acceptor issue. Possible sources of O-coordination could be water, urea, or sulfate. Analysis suggests at least part of this coordination is due to urea or sulfate. However, urea is the more likely source of O-coordination.

The next effort was to remove relatively strong ligands such as chloride and form the first deep eutectic solvents without a chloride anion. Eutectic mixtures can be formed with the double salt $\text{KCr}(\text{SO}_4)_2 \cdot 12\text{H}_2\text{O}$. A trivalent cationic chromium species was produced for a DES for the first time and this had relatively a higher conductivity than any similar liquid previously described. Using this liquid black, adherent, hard chromium was obtained by electroreduction which contrasted with softer, black, less crystalline deposits which were obtained when speciation was less well defined.

7.1.3 The effect of additives on the Cr electrodeposition

Brighteners are vital to most electroplating systems and act to reduce the surface roughness and increase reflectivity. The investigation was extended to determine the effect of the classical additives on the Cr electrodeposition mechanism. Insufficient aqueous electrodeposition procedures consist of electrolyte and metal salt alone; a wide range of additives are commonly introduced to the electroplating solution as levellers, brighteners and complexing agents. Nevertheless, little consideration has been given to the effect of additives in ionic liquid/ deep eutectic solvent electroplating procedures.

In this thesis it has been shown that water and the organic additives boric acid and NaBr have a significant effect on the Cr electrodeposition mechanism in both urea: $\text{CrCl}_3 \cdot 6\text{H}_2\text{O}$ and urea: $\text{KCr}(\text{SO}_4)_2 \cdot 12\text{H}_2\text{O}$ systems. Water and boric acid were shown to significantly alter the deposited Cr morphology. Corresponding changes in the cyclic voltammetry and UV-vis spectroscopy were indicative of a change in the Cr electrodeposition mechanism this was investigated using both electrochemical and microscopic methods.

Brighteners are believed to act in one of two ways in aqueous electrolytes:

- i. They act to complex the metal in solution making it harder to reduce
- ii. They are adsorbed at the electrode surface, inhibiting nucleation.

It was therefore proposed that the differences in electrochemical behaviour and deposit morphology were due to the relative hydrogen bond donor strength of the additives.

In this investigation we show how the incorporation of water, NaBr and boric acid affects the viscosity, conductivity and species present in the deep eutectic solvents and how this in turn these change the morphology of the deposit.

7.2 Future directions

This thesis has highlighted the complexity of electrodeposition processes in deep eutectic solvents. It is clear that the electrodeposition mechanism is powerfully reliant on the solvent used and the concentration of solute.

The coordination geometry around a Cr^{III} centre is controlled by making a complex which affects the properties of the eutectic mixture. It is shown that markedly different properties are obtained together with different deposit morphology, when the chromium ligand has been exchanged. This approach could lead to the design of improved DESs and an understanding of which ligand can improve the properties of the plating solution. Additionally it has been shown that some organic additives can be used as brighteners in these systems and while their mode of action is not fully understood it is clear that they do not significantly affect speciation. This is a research area, which to date has been rather under represented and it would be helpful to carry out a systematic analysis of functional groups to determine the mechanism by which brighteners work in these liquids. Other additives such as nicotinic acid, methyl nicotine and dimethyl-hydantoin have been shown to be very effective in other DESs and it would be useful to determine their efficacy in these liquids.

The adsorption of cations on metal surfaces has been studied by Endres using STM.¹ It would be useful to apply this technique to these systems as it would also provide information about the magnitude of the adsorption energy and the structure of the double layer. It would also be helpful to use spectroscopic or impedance techniques to study adsorption but the main difficulties are the high extinction coefficient for visible spectroscopy and large number of IR active functional groups in the liquid.

Data presented in this thesis suggests that the changes in Cr deposition, from these three electrolytes studied and upon the addition of organic additives, is due to a difference in Cl⁻ activity and the structure of the electrochemical double layer. However, it would be also useful to study the structure of the double layer in these deep eutectic solvents which could be done through capacitance measurements.

To investigate what affect the choice of cation or hydrogen bond donor has on the formation of the chloro-complex, it would be vital to examine other hydrogen bond

donors such as glycerol and ethylene glycol with the selected chromium salts. We have shown that they are in general slightly less conducting but they may have enhanced electrochemical stability and may affect the double layer structure more markedly.

It would be interesting to investigate the anodic reaction which is an area already being studied in the group. To date it is known that the anodic reaction is either the evolution of hydrogen or the evolution of chlorine depending on the electrolyte and electrode material. It would be useful to study possible sacrificial additives or soluble anodes. It has also been shown within the group that pulse plating is effective at re-establishing equilibrium in the double layer during electrodeposition.

Preliminary data suggests that the viscosity of the solutions behaves as non-Newtonian fluid at low temperature and behaves as Newtonian fluid at relatively high temperature. Also, adding water from 5-20 wt% will change the non-Newtonian behaviour to the Newtonian. The causes underlying this would be interesting to study. The most probably cause of this phenomenon is an increase in free volume and an increase in the freezing holes in the liquid structure. This could be studied by simple viscosity measurements and corroborated using different spindle speed.

The current electrolytic solutions, works successfully for a lab scale. The next steps would be to scale this process up and to potentially create a flow process, such that pre-treatment and plating can be done straightforwardly. It was also be interesting to examine the separation and recovery of the solution on a small scale after using in a great detail.

A large number of alloy electrodeposits have been described from deep eutectic solvents. Very little is known about the Cr alloy and the phase formation in addition to the relative structure of the co-deposit. *Ex-situ* AFM study can be carried out to study the nucleation and growth mechanism of metals in the co-deposit and the correlation of the electrolyte composition and the electrodeposition parameters to the structure of the co-deposit at the early stages of deposition.

7.3 References

1. E. M. Moustafa, S. Zein El Abedin, A. Shkurankov, E. Zschippang, A. Y. Saad, A. Bund and F. Endres, *The Journal of Physical Chemistry B*, 2007, **111**, 4693-4704.

Chapter 8: Appendix

8.1 Viscosity and conductivity

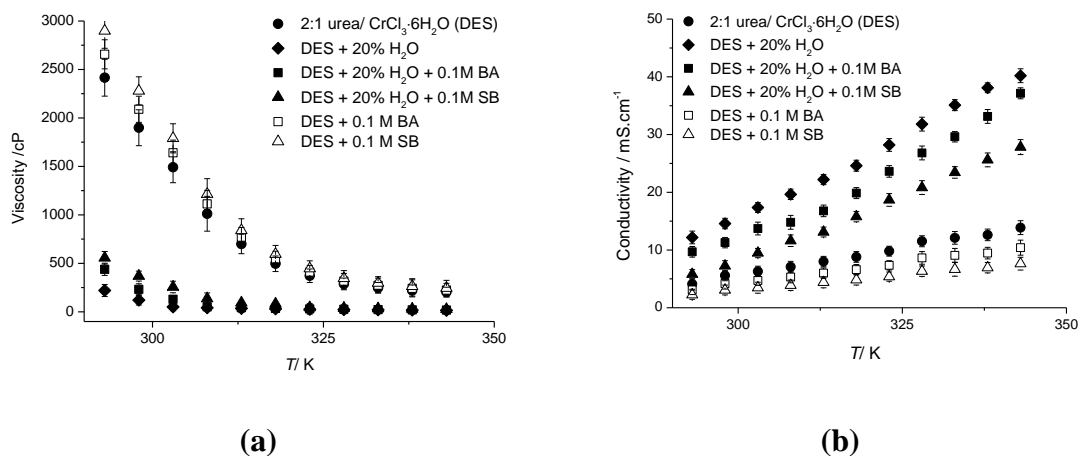
(i) 2 urea: $\text{CrCl}_3 \cdot 6\text{H}_2\text{O}$ system

Figure 8.1: (a) Viscosity and (b) conductivity of 2 urea: $\text{CrCl}_3 \cdot 6\text{H}_2\text{O}$ mixtures as a function of temperature and additives

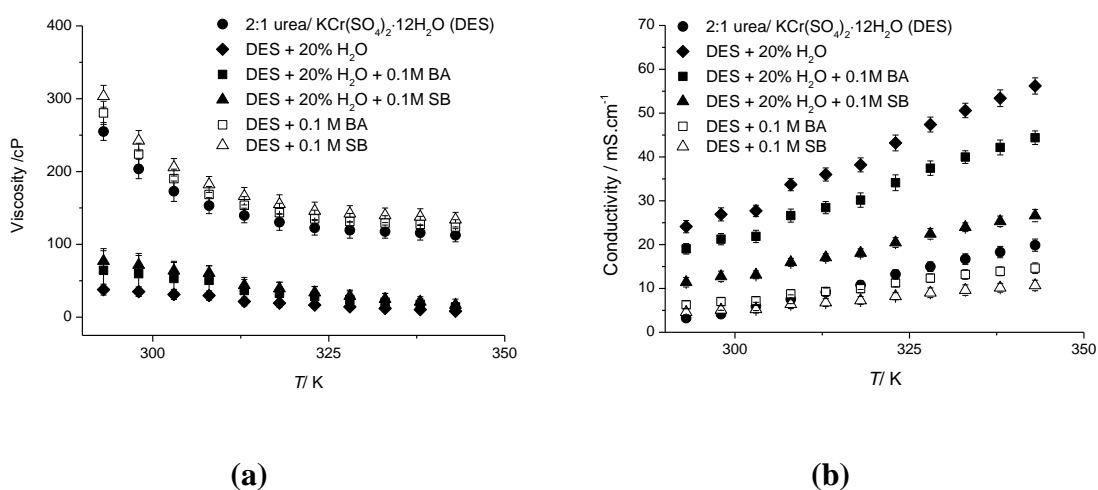
(ii) urea/ $\text{KCr}(\text{SO}_4)_2 \cdot 12\text{H}_2\text{O}$ system

Figure 8.2: (a) Viscosity and (b) conductivity of 2urea: $\text{KCr}(\text{SO}_4)_2 \cdot 12\text{H}_2\text{O}$ mixtures as a function of temperature and additives

(iii) Activation energies

Table 8.1: Activation energies for viscous flow (E_η) and conductivity (E_A) as a function of liquid composition. Coefficients of correlation (r).

Systems	E_η [kJ·mol ⁻¹]	r	E_A [kJ·mol ⁻¹]	$-r$
2urea: CrCl ₃ ·6H ₂ O	46.30	0.983	19.09	0.977
DES + 20% H ₂ O	38.59	0.907	20.03	0.993
DES + 0.1M boric acid	45.09	0.982	19.09	0.977
DES + 0.1M NaBr	45.18	0.990	19.13	0.968
DES + 20% H ₂ O + 0.1M boric acid	50.76	0.958	22.62	0.996
DES + 20% H ₂ O + 0.1M NaBr	53.12	0.964	26.19	0.985

Table 8.3: Activation energies for viscous flow (E_η) and conductivity (E_A) as a function of liquid composition. Coefficients of correlation (r) for the fits to Equations 6.2 and 6.3 are also given.

Systems	E_η [kJ·mol ⁻¹]	r	E_A [kJ·mol ⁻¹]	$-r$
DES 2urea: KCr(SO ₄) ₂ ·12H ₂ O	12.56	0.953	30.48	0.977
H ₂ O DES + 20 % H ₂ O	25.89	0.907	14.68	0.989
Boric acid DES + 0.1M boric acid	12.58	0.952	14.69	0.987
NaBr DES + 0.1M NaBr	12.60	0.950	14.70	0.958
Boric acid+ H ₂ O DES + 20 % H ₂ O + 0.1M boric acid	25.92	0.908	14.72	0.986
NaBr+ H ₂ O DES + 20 % H ₂ O + 0.1M NaBr	25.90	0.914	14.73	0.955